Heinrich Heine Universität Düsseldorf

Quantitative secretome analysis of cardiac fibroblasts in the control heart and after myocardial infarction

---

Inaugural dissertation

Submitted to the

Faculty of Mathematics and Natural Sciences

of the Heinrich Heine University Düsseldorf, Germany

for the degree of

Doctor of Natural Sciences

Submitted by

Jasmin Bahr

born in Duisburg, Germany

Düsseldorf, December 2023

From the Department of Molecular Cardiology, Medical Faculty and University Hospital Düsseldorf, Heinrich Heine University Düsseldorf

Printed with the permission of the Faculty of Mathematics and Natural Sciences of the Heinrich Heine University Düsseldorf

1. Assessor: Prof. Dr. Jürgen Schrader

Department of Molecular Cardiology, Heinrich Heine University Düsseldorf

Universitätsstraße 1

40225 Düsseldorf

2. Assessor: Prof. Dr. Axel Gödecke

Department of Cardiovascular Physiology, Heinrich Heine University Düsseldorf

Universitätsstraße 1

40225 Düsseldorf

Day of oral exam: 15.04.2024

Summary

Myocardial infarction (MI) is still the leading cause of death worldwide. Especially cardiac fibrosis, which mediates myocardial stiffness and impairs cardiac function resulting in heart failure (HF) and death, is a common feature of this ischemic heart disease. Cardiac fibroblasts (CF) play a crucial role in cardiac remodeling post MI. However, little is known about CF-secreted factors and how they could be used as therapeutic targets to prevent excessive fibrosis and heart failure.

To obtain deeper insights into the mechanisms of cardiac remodeling and fibrosis, a combination of stable isotope labeling with amino acids in cell culture (SILAC) and click-chemistry-based protein enrichment to analyze the CF secretome in healthy control and post-MI hearts (50 min ischemia/reperfusion), was established. This method allowed the enrichment of newly synthesized proteins in serum-containing (10% FBS) medium that can be analyzed via liquid chromatography with tandem mass spectrometry (LC-MS/MS). Additionally, single-cell/single-nucleus RNA sequencing (scRNA-seq/snRNA-seq) data were evaluated to study cellular expression of the identified proteins.

Secretome analysis of cultured CF under basal conditions identified 122 proteins which, besides several ECM-related proteins, included 57 paracrine/autocrine factors reported to be involved in fibrosis inhibition (PAI-1, GSN, SFRP1, SLIT2), immune homeostasis (AXL, CCL2, SOD3), angiogenesis (IGFBP4, ANGPTL4, NGF, PEDF), and cardioprotection (IGFBP4, NGF, PCSK6, SFRP1). Plasminogen activator 1 (PAI-1) was the most abundant paracrine factor by far. Gene expression analysis (scRNA-seq) showed a high degree of agreement with proteins secreted by CF in the healthy heart. CF obtained after MI showed a significantly higher abundance of 79 proteins 3 d post MI and 28 proteins 5 d post MI compared to Sham control. Some of these factors are known to promote fibrosis (BMP1, LOXL3), angiogenesis (TIMP3, GDF6), inflammation (SEMA7A), cardioprotection (CPE, SFRP1, SLIT2), but also apoptosis of cardiomyocytes (PXDN, FN1). Within the paracrine/autocrine factors, there were two proteins only detectable after MI: osteoprotegerin (OPG), which is known to enhance cardiomyocyte proliferation, and DnaJ heat shock protein family (Hsp40) member B11 (DNAJB11), whose function in cardiac remodeling is still unclear. ScRNA analyses revealed that the significantly higher secreted proteins were preferentially expressed by CF and were mostly enhanced post MI.

In addition, an attempt was made to study the fibroblast-specific secretome of murine infarct-induced aCF *in vivo* by using AAV9-mediated biotinylation of $POSTN^+$ CF-secreted proteins in the heart. To this end, an ER-localized biotin ligase (ER-TurboID), under control of an aCF specific promoter (AAV9-POSTN-ER-TurboID), was applied *in vivo* to enable measurements of the dynamic changes of the MI-induced aCF secretome in the coronary effluent of isolated perfused hearts. Analysis of $POSTN^+$ CF secretome was limited by plasma proteins still present and low intensity distribution. However, some ECM-related and paracrine/autocrine factors were identified post MI that were also found to be significantly increased in the secretome of cultured CF after MI.

In summary, CF in the infarcted heart specifically secrete a set of matrix proteins and several paracrine factors which can signal to surrounding cells and thus might be important in cardioprotection and fibrosis. Identified proteins may be therapeutic targets in the future to limit cardiac fibrosis. In addition, some of these proteins may be suitable as biomarkers to monitor the activation state of CF.

Publications

Parts of this thesis have been published in following publications:

Defining the cardiac fibroblast secretome in the healthy and post-MI heart

Jasmin Bahr, Gereon Poschmann, Zhaoping Ding, Ria Zalfen, Julia Steinhausen, Thorsten Wachtmeister, Daniel Rickert, Tobias Lautwein, Christina Alter, Junedh M. Amrute, Kory J. Lavine, Karl Köhrer, Kai Stühler, Julia Hesse, Jürgen Schrader

Under review in:	Nature Cardiovascular Research
	(reference number: NCVR-2023-11-2326-T)
Impact factor:	Journal was founded in 2022, impact factor is expected in 2024
Own contribution:	60%
	Performance of biological experiments
	Data analysis
	Concept development and manuscript writing

Secretomics-A Key to a Comprehensive Picture of Unconventional Protein Secretion

Gereon Poschmann, Jasmin Bahr, Jürgen Schrader, Ioana Stejerean-Todoran, Ivan Bogeski, Kai Stühler

Published in:	Frontiers in Cell and Developmental Biology, 2022
Impact factor:	5.5
Own contribution:	30%
	Performance of biological experiments

Abbreviations

Table 1: Abbreviations

***P**	P-value
$^{13}C_6$ Arg	$^{13}C_6$ L-arginine
$^{13}C_6{}^{15}N_4$ Arg	$^{13}C_6{}^{15}N_4$ L-arginine
$^{13}C_6{}^{15}N_2$ Lys	$^{13}C_6{}^{15}N_2$ L-lysine
α-SMA	Alpha-smooth muscle actin
AAV	Adeno-associated virus
AAV9	Adeno-associated virus of serotype 9
aCF	Activated cardiac fibroblasts
ACTB	Actin beta
ACTG1	Actin gamma 1
ACTIVIN-A	Homodimer of two INHBA subunits
ADAM	A disintegrin and metalloproteinases
ADAM12	A disintegrin and metalloproteinase 12
ADAM15	A disintegrin and metalloproteinase 15
ADAMTS1	A disintegrin and metalloproteinase with thrombospondin motifs 1
ADAMTS2	A disintegrin and metalloproteinase with thrombospondin motifs 2
ADAMTSL3	A disintegrin and metalloproteinase with thrombospondin motifs like 3
ADM	Adrenomedullin
AEBP1	Adipocyte enhancer-binding protein 1
AF	Alexa Fluor
AHA	L-azidohomoalanine
AHSG	Alpha 2-HS Glycoprotein
AMI	Acute myocardial infarction
AMP	Adenosine monophosphate
ANGPTL4	Angiopoietin-like 4
AP	Alkaline phosphatase
APP	Amyloid precursor protein
APOE	Apolipoprotein E
APOH	Apolipoprotein H
APP	Amyloid-beta precursor
Arg	L-arginine
ASPN	Asporin
ATP	Adenosine triphosphate
AXL	Receptor protein tyrosine kinase receptor UFO
B2M	Beta-2 microglobulin
BCA	Bicinchoninic acid
BGN	Biglycan
Bis-Tris	Bis(2-hydroxyethyl) iminotris(hydroxymethyl)methane
BMP1	Bone morphogenic protein 1
BSA	Bovine serum albumin
C1-INH (SERPING1)	C1-Esterase-Inhibitor
C3	Complement C3
C4B	Complement C4b
C4BP	C4b-binding protein
C57Bl/6	C57 black six mice (inbred strain)
CCDC80	Coiled-coil domain containing 80
CCK-8	Cell Counting Kit 8
CCL2	CC-Chemokin-Ligand-2
CCL9	CC-Chemokin-Ligand-9

Cd31	Cluster of differentiation 31
Cd45	Cluster of differentiation 45
Cd90	Cluster of differentiation 90
CF	Cardiac fibroblasts
CFH	Complement factor H
CFI	Complement factor I
CHAPS	3-[(3-Cholamidopropyl) dimethylammonium]-1-propanesulfonate hydrate
CLSTN1	Calsyntenin 1
CLU	Clusterin
CM	Cardiomyocytes
COL	Collagen
COL1A1	Collagen type I alpha 1 chain
COL1A2	Collagen type I alpha 2 chain
COL3A1	Collagen type III alpha 1 chain
COL4A1	Collagen type IV alpha 1 chain
COL4A2	Collagen type IV alpha 2 chain
COL4A5	Collagen type IV alpha 5 chain
COL5A2	Collagen type V alpha 2 chain
COL5A3	Collagen type V alpha 3 chain
COL6A1	Collagen type VI alpha 1 chain
COL6A3	Collagen type VI alpha 3 chain
COL8A1	Collagen type VIII alpha 1 chain
COL12A1	Collagen type XII alpha 1 chain
COL16A1	Collagen type XVI alpha 1 chain
Conv	Conventional protein secretion
COTL1	Coactosin-like protein
CP	Ceruloplasmin
CPE	Carboxypeptidase E
CRLF1	Cytokine receptor like factor 1
CSF1	Macrophage colony-stimulating factor
CST3	Cystatin C
CTGF	Connective tissue growth factor
cTn	Cardiac troponin
Ctrl	Control
CTSA	Cathepsin A
CTSB	Cathepsin B
CTSD	Cathepsin D
CYCS	Cytochrome C
D-DMEM	Depletion DMEM
D4 Lys	[4,4,5,5- D4] L-lysine
DAG1	Dystroglycan 1
DAPI	4’,6-diamidino-2-phenylindole
DAMPs	Damage-associated molecular patterns
DC	Dendritic cells
DCN	Decorin
Ddr2	Discoidin domain receptor 2
DMEM	Dulbecco’s Modified Eagle Medium
DMSO	Dimethyl sulfoxide
DNA	Deoxyribonucleic acid
DNAH7B	Dynein axonemal heavy chain 7
DNAJB11	DnaJ heat shock protein family (Hsp40) member B11
DPT	Dermatopontin
DTT	Dithiothreitol
E. coli	*Escherichia coli*
ECG	Electrocardiogram
ECM	Extracellular matrix

EC	Endothelial cells
ECM1	Extracellular matrix protein 1
EDTA	Ethylenediaminetetraacetic acid
EEF2	Elongation factor 2
EFEMP1	EGF-containing fibulin-like extracellular matrix protein 1
EFEMP2	EGF-containing fibulin-like extracellular matrix protein 2
EGTA	Ethylene glycol-bis (β-aminoethyl ether)-N,N,N',N'-tetra acetic acid
EMILIN1	Elastin microfibril interfacer 1
EMT	Epithelial-mesenchymal transition
EndoMT	Endothelial-to-mesenchymal transition
EPDC	Epicardium-derived cells
ER	Endoplasmic reticulum
ESI	Electrospray ionization
F13B	Coagulation factor XIII b chain
FBLN1	Fibulin 1
FBLN2	Fibulin 2
FBLN5	Fibulin 5
FBN1	Fibrillin 1
FBN2	Fibrillin 2
FBS	Fetal bovine serum
FC	Fold change
FDR	False discovery rate
FGF	Fibroblasts growth factor
FMOD	Fibromodulin
FN1	Fibronectin
FNDC1	Fibronectin type III domain containing 1
FRZB	Frizzled related protein
FSP1	Fibroblast-specific protein 1
FSTL1	Follistatin-related protein 1
GANAB	Glucosidase II alpha subunit
GAS6	Growth arrest-specific-protein-6
gc	Genome copies
GDF6	Growth differentiation factor 6
GDF15	Growth differentiation factor 15
GDN (SERPINE2)	Glyco-diosgenin
GFP	Green fluorescent protein
GM-CSF	Granulocyte macrophage colony stimulating factor
GOBP	Gene ontology biological process
GOCC	Gene ontology cellular component
GSN	Gelsolin
GRN	Granulin
HA	Human influenza hemagglutinin
HBA2	Hemoglobin subunit alpha-2
HBB-B2	Hemoglobin subunit beta-2
HBBT1	Beta-globin
HEK293T	Human embryonic kidney 293 cells containing the SV40 large T antigen
HF	Heart failure
HSP	Heat shock protein
HSP47 (SERPINH1)	Heat shock protein 47
HSP90B1	Heat shock protein 90kDa beta member 1
HSPA5	Heat shock protein family A (Hsp70) member 5
HSPG2	Heparan sulfate proteoglycan 2

IAA	Iodoacetamide
IC	Intracellular
IGF1	Insulin-like growth factor 1
IGFBP2	Insulin-like growth factor binding protein 2
IGFBP4	Insulin-like growth factor binding protein 4
IGFBP7	Insulin-like growth factor binding protein 7
IgG	Immunoglobulin G
IF	Immune fluorescence
IFN	Interferon
IL-1	Interleukin-1
IL-1β	Interleukin-1 beta
IL-10	Interleukin 10
INHBA	Inhibin A
IKBIP	I kappa B kinase interacting
I/R	Ischemia/reperfusion
IVC	Vena carva inferior
KHB	Krebs-Henseleit buffer
KLKB1	Kallikrein b1
KRT1	Keratin 1
KRT2	Keratin 2
KRT10	Keratin 10
LAD	Left anterior descending coronary artery
LAMA2	Laminin subunit alpha 1
LAMA4	Laminin subunit alpha 4
LAMB1	Laminin subunit beta 1
LAMB2	Laminin subunit beta 2
LAMC1	Laminin subunit gamma 1
LANUV	Landesamt für Natur, Umwelt und Verbraucherschutz Nordrhein-Westfalen
LC	Liquid chromatography
LC MS/MS	Liquid chromatography with tandem mass spectrometry
LGALS3BP	Galectin 3 binding protein
LGMN	Legumain
LOX	Lysyl oxidase
LOXL1	Lysyl oxidase like 1
LOXL2	Lysyl oxidase like 2
LOXL3	Lysyl oxidase like 3
LPL	Lipoprotein lipase
LTBP1	Latent TGF-β binding protein 1
LTBP2	Latent TGF-β binding protein 2
LTBP3	Latent TGF-β binding protein 3
LTBP4	Latent TGF-β binding protein 4
LUM	Lumican
Lys	L-lysine
m/z	Mass-to-charge ratio
MATN2	Matrilin 2
MBL2	Mannose binding lectin 2
MFAP4	Microfibril associated protein 5
MFAP5	Microfibril associated protein 5
MFGE8	Milk fat globule EGF factor 8
Met	L-methionine
METRNL	Meteorin-like protein
MGP	Matrix-GLA-protein
MI	Myocardial infarction
MIA3	Melanoma inhibitory activity protein 3
miRNA	Micro-ribonucleic acid

MMP	Matrix metalloproteinase
MMP2	Matrix metalloproteinase 2
MMP3	Matrix metalloproteinase 2
MMP14	Matrix metalloproteinase 2
MS	Mass spectrometer
mRNA	Messenger ribonucleic acid
MW	Molecular weight
NCBI	National Center for Biotechnology Information
NF-κB	Nuclear factor-kappa B
NGF	Beta-nerve growth factor
NGS	Normal goat serum
NHDF	Normal human dermal fibroblasts
NID	Nidogen
NID1	Nidogen 1
NID2	Nidogen 2
NTN4	Netrin 4
NUCB	Nucleobindin
NUCB1	Nucleobindin 1
NUCB2	Nucleobindin 2
OAF	Out at first homolog
OGN	Osteoglycin
OLFML3	Olfactomedin-like protein 3
OPG (TNFRSF11B)	Osteoprotegerin/ TNF receptor superfamily member 11b
P4HB	Protein disulfide-isomerase
PAI-1 (SERPINE1)	Plasminogen activator inhibitor
PAM	Peptidylglycine alpha-Amidating Monooxygenase
PBS	Phosphate-buffered saline
PCOLCE	Procollagen C-endopeptidase enhancer
PCOLCE2	Procollagen C-endopeptidase enhancer 2
PCSK6	Proprotein convertase subtilis/kexin 6
Pdgfrα	Platelet-derived growth factor receptor alpha
PDIA3	Protein disulfide-isomerase A3
PEDF (SERPINF1)	Pigment epithelium-derived factor
PFA	Paraformaldehyde
PLAT	Tissue-type plasminogen activator
PLAU	Plasminogen activator urokinase
PLG	Plasminogen
PLOD1	Procollagen-Lysine, 2 Oxoglutarate 5-Dioxygenase 1
PLOD3	Procollagen-Lysine, 2 Oxoglutarate 5-Dioxygenase 3
POSTN	Periostin
PRDX4	Peroxiredoxin-4
PRELP	Proline and arginine rich end leucine rich repeat protein
PROS1	Protein S
PSAP	Prosaposin
P/S/G	Penicillin/Streptomycin/Glutamine
pSILAC	Pulsed stable isotope labeling using amino acids in cell culture
PTX3	Pentraxin-related protein 3
PVDF	Polyvinylidene difluoride
PXDN	Peroxidasin

QPCT	Glutaminyl-peptide cyclotransferase-like protein
QSOX1	Sulfhydryl oxidase 1
RCN3	Reticulocalbin-3
RIPA	Radioimmunoprecipitation assay
RNA	Ribonucleic acid
RNASE4	Ribonuclease 4
ROS	Reactive oxygen species
RT	Room temperature
S_0	Exchangeability factor for denominator of test statistic
SAM	Analysis of microarray approach
ScRNA-seq	Single-cell RNA sequencing
SnRNA-seq	Single-nuclei RNA sequencing
SDF4	Stromal cell derived factor 4
SDS	Sodium dodecyl sulfate
SEM	Standard error of the mean
SEMA7A	Semaphorin 7A
SERPINA1	Alpha-1-anititrypsin
SERPINA3N	Serine protease inhibitor A3N
SERPINE1 (PAI-1)	Plasminogen activator inhibitor 1
SERPINE2 (GDN)	Glyco-diosgenin
SERPINF1 (PEDF)	Pigment epithelium-derived factor
SERPING1 (C1-INH)	C1 esterase inhibitor
SERPINH1 (HSP47)	Heat shock protein 47
SFRP1	Secreted frizzled related protein 1
SFRP2	Secreted frizzled related protein 2
SILAC	Stable isotope labeling using amino acids in cell culture
SLIT2	Slit guidance ligand 2
SLIT3	Slit guidance ligand 3
SMC	Smooth muscle cells
SOD3	Superoxide dismutase 3
SPARC	Secreted protein acidic and rich in cysteine (Osteonectin)
SPARCL1	Sparc-like protein 1
SPON2	Spondin-2
SRL	Sarcalumenin
SRPX	Sushi repeat-containing protein
SRPX2	Sushi repeat-containing protein 2
SV40	Simian vacuolating virus 40
SVC	Vena carva superior
SVEP1	Sushi von Willebrand factor type A
Tbg	Thyroxine-binding globulin
TBS	Tris-buffered saline
TBST	Tris-buffered saline + Tween 20
Tbx18	T-box transcription factor TBX18
TC	Tissue culture treated
Tcf21	Transcription factor 21
TCN2	Transcobalamin 2
TF	Transferrin protein
TFA	Trifluoracetic acid
TGB	Thyroxine binding globulin
TGF-β	Transforming growth factor beta
TGF-β1	Transforming growth factor beta 1
TGF-βI	Transforming growth factor beta-induced
THBS1	Thrombospondin 1
THBS2	Thrombospondin 2

THBS4	Thrombospondin 4
TIMP	Tissue inhibitors of metalloproteinases
TIMP1	Tissue inhibitors of metalloproteinases 1
TIMP2	Tissue inhibitors of metalloproteinases 2
TIMP3	Tissue inhibitors of metalloproteinases 3
TIMPs	Tissue inhibitors of metalloproteinases
TM	Transmembrane
TMTC3	Transmembrane and TPR repeat-containing protein 3
TNC	Tenascin-C
TNF-α	Tumor necrosis factor-alpha
TNFRSF11B (OPG)	Osteoprotegerin/ TNF receptor superfamily member 11b
TLR	Toll-like receptor
Tris-HCl	Tris-(hydroxymethyl)-aminomethane hydrochloride
tRNA	Transfer ribonucleic acid
TUBB5	Tubulin beta-5 chain
Tween 20	Polyethylene glycol sorbitan monolaurate
UGGT1	UDP-glucose: glycoprotein glycosyltransferase 1
UPS	Unconventional protein secretion
VDAC1	Voltage-dependent anion-selective channel protein 1
Vim	Vimentin
w/o	Without
WB	Western Blot
WISP2	WNT-inducible-signaling pathway protein 2
Wntx	Wnt signaling pathway related
Wt1	Wilms tumor protein
w/v	Weight per volume
ZETT	Zentrale Einrichtung für Tierforschung und wissenschaftliche Tierschutzaufgaben
ZFP462	Zinc finger protein 462

Contents

Summary II
Publications III
Abbreviations IV
1. Introduction 1
1.1 Cellular composition of the heart 1
1.2 Cardiac fibroblasts 2
1.3 Myocardial infarction 3
1.4 Cardiac remodeling after MI 4
1.5 Heterogeneity of CF in MI 6
1.6 Quantitative secretome analysis using mass spectrometry 6
1.6.1 Secretome analysis of cultured cells 7
1.6.2 *In vivo* secretome analysis 9
1.7 Aims of the study 11
2. Materials 13
2.1 Devices and equipment 13
2.2 Expendable materials 15
2.3 Chemicals 16
2.4 Media 18
2.5 Solutions 19
2.6 Buffer 19
2.7 Kits 22
2.8 Antibodies 22
2.8.1 Primary antibodies 22
2.8.2 Secondary antibodies 22
2.8.3 Fluorochromes 23
2.9 Cell lines 23
2.10 Vectors 23
2.11 Adeno-associated virus 24
2.12 Software 24
2.13 Databases 24
3. Methods 25
3.1 Laboratory animals and housing conditions 25
3.2 Induction of MI 25
3.3 Collection of blood and serum 25
3.4 Collection of organs 25
3.5 Collection of coronary effluent 25

3.6 Isolation of CF 26
3.7 Cell culture 26
3.7.1 Cultivation of CF 26
3.7.2 Cultivation of Normal Adult Human Dermal Fibroblasts (NHDF) 26
3.7.3 Cell number determination 27
3.8 Cell viability assay 27
3.9 Lysis of cultured cells 28
3.10 Protein concentration determination 28
3.11 Bis(2-hydroxyethyl)iminotris(hydroxymethyl)methan) gels (Bis-Tris gels) 28
3.11.1 Silver staining 29
3.12 Western Blot 29
3.13 Histology 30
3.14 Immunofluorescence imaging 30
3.15 Secretome analysis of cultured fibroblasts 30
3.15.1 Pulsed SILAC labeling of secreted proteins 30
3.15.2 Click-chemistry for protein enrichment 31
3.15.3 Click-chemistry determination 32
3.15.4 Cell lysate sample preparation 33
3.16 *In vivo* secretome analysis of POSTN^{+} CF post MI 34
3.16.1 Viral transduction 34
3.16.2 *In vivo* biotinylation of cell type-selective secreted proteins 34
3.16.3 Preparation of serum, coronary effluent, and tissue 34
3.16.4 Concentration of coronary effluent 35
3.16.5 Enrichment of biotinylated proteins 35
3.17 MS analysis 35
3.17.1 MS analysis of cultivated fibroblast secretome and proteome 36
3.17.2 MS analysis of POSTN^{+} CF-specific peptides 37
3.18 Single-cell/ single-nuclei RNA sequencing data analysis 38
3.19 Statistics 39
4. Results 40
4.1 Establishment of combined pSILAC and click-chemistry for secretome analysis of NHDF cells 40
4.1.1 Cell viability 40
4.1.2 Click reaction 41
4.1.3 Incorporation of amino acid isotopes 42
4.1.4 Protocol optimization 44
4.1.5 Influence of AHA labeling on NHDF proteome 44
4.1.6 Influence of serum starvation on NHDF secretome 46

4.2 Establishment of combined pSILAC and click-chemistry for secretome analysis of murine CF 48
4.2.1 Cell viability 48
4.2.2 Click-chemistry 49
4.3 Secretome analysis of cultured murine CF 50
4.3.1 Secretome analysis of cultured CF under basal conditions 50
4.3.2 Secretome analysis of cultured CF after MI 53
4.3.3 Gene ontology analysis of CF-secreted proteins after MI 57
4.3.4 Gene expression levels of CF-secreted proteins 5 d post MI compared to Sham 58
4.4 Specific *in vivo* secretome analysis of POSTN$^+$ CF 60
4.4.1 Establishment of POSTN$^+$ CF specific *in vivo* secretome analysis 60
4.4.2 *In vivo* secretome analysis of POSTN$^+$ CF 64
4.4.3 Analysis of the POSTN$^+$ CF-specific proteome 65
5. Discussion 68
5.1 Combining pSILAC labeling and click-chemistry for secretome analysis of fibroblasts 68
5.2 Defining the CF secretome under basal conditions 68
5.3 Comparative secretome analysis of CF after MI and Sham 71
5.4 Method for POSTN$^+$ CF-specific *in vivo* secretome analysis post MI 77
5.5 POSTN$^+$ CF-specific *in vivo* proteome analysis post MI 78
5.6 Outlook 80
6. References 83
7. Appendix XIV
8. Acknowledgement XXXVII
9. Affidavit XXXIX

1. Introduction

1.1 Cellular composition of the heart

The heart is the motor of the body, as it supplies the body with oxygen, nutrients, hormones, components of the immune system, and other metabolites[1]. The heart is divided into the right and left heart, containing four chambers which are separated from each other by the septum and valves[2] (Figure 1). The right heart transports venous blood from the right atrium via the right ventricle into the pulmonary system. The blood becomes oxygenated in the lung and then passes through the left atrium and ventricle, entering the large circulatory system via the aorta[2]. Part of this blood is separately used to supply the heart with oxygen and nutrients via coronary arteries[3].

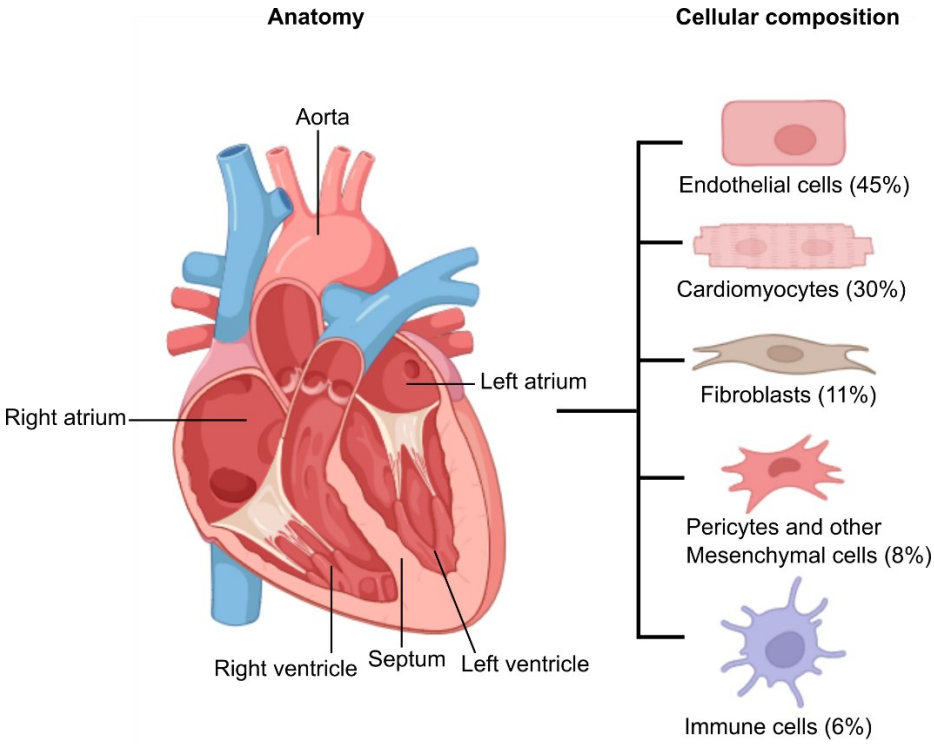

Figure 1: Frontal section view and cellular composition of the heart (adapted from Berry, J. 2020, BioRender[4] and Lafuse *et al*. 2021[5]). The right and the left heart are divided by the septum. They both have an atrium and ventricle separated by valves. The right atrium is filled with deoxygenated blood which is transported into the pulmonary system. Oxygenated blood flows into the left atrium and is transferred into the left ventricle, where it is pumped into the large circulatory system via the aorta. The heart is composed of different cell types (endothelial cells, cardiomyocytes, fibroblasts, other mesenchymal cells like pericytes and smooth muscle cells, and immune cells). The proportion of the total cell count is given as percentage.

The heart is composed of different cell types. These include endothelial cells (EC), cardiomyocytes (CM), immune cells, cardiac fibroblasts (CF), and other mesenchymal cells such as pericytes, and smooth muscle cells (SMC) (Figure 1), with EC making up the largest proportion of the total cell count (~ 45%)[5,6]. CM are heart muscle cells and therefore generate contractile force and maintain contractility of the heart[7]. They make up about 30% of all cells in the heart[6]. CF (~ 11%) are known to produce extracellular matrix (ECM) proteins, which provide structural support. These cells are key players in cardiac remodeling and healing[8]. SMC maintain the elasticity of arteries but are also involved in vascular contraction and ECM generation[9]. Pericytes are important for homeostasis and angiogenesis in the heart[10], as well

as EC, which form the inner layer of vessels and therefore regulate the bloodflow[11]. In the steady state, immune cells like macrophages, which are very important in heart development, monocytes, dendritic cells, B cells, and T cells reside in the heart in small number[12].

For maintaining cardiac function, the different cell types communicate with each other[13]. Especially CF are described to communicate with CM and are also important for communication between different myocardial layers[14]. Crosstalk between cells and the cellular composition of the heart change when it comes to injury like myocardial infarction (MI)[12,13]. In this case, immune cells are attracted to the infarcted area, releasing inflammatory proteins leading to an augmentation and activation of CF as initial step for cardiac repair[12,13].

1.2 Cardiac fibroblasts

CF can be found all over the entire heart[15]. They start to develop during embryogenesis and mostly originate from cells of the proepicardial organ[16,17] that undergo epithelial-mesenchymal transition (EMT). EMT leads to the formation of mesenchymal progenitor cells, which are called epicardium-derived cells (EPDC). EPDC express *transcription factor 21* (*Tcf21*), *Wilms tumor protein* (*Wt1*), and *t-box transcription factor TBX18* (*Tbx18*)[18,19]. These cells migrate into the myocardium where they can differentiate into CF (Figure 2)[16]. About 80% of CF have an epicardial origin, whereas approximately 18% of CF are derived from endocardial cells, which undergo endothelial-to-mesenchymal transition (EndoMT). Only a minority of CF are derived from the neural crest[20,16].

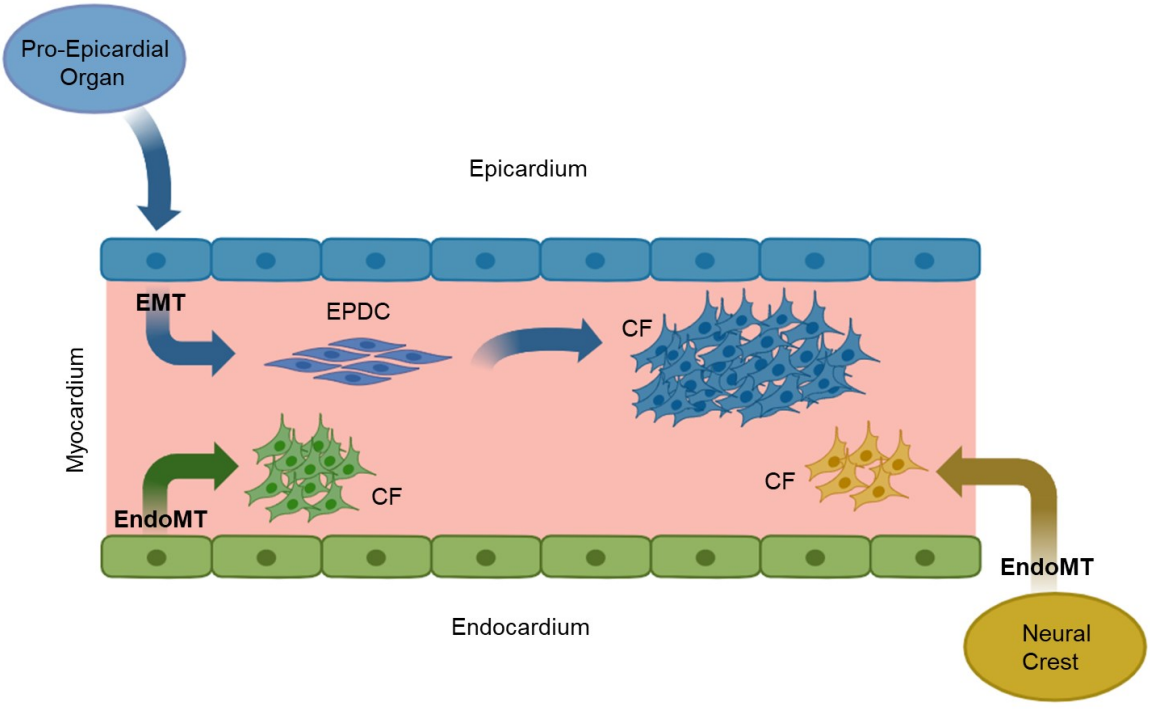

Figure 2: Scheme of the development of cardiac fibroblasts (modified from Doppler *et al.* 2017[16]). Cardiac fibroblasts (CF) derive from three different types of progenitor cells. Most CF derive from epicardial cells that undergo epithelial-mesenchymal transition (EMT). CF can also originate from cells of the endocardium or neural crest cells undergoing endothelial-mesenchymal transition (EndoMT).

CF are defined as mesenchymal cells that produce ECM proteins like different collagens, glycoproteins or fibronectin (FN1)[21,22]. Therefore, they are mainly responsible for cardiac

structure and function by maintaining the ECM homeostasis[23]. Their morphology can be described as spindle-shaped cells[22]. CF are a very heterogeneous cell population[24] and can be characterized by expression of multiple genes like *discoidin domain receptor 2* (*Ddr2*)[25], *Tcf21*[18], *cluster of differentiation 90* (*Cd90*)[20], *collagen type I alpha 1 chain* (*Col1a1*)[26], *platelet-derived growth factor receptor alpha* (*Pdgfrα*)[27], and *vimentin* (*Vim*)[28]. However, there is no specific CF marker as these genes are also expressed by other cell types[16,29]. Therefore, a combination of markers is generally used to identify CF.

1.3 Myocardial infarction

In order to maintain the pumping capacity of the heart, an adequate supply of oxygen of the myocardium must be ensured, which is accomplished by the right and left coronary arteries[2]. The left coronary arteries account for about 80% of the blood flow, which supplies the heart with oxygen[30]. In MI, which is still the leading cause of death worldwide[31], a non-sufficient oxygen supply of a coronary artery results in ischemia of the affected area[30]. Due to a lack of oxygen, affected CM undergo apoptosis, resulting in significant functional impairment of the heart. There are different triggers which can lead to an infarction, thus, MI is classified in five different groups, with type 1 and type 2 being the most prevalent[32]. MI type 1 occurs due to rupture of an atherosclerotic plaque (Figure 3)[33]. This acute myocardial infarction (AMI) leads to a total occlusion of the vessel, resulting in no oxygen supply and has the highest prevalence[34,35].

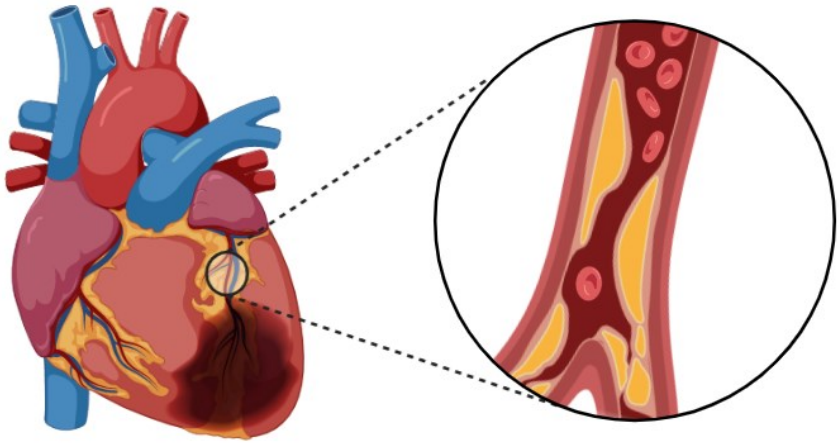

Figure 3: Development of a myocardial infarction type 1 (adapted from BioRender, 2022[36]). Rupture or erosion of an atherosclerotic plaque leads to thrombus formation which occludes a coronary artery resulting in a critical reduction of heart tissue oxygen supply.

MI type 2 is not attributed to an atherosclerotic plaque, but there is also a reduced oxygen supply[37]. It can occur due to a reduction in the diameter of a coronary artery, for example, during vasoconstrictions, atherosclerosis, or other vessel dissections. It may also occur due to an increased oxygen demand, like during severe hypertension or tachyarrhythmia[33].

There are several biomarkers for AMI in the clinics, with elevated cardiac troponin (cTn) levels in the blood being very specific for myocardial damage[38]. The subunits I and T of cardiac troponin are only synthesized in CM and are released into the peripheral blood when CM

undergo necrosis[39]. Determining the cTn levels has highly improved MI diagnostics, but there are other factors which can lead to false positive cTn levels, like heterophilic antibodies[40].

After diagnosis of AMI, rapid reperfusion of the occluded coronary artery to the myocardium is the most often used intervention to revitalize the undersupplied tissue. This minimizes myocardial tissue loss, which has been shown to significantly increase survival after AMI[41]. However, the resulting tissue damage and heart stiffness due to scar formation often lead to a permanent reduction in cardiac performance and heart failure (HF)[42,43]. For this reason, it is important to further study the molecular mechanisms underlying the remodeling process after MI. It is particularly important to understand the signals generated by activated CF (aCF), which finally result in excessive fibrosis, and to develop new therapies preventing cardiac fibrosis post MI.

1.4 Cardiac remodeling after MI

During myocardial ischemia, there is substantial loss of CM by necrosis and apoptosis that cannot be compensated by the adult mammalian heart[44]. Therefore, formation of a collagen-rich scar is a main point in cardiac repair[45]. This process can be divided into three overlapping phases: inflammatory phase (3 hours - 3 days after MI), proliferative phase (3 – 14 days post MI), and maturation phase (14 days - 2 month after MI)[14]. In all these phases, CF play a crucial role and undergo changes in their phenotypes[46].

Following reperfusion after ischemia, reactive oxygen species (ROS) are generated due to re-oxygenation[47]. Additionally, necrotic CM and damaged ECM release molecules, so-called damage-associated molecular patterns (DAMPs), that function as a warning system and initiate the inflammatory response[44,47], starting with the innate immune system[44]. As a result, Toll-like receptor (TLR)-mediated pathways, the complement system and nuclear factor-kappaB (NF)-κB pathway are activated[48]. This leads to a release of soluble factors like cytokines or chemokines that attract neutrophils into the infarct zone[49,50]. Neutrophils secrete factors which cause tissue damage, inflammation, and matrix degradation like ROS, cytokines, lipids, and proteases[50] resulting in a further increase of immune cell recruitment. Lymphocytes and monocytes are recruited to the infarcted area where the latter of the two maturate into M1 macrophages that phagocytize apoptotic cells[51,52].

In the first hours and days post MI, resident CF are activated. First these aCF have a pro-inflammatory phenotype which is predominant until day 3 post MI. In this state, aCF produce several pro-inflammatory cytokines like interleukin-1β (IL-1β) or tumor necrosis factor-α (TNF-α) triggered by ROS and TLRs, leading to an additional secretion of several cytokines and chemokines that contribute to leukocyte attraction[45,47]. Furthermore, these pro-inflammatory aCF secrete matrix metalloproteinases (MMPs) which degrade extracellular matrix into fragments that again maintain inflammation (Figure 4)[14]. This also leads to an increase in fibrin and fibrinogen which are extravasated by the hyperpermeable vascular system and form a provisional fibrin matrix[53]. There is some evidence that aCF are also able to phagocyte apoptotic cells in the infarcted area, but the role of fibroblasts in phagocytosis remains unknown[14].

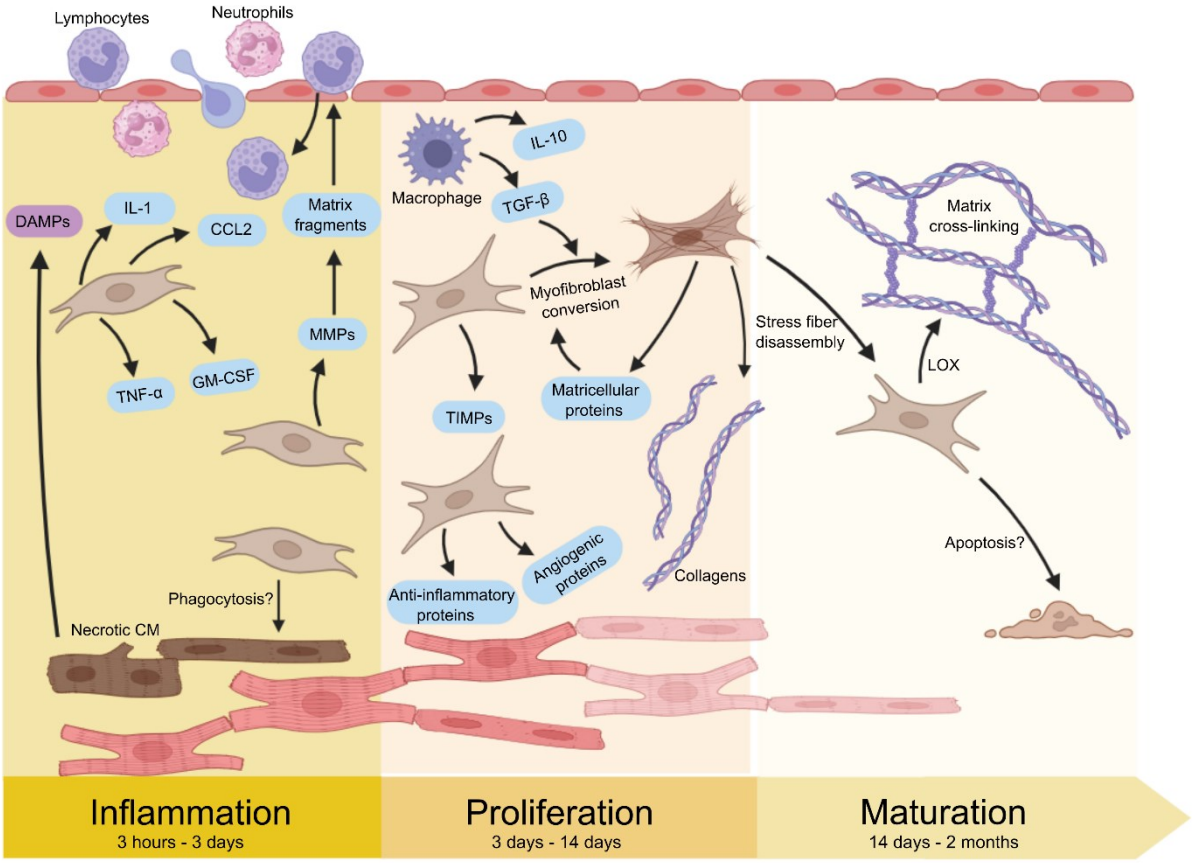

Figure 4: CF in the three different phases of cardiac remodeling post MI (adapted from Humeres *et al.*, 2019[14]). The process of remodeling is divided into three overlapping phases: inflammatory phase (3 hours - 3 days after MI), proliferative phase (3 – 14 days post MI), and maturation phase (14 days - 2 month after MI). During the first hours after MI, necrotic cardiomyocytes release damage-associated molecular patterns (DAMPs), resulting in activation of the innate immune system and attraction of leukocytes. Furthermore, fibroblasts are activated (aCF) and secrete pro-inflammatory proteins like CC-chemokin-ligand-2 (CCL2), interleukin-1 (IL-1), tumor necrosis factor-α (TNF-α), granulocyte macrophage colony-stimulating factor (GM-CSF), and different matrix metalloproteinases (MMPs). There is also evidence that some fibroblasts have phagocytic properties, but their role in phagocytosis is still unknown. After most damaged tissue is cleared, there is a switch of macrophage phenotype promoting the secretion of anti-inflammatory proteins like transforming growth factor-β (TGF-β). Anti-inflammatory signals lead to a change in protein secretion. Activated CF secrete anti-inflammatory, angiogenic, and ECM-related proteins like collagens that are important for later scar formation and matrix reassembly. As the scar matures, the number of aCF decreases. The underlying mechanism, however, is presently not fully understood. It might involve the loss of α-SMA-decorated stress fibers which leads to a change in phenotype. At this timepoint matrix cross-linking proteins like lysyl oxidases (LOX) are secreted to promote cross-linking of collagen fibers leading to the maturation of a collagen-rich scar.

Three days after infarction, most damaged tissue is cleared, and neutrophils undergo apoptosis, leading to a phenotype change of macrophages to an M2 phenotype[54]. These macrophages secrete anti-inflammatory proteins like interleukin-10 (IL-10) or transforming growth factor-β (TGF-β) that initiate the proliferation phase[55]. Additionally, T cells infiltrate into the infarct area, which also secrete anti-inflammatory proteins[56]. At this stage, proliferation of aCF is induced, as well as a shift to an anti-inflammatory and angiogenic aCF phenotype[57]. Additionally, aCF secrete proteins that inhibit MMP, so-called tissue inhibitors of metalloproteinases (TIMP), to prevent further matrix degradation[58]. At that time, aCF are the dominant cell type in the infarction zone as they migrate to the border zone of the infarcted area and infiltrate it mediated by growth factors like TGF-β or fibroblasts growth factors (FGFs), cytokines, and chemokines[14,59]. These factors also lead to an aCF phenotype conversion into so-called myofibroblasts, which are characterized by their contractility generated by the expression of α-smooth muscle actin (α-SMA)[15]. These aCF are associated with production of

ECM proteins like different collagens, FN1, tenascin-C (TNC) or periostin (POSTN)[57,60]. Thus, a collagen-based matrix can be formed, that replaces the fibrin matrix which was formed in the inflammatory phase[61].

In the final phase of wound healing, the scar matures, and the number of α-SMA-expressing aCF decreases[62] as there is a breakdown of α-SMA-decorated stress fibers leading to a change of aCF from a myofibroblast phenotype into a matrifibrocyte phenotype (Figure 4)[14,63]. At that timepoint, aCF secrete matrix cross-linking enzymes like lysyl oxidases (LOX), which are leading to a further scar maturation and strengthening due to the cross-linking of different collagen fibers[64]. At the end of maturation, reparative cells like immune cells, endothelial cells undergo apoptosis, whereas matrifibrocytes remain within the scar or may undergo apoptosis[14,47,63].

The extend and time course of cardiac remodeling after MI do not only depend on infarct size and the amount of CM loss but also on the reparative response on the cellular level and scar formation[65]. The newly formed collagen-rich scar minimizes the risk of rupture. However, an excessive fibrotic response may have a negative impact on pump function due to the resulting stiffness of the myocardium which can cause heart failure[65,66]. Therefore, the fibrotic response has to be well balanced.

1.5 Heterogeneity of CF in MI

Although CF play a crucial role in cardiac remodeling after MI, the different phenotypes, as well as the heterogenous subpopulations during myocardial healing, are still poorly understood[14]. Recent scRNA-seq analysis of C57Bl/6 mice revealed that CF are comprised of at least 11 fibroblast subpopulations which dramatically change their proportion after MI[67–69]. In a recent scRNA-seq study comparing 5 d post MI to Sham-operated control, our group has shown comparable results concerning the different clusters and upregulated genes[68]. A heterogeneous gene expression of various cytokines, chemokines, growth factors, and ECM-associated proteins was detectable within the different subpopulations of aCF 5 d post MI. In this analysis, numerous paracrine factors were identified which are known to be cardioprotective and may have the potential to influence inflammation and myocardial contraction[68].

To what extent the findings by scRNA-seq can be translated to protein level and, in particular, the secretome has not been investigated yet and is of high interest.

1.6 Quantitative secretome analysis using mass spectrometry

The secretome describes all proteins which can either be conventionally or unconventionally secreted[70]. Conventionally secreted proteins contain an N-terminal signal sequence and are guided to the endoplasmic reticulum (ER) and then transported to the Golgi apparatus before secretion[71]. Unconventionally secreted proteins are secreted independently from the ER-Golgi pathway[72]. Secreted proteins are of high interest because they are dynamically changing and play a key role in physiological and pathological processes like cell-cell signaling, cell communication, and cell growth[73–75]. Consequently, they can be used as biomarkers or drug targets in different diseases.

For sake of convenience, the secretome of cells is usually studied *in vitro* using conditioned medium. These approaches cannot fully mirror the *in vivo* situation but can give first important insights into biological pathways that were conserved in cell culture[74]. The general workflow of *in vitro* secretome analysis follows the steps shown in Figure 5. Cells are cultured in medium containing at least 10% fetal bovine serum (FBS). During treatment, e.g., with drugs, the FBS concentration needs to be decreased to ≤ 2%, because otherwise low abundant proteins cannot be detected[76,77]. After stimulating the cells for a specific time, supernatant is collected, and proteins are enriched, followed by fractionation via liquid chromatography, and mass spectrometry analysis[74]. As a control, this procedure is performed without stimulating drugs. A drawback of this procedure is that starving cells may induce cell activation, thereby critically influencing the secretome. After the mass spectrometry analysis, proteins have to be identified with the help of databases as provided by NCBI or UniProt. Afterwards, pathway analysis and prediction models can be used[74].

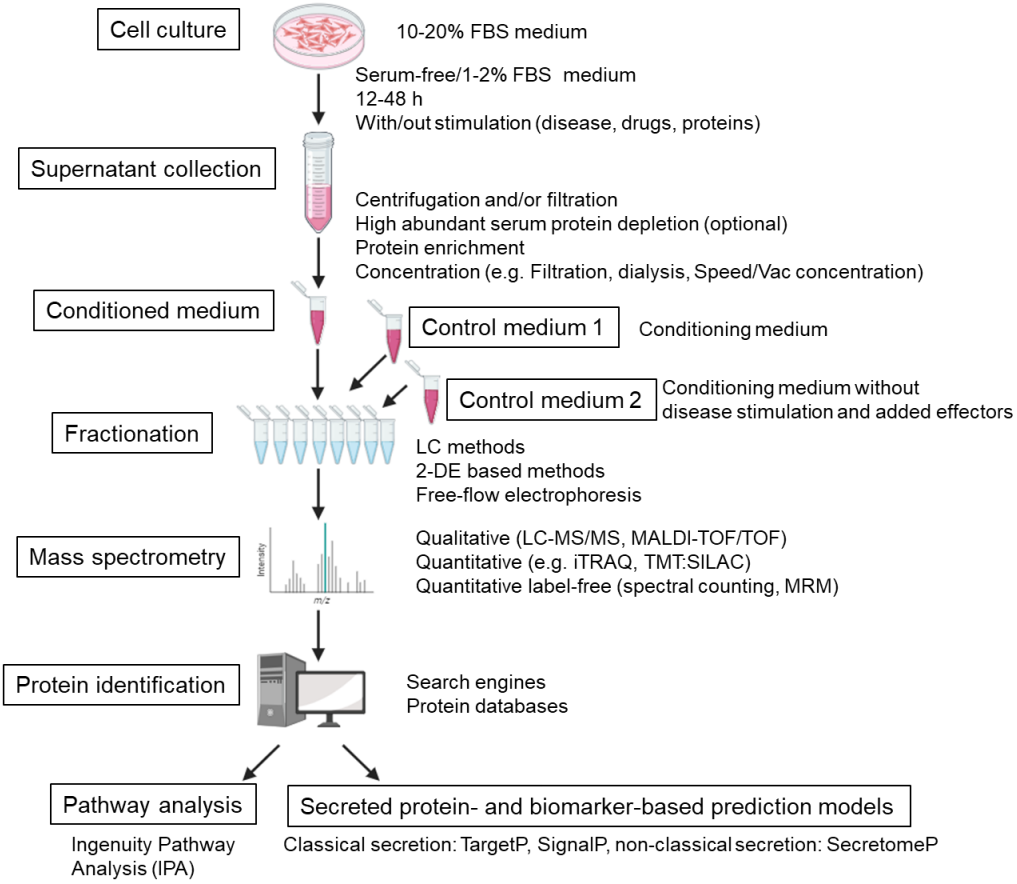

Figure 5: Workflow of state-of-the-art secretome analysis from cultured cells (adapted from Stastna *et al.* 2012[74]). Cells are cultured in medium containing 10-20% fetal bovine serum (FBS). During treatment, FBS concentration is lowered (≤ 2%). After stimulation, supernatants of stimulated cells and control cells are collected, and proteins are enriched by fractionation via liquid chromatography, followed by mass spectrometry analysis. For protein identification, protein databases as provided by NCBI can be used. After this, pathway analysis and prediction models can be carried out.

1.6.1 Secretome analysis of cultured cells

In MS-based secretome analysis of cultured cells, as described above, a major problem is that culture medium usually contains FBS, and thus low-abundant proteins cannot be detected. Therefore, the FBS concentration is lowered, but this has been reported to result in changes

of the secretome[76,77]. To address this issue, Eichelbaum and Krijgsveld established a combination of pulsed stable isotope labeling using amino acids in cell culture (pSILAC) and click-chemistry[78]. This approach enables the quantitative secretome analysis of newly secreted proteins without disturbing background proteins.

SILAC labeling is based on the incorporation of non-radioactive amino acid isotopes with the help of medium lacking specific amino acids, which is supplemented with labeled amino acid isotopes[79]. During a typical pSILAC labeling experiment, cells are exposed to different isotopes of amino acids (heavy or intermediate) for a short time period, allowing the comparison of two different conditions in parallel[80]. For this purpose, the cells to be analyzed are divided in two preparations. For example, cells are depleted of the amino acids L-arginine (Arg), L-lysine (Lys), and L-methionine (Met) using medium without these amino acids. This is followed by labeling the cells with heavy Arg and Lys ([$^{13}C_6$, $^{15}N_4$] Arg, and [$^{13}C_6$, $^{15}N_2$] Lys) or intermediate Arg and Lys ([$^{13}C_6$] Arg and [4,4,5,5-D4] Lys), and the different treatments, respectively. During protein biosynthesis, the amino acid isotopes are incorporated into newly synthesized proteins. These proteins are heavier than the remaining proteins and can be identified by MS. To optimally compare two different conditions at the same time, supernatants containing the secreted proteins are combined, the proteins are digested, and then measured. In this way, random errors can be minimized, and the measurement results of the different conditions are more comparable.

The principle of click-chemistry is to incorporate an azide-bearing biomolecule into the proteins and, in a second step, use the chemo-selective reaction between the azide and an alkyne[81]. Using this technique, newly secreted proteins are bound to an alkyne resin via ring formation (click reaction), which allows separating them from the remaining proteins (Figure 6B). For this purpose, the methionine analogue L-azidohomoalanine (AHA) is used, which carries an azide group (Figure 6A). For the implementation of the method, a depletion of Met must be carried out before adding AHA. Due to the absence of Met in the medium, AHA is incorporated into the newly formed proteins during protein biosynthesis.

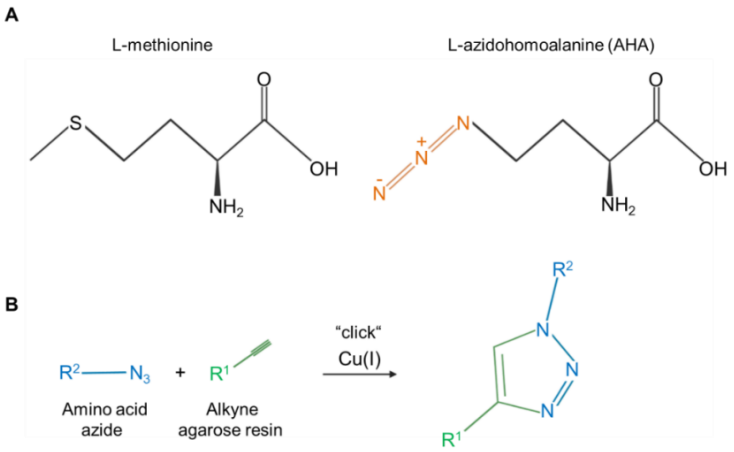

Figure 6: Molecular structure of L-methionine and L-azidohomoalanine (AHA) (adapted from Imami *et al.*, 2019[82]) and mechanism of the click reaction between an alkyne and an azide (adapted from Innovate Peptide Solutions, 2020[83]). A) The L-methionine analogue AHA contains an azide group instead of a sulfur group. **B)** An alkyne and an azide react catalyzed by Cu (I) to form a triazole conjugate (click reaction).

The labeled and azide-containing newly synthesized proteins are bound to an agarose-resin that contains an alkyne, and unbound proteins can be removed by stringent washing[80] (Figure 7). The bound proteins are subsequently digested and eluted as peptides, which can be analyzed by LC-MS/MS based on their different SILAC label.

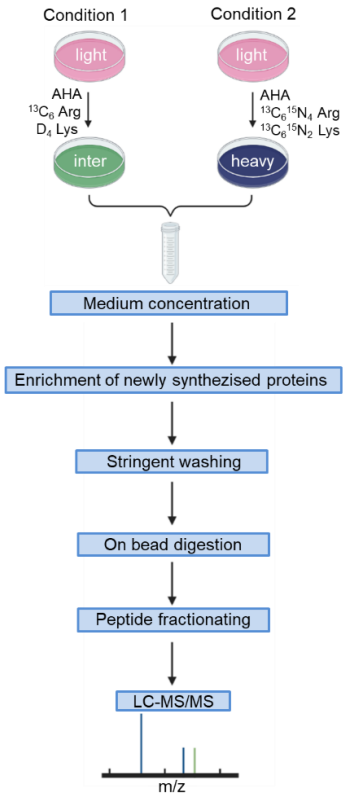

Figure 7: Workflow of combined pulsed SILAC labeling and click-chemistry for enrichment of newly synthesized proteins (modified from Eichelbaum *et al.*, 2012[80]). Cells are divided into two samples and cultivated in medium to adhere. This is followed by depletion of the amino acids Arg, Lys, and Met using depletion medium, which does not contain these three amino acids. Cells are treated under different conditions and incubated in depletion medium plus L-azidohomoalanine (AHA) and heavy- or intermediate (inter) labeled Arg and Lys. Then the supernatants are combined, and the AHA-containing newly synthesized proteins are bound to an agarose-resin by the click-chemistry procedure. The non-bound proteins are washed away, and the bound proteins are digested to elute the peptides. This is followed by analysis of the peptides by LC-MS/MS.

1.6.2 *In vivo* secretome analysis

A method for cell-specific *in vivo* secretome analysis was published for hepatocytes recently[84]. This protocol is based on labeling proteins of interest with biotin using an ER-located biotin ligase TurboID[84]. With this methodology, proteins located in the vicinity of TurboID, which are secreted later, are labeled with biotin and can be subsequently enriched and analyzed.

TurboID is a biotin ligase derived from *E. coli* (*BirA R118S*)[85] that catalyzes the binding of adenosine triphosphate (ATP) to biotin with cleavage of two phosphates. The reactive biotin-5'-adenosine monophosphate (AMP) compound can react with primary amines of nearby proteins. As a result, these proteins are biotinylated under the catalytic action of TurboID[86] (Figure 8).

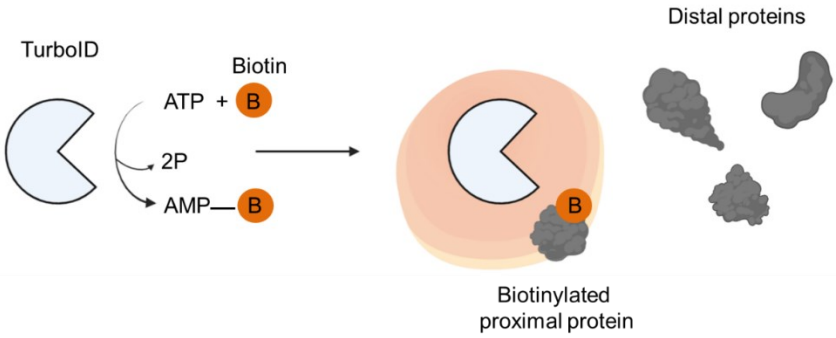

Figure 8: Proximity labeling of secreted proteins using a TurboID biotin ligase (adapted from Cho *et al.*, 2020[87]). In the first step, TurboID catalyzes the binding of adenosine triphosphate (ATP) to biotin with cleavage of two phosphates (2P). Thus, a reactive biotin-5'-adenosine monophosphate (AMP) compound is formed. In the second step, this compound can react with the primary amines of proximate proteins catalyzed by TurboID, leading to protein biotinylation[87].

Biotin labeling of the desired proteins can only be performed when the TurboID is delivered to and expressed in the corresponding tissue, and biotin is added as a substrate. For this purpose, an adeno-associated virus (AAV) vector system can be used, and biotin is added via drinking water[84].

1.7 Aims of the study

CF are key players in remodeling after MI and could be a therapeutic target in treatment of MI to prevent excessive fibrosis[48]. In recent work of our group, the transcriptome of CF from infarcted mouse hearts was investigated by scRNA-seq, showing that infarct-induced aCF expressed various cytokines, chemokines, growth factors, and proteins important for ECM formation[68]. Together, these findings suggested that aCF secrete not only proteins of the ECM but also proteins with paracrine/autocrine activity, which may signal to surrounding cardiac cells. These factors, therefore, might be important in the remodeling process post MI.

The secretome of CF has already been investigated in human, mice and rats *in vitro* under conditions like treatment with TNF-α and TGF-β or exposure to hypoxia and normoxia[88–91]. No secretome study has been reported on CF so far, comparing secreted proteins post MI and control. Additionally, in all reported studies CF were cultivated over a long time period or were passaged, which results in CF activation[92]. Furthermore, serum starvation of CF was regularly used to perform secretome analysis in all reported studies. These procedures are all known to result in changes of the secretome[93]. Therefore, to perform a complete analysis of newly secreted proteins under optimal growth conditions and to minimize factors which lead to changes in secretome, a combination of pSILAC and click-chemistry according to Eichelbaum and Krijgsveld, 2014[78], was adapted for the first time for CF in this thesis. This method has already been performed on macrophages, various cancer cell lines and primary cells[78]. After successful method establishment, CF-secreted proteins were analyzed on different days post MI and compared to secreted proteins from Sham-operated control CF. To minimize the influence of cell culture on secretome analysis, CF were cultured no longer than 60 h after isolation.

So far, not much is known about the composition and dynamics of the secretome of CF in the living heart. Therefore, an additional aim of this study was to establish a technique which permits the study of the CF secretome under *in vivo* conditions. If successful, this should enable the study of the dynamics of protein secretion by CF. For this purpose, a cell-specific *in vivo* secretome analysis of CF in the post-MI heart was adapted according to methods originally described for hepatocytes by Wei *et al.* 2021[84].

For targeting infarct-induced aCF, an adeno associated virus serotype 9 (AAV9) was used in this study due to its known affinity for heart cells[94]. The vector system carried a plasmid containing an ER-localized TurboID sequence, expressed under the control of a *Postn* promoter, as aCF are known to highly express *Postn*[60]. Previous studies have demonstrated that the combination of AAV9 with a *Postn* promoter has a high affinity to aCF[95]. Therefore, the utilization of TurboID under control of the *Postn* promoter enables targeted ER-TurboID expression, serving as a biotin ligase for nearby proteins (Figure 9). In addition to ER-TurboID, tags like V5 were also expressed under the control of the *Postn* promoter to perform Western Blot and immune fluorescence imaging analyses.

The planned experimental workflow is outlined in Figure 9. For *in vivo* secretome analysis, AAV9-POSTN-ER-TurboID was injected intravenously after MI (50 min ischemia/reperfusion), which leads to an activation of CF and expression of *Postn* concomitant with expression of ER-located ER-TurboID. Since there is no substrate for ER-TurboID promoted labeling of newly synthesized proteins from $POSTN^+$ CF, exogenous biotin was subsequently administered via drinking water so the ER-TurboID was able to catalyze the biotin labeling of the proteins *in*

vivo. Thereafter, the biotin-labeled secreted proteins were enriched from the coronary effluent of the isolated perfused heart of the mice and analyzed by MS.

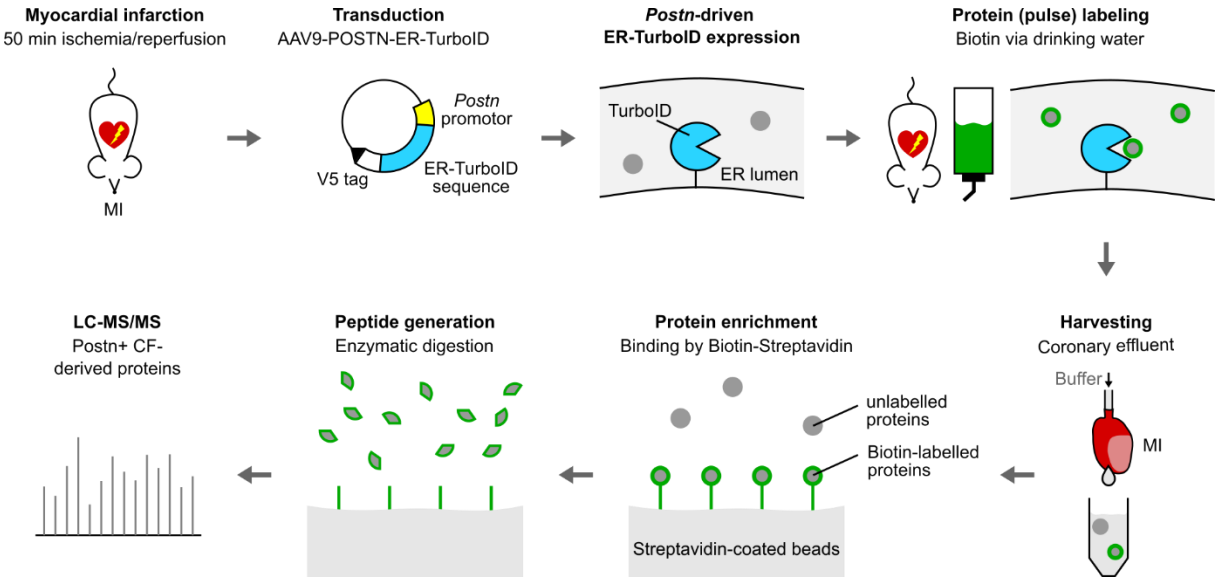

Figure 9: Workflow of *in vivo* secretome analysis for POSTN⁺ CF (according to Wei *et al.*, 2021[84]). An adeno-associated Virus of serotype 9 (AAV9) carrying a vector containing the ER-located biotin ligase ER-TurboID and a V5 tag under control of a *Periostin* (*Postn*) promoter is injected into the tail vein of C57Bl/6 mice one day after MI (50 min ischemia/reperfusion). Due to ischemia, cardiac fibroblasts are activated and express *Postn*, leading to an expression of the ER-TurboID. To label proximate proteins with the help of the ER-TurboID, biotin is applied to mice via drinking water on three consecutive days. After biotin labeling, coronary effluent is collected and biotinylated proteins are enriched using magnetic streptavidin beads. After this procedure, proteins can be analyzed via LC-MS/MS.

The overreaching aim of the present work was to establish and adapt state-of-the-art techniques for the secretome analysis of CF after MI under both *in vitro* and *in vivo* conditions. The results obtained will be integrated into a larger picture of how CF communicate with surrounding cardiac cells and identify factors that may be crucial for the development of cardiac fibrosis and remodeling post MI.

2. Materials

2.1 Devices and equipment

Table 2: Used devices and equipment

Device	Manufacturer	Type Designation
Analytical balance	Ohaus Europe (Greifensee, Switzerland)	PA214
Autoclave	F. & M. Lautenschläger (Köln, Germany)	5169
Centrifuges	Eppendorf (Hamburg, Germany),	5424R
	Beckman Coulter (Brea, USA)	Allegra X-30R
	Hettich Zentrifugen (Tuttlingen, Germany)	ROTANTA 460R
Cryostat	Leica Biosystems (Nussloch, Germany)	Leica CM1520
Data Acquisition Hardware Device	ADInstruments (Spechbach, Germany),	PowerLab/16SP
Electrophoresis power supply	Consort bvba (Turnhout, Belgium)	EV231
Fluorescence microscope	Olympus (Tokyo, Japan)	BX61
Gel electrophoresis system	Thermo Fisher Scientific (Waltham, USA)	Mini Gel Tank
Heating block	Eppendorf (Hamburg, Germany)	Thermomixer compact
Heating circulator bath	Thermo Haake (Karlsruhe, Germany)	DC1-B3
Drying cabinet	Memmert (Büchenbach, Germany)	UN30
Imaging System	Thermo Fisher (Rockford, USA)	iBright™ FL1000
Incubator	Thermo Fisher (Rockford, USA)	Heracell 150i
Langendorff equipment	Physiology workshop, University Düsseldorf	
High-performance liquid chromatography system	Thermo Fisher Scientific (Waltham, USA)	UltiMate™ 3000 Rapid Separation HPLC System
Magnet	BioLegend (San Diego, USA)	Mojosort™ Magnet
Magnetic stirrer	IKA Werke (Staufen, Germany)	RCT basic
Mass spectrometer	Thermo Fisher Scientific (Waltham, USA)	Orbitrap Fusion™ Lumos™ Tribrid™ Mass Spectrometer
	Thermo Fisher Scientific (Waltham, USA)	Q Exactive™ Plus Hybrid Quadrupol-Orbitrap™ Mass Spectrometer
Micro forceps	Aesculap (Tuttlingen, Germany)	MICRO FCPS 20 MM 115 MM
Micro scissors	Aesculap (Tuttlingen, Germany)	Vannas Scissors, straight, 85 mm

Device	Manufacturer	Type Designation
	Aesculap (Tuttlingen, Germany)	Vannas Scissors, curved, 85mm
	Aesculap (Tuttlingen, Germany)	Vannas Scissors, curved, 160 mm
Microplate Reader	BMG Labtech (Ortenberg, Germany)	FLUOstar OPTIMA
Microscope	Leica Biosystems (Nußloch, Germany)	LEICA MZ6
Microscopy scissors	Roth (Karlsruhe, Germany)	Scissors stem, round
Neubauer counting chamber	neoLab Migge GmbH (Heidelberg, Germany)	Neubauer counting chamber 0,100 mm depth, 0,0025 mm^2
Peristaltic pumps	GILSON Company Inc. (Ohio USA)	MINIPULS3
pH meter	Knick (Berlin, Germany),	766 Calimatic
Pipettes	Eppendorf (Hamburg, Germany)	Research
Plate shaker	IKA Werke (Staufen, Germany)	MTS 2/4
Rotational-vacuum-concentrator	Christ (Osterode am Harz, Germany)	RVC 2-19 CD plus
Rotator	Miltenyi Biotec (Bergisch Gladbach, Germany)	MACSmix™ Tube Rotator
Scanner	Biostep (Burkhardtsdorf, Germany)	ViewPix 700
Sterile bench	Labogene (Lynge, Denmark)	Scanlaf Mars Pro Cytosafe Class 2
Small animal blood flow meter	Transonic Systems Inc. (New York, USA)	T160
TissueLyser LT	Qiagen (Hilden, Germany)	85600
Transblot system	Thermo Fisher (Rockford, USA)	iBlot™ 2 Dry Blotting System
Tweezers	Roth (Karlsruhe, Germany)	Tweezers straight pointed, 130 mm
Ultrasonic bath	Bandelin (Berlin, Germany)	Sonorex RK 100 H
Vacuum manifold	Waters (Milford, USA)	20-position cartridge manifold
Vacuum pump	KNF Group (Sursee, Switzerland)	Laboport® N86 KN.18
Vortexer	neoLab (Heidelberg, Germany)	Vortex-Genie 2

2.2 Expendable materials

Table 3: Used expendable materials.

Material	Manufacturer
10 cm Cell culture dishes	Corning (New York, USA)
Pierce™ 3kDa protein concentrator, 5-20 ml	Thermo Fisher Scientific (Waltham, USA)
Pierce™10kDa protein concentrator, 5-20 ml	Thermo Fisher Scientific (Waltham, USA)
0,5 ml Insulin syringes	Becton Dickinson (New Jersey, USA)
20 ml Syringes	Braun (Melsungen, Germany)
18 Gx1 1/1 1.2x40 mm Cannulas	Braun (Melsungen, Germany)
6-Well plates suspension	Greiner Bio One (Kremsmunster, Austria)
6-Well plates TC	Greiner Bio One (Kremsmunster, Austria)
96-Well plates TC	Greiner Bio One (Kremsmunster, Austria)
Cell-culture flask 25 cm^2, 75 cm^2, 175 cm^2	Greiner Bio One (Kremsmunster, Austria)
Syringe filter 0.22 µm	Becton Dickinson (Heidelberg, Germany)
Cell scraper	Roth (Karlsruhe, Germany)
Centrifuge tubes (50 ml; 15 ml)	Greiner Bio One (Kremsmunster, Austria)
Chromatography columns 1.2 ml bed volume	Bio-Rad Laboratories (Hercules, USA)
Coverslips 18x18 mm	Roth (Karlsruhe, Germany)
Easystrainer 100 µm	Greiner Bio One (Kremsmunster, Austria)
Easystrainer 30 µm	Greiner Bio One (Kremsmunster, Austria)
iBlot™ Transfer Stack, PVDF mini	Thermo Fisher Scientific (Waltham, USA)
ImmEdge® Hydrophobic Barrier PAP Pen	BIOZOL Diagnostica Vertrieb GmbH (Eching, Germany)
Low retention filter tips	Greiner Bio One (Kremsmunster, Austria)
Microscope slides 76 mmx 26 mm x 1 mm	Engelbrecht Medizin und Labortechnik GmbH (Edermünde, Germany)
Mini Bio-Spin® Chromatography 1.2 ml	Bio-Rad Laboratories (Hercules, USA)
Mr. Frosty™ freezing container	Thermo Fisher Scientific (Waltham, USA)
NuPAGE™ 4-12% Bis-Tris 1.0-1.5 mm Mini Protein Gels	Thermo Fisher Scientific (Waltham, USA)
Reaction tube low retention 2 ml, 1.5 ml	Eppendorf (Hamburg, Germany)
Roundbottom tubes	Becton Dickinson (New Jersey, USA)
Scalpel No. 10	Feather Safety Razor Co. (Osaka, Japan)
Stainless Steel Beads, 5 mm	Qiagen (Hilden, Germany)
Stripets (2 ml, 5 ml, 10 ml, 25 ml, 50 ml)	Greiner Bio One (Kremsmunster, Austria)
tC18 Cartridges Sep-Pak® Vac 1cc (50 mg)	Waters (Milford, USA)

2.3 Chemicals

Table 4: Chemicals used in the experiments

Chemical	Manufacturer
[4,4,5,5-D4] L-lysine	Cambridge Isotope Laboratories, Inc. (Tewksbury, USA)
[$^{13}C_6$] L-arginine	Cambridge Isotope Laboratories, Inc. (Tewksbury, USA)
[$^{13}C_6$, $^{15}N_4$] L-arginine	Cambridge Isotope Laboratories, Inc. (Tewksbury, USA)
[$^{13}C_6$, $^{15}N_2$] L-lysine	Cambridge Isotope Laboratories, Inc. (Tewksbury, USA)
4X Bolt™ LDS sample buffer	Thermo Fisher Scientific (Waltham, USA)
10X Bolt™ sample reducing agent	Thermo Fisher Scientific (Waltham, USA)
Acetic acid MS grade	Roth (Karlsruhe, Germany)
Acetonitrile MS grade	Roth (Karlsruhe, Germany)
Ammonium hydrogen carbonate (Na_2HCO_3)	Honeywell International Inc. (Morristown, USA)
Biotin MS grade	Sigma-Aldrich (St. Louis, USA)
Bolt™ MES SDS Running Buffer (20x)	Thermo Fisher Scientific (Waltham, USA)
Bovine Serum Albumin (BSA)	Thermo Fisher Scientific (Waltham, USA)
3-[(3-Cholamidopropyl) dimethylammonium]-1-propanesulfonate hydrate (CHAPS)	Sigma-Aldrich (St. Louis, USA)
Chloroform	Roth (Karlsruhe, Germany)
Calciumchloride ($CaCl_2$)	Roth (Karlsruhe, Germany)
Click-iT™ L-azidohomoalanine	Thermo Fisher Scientific (Waltham, USA)
Collagenase Type II	Worthington Biochemical Corporation (Lakewood, USA)
Coomassie Brilliant Blue	Sigma-Aldrich (St. Louis, USA)
Deionized water 18 MΩ MS grade	BMFZ, University Düsseldorf
Dimethyl sulfoxide (DMSO)	Sigma-Aldrich (St. Louis, USA)
Dithiothreitol (DTT)	Merck (Darmstadt, Germany)
Dynabeads™ MyOne™ Streptavidin T1	Thermo Fisher Scientific (Waltham, USA)
Ethanol	Thermo Fisher Scientific (Waltham, USA)
Ethylenediaminetetraacetic acid EDTA (0.5 M pH 8)	Thermo Fisher Scientific (Waltham, USA)
Ethylene glycol-bis (β-aminoethyl ether)-N,N,N',N'-tetra acetic acid (EGTA)	Thermo Fisher Scientific (Waltham, USA)
Fetal Bovine Serum, dialyzed (FBS)	Thermo Fisher Scientific (Waltham, USA)
Formaldehyde 37%	Merck (Darmstadt, Germany)
Glucose	Merck (Darmstadt, Germany)
Glutamax™	Thermo Fisher Scientific (Waltham, USA)
Halt™ Protease-Inhibitor-Cocktail (100x)	Thermo Fisher Scientific (Waltham, USA)
Hydrochloric acid 35%	Thermo Fisher Scientific (Waltham, USA)
Iodoacetamide	Sigma-Aldrich (St. Louis, USA)
Isoflurane	Actavis GmbH (Wien, Austria)
Isopropanol MS grade	Roth (Karlsruhe, Germany)
Ketaset® 100 mg/ml (Ketamine hydrochloride)	Zoetis (Parsippany-Troy Hills Township, USA)
KP-CryoCompund	ImmunoLogic (Duiven, Netherlands)
L-arginine	Merck (Darmstadt, Germany)
L-lysine	Merck (Darmstadt, Germany)
L-methionine	Merck (Darmstadt, Germany)
Magnesium chloride ($MgCl_2$)	Merck (Darmstadt, Germany)

Chemical	Manufacturer
Magnesium sulfate heptahydrate ($MgSO_4$ x $7H_2O$)	Merck (Darmstadt, Germany)
Methanol	Roth (Karlsruhe, Germany)
Monopotassium phosphate (KH_2PO_4)	Merck (Darmstadt, Germany)
Monosodium phosphate (NaH_2PO_4)	Roth (Karlsruhe, Germany)
Nail polish	Essie (New York, USA)
Normal Goat Serum (NGS)	Thermo Fisher Scientific (Waltham, USA)
Nonfat-Dried Milk bovine	Sigma-Aldrich (St. Louis, USA)
Novex™ AP Chemiluminescent Substrate	Thermo Fisher Scientific (Waltham, USA)
Novex™ Sharp Pre-stained Protein Standard	Thermo Fisher Scientific (Waltham, USA)
NP-40	Merck (Darmstadt, Germany)
NuPAGE™ LDS-Sample buffer (4x)	Thermo Fisher Scientific (Waltham, USA)
Paraformaldehyde (PFA) 4%	Labochem international
Penicillin/Streptomycin/ Glutamine (10.000 U/ml)	Biochrom GmbH (Berlin, Germany)
Potassium chloride (KCl)	Roth (Karlsruhe, Germany)
Pierce™ Streptavidin Protein, Alkaline Phosphatase (AP) Conjugate	Thermo Fisher Scientific (Waltham, USA)
ProLong™ Gold antifade reagent with DAPI	Thermo Fisher Scientific (Waltham, USA)
Recombinant mouse TGF-beta1 protein	R&D Systems (Minneapolis, USA)
Restore™ Western Blot Stripping Buffer	Thermo Fisher Scientific (Waltham, USA)
Rompun 2% (Xylazine hydrochloride)	Bayer (Leverkusen, Germany)
Saponin	Merck (Darmstadt, Germany)
Silver nitrate ($AgNO_3$)	Merck (Darmstadt, Germany)
Sodium acetate (CH_3COONa)	Merck (Darmstadt, Germany)
Sodium bicarbonate ($NaHCO_3$)	Roth (Karlsruhe, Germany)
Sodium carbonate (Na_2CO_3)	Roth (Karlsruhe, Germany)
Sodium chloride (NaCl)	Roth (Karlsruhe, Germany)
Sodium dodecyl sulfate (SDS) solution 20%	Bio-Rad Laboratories (Hercules, USA)
Sodium pyruvate (100 mM)	Thermo Fisher Scientific (Waltham, USA)
Sodium thiosulfate ($Na_2S_2O_3$)	Honeywell International Inc. (Morristown, USA)
Streptavidin Nanobeads, Mojosort™	BioLegend (San Diego, USA)
SuperSignal™ West Femto Maximum Sensitivity Substrate	Thermo Fisher Scientific (Waltham, USA)
Thiourea	Sigma-Aldrich (St. Louis, USA)
Trifluoracetic acid (TFA)	Merck (Darmstadt, Germany)
Tris-(hydroxymethyl)-aminomethane (Trizma® base)	Sigma-Aldrich (St. Louis, USA)
Tris-(hydroxymethyl)-aminomethane hydrochloride (Tris-HCl) 1M pH 8	Serva Electrophoresis GmbH (Heidelberg, Germany)
Trypan blue stain (0.4%)	Thermo Fisher Scientific (Waltham, USA)
Trypsin sequencing grade modified	Promega (Fitchburg, USA)
Trypsin-EDTA (0.05%)	Thermo Fisher Scientific (Waltham, USA)
Tween® 20 (Polyethylene glycol sorbitan monolaurate)	Sigma-Aldrich (St. Louis, USA)
Urea MS grade	Merck (Darmstadt, Germany)

2.4 Media

Table 5: Used media for cell culture experiments.

Media	Components	Manufacturer
DMEM w/o FBS	DMEM high Glucose 1% Penicillin/ Streptomycin 1% Glutamax	PAN Biotech GmbH (Aidenbach, Germany)
DMEM	DMEM high Glucose 10% dialyzed FBS 1% Penicillin/ Streptomycin 1% Glutamax	PAN Biotech GmbH (Aidenbach, Germany)
Depletion DMEM	DMEM high Glucose w/o Methionine, arginine, lysine 1% Penicilin/ Streptomycin 1% Glutamax	PAN Biotech GmbH (Aidenbach, Germany)
Depletion DMEM	DMEM high Glucose w/o Methionine, arginine, lysine 10% dialyzed FBS 1% Penicillin/ Streptomycin 1% Glutamax	PAN Biotech GmbH (Aidenbach, Germany)
Labeling DMEM heavy w/o FBS	DMEM high Glucose w/o Methionine, arginine, lysine 1% Penicillin/ Streptomycin 1% Glutamax 0.1 mM L-azidohomoalanine 84 µg/ml $^{13}C_6{}^{15}N_4$ L-arginine 146 µg/ml $^{13}C_6{}^{15}N_2$ L-lysine	PAN Biotech GmbH (Aidenbach, Germany)
Labeling DMEM heavy	DMEM high Glucose w/o Methionine, arginine, lysine 10% dialyzed FBS 1% Penicillin/ Streptomycin 1% Glutamax 0.1 mM L-azidohomoalanine 84 µg/ml $^{13}C_6{}^{15}N_4$ L-arginine 146 µg/ml $^{13}C_6{}^{15}N_2$ L-lysine	PAN Biotech GmbH (Aidenbach, Germany)
Labeling Medium intermediate w/o FBS	DMEM high Glucose w/o Methionine, arginine, lysine 1% Penicillin/ Streptomycin 1% Glutamax 0.1 mM L-azidohomoalanine 84 µg/ml $^{13}C_6$ L-arginine 146 µg/ml [4,4,5,5- D4] L-lysine	PAN Biotech GmbH (Aidenbach, Germany)
Labeling DMEM intermediate	DMEM high Glucose w/o Methionine, arginine, lysine 10% dialyzed FBS 1% Penicillin/ Streptomycin 1% Glutamax 0.1 mM L-azidohomoalanine 84 µg/ml $^{13}C_6$ L-arginine 146 µg/ml [4,4,5,5- D4] L-lysine	PAN Biotech GmbH (Aidenbach, Germany)

2.5 Solutions

Table 6: Solutions used for experiments.

Solutions	Components
L-azidohomoalanine 500 mM	L-azidohomoalanine DMSO
$^{13}C_6$ L-arginine 84 µg/ml	$^{13}C_6$ L-arginine Deionized H_2O
[4,4,5,5- D4] L-lysine 146 µg/ml	[4,4,5,5- D4] L-lysine Deionized H_2O
$^{13}C_6{}^{15}N_4$ L-arginine 84 µg/ml	$^{13}C_6{}^{15}N_4$ L-arginine Deionized H_2O
$^{13}C_6{}^{15}N_2$ L-lysine 146 µg/ml	$^{13}C_6{}^{15}N_2$ L-lysine Deionized H_2O
Acetic acid 0.5%	Acetic acid Deionized H_2O
Acetonitrile 50%+ 0.5% Acetic acid	Acetonitrile Acetic acid Deionized H_2O
Acetonitrile 20%	Acetonitrile Deionized H_2O
Biotin 25 mM	Biotin Deionized H_2O
Dithiothreitol 1 M	Dithiothreitol Deionized H_2O
Isopropanol 20%	Isopropanol Deionized H_2O
Iodoacetamide 40 mM	Iodoacetamide SDS washing buffer
Trifluoracetic acid 10%	Trifluoracetic acid Deionized H_2O
Trifluoracetic acid 0.1%	Trifluoracetic acid Deionized H_2O

2.6 Buffer

Table 7: Buffers used for experiments.

Buffer	Components
Alkylation buffer	55 mM Iodoacetamide 50 mM NH_4HCO_3 Deionized H_2O
Band washing buffer	10 mM NH_4HCO_3 50% Acetonitrile Deionized H_2O
Blocking buffer	TBS 5% Nonfat-dried milk
Cell lysis buffer	50 mM Tris-HCl 1% SDS 1X Protease Inhibitor Deionized H_2O pH 8

Buffer	Components
Cell sorting buffer	PBS 0.5% BSA 5 mM EDTA
CF cell lysis buffer	30 mM Tris-HCl 2 M Thiourea 7 M Urea 4% CHAPS (w/v) in water Deionized H_2O pH 8.5
Coomassie staining solution	40% Ethanol 10% Acetic acid 250 mg/L Coomassie Brilliant Blue Deionized H_2O
Destaining solution	50% Ethanol 10% Acetic acid Deionized H_2O
Developing buffer	236 mM Sodium carbonate Deionized H_{2O}
Digestion buffer	100 mM Tris-HCl pH 8 10% Acetonitrile 2mM Ca_2Cl Deionized H_2O
Dilution buffer	TBST 1% Nonfat-dried milk
Extraction buffer	0.1% TFA Acetonitrile (1:1)
Fixation buffer	50% Ethanol 10% Acetic acid Deionized H_2O
Gel washing buffer	236 mM Sodium carbonate Deionized H_2O
Immunofluorescence blocking buffer	PBS 0.2% Saponin 5% NGS 1:50 IgG anti mouse
Lysis buffer	50 mM Tris HCl 150 mM NaCl 0.4% SDS 1% NP-40 1 mM EGTA 1.5 mM MgCl2 Protease inhibitor (1 µl/ml) Deionized H_2O pH 7.4

Buffer	Components
Krebs-Henseleit buffer	6.78 g/l NaCl 0.345 g/l KCl 0.27 g/l $MgSO_4$ x $7H_2O$ 2.09 g/l $NaHCO_3$ 0.37 g/l $CaCl_2$ 0.165 g/l KH_2PO_4 1.495 g/l Glucose 20 ml/l Sodium pyruvate (100 mM) Deionized H_2O
Phosphate buffered saline (PBS)	137 mM NaCl 2.7 mM KCl 10 mM NaH_2PO_4 1.8 mM KH_2PO_4 Deionized H_2O pH 7.2
RIPA	50 mM Tris-HCl 150 mM NaCl 1% NP-40 0.5% Sodium deoxycholate 0,1% SDS Deionized H_2O pH 8
Reducing buffer	10 mM DTT 50mM NH_4HCO_3 Deionized H_2O
Tris-buffered saline (TBS)	20 mM Tris-HCl 140 mM NaCl Deionized H_2O pH 7.5
Tris-buffered saline + Tween 20 (TBST)	20 mM Tris-HCl 140 mM NaCl 0.1% Tween 20 Deionized H_2O pH 7.5
SDS-PAGE loading buffer	25% of 4X Bolt™ LDS sample buffer 10% of 10X Bolt™ sample reducing agent
SDS-PAGE running buffer	1X Bolt™ MES SDS Running Buffer (20X) Deionized H_2O
SDS washing buffer	100 mM Tris-HCl pH 8 1% SDS 250 mM NaCl 5 mM EDTA Deionized H_2O
Sensitivity buffer	30% Ethanol 500 mM Sodium acetate 8 mM Sodium thiosulfate Deionized H_2O
Staining buffer	6 mM Silver nitrate Deionized H_2O
Stopping buffer	50 mM EDTA Deionized H_2O
8M Urea buffer	100 mM Tris-HCl pH 8 8 M Urea Deionized H_2O

Buffer	Components
Washing buffer	50 mM Tris HCl 2% SDS Deionized H_2O pH 7.5

2.7 Kits

Table 8: Kits that were used.

Kit	Manufacturer
Click-iT™ Biotin Protein Analysis Detection Kit	Thermo Fisher Scientific (Waltham, USA)
Click-iT™ Protein Enrichment Kit	Thermo Fisher Scientific (Waltham, USA)
Cell Counting Kit-8 (CCK-8)	Tebu-bio (Le Perray-en-Yvelines, France)
Novex™ AP Chemiluminescent Substrate	Thermo Fisher Scientific (Waltham, USA)
Pierce™ BCA Protein Assay Kit	Thermo Fisher Scientific (Waltham, USA)

2.8 Antibodies

2.8.1 Primary antibodies

Table 9: Primary antibodies used for Western Blots and immunofluorescent imaging.

Specifity	Clone	Host	Application	Dilution	Manufacturer
Biotin-anti - mouse CD31	MEC13.3	rat	CF isolation	1:10	BioLegend (San Diego, USA)
Anti-V5 tag	2F11F7	mouse	WB/IF	1:5000/ 1:100	Thermo Fisher Scientific (Waltham, USA)
Anti-HA tag	2-2.2.14	mouse	IF	1:100	Thermo Fisher Scientific (Waltham, USA)
Anti-Vimentin	EPR3776	rabbit	IF	1:400	Abcam (Cambridge, UK)
Anti-Postn	polyclonal	rabbit	WB/IF	1:1000/ 1:100	OriGene (Rockville, USA)
Anti-mouse IgG	polyclonal	goat	IF	1:50	R&D Systems
Anti-β-actin	15G5A11/E2	mouse	WB	1:2000	Thermo Fisher Scientific (Waltham, USA)

2.8.2 Secondary antibodies

Table 10: Secondary antibodies used for Western Blots and immunofluorescent imaging.

Specificity	Conjugate	Clone	Host	Application	Dilution	Manufacturer
Anti-mouse IgG	AF800	polyclonal	goat	WB	1:20,000	Thermo Fisher Scientific

Specificity	Conjugate	Clone	Host	Application	Dilution	Manufacturer
						(Waltham, USA)
Anti - mouse IgG	AF 594	polyclonal	goat	IF	1:1000	Thermo Fisher Scientific (Waltham, USA)
Anti-rabbit IgG	AF 488	polyclonal	goat	IF	1:1000	Thermo Fisher Scientific (Waltham, USA)
Anti-rabbit IgG	Horse-radish Peroxidase	polyclonal	goat	WB	1:50,000	Thermo Fisher Scientific (Waltham, USA)
Anti-mouse IgG	Horse-radish Peroxidase	polyclonal	goat	WB	1:50,000	Thermo Fisher Scientific (Waltham, USA)

2.8.3 Fluorochromes

Table 11: Fluorochromes used for Western Blots and immunofluorescent imaging

Fluorochrome	Abbreviation	Excitation [nm]	Emission [nm]
Alexa Fluor 488	AF 488	495	519
Alexa Fluor 594	AF 594	590	617
Alexa Fluor 800	AF 800	787	795

2.9 Cell lines

Table 12: Used cell lines

Cell line	ATCC number	Manufacturer
Normal Human Dermal Fibroblasts (NHDF)	PCS-201-012	PromoCell GmbH (Heidelberg, Germany)

2.10 Vectors

Table 13: Used vectors

Vector
pAAV-POSTN-ER-TurboID

The plasmid was constructed by the research group of Prof. Dr. Patrick Most, University Medical Center Freiburg using *pAAV-TBG-ER-TurboID* purchased from Addgene (#149415) and exchanging the *TBG* promoter for the *Periostin* promoter from Lindsley *et al.*[96].

2.11 Adeno-associated virus

Table 14: Used adeno-associated virus

AAV Type	Name
AAV9	POSTN-ER-TurboID

2.12 Software

Table 15: Used software

Software	Version	Manufacturer
ImageJ/Fiji	1.53s	Rasband, W.S., ImageJ, U. S. National Institutes of Health, (Bethesda, USA)
Inkscape	1.3.2	Freedom Conservancy (New York, USA)
MaxQuant	1.6.17.0 2.1.3.0 2.2.0.0	MaxPlack Institute for Biochemistry (Planegg, Germany)
Office	365	Microsoft (Redmond, USA)
Perseus	1.6.6.0	MaxPlack Institute for Biochemistry (Planegg, Germany)
Prism	9	GraphPad Software Inc (La Jolla, USA)
R	4.2.1	R Foundation Vienna, Austria)
RStudio	2022.07.2	R Foundation Vienna, Austria)
Seurat	3.0	Satija Lab, New York Genome Center (New York, USA)

2.13 Databases

Table 16: Used databases

Species	Entries	Database	Date
Homo sapiens	75777	UP000005640	01/27/2021
Mus musculus	55268	UP000000589	01/12/2023
Mus musculus	55341	UP000000589	01/18/2022

3. Methods

3.1 Laboratory animals and housing conditions

The animals used for the experiments were kept at the Zentrale Einrichtung für Tierforschung und wissenschaftliche Tierschutzaufgaben (ZETT) of the Heinrich Heine University Düsseldorf, where they were provided with standard chow and water *ad libitum*. Animal experiments were conducted in accordance with ethical standards and were approved by the Landesamt für Natur, Umwelt und Verbraucherschutz Nordrhein-Westfalen (LANUV), reference number 81-02.04.2020.A351. The experiments were carried out with 10–12-week-old C57Bl/6J wildtype mice purchased from Janvier (Le Genest Isle, France) and they complied with all relevant animal welfare regulations.

3.2 Induction of MI

Before MI induction, mice were sedated with isoflurane and intubated for artificial ventilation to keep respiratory rate at about 150 breaths per minute. During surgery, a constant supply of 1.5% isoflurane was provided to anesthetize the animals. To sustain body temperature, mice were placed on a hot plate. In addition, an electrocardiogram (ECG) was connected by attaching electrodes to the paws. MI was induced by opening the chest and ligating the left anterior descending coronary artery (LAD) with an 8-0 polypropylene thread for 50 min. Ischemia was confirmed by ST-segment elevation on the ECG. After 50 min of ligation, the polypropylene thread was released to initiate reperfusion. Subsequently, the ST-segment elevation was checked to confirm normalization on the ECG. The chest was closed by suturing and was disinfected. Sham surgeries were performed similarly, but the thread was not knotted. All surgeries were kindly performed by Zhaoping Ding, MD.

3.3 Collection of blood and serum

To obtain blood serum, a final blood sample was collected via the vena cava after mice were heparinized and treated with xylazine and ketamine. The blood was centrifuged for 10 min at 2000 x*g* and 4°C. After this, the serum was carefully extracted and frozen at -80°C.

3.4 Collection of organs

After final blood collection (section 3.3), organs such as the liver, lungs, pancreas, spleen and kidney were removed using scissors, immediately frozen in liquid nitrogen and stored at -80°C.

3.5 Collection of coronary effluent

After the blood was collected (section 3.3), the heart was removed and transferred to ice-cold PBS. Lungs, thymus, esophagus, trachea and adipose tissue were subsequently excised from the heart. Following this, the heart was cannulated via the aorta and retrogradely perfused in a Langendorff apparatus with oxygenated Krebs-Henseleit buffer. The perfusion pressure was maintained at 1 m H_2O. After 3 min of perfusion, aimed at washing out residual blood and to

stabilizing the heart rate, coronary effluent was collected for 60 min using 50 ml centrifuge tubes kept on ice. After collection, 1X of Halt™ Protease-Inhibitor-Cocktail 100X (Thermo Fisher Scientific (Waltham, USA) was added to prevent protein degradation. Both effluent samples and the heart were snap-frozen in liquid nitrogen and stored at -80°C.

3.6 Isolation of CF

Mice were heparinized and thereafter euthanized by cerebral dislocation. The thorax was opened and the heart was removed and transferred to ice-cold PBS. The lungs, thymus, esophagus, trachea and adipose tissue were excised from the heart. Afterwards the heart was cannulated via the aorta on a Langendorff apparatus. Retrograde perfusion with pre-warmed PBS for 3 min (constant flow of 2 ml/min) at 37°C was performed to wash out the residual blood from the coronaries. After washing, the system was switched to a pre-warmed 1000 U/ml collagenase type II solution (Worthington Biochemical Corporation, Lakewood, USA) for 8 min to digest the tissue. At the same time, the heart was placed in a 5 ml reaction tube filled with collagenase solution and continuously exposed to moderate shear forces (80 *rpm*) to remove epicardial stromal cells. After this procedure, the heart was removed from the canula and atria and aorta were excised. The digested tissue was carefully dissociated with forceps and scalpel and transferred to 5 ml DMEM medium containing 10% FBS and 1% Penicillin/Streptomycin/Glutamine (P/S/G) to stop collagenase activity. After up-and-down pipetting, the cell suspension was filtered through a 100 µl strainer and centrifuged for 1 minute at 55 x*g* and 15°C to pellet CM. The supernatant containing CF was filtered through a 40 µm strainer and centrifuged for 7 min at 300 x*g* and 15°C.

3.7 Cell culture

3.7.1 Cultivation of CF

For further cultivation, the CF-containing supernatant (section 3.6) was depleted of $CD31^+$ cells (endothelial cells) and $CD45^+$ cells (immune cells) via magnetic sorting with Mojosort Nanobeads and a Mojosort Magnet (BioLegend, San Diego, USA). According to the manufactures protocol, cells were resuspended in 200 µl cell sorting buffer and incubated with 20 µl biotin anti-mouse CD31 antibodies (BioLegend, San Diego, USA) for 15 min at 4°C in the dark. After this, cells were incubated with 20 µl MojoSort Mouse CD45 Nanobeads (BioLegend, San Diego, USA) and 20 µl Mojosort Streptavidin Nanobeads (BioLegend, San Diego, USA) for 15 min at 4°C in the dark. Depletion was performed using the Mojosort magnet for 5 min. The $CD31^-/CD45^-$ fraction was collected and centrifuged for 5 min at 300 x*g* and room temperature (RT). Cells were resuspended in pre-warmed DMEM, seeded in culture plates and cultivated at 37°C and 5% CO_2. On the following day, cells were washed four to six times with pre-warmed PBS to remove residual cell debris.

3.7.2 Cultivation of Normal Adult Human Dermal Fibroblasts (NHDF)

NHDF cells are derived from the dermis of adult skin and were obtained from PromoCell GmbH, kindly provided by Prof. Dr. Kai Stühler (Molecular Proteomics Laboratory, BMFZ, Heinrich Heine University Düsseldorf).

At the initiation of cultivation, approximately 5x10^6 NHDF cells were retrieved from liquid nitrogen and thawed in a water bath at 37°C. Cells were resuspended in 10 ml DMEM and centrifuged for 10 min at 200 x*g* and room temperature. The supernatant was discarded and the cell pellet was resuspended in 10 ml medium before being plated in a T75 cell culture flask. Cells were cultivated at 37°C and 5% CO_2. The medium was replaced after 24 h and cells were cultured to 70-90% confluency. Subsequently, cells were split at a 1:3 ratio every 2 to 3 days, depending on their confluency. For this, cells were washed three times with pre-warmed PBS. To detach cells, they were covered with 3 ml trypsin-EDTA (0.05%) and incubated for 5 min at 37°C. Following this, trypsin was neutralized with medium and cells were centrifuged for 5 min at 300 x*g*. Cells were resuspended in medium and plated in culture flasks or plates.

To freeze the cells, a total of 5x10^6 cells were placed in 1 ml of freezing medium (DMEM containing 10% FBS 1% P/S/G with 10% DMSO). Cells were then placed in a Mr. Frosty freezing container (Thermo Fisher Scientific, Waltham, USA) containing isopropanol for 24 h at -80°C and then stored in liquid nitrogen.

3.7.3 Cell number determination

The number of living cells was determined using the Neubauer counting chamber. To this end, cells were diluted at a 1:2 ration with trypan blue. Subsequently, 10 µl of this dilution were placed into the counting chamber and the cells in the four specified squares were counted. Living cells, which were not stained, were differentiated from dead cells, which appeared blue. The number of living cells was calculated using the following formula:

$$\frac{number\ of\ total\ cells}{4} * 10^4\ \frac{1}{ml} * dilution\ factor = number\ of\ cells\ per\ ml$$

3.8 Cell viability assay

For cell viability determination, Cell Counting Kit 8 (Tebu-bio Le Perray-en-Yvelines, France) was used. The solution contains a light-yellow tetrazolium salt that is reduced to an orange formazan by dehydrogenases in living cells. The absorbance can be measured at 450 nm. Due to the proportional correlation between the amount of produced formazan and living cells, the number of living cells can be determined.

To investigate the influence of different depletion and labeling times on the different cells, 5x10^3 cells (in 100 µl) per well were plated in a 96-well plate and incubated 24 h at 37°C and 5% CO_2. After this, cells were washed with PBS and treated with different medium conditions for various time points. After this, 10 µl Cell Counting Kit 8 (CCK-8) dye was added to each well for 3 h and absorbance was measured in the microplate reader FLUOstar OPTIMA (BMG Labtech, Ortenberg, Germany) at 450 nm. As a control, cells were treated with DMEM medium and under these conditions, a live cell count of 100% was assumed. In addition, medium was incubated without cells for background subtraction.

To determine if depleting cells for the amino acids Arg, Lys, and Met has an impact on cell viability, cells were cultivated either with DMEM or Depletion DMEM (D-DMEM) for 30 min, 60 min or 90 min.

To investigate the impact of cultivating cells with FBS, cells were cultured with DMEM and DMEM without FBS (DMEM w/o FBS) for 24 h and 48 h.

To assess if labeling with different amino acids affects cell viability, cells were depleted for 60 min with D-DMEM and washed with PBS. Thereafter, cells were labeled with the different amino acids: 0.1 mM AHA (Thermo Fisher Scientific Waltham, USA), 84 µg/ml $^{13}C_6$ Arg, 146 µg/ml [4,4,5,5- D4] Lys (D4 Lys), 84 µg/ml $^{13}C_6{}^{15}N_4$ Arg, 146 µg/ $^{13}C_6{}^{15}N_2$ Lys (Cambridge Isotope Laboratories, Inc. Tewksbury, USA) and incubated for different time points (6 h, 8 h, 16 h, 24 h, 48 h).

3.9 Lysis of cultured cells

Cells were lysed for 30 min on ice using 0.5 ml cell lysis buffer (1% SDS, 50 mM Tris-HCl, 1X protease inhibitor, pH 8). Thereafter, cells were vortexed and centrifuged for 5 min at 13,000 x*g* and 4°C. The supernatant containing proteins was transferred to a clean 2 ml-tube and protein concentration was measured (see 3.10). Samples were stored at -20°C until further use.

3.10 Protein concentration determination

To determine the total concentration of proteins in a sample, the Pierce BCA Protein Assay (Thermo Fisher Scientific Waltham, USA) was used according to the manufacturer's protocol. This assay is based on the reduction property of peptide bonds in an alkaline environment. In this assay Cu^{2+} is reduced to Cu^{1+} and the amount of reduced copper is proportional to the total amount of proteins in the solution. After the initial reaction, the bicinchoninic acid (BCA) reagent is building a purple complex with Cu^{1+}. The absorption can be detected at a wavelength of 562 nm. To determine concentration of the samples, the following dilutions of the standard solution were prepared: 0 µg/ml, 25 µg/ml, 125 µg/ml, 250 µg/ml, 500 µg/ml, 750 µg/ml, 1000 µg/ml, 1500 µg/ml, and 2000 µg/ml. The samples were applied in a dilution of 1:2, 1:10, and 1:20. All samples and standards were measured in duplicates using microplate reader FLUOstar OPTIMA (BMG Labtech, Ortenberg, Germany).

3.11 Bis(2-hydroxyethyl)iminotris(hydroxymethyl)methan) gels (Bis-Tris gels)

For later analyses, protein samples were separated by Bis-Tris polyacrylamide gels. To this end, NuPAGE 4-12% Bis-Tris 1.0-1.5 mm Mini Protein Gels (Thermo Fisher Scientific, Waltham, USA) were positioned in the Mini Gel Tank Gel electrophoresis system (Thermo Fisher Scientific, Waltham, USA) and SDS-PAGE running buffer was added. Samples containing 20 µg protein (for silver staining 1/10 of sample) were prepared in SDS-PAGE loading buffer and heated for 10 min at 70°C in a thermomixer. Subsequently, 3 µl of Novex Sharp Pre-stained protein standard (Thermo Fisher Scientific, Waltham, USA) and the samples were applied to the gels. The device was connected to the electrophoresis power supply (Consort bvba, Turnhout, Belgium) and the electrophoresis was conducted at 200 V for 25 min.

3.11.1 Silver staining

For silver staining, the gel was fixed for 15 min in 15 ml fixation buffer (50% ethanol, 10% acetic acid) on a shaker, followed by 15 min incubation with 15 ml of sensitivity buffer (30% ethanol, 500 mM sodium acetate, 8 mM sodium thiosulfate). Subsequently, the gel was washed 3 times for 5 min with deionized H_2O. After that, the gel was stained for 20 min using 15 ml staining buffer (6 mM silver nitrate) and washed with deionized H_2O 3 times for 5 min. Following this, the gel was washed for 1 min in gel washing buffer (236 mM sodium carbonate) to remove the remaining silver followed by gel development with developing buffer (236 mM sodium carbonate, 0.01% formaldehyde) for 1-7 min. The developing reaction was stopped using a 50 mM EDTA solution (stopping buffer). Again, the gel was washed 3 times with deionized H_2O for 10 min each. Afterwards, the gel was scanned using ViewPix 700 (Biostep, Burkhardtsdorf, Germany).

3.12 Western Blot

For transferring the electrophoresis gels to a membrane, iBlot Transfer Stack, PVDF mini was used according to the manufacturer's protocol and placed in the iBlot 2 Dry Blotting System (Thermo Fisher, Rockford, USA). Gels were placed onto the membrane bubbles-free, a pre-soaked filter paper was added and an absorbent pad was placed on top. The membrane was blotted at 20 V for 7 min.

To prevent unspecific binding, the membrane was blocked for 60 min with 15 ml blocking buffer (TBS, 5% nonfat-dried milk) at room temperature on a plate shaker. The membrane was washed three times with TBST for 5 min and incubated with the respective primary antibody at desired concentration for 60 min in 15 ml dilution buffer (TBST, 1% nonfat-dried milk). After incubation, the membrane was washed three times with 15 ml TBST. The membrane was incubated with the secondary antibody at desired concentration for 60 min in 15 ml dilution buffer (in the dark) and washed three times with 15 ml TBST afterwards for 5 min. After incubating the membrane with goat anti-rabbit or goat anti-mouse IgG peroxidase conjugate, it was washed two times with TBST and once with H_2O. For detection, the membrane was incubated with SuperSignal West Femto Maximum Sensitivity Substrate (Thermo Fisher Scientific, Waltham, USA) for 5 min.

For biotin detection, membranes were first incubated with Pierce Streptavidin-Alkaline Phosphatase Conjugate (Thermo Fisher Scientific, Waltham, USA) in a 1:2000 dilution in 15 ml dilution buffer for 60 min on a plate shaker. The membrane was washed two times with TBST and once with H_2O. For detection, the membrane was incubated with Novex AP Chemiluminescent Substrate (Thermo Fisher Scientific, Waltham, USA) for 5 min.

Images were captured using iBright FL1000 Imaging System (Thermo Fisher Scientific, Waltham, USA). Blue bands were detected using a filter range of 675-720 nm, red bands were detected using a filter range of 565-615 nm. Green bands and signal of AF800 coupled secondary antibodies were detected using a filter range of 810-850 nm. The signal of alkaline phosphatase- and peroxidase-coupled secondary antibodies were detected using chemiluminescence.

3.13 Histology

To prepare histological cryo-sections of heart tissue, mouse hearts were explanted and washed in ice-cold PBS. Afterwards, hearts were embedded in KP-CryoCompound and frozen at -40°C in isopropanol. Hearts were stored at -80°C. Cryo-sections were prepared using a cryostat, with a thickness of 10 µm and placed on microscope slides. Sections were stored at -20°C until use.

3.14 Immunofluorescence imaging

To prepare immunofluorescence staining, cryo-sections were first outlined with a hydrophobic barrier pen and then fixed with 4% PFA for 15 min. For permeabilization, sections were washed three times with PBS and 0.2% saponin for 5 min on a plate shaker. To prevent unspecific binding, sections were blocked with 150 µl immunofluorescence blocking buffer (PBS, 0.2% saponin, 5% NGS, 1:50 IgG anti mouse) afterwards for 60 min at room temperature. Then samples were incubated with the respective primary antibody at desired concentration (section 2.8.1) over night at 4°C. On the following day, sections were washed three times with PBS and 0.2% saponin on a plate shaker to remove unbound antibody residues. Afterwards, samples were incubated with the secondary antibody at desired concentration (section 2.8.2) for 1.5 h at room temperature in the dark and afterwards washed two times with PBS and 0.2% saponin and one time with PBS for 5 min on a plate shaker. Subsequently the sections were embedded with ProLong Gold Antifade Reagent with DAPI to stain the nuclei. Samples were covered with a cover slip, outlined with nail polish and dried in the dark at 37°C. Samples were stored at -20°C. Fluorescence images were taken with the fluorescence microscope BX61 (Olympus, Tokyo, Japan) using different objectives (4x, 10x) and processed with ImageJ/Fiji 1.53s software.

3.15 Secretome analysis of cultured fibroblasts

To perform mass spectrometry analysis of newly synthesized proteins under serum-containing conditions, a combination of pulsed SILAC labeling and click-chemistry was used. Initially, fibroblasts were depleted of Arg, Lys, and Met for 60 min and afterwards labeled with medium containing heavy/intermediate Arg and Lys isotopes along with AHA (section 1.6.1, Figure 7). This approach allows the measurement of secreted proteins from differently treated cells in a single analysis. After sufficient labeling, supernatants containing secreted proteins were collected and pooled. AHA-labeled proteins were then bound to an agarose resin via click-chemistry reaction (section 1.6.1, Figure 6). Non-bound proteins were removed through stringent washing and the bound proteins were digested to elute the peptides of interest. Subsequently, mass spectrometry analysis of the peptides was conducted using Liquid Chromatography Tandem Mass Spectrometry (LC-MS/MS).

3.15.1 Pulsed SILAC labeling of secreted proteins

NHDF cells were cultured as previously described (section 3.7.2). A total of $1x10^6$ cells were plated on a 10 cm^2 culture plate in 8 ml DMEM medium and incubated for 24 h at 37°C and 5% CO_2. CF were isolated as described before (section 3.6) and cultured in a 10 cm^2 culture

plate in 8 ml DMEM. On the following day, cells were washed four to six times with pre-warmed PBS to remove residual cell debris and then incubated for 24 h at 37°C and 5%CO_2.

For depletion of Arg, Lys, and Met, the medium was removed and cells were washed four times with pre-warmed PBS. Cells were incubated with 4 ml of D-DMEM for 60 min at 37°C and 5% CO_2. Medium was removed and cells were washed four times with pre-warmed PBS. Cells were labeled either with 4 ml of intermediate labeling DMEM (D-DMEM + 0.1 mM AHA, 84 µg/ml $^{13}C_6$ Arg and 146 µg/ml D4 Lys) or heavy labeling DMEM (D-DMEM + 0.1 mM AHA, 84 µg/ml $^{13}C_6{}^{15}N_4$ Arg and 146 µg/ml $^{13}C_6{}^{15}N_2$ Lys) for 8 h. Throughout this labeling period, the amino acid isotopes, as well as the AHA, were incorporated into the newly synthesized proteins by protein biosynthesis. The medium volume was reduced to 4 ml to increase the ratio of labeled proteins to FBS contaminants. After labeling, the medium was collected and centrifuged for 5 min at 1000 x*g* and 4°C to pellet undesired cells and debris. The supernatant was transferred to a fresh 15 ml centrifuge tube supplemented with 1X Halt™ Protease-Inhibitor-Cocktail (Thermo Fisher Scientific, Waltham, USA) and stored at -80°C. Cells were washed four times with ice-cold PBS. Subsequently, 1.5 ml PBS was added, cells were scraped off the dish and transferred into a 2 ml-tube. Cells were centrifuged for 5 min at 800 x*g* and 4°C. Afterwards, the supernatant was discarded and cell pellets were stored at -80°C. Cells can be used to check labeling efficiency or analyze intracellular proteins.

For protein enrichment, the medium containing labeled newly synthesized proteins was thawed and concentrated in Pierce 3 kDa protein concentrators (Thermo Fisher Scientific, Waltham, USA) until a volume of 250 µl was reached. Samples were kept on ice.

3.15.2 Click-chemistry for protein enrichment

For enrichment of newly synthesized proteins, Click-iT Protein Enrichment Kit (Thermo Fisher Scientific, Waltham, USA) was used according to the protocol of Eichelbaum and Krijgsveld et. al[78]. A volume of 250 µl urea buffer provided in the kit was added to the samples. For each sample, 100 µl of the agarose resin (provided) were washed with 900 µl H_2O for 5 min at 1000 x*g* and supernatant was discarded. After this, agarose resin was added to the samples. Then 10 µl of dissolved Reaction Additive 2 (Component F), 10 µl 10 mM Copper (II) sulfate (Component E) and 63 µl Reaction Additive 1 (Component D) were added and the samples were vortexed. For clicking the newly synthesized proteins onto the agarose resin, samples were rotated overnight at 20 *rpm* and room temperature using the MACSmix Tube Rotator (Miltenyi Biotec, Bergisch Gladbach, Germany). On the next day, samples were centrifuged for 1 min at 1000 x*g* and supernatant was discarded. A volume of 900 µl H_2O was added to the resin and samples were vortexed. Afterwards, samples were centrifuged for 1 min at 1000 x*g* and supernatant was discarded. This step was repeated four times in contrast to the protocol of Eichelbaum and Krijgsveld, 2014[78]. The resin was resuspended in 500 µl of pre-warmed SDS washing buffer (100 mM Tris-HCl pH 8, 1% SDS, 250 mM NaCl, 5 mM EDTA) and 5 µl 1M Dithiothreitol (DTT), vortexed and heated for 15 min at 70°C in a heating block. Afterwards, the samples were cooled for 15 min at room temperature and centrifuged for 5 min at 1000 x*g*. Supernatant was discarded and the resin was resuspended in 500 µl of a freshly prepared 40 mM iodoacetamide (IAA) solution. Samples were vortexed and shaken in the dark for 30 min at 500 *rpm*.

For gravity flow washing of the resin, chromatography columns (Bio-Rad Laboratories, Hercules, USA) were put on an 18 Gx1 1/1 1,2x40 mm Cannula (Braun, Melsungen, Germany). This cannula was pierced through the lid of a 50 ml centrifuge tube, which was placed on top of that tube. Samples were transferred to the column and washed with 20 ml of SDS washing buffer. After that, resin was washed with 20 ml of 8 M urea buffer (100 mM Tris-HCl pH 8, 8 M Urea), 20 ml of 20% isopropanol and 20 ml of 20% acetonitrile according to Eichelbaum and Krijgsveld, 2014[78].

To improve protein enrichment, the washing steps were modified. The resin was transferred to a Mini Bio-Spin Chromatography column, which was placed in a 2 ml reaction tube and washed ten times with 0.8 µl of SDS washing buffer by centrifuging for 30 sec at 1000 *xg*. After that, resin was washed 20 times with 0.8 µl 8 M urea buffer, 20 times with 0.8 µl isopropanol and 20 times with 0.8 µl of acetonitrile.

Following that, the column was sealed with a cap and 500 µl digestion buffer (100 mM Tris-HCl pH 8, 10% Acetonitrile, 2 mM Ca_2Cl) was added to the resin. The samples were transferred into a clean 2 ml-tube. Again 500 µl digestion buffer was added to the column and transferred into the 2 ml-tube. The resin was pelleted via 5 min of centrifugation at 1000 x*g* and supernatant was discarded (approximately 200 µl were left in the tube). For digestion, 0.5 µg trypsin was added, sample were vortexed and shaken overnight at 37°C. On the next day, samples were centrifuged for 5 min at 1000 x*g* to pellet the resin and the supernatant containing the peptides was transferred into a clean 2 ml-tube. Resin was resuspended in 500 µl H_2O and again centrifuged 5 min at 1000 x*g*. The supernatant was added to the 2 ml-tube and filled up with water to a final volume of 1 ml to dilute the acetonitrile to an appropriate dilution of 2%. After that, samples were acidified with 20 µl of 10% trifluoracetic acid (TFA).

For the desalting of proteins, Sep-Pak Cartridges (Vac 1cc (50 mg) tC18) were placed in a 20-position cartridge manifold (Waters, Milford, USA) and connected to a vacuum pump. Cartridges were washed and conditioned with 900 µl acetonitrile then washed with 300 µl of 50% acetonitrile and 0,5% acetic acid. Following this, cartridges were equilibrated with 900 µl 0.1% TFA and samples containing the peptides were load onto the cartridges. Peptides were desalted with 900 µl 0.1% TFA, washed with 900 µl 0.5% acetic acid and eluted with 300 µl 50% acetonitrile and 0.5% acetic acid into a clean 2 ml-tube. Afterwards, samples were dried using a rotational-vacuum-concentrator (Christ, Osterode am Harz, Germany) and stored at -80°C until further use.

3.15.3 Click-chemistry determination

To verify the suitability of the click-chemistry mechanism for fibroblasts, Click-iT Biotin Protein Analysis Detection Kit (Thermo Fisher Scientific, Waltham, USA) was used according to the manufacturer's protocol. Therefore, cells were incubated as described before (section 3.7.1), depleted of Arg, Lys, and Met for 60 min and after this labeled with heavy Arg, Lys, and AHA for 24 h. Then cells were washed four times with PBS and lysed 30 min on ice using 0.5 ml cell lysis buffer (1 % SDS, 50 mM Tris-HCl, 1X protease inhibitor, pH 8). The lysate was vortexed and centrifuged for 5 min at 13,000 x*g* and 4°C and the supernatant, containing proteins, was transferred to a clean 2 ml-tube. Protein concentration was measured (see 3.9) and samples were stored at -20°C until further use.

For click reaction, 200 µg of the sample, in a maximum volume of 50 µl, were used and 100 µl of 2X Click-iT reaction buffer (provided), which contains a biotin alkaline detection reagent, was added. Water was added to reach a total volume of 160 µl and the samples were vortexed. After that, 10 µl $CuSO_4$ (component C) was added and samples were vortexed again. Subsequently, 10 µl Click-iT™ reaction buffer additive 1 (component D) was added, samples were vortexed and incubated for 3 min, followed by adding 20 µl Click-iT reaction buffer additive 2 (component E). Samples were vortexed and rotated over end in the dark for 20 min at 20 *rpm* using MACSmix Tube Rotator to click the azide bearing peptides to the biotin alkyne.

For Western Blot analysis, samples were mixed with 600 µl methanol, followed by 150 µl of chloroform and 400 µl water and vortexed. After that, samples were centrifuged for 5 min at 13,000 x*g* and the upper aqueous phase (bright orange) was discarded. A volume of 450 µl methanol was added and samples were vortexed again, followed by centrifugation to pellet the proteins. The supernatant was discarded and the step was repeated. After that, protein pellets were air-dried and stored at -20°C until use.

As azide containing peptides were clicked to a biotin alkyne, they can be detected via Western Blot (see section 3.12) using Pierce Streptavidin-Alkaline Phosphatase Conjugate and Novex AP Chemiluminescent Substrate.

3.15.4 Cell lysate sample preparation

Frozen NHDF and CF were lysed by bead-milling in 2x 30 µl CF cell lysis buffer (see 2.6). After that, 2.5 µg protein from intermediate and heavy labeled cells were combined and shortly stacked into a polyacrylamide gel (see 3.11). Electrophoresis was run for 10 min at 50 V. Then the gel was stained with Coomassie staining solution (40% ethanol, 10% acetic acid, 250 mg/L Coomassie Brilliant Blue) for 1 h on a shaker to visualize peptides, followed by washing with destaining solution (50% ethanol, 10% acetic acid) for 5 min. After that, new destaining solution was added and gel was incubated for 10 min, followed by removing and adding again new destaining solution for overnight incubation. On the next day, the gel was washed with deionized H_2O for 20 min. Afterwards, the gel was scanned using ViewPix 700 (Biostep; Burkhardtsdorf, Germany) and protein bands were excised from the gel with a scalpel and transferred into a 2 ml-tube. The bands were washed with 100 µl of 10 mM NH_4HCO_3 solution for 4 min and supernatant was discarded, followed by washing with 100 µl of band washing buffer (10 mM NH_4HCO_3, 50% acetonitrile) for 10 min. This washing procedure was repeated 2 times. After that, samples were dried in a vacuum concentrator.

Then proteins were reduced with 70 µl of reducing buffer (10 mM DTT in 10 mM NH_4HCO_3) for 45 min at 56°C. After that, proteins were alkylated (in the dark) with 70 µl of alkylation buffer (55 mM IAA in 50 mM NH_4HCO_3) and again washed with 100 µl of 10 mM NH_4HCO_3 for 4 min, followed by 4 min washing with band washing buffer. This step was repeated once and bands were dried using a vacuum concentrator. Then, bands were digested with 1:50 trypsin in 10 mM HCl for 1 min (if band did not get clearer 3-7 µl 10 mM NH_4HCO_3 was added). Subsequently, bands were incubated over night at 37°C. On the next day, peptides were extracted using 35 µl extraction buffer (0.1% TFA with acetonitrile (1:1)). Samples were put into a sonicator for 15 min and supernatant was transferred into a 2 ml-tube. This process was repeated once and supernatants were pooled and dried in a vacuum concentrator. A total amount of 500 ng was prepared for MS analysis in 0.1% TFA.

3.16 *In vivo* secretome analysis of POSTN$^+$ CF post MI

3.16.1 Viral transduction

Cell type-specific *in vivo* secretome analysis is based on proximity labeling using the biotin ligase TurboID[84]. As *Postn* serves as a marker gene of infarct-induced aCF, a *Postn* promoter was used to specifically label a substantial proportion of these cells. To target POSTN$^+$ CF in the heart, vector system AAV9 was utilized due to its specificity for heart cells.

For this purpose, the group of Prof. Most, Heidelberg, engineered an AAV9 carrying the plasmid (POSTN-ER-TurboID), which contains TurboID according to Wei *et al.*[84]. This construct is expressed under the control of a *Postn* promoter. To produce the transfer plasmid *pAAV-POSTN-ER-TurboID*, the existing thyroxine binding globulin (*Tgb*) promoter in the AAV transfer plasmid *pAAV-TBG-ER-TurboID* purchased from Addgene (#149415) (Appendix; Figure 32), was replaced with the *Postn* promoter from Lindsley *et al.*[96]. The vector cloning process was conducted in *E. coli* (VB UltraStable, strain K12). The plasmid of the *pAAV-POSTN-ER-TurboID* is shown in Figure 33 (Appendix).

Prof. Dr. Patrick Most's research group also performed the production of replication-defective AAV9 particles (AAV particles POSTN-ER-TurboID) through the co-transfection of the transfer plasmid and helper plasmids (coding for the AAV proteins required for virus sub particle production) in packaging cells (HEK293T). Additionally, they handled the purification of the virus particles and titer determination. The AAV9 particles POSTN-ER-TurboID were dissolved in PBS with a titer of 2.02×10^{13} gc/ml.

For transduction, 1×10^{12} genome copies AAV9-POSTN-ER-TurboID were injected into the tail vein of 10 weeks-old C57Bl/6 mice one day post MI/Sham (section 3.2). The genetically engineered biotin ligase TurboID, with a localization signal for the ER membrane[85], should be specifically expressed in CF of C57Bl/6 mice that are positive for *Postn*.

3.16.2 *In vivo* biotinylation of cell type-selective secreted proteins

Due to the *Postn* expression of CF after MI, TurboID is also expressed and can biotinylate proteins that are located in proximity. For the labeling process, external biotin is needed, which was provided via drinking water. For this, biotin was added to the drinking water at a concentration of 0.5 mg/ml for 3 consecutive days.

3.16.3 Preparation of serum, coronary effluent, and tissue

One day after the final dose of biotin, serum, coronary effluent, and organs were collected (sections 3.3-3.5) and stored at -80°C until further use.

For later protein analyses, organ tissues were disrupted and homogenized mechanically using TissueLyser LT (Qiagen, Hilden, Germany). For this, tissue was transferred into a 2 ml-tube and weighed. After that, a threefold amount of lysis buffer (see section 2.6) was added, along with one stainless steel bead. Cells were disrupted in the TissueLyser LT for 1 min at 40 Hz, followed by six times 10 sec sonication in an ultrasonic bath. Between the sonication steps,

samples were cooled down for 10 sec. After sonication, cell lysate was centrifuged for 15 min at 16,000 *xg* and 4°C. The supernatant was transferred into a new tube and kept on ice. The cell pellet was resuspended in twofold weight lysis buffer. Cells were sonicated again as described before. The cell lysate was centrifuged for 15 min at 16,000 *xg* and 4°C, both supernatants were combined, and protein concentration was determined. The lysate was stored at -80°C until further use. This protocol was kindly performed by Dr. Gereon Poschmann.

Biotin, POSTN, and V5-tag were detected in coronary effluent and lysed organs by Western Blot (section 3.12).

3.16.4 Concentration of coronary effluent

To concentrate the large-volume effluent samples (approximately 45-60 ml) to a volume of 250 µl for further measurements, 10 kDa protein concentrators were used. Samples were centrifuged at 4000 x*g* and 4°C until the desired volume was achieved. Subsequently, the samples were stored at -80°C.

3.16.5 Enrichment of biotinylated proteins

For the enrichment of biotinylated proteins, Dynabeads MyOne Streptavidin T1 (Thermo Fisher Scientific, Waltham, USA) were used according to the protocols of Wei *et al.*[84] and Cheah and Yamada[97]. A volume of 200 µl Dynabeads was washed twice with 1 ml lysis buffer (50 mM Tris HCl, 150 mM NaCl, 0.4% SDS, 1% NP-40, 1 mM EGTA, 1.5 mM $MgCl_2$, protease inhibitor (1 µl/ml), pH 7.4) by centrifugating 2 min at 2000 x*g*. The pellet was resuspended in 100 µl lysis buffer and 200 µl of the concentrated effluent (3.16.4) was added to the Dynabeads and rotated over end overnight at 20 *rpm* and 4°C using the MACSmix Tube Rotator. On the next day, samples were washed with 1 ml lysis buffer, 1 ml washing buffer (50 mM Tris HCl, 2% SDS, pH 7.5) and twice with 1 ml lysis buffer. For elution, 15 µl of a 25 mM biotin solution was added to the beads and samples were heated in a heating block for 5 min at 95°C. Samples were centrifuged for 2 min at 2000 x*g* and supernatant containing biotinylated peptides was transferred into clean 2 ml-tubes. This step was repeated once and peptides were stored at -80°C until further use. For later MS analysis, 5 µg of the samples were shortly stacked into a polyacrylamide gel which was stained with Coomassie Brilliant Blue (see 3.15.4). The protein-containing bands were cut out, de-stained, reduced with DTT, alkylated with IAA and digested with trypsin overnight. After extraction the peptides were dried in a vacuum concentrator and a total amount of 500 ng was prepared for MS analysis in 0.1% TFA.

3.17 MS analysis

In order to measure the enriched peptide samples using MS, they first needed to be separated and ionized. Therefore, the liquid phase containing all peptides (mobile phase) was flushed through a column (stationary phase) containing hydrophobic particles[98]. Due to their mass and charge, the peptides within the mobile phase interact differently with the stationary phase and were eluted at different timepoints based on their physical properties[98]. For ionize the analytes, electrospray ionization (ESI) was used, which is a gentle ionization process to transfer ions from liquid phase to gas phase[99]. The liquid sample was passed through a small capillary to which a large voltage was applied, leading to the creation of small, charged droplets. These

droplets were passed through a stream of nitrogen, evaporating and reducing in size until the charge density exceeded the surface tension, leading to the decay of droplets and the transfer of ions to the gas phase[99,100]. To precisely analyze the ionized analytes, MS/MS was used. In this technique, at least two mass spectrometers are coupled[99]. The ions were first separated based on their mass-to-charge ratio (m/z) and selectively further fragmentated (product ions)[101]. Then m/z of these product ions was measured and results were compared to extensive databases.

3.17.1 MS analysis of cultivated fibroblast secretome and proteome

The fibroblast-secreted peptides of NHDF and CF, as well as cell lysate peptides of NHDF (see section 3.15), were separated on C18 columns using an Ultimate3000 rapid separation liquid chromatography system (Thermo Fisher Scientific). A 2 h gradient was applied, following a protocol essentially described by Brenig, Grube *et al.*, 2020[102]. Subsequently, the peptides were injected into the respective mass spectrometer (operated in positive mode) via an electrospray nano-source interface (compare Table 17).

Table 17: Used MS settings for NHDF secretome and proteome and CF secretome analysis

Experiment	Instrument	Gradient	Software	Database
NHDF secretome +/- FCS	QExactive Plus	2 h	Maxquant 1.6.17.0	20210127 homo sapiens UP000005640 75777 entries
NHDF lysate +/- AHA	QExactive Plus	2 h	Maxquant 1.6.17.0	20210127 homo sapiens UP000005640 75777 entries
CF secretome MI/Sham	Fusion Lumos	2 h	Maxquant 2.1.3.0	20220118 mus musculus UP000000589 55341 entries

At the beginning of the measurement, survey scans were recorded using an orbitrap analyzer (used parameters see Table 17). Subsequently, precursor ions were selected by the quadrupole and fragmented spectra recorded either in the orbitrap analyzer (QExactive Plus) or linear ion trap (Fusion Lumos). Parameters employed are detailed in Table 18. For data analysis, MaxQuant (Max Planck Institute for Biochemistry, Planegg, Germany) was utilized, with software versions specified in Table 17.

Only proteins identified with at least two different peptides were considered. Normalization was performed separately for the different sample groups based on the median intensity per sample.

Table 18: Used MS parameters for NHDF secretome and proteome and CF secretome analysis

	NHDF secretome +/- FCS	NHDF lysate +/- AHA	CF secretome MI/Sham
MS1 (Orbitrap)			
Resolution	140000	140000	120000
Target value advanced gain control	3000000	3000000	250000
Maximum injection time [ms]	80	80	60
Scan range [m/z]	350-2000	350-2000	200-2000
Data type	profile	profile	profile

Isolation (Quadrupole)			
Isolated precursor charges	2 and 3	2 and 3	2-7
Isolation window [m/z]	2	2	1.6
Collision energy HDC	30%	30%	35%
MS2			
MS2 analyzer	Orbitrap	Orbitrap	Linear ion trap
Scan rate/resolution	17500	17500	rapid
Target value advanced gain control	100000	100000	10000
Maximum injection time [ms]	60	60	50
Data type	centroid	centroid	centroid
Cale time [s]	-	-	2
TopN	10	10	-
Dynamic exclusion [s]	100	1000	60

To determine differences in protein abundance, only proteins that showed at least three valid values in one sample group for the secretome or at least 5 valid values in one group for the proteome were considered. Significance analysis was performed using microarrays method[103] based on Student's t-tests and permutation-based control of the false discovery rate (FDR) with setting shown in Table 19. In instances of missing values, random values drawn from a downshifted normal distribution were imputed.

Data searches were conducted using secretome and proteome sequences from homo sapiens and mus musculus (see Table 17), obtained from UniProt KB. For further quantitative data processing and gene ontology categorization, Perseus 1.6.6.0 (Max Planck Institute for Biochemistry, Planegg, Germany) was used. One-dimensional annotation enrichment analysis was performed following the method outlined by Cox and Mann, 2012[104] and secretion pathways were predicted using OutCyte[105]. It is important to note that measured intensities may be influenced by the availability of tryptic peptides and modifications of peptides can vary between proteins. Consequently, measured intensities do not necessarily reflect absolute protein abundance.

Table 19: Used analysis parameters for NHDF secretome and proteome and CF secretome

Experiment	Valid values	Fill in of missing values	t-test /SAM
NHDF secretome +/- FCS	3 in at least one group	width: 0.3 SD, down shift 1.8 SD	5% FDR, S_0=0.1
NHDF lysate +/- AHA	5 in at least one group	width: 0.3 SD, down shift 1.8 SD	5% FDR, S_0=0.6
CF secretome MI/Sham	3 in at least one group	width: 0.3 SD, down shift 1.8 SD	5% FDR, S_0=0.6

3.17.2 MS analysis of POSTN$^+$ CF-specific peptides

MS analysis of POSTN$^+$ CF-specific peptides was performed as described before (see section 3.17.1) using the specified mass spectrometers and settings (Table 20), MS parameters (Table 21), and analysis parameters (Table 22).

Table 20: Used MS settings for POSTN$^+$ CF *in vivo* secretome and proteome analysis

Experiment	Instrument	Gradient	Software	Database

Coronary effluent MI/Sham	Fusion Lumos	1 h	Maxquant 2.2.0.0. minimum ratio count 1	20230112 mus musculus UP000000589 55268 entries
Heart tissue MI/Sham	Fusion Lumos	40 min	Thermo Proteome discoverer 2.4.1.15	20230112 mus musculus UP000000589 55268 entries

Table 21: Used MS parameters for POSTN$^+$ CF *in vivo* secretome and proteome analysis

	Coronary effluent MI/Sham	**Heart tissue MI/Sham**
MS1 (Orbitrap)		
Resolution	120000	120000
Target value advanced gain control	400000	400000
Maximum injection time [ms]	60	50
Scan range [m/z]	200-2000	350-2000
Data type	profile	profile
Isolation (Quadrupole)		
Isolated precursor charges	2-7	2-6
Isolation window [m/z]	1.6	1.6
Collision energy HDC	35%	35%
MS2		
MS2 analyzer	Linear ion trap	Linear ion trap
Scan rate/resolution	rapid	rapid
Target value advanced gain control	10000	10000
Maximum injection time [ms]	150	35
Data type	centroid	centroid
Cale time [s]	2	1
TopN	-	-
Dynamic exclusion [s]	60	60

Table 22: Used analysis parameters for POSTN$^+$ CF secretome and proteome analysis *in vivo*

Experiment	**Valid values**	**Fill in of missing values**	**t-test /SAM**
Coronary effluent MI/Sham	4 in at least one group	width: 0.3 SD, down shift 1.8 SD	5% FDR, S_0=0.1
Heart tissue MI/Sham	4 in at least one group	width: 0.3 SD, down shift 1.8 SD	5% FDR, S_0=0.1

3.18 Single-cell/ single-nuclei RNA sequencing data analysis

ScRNA-seq and snRNA-seq published data were processed using R Studio version 2022.07.2 and the R Seurat package[106] version 3.0.

To compare basal gene expression levels between different cardiac cell types, including cardiomyocytes, a snRNA-seq data set of cardiac cells isolated from a healthy 12-week-old mouse[107] (ArrayExpress E-MTAB-7869, sample Y1) was utilized.

To compare gene expression level in CF 5 days after MI/Sam or among different cardiac cell types 5 days post MI, scRNA-seq datasets previously published by our group[108,109] were re-

analyzed. Names of CF populations were annotated based on the expression of CF population markers according to Shi *et al.*[110] and Farbehi *et al.*[67].

3.19 Statistics

Statistics were performed using Prism and MaxQuant (software versions see Table 15). The different applied tests are displayed in the corresponding figure descriptions (section 4).

In experiments for cell viability determination, a Two-way ANOVA followed by Tukey multiple comparisons test was used. *P* values < 0.05 were considered to be significant (**P*< 0.05; ***P*< 0.01; ****P*< 0.001). Data is shown as mean with SEM.

To determine differentially abundant proteins, Student's t-test-based significance analysis of microarray approach (SAM) (Tusher *et al.*, 2001)[103] was employed. The significance of protein intensities was determined through Student's t-test-based SAM analysis (unpaired two-sided T-test; permutation-based FDR). In case of missing values, random values drawn from a downshifted normal distribution were filled in. Used parameters are listed in section 3.17.

For protein annotation, gene ontology categories by Perseus were used and secretion pathways were predicted by OutCyte[105].

Analysis of global abundance shifts was displayed by showing selected GOCC and GOBP categories grouped by gene ontology annotations (Cox and Mann, 2012)[104].

4. Results

4.1 Establishment of combined pSILAC and click-chemistry for secretome analysis of NHDF cells

The described protocol, using pSILAC and click-chemistry for secretome analysis, has not yet been applied for fibroblasts. Establishing the method requires a high cell count, but the number of CF obtained from one mouse heart varies between only $2x10^5$-$4x10^5$ cells. To overcome these limitations, the fibroblast cell line NHDF was used for protocol establishment and optimization. This approach also minimized the number of mice used, aligning with animal welfare guidelines. In order to adapt the protocol for specific cells, certain prerequisite, such as ensuring cell viability, a functional click mechanism and proper amino acid incorporation, have to be addressed in advance.

4.1.1 Cell viability

For pulse labeling the cells with different amino acid isotopes of Arg, Lys and Met, they must be depleted of these amino acids initially. This was achieved by using depletion medium lacking these amino acids.

During the labeling time, it is crucial to ensure that the cells are depleted for a sufficient duration in order to allow subsequent incorporation of the amino acids but not for so long that it attenuates cell viability.

Following the recommendation of Eichelbaum and Krijgsveld for cell depletion of 30-60 min[78], cell viability was determined for Arg, Lys, and Met depletion at 30 min, 60 min, and 90 min using depletion medium (D-DMEM) in comparison to DMEM as a control. In addition, cell viability was measured after labeling cells with the desired concentrations of AHA, $^{13}C_6$ Arg, D4 Lys, $^{13}C_6{}^{15}N_4$ Arg, and $^{13}C_6{}^{15}N_2$ Lys for 24 h and 48 h. Furthermore, cells were treated with a combination of intermediate Arg ($^{13}C_6$ Arg) and Lys (D4 Lys) and heavy Arg ($^{13}C_6{}^{15}N_4$ Arg) and Lys ($^{13}C_6{}^{15}N_2$ Lys) plus AHA for 24 h and 48 h. Considering their impact on the secretome, for example AHA incorporating more slowly into tRNA than Met[111], it was recommended by the Krijgsveld group not to exceed a labeling time of 24

Cell viability was measured using Cell Counting Kit 8, with NHDF treated with control DMEM were assumed to have a cell viability of 100%. For all three depletion time points, there were no differences in cell viability compared to control (Figure 10A). Additionally, there were no changes in cell viability after treating cells with the different intermediate and heavy amino acids and AHA for 24 h and 48 h (Figure 10B).

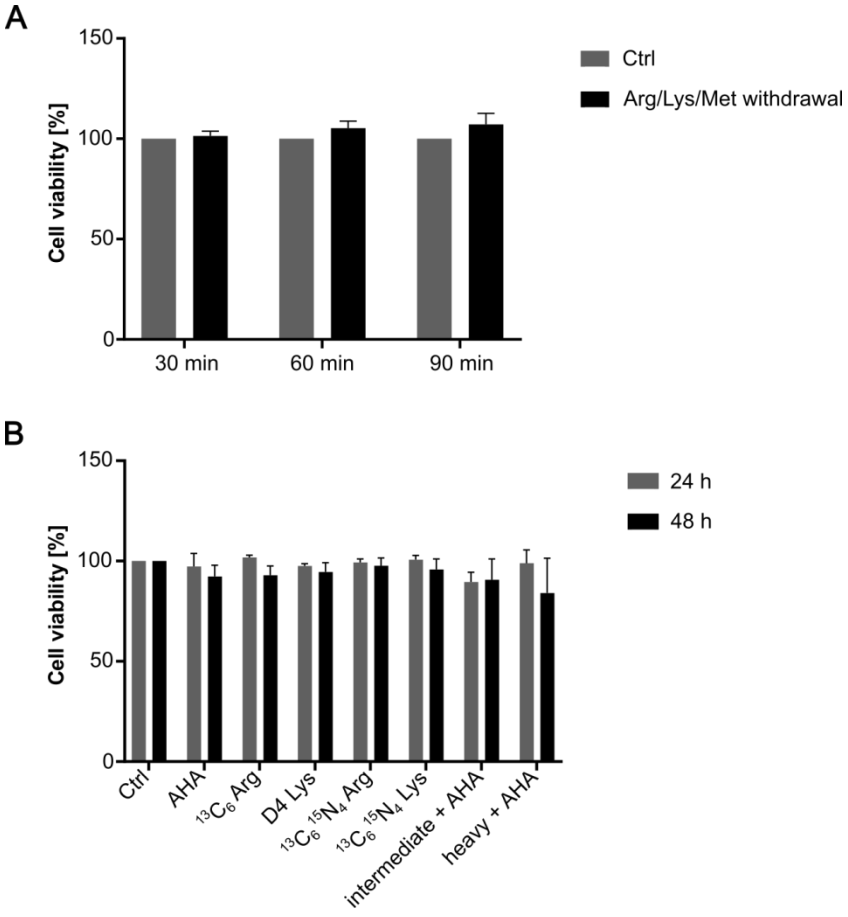

Figure 10: Arg, Lys, and Met depletion as well as the treatment with different amino acid isotopic analogues of Arg and Lys plus azidohomoalanine (AHA), had no influence on NHDF cell viability after 24 h and 48 h of labeling. A) NHDF cells were depleted of Arg, Lys and Met for 30 min, 60 min, and 90 min using depletion medium lacking these amino acids. As a control, NHDF cells were cultivated with DMEM (Ctrl). **B)** NHDF cells were depleted of Arg, Lys, Met for 60 min and labeled with different amino acid isotopic analogues, $^{13}C_6$ Arg, [4,4,5,5-D4] Lys (D4 Lys), $^{13}C_6{}^{15}N_4$ Arg and $^{13}C_6{}^{15}N_2$ Lys or L-azidohomoalanine (AHA) instead of Met for 24 h and 48 h. Additionally, cells were treated with a combination of intermediate $^{13}C_6$ Arg and D4 Lys and heavy $^{13}C_6{}^{15}N_4$ Arg and $^{13}C_6{}^{15}N_2$ Lys plus AHA for 24 h and 48 h. As a control (Ctrl), cells were treated with DMEM. Cell viability was measured in triplicates using CCK-8, assuming the control group had a cell viability of 100%. Data points are present as mean ± SEM (n=3). Two-way ANOVA followed by Tukey multiple comparisons test was used for statistical analysis (*P< 0.05).

As there was no diminished cell viability after 60 min and even 90 min of depletion, the recommended depletion time by the Krijgsveld group of 60 min was used for further investigations. There was no significant change in cell viability after 24 h and 48 h of AHA labeling. Considering the potential toxicity of azides over time and their possible impact on the alteration of secreted proteins, the labeling time for NHDF cells was set to 24 h for the following experiments to ensure sufficient labeling without compromising cell viability.

4.1.2 Click reaction

To enrich the newly synthesized proteins of NHDF for further MS analysis, it is essential that proteins which incorporated AHA bind to an alkyne resin via click-chemistry reaction (see section 3.15.2). This allows the removal of all other proteins through washing. Therefore, it has to be ensured that this mechanism functions effectively for the specific cell type used, ensuring that newly synthesized proteins containing azides bind to alkynes, in contrast to non-AHA containing proteins.

Click-chemistry suitability was assessed by Western Blot (see section 3.12). Therefore, NHDF cells were depleted of Arg, Lys, and Met for 60 min and thereafter labeled with heavy Arg, Lys, and AHA for 24 h. As a control, NHDF cells were used that were incubated with DMEM. After incubation, cells were lysed and intracellular proteins were clicked to an alkyne biotin using the same reagents as for the alkyne agarose binding reaction (see section 3.15.3). Proteins that were bound to biotin were detectable using alkaline phosphatase (AP) coupled streptavidin, which binds to biotin.

Western Blot analysis showed that only proteins of the AHA-treated cells were bound to the alkyne biotin (Figure 11) across various molecular weights, whereas no biotin-containing proteins was detected in the control (Figure 11A left). To ensure that the control sample was added in an appropriate concentration, the housekeeper protein β-actin, which has a molecular weight of 42 kDa, was used as a loading control. It was detected in both cell lysate samples (Figure 11 right), indicating that clicking of AHA-treated fibroblast was successful and that this method can be used for enrichment of de novo proteins.

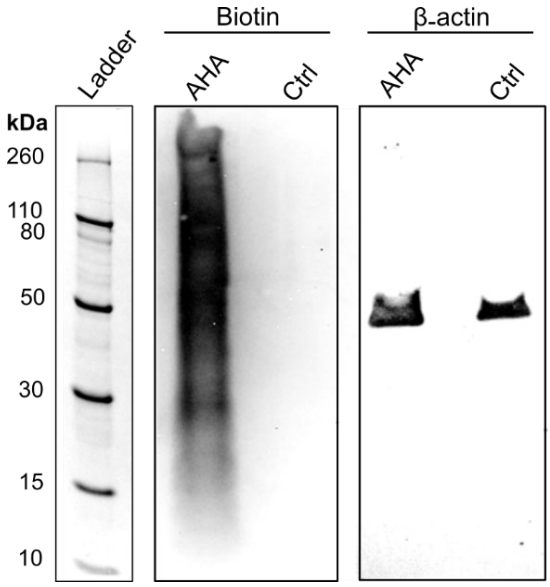

Figure 11: Click-chemistry reaction was suitable for AHA-labeled NHDF proteins. NHDF cells were either depleted of Met and labeled with AHA for 24 h (AHA) or incubated with DMEM (Ctrl). Cells were lysed and intracellular proteins were coupled with an alkyne biotin via click-chemistry mechanism. Western Blot of AHA-labeled intracellular proteins and intracellular proteins of DMEM-incubated NHDF is present. Biotin, detected via chemiluminescence using alkaline phosphatase-coupled streptavidin, is shown on the left and the housekeeping protein β-actin, with a molecular weight of 42 kDa, was detected using a mouse anti-β-actin antibody and secondary antibody goat anti-mouse IgG AF 800 with a filter range of 810-850 nm, shown on the right. For Bis-Tris gel electrophoresis, 20 ng of protein was applied per sample. Novex Sharp Pre-stained protein standard was used as a protein ladder (3 µl). Representative image of n=2 experiments.

4.1.3 Incorporation of amino acid isotopes

After confirming the efficiency of coupling AHA-bearing proteins to alkynes, it was explored, whether the incorporation of amino acid isotopes and AHA was sufficient. Therefore, NHDF cells were depleted of Arg, Lys, Met for 60 min and labeled with heavy Arg and Lys plus AHA for 24 h. As a control, NHDF cells were incubated with DMEM. Subsequently, cells were lysed (see section 3.9) and intracellular proteins were detected via LC MS/MS.

In the lysate sample of cells treated with heavy Arg and Lys, there where high numbers of heavy-labeled peptides with different intensities, but also some peptides that were not heavy labeled, showing lower intensities (Figure 12A). In the control lysate sample of unlabeled cells, most peptides were not heavy labeled and a few heavy-labeled peptides with low intensities were detected. To ensure that amino acid isotope-labeled proteins can be enriched using click-chemistry, they must also have incorporated AHA. In the LC-MS/MS analysis, most of the heavy-labeled peptides also showed incorporated AHA (Figure 12B). Only a few light peptides with low intensity were also positive for AHA, demonstrating that the incorporation of different amino acid isotopes and AHA was successful.

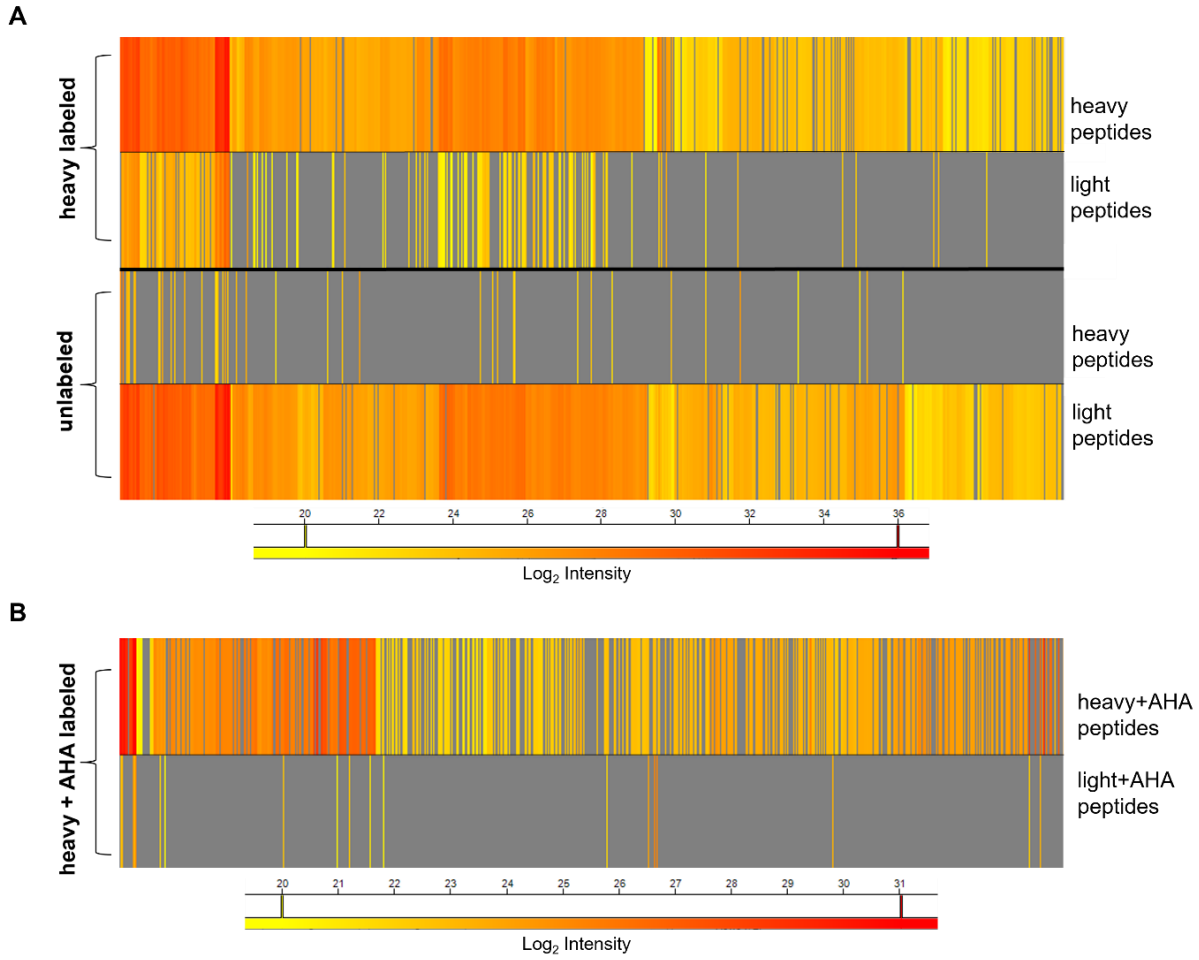

Figure 12: NHDF cells incorporated heavy amino acid isotopes and L-azidohomoalanine (AHA) into their proteins. A) NHDF cells were depleted of Arg, Lys and Met for 60 min and labeled with heavy Arg and Lys plus AHA (heavy labeled) or incubated with control medium (unlabeled). Cells were lysed and intracellular peptides were analyzed via LC-MS/MS for their Log_2 intensity and distribution, divided into heavy-labeled peptides (heavy peptides) and peptides that had no heavy amino acids incorporated (light peptides). **B)** NHDF cells were depleted of Arg, Lys, and Met for 60 min and labeled with heavy Arg and Lys plus AHA (heavy + AHA labeled). Cells were lysed and intracellular peptides were analyzed via LC-MS/MS for their Log_2 intensity and distribution, divided into peptides that incorporated both AHA and heavy amino acids (heavy + AHA peptides) and peptides that only incorporated AHA (light + AHA peptides). The scale bar of Log_2 intensity is shown below the illustrations of the respective measurements.

4.1.4 Protocol optimization

After ensuring cell viability and incorporation of amino acid isotopes and AHA, the secretome of labeled NHDF cells was analyzed via LC-MS/MS. In a first experimental series, the protocol described by Eichelbaum and Krijgsveld in 2014[78] was used. However, despite applying click-chemistry for protein enrichment of AHA-bearing proteins, serum contaminants like bovine serum albumin (BSA) (39%) were found to be highly enriched (Figure 13A). Approximately 72% of the analyzed proteins appeared to be serum contaminants. Besides that, a high proportion of transforming growth factor beta-induced (TGF-βI) (6%) and FN1 (3%) was identified in the NHDF secretome. To address these contaminants, the washing steps of the proteins bound to resin were increased fourfold compared to the previous protocol (section 3.15.2). Furthermore, the method of gravity flow washing of the resin using chromatography columns was changed to washing the resin by centrifugation (see 3.15.2). With this optimized protocol, secretome analysis revealed fewer contaminants (24%), of which BSA accounted for 13%. Furthermore, there was a high proportion of FN1 (12%), collagen type I alpha 2 chain (COL1A2) (8%), matrix metalloproteinase 2 (MMP2) (5%), metalloproteinase inhibitor 1 (TIMP1) (5%), TGF-βI (4%), thrombospondin 1 (THBS1) (3%), COL1A1 (3%), collagen type VI alpha 3 chain (COL6A3) (3%), and collagen type VI alpha 1 chain (COL6A1) (1%). As the number of contaminants was considerably reduced by increasing and modifying the washing steps, the optimized protocol was used for further analysis.

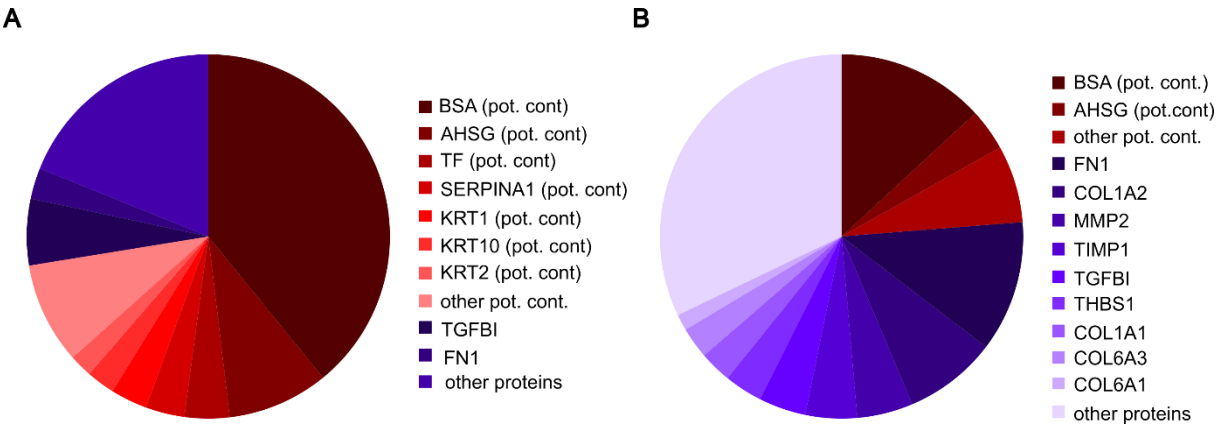

Figure 13: An increase of washing steps in the protein enrichment protocol reduced the number of serum contaminants in the NHDF secretome. A) Percentage distribution of proteins identified in LC-MS/MS analysis of NHDF cells using protein enrichment protocol of Eichelbaum and Krijgsveld, 2014[78]. **B)** Distribution of NHDF-secreted proteins using the protein enrichment protocol of Eichelbaum and Krijgsveld, 2014, with an increase in washing steps and using centrifugation instead of gravity flow. (Pot. cont = potential contaminant).

4.1.5 Influence of AHA labeling on NHDF proteome

AHA labeling did not alter the NHDF cell viability but might influence the secretome, for example, by a reduced rate of incorporation in comparison to Met[112]. A direct measurement of AHA's impact on the secretome is not possible because AHA is needed to enrich the newly synthesized proteins using click-chemistry. Therefore, the influence of AHA on intracellular proteins at different labeling time points (6 h, 24 h) was investigated. To do so, NHDF cells were depleted of Met, Arg, and Lys for 60 min and labeled with either AHA, $^{13}C_6{}^{15}N_4$ Arg and $^{13}C_6{}^{15}N_2$ Lys or Met, $^{13}C_6{}^{15}N_4$ Arg, and $^{13}C_6{}^{15}N_2$ Lys. After 6 h, only two significant changes in protein abundance between AHA and Met labeling, out of a total of 2441 proteins (Figure 14A

left, Figure 14B), were detected, but after 24 h, the number of significantly altered proteins strongly increased (194 out of 2141) (Figure 14A right, Figure 14B).

Even though only two proteins changed their abundance 6h after AHA labeling, there was a decrease in abundance of ribosomal- and translational-associated proteins, which continued after 24 h of AHA labeling (Figure 14C Q4). Golgi-associated proteins only increased their abundance after 24 h of labeling (Figure 14C Q2). Proteins associated with the response to DNA damage and DNA replication were higher abundant 6 h after AHA labeling, whereas they had a lower abundance after 24 h of AHA labeling (Figure 14C Q3). Furthermore, proteins associated with ECM, cell surface, protein glycosylation, and ER showed a lower abundance after 6 h, which increased to a higher abundance after 24 h of AHA labeling (Figure 14 C Q1).

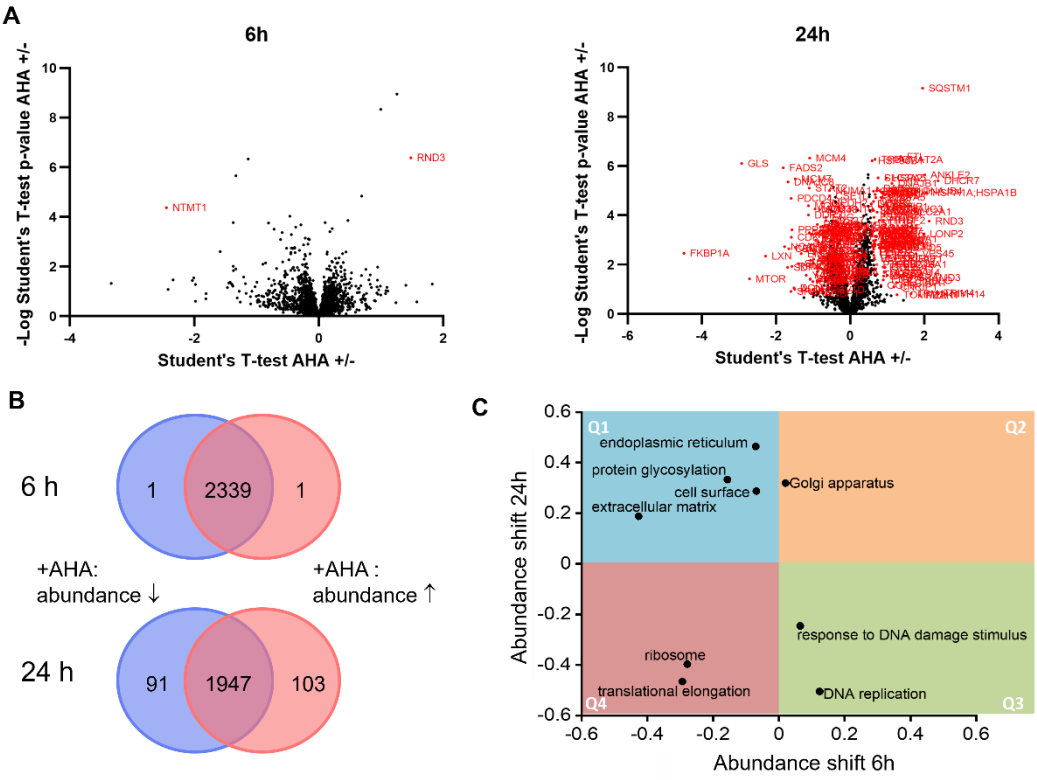

Figure 14: L-azidohomoalanine (AHA) labeling altered the proteome of NHDF cells (based on Poschmann *et al.*, 2022[70]). The proteome of NHDF cells was analyzed after labeling with AHA or Met as a control for 6 h and 24 h. **A)** Different abundant intracellular proteins, which were determined by Student's t-test-based significance analysis of microarray approach (Tusher *et al.*, 2001)[103] (n=5). Proteins with significant differences in intensity (Student's t-test-based SAM analysis, 5% FDR, S_0=0.6) are highlighted in red. **B)** Venn diagram of secretome changes 6 h and 24 h after AHA labeling. Proteins with lower abundance after AHA labeling compared to control are shown in blue, while higher abundant proteins are shown in red. **C)** Analysis of global abundance shifts showing selected GOCC and GOBP categories grouped by gene ontology annotations (Cox and Mann, 2012)[104]. Proteins that changed abundance in the same way after 6 h and 24 h of AHA incubation are shown in quadrant Q2 and Q4. In quadrant Q1 and Q3, proteins are shown that changed their abundance direction between 6 h and 24 h in the opposite way.

As differences in the abundance of intracellular proteins were observed even after only 6 h of AHA labeling, it is highly probable that changes in the secretome would occur with longer AHA incubation times. This needs to be considered when determining the incubation time for further secretome analyses.

4.1.6 Influence of serum starvation on NHDF secretome

Since the majority of published secretome analyses were performed under serum starvation conditions, the study aimed to investigate changes in cellular secretome between serum starvation and serum-containing conditions (10% FBS). To this end, NHDF cells were cultured with DMEM without FBS for 6 h and 24 h. As a control, cells were cultivated with DMEM including 10% FBS. Cell viability of NHDF cells was measured after 24 h starvation in contrast to conditions using 10% FBS. This measurement revealed no changes in cell viability between the two conditions (Figure 15A). However, after 6 h of cultivation with 10% FBS, 48 (out of 225) proteins were detected that were not detectable when cultivating without FBS (Figure 15B). Additionally, there was one protein that was only secreted under serum starvation conditions. After 24 h of serum starvation, protein was detectable that was not secreted under 10% serum cultivation, but 32 proteins (out of 278) were only secreted when culturing the NHDF cells with 10% FBS. After 6 h of serum depletion, 123 proteins were significantly altered compared to cultivation with 10% FBS, whereas after 24 h, a total of 159 proteins showed significantly altered abundance (Figure 15C). In general, in both approaches with serum starvation, fewer proteins were found, and the average intensity distribution of detected proteins was lower (Figure 15D).

As expected, more secreted proteins could be detected after a longer labeling period of 24 h in contrast to the short incubation time of 6 h. These findings underline the importance of serum-containing conditions and efficient labeling times to comprehensively cover the secretome.

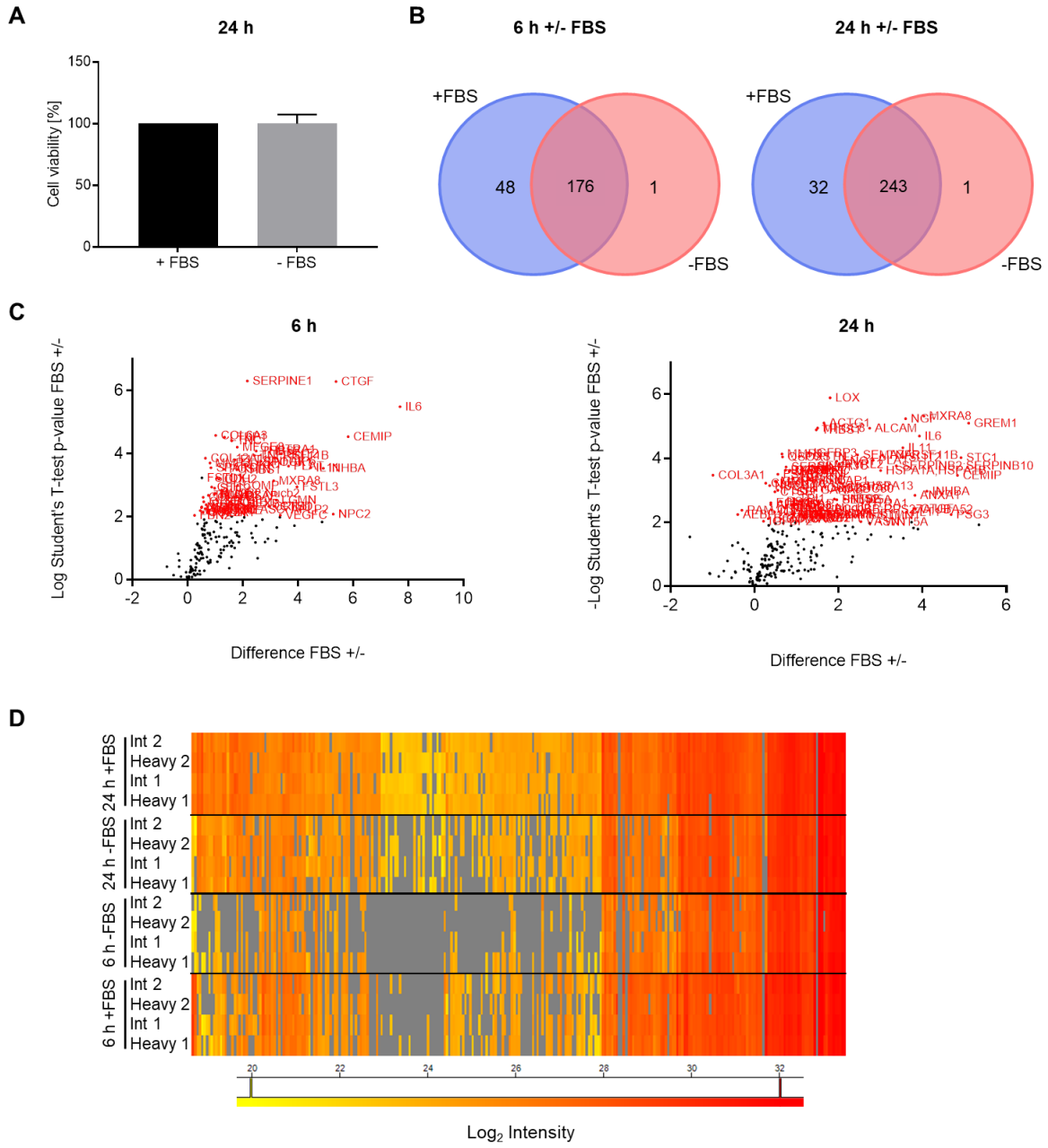

Figure 15: Serum starvation altered the secretome of NHDF cells despite unaffected cell viability. A) Cell viability of NHDF cells incubated with DMEM containing 10% FBS (FBS+) or DMEM without FBS (FBS-) was measured in triplicates using CCK-8, assuming the control group cultivated with 10% FBS had a cell viability of 100%. Data points are present as mean ± SEM (n=3). Two-way ANOVA followed by Tukey multiple comparisons test was used for statistical analysis. **B)** NHDF cells were depleted of Arg, Lys, and Met for 60 min and labeled with heavy or intermediate (int) Arg and Lys plus AHA either with 10% FBS or without FBS. Cells were lysed, and intracellular peptides were analyzed via LC-MS/MS (n=4). **C)** Volcano plot illustrating secreted proteins after 6 h and 24 h of serum depletion compared to the control (10% FBS). Different abundant proteins were determined using a Student's t-test-based significance analysis of microarray approach (Tusher *et al.*, 2001)[103] (n=4). Proteins with significant differences in intensity (Student's t-test-based SAM analysis, 5% FDR, S_0=0.1) are highlighted red. **D)** Log_2 intensity and distribution of secreted proteins after 6 h and 24 h of serum starvation (n=4) using int and heavy labeling two times in each case.

4.2 Establishment of combined pSILAC and click-chemistry for secretome analysis of murine CF

After successfully establishing the quantitative secretome analysis using pSILAC and click-chemistry for the fibroblast cell line NHDF, this protocol served as the foundation for analyzing the secretome of murine CF isolated from both control and infarcted hearts. Given that CF were freshly isolated and subjected to short-term culture, it was necessary to investigate whether the chosen protocol had any impact on viability and click-chemistry efficiency.

4.2.1 Cell viability

Cells were depleted of Arg, Lys, and Met for 30 min, 60 min, and 90 min using D-DMEM, which does not contain these three amino acids. As a control, cells were incubated with DMEM. Cell viability was measured using CCK-8. The different depletion times had no influence on CF cell viability (Figure 16A).

Furthermore, cells were depleted for 60 min and then labeled with the desired concentrations of AHA, $^{13}C_6$ Arg, D4 Lys, $^{13}C_6{}^{15}N_4$ Arg, and $^{13}C_6{}^{15}N_2$ Lys. Additionally, cells were treated with a combination of intermediate Arg and Lys as well as heavy Arg and Lys plus AHA for 6 h, 8 h, 16 h, and 24 h. The different amino acid isotopes had no effect on cell viability, whereas all cells treated with AHA showed a significant decrease in cell viability after 24 h (Figure 16B). Already after 16 h of AHA labeling, there was a tendency of loss in cell viability.

As AHA decreased cell viability over time, it is likely that it will also influence its secretome. Thus, in the following experiments, a labeling time of 8 h was chosen.

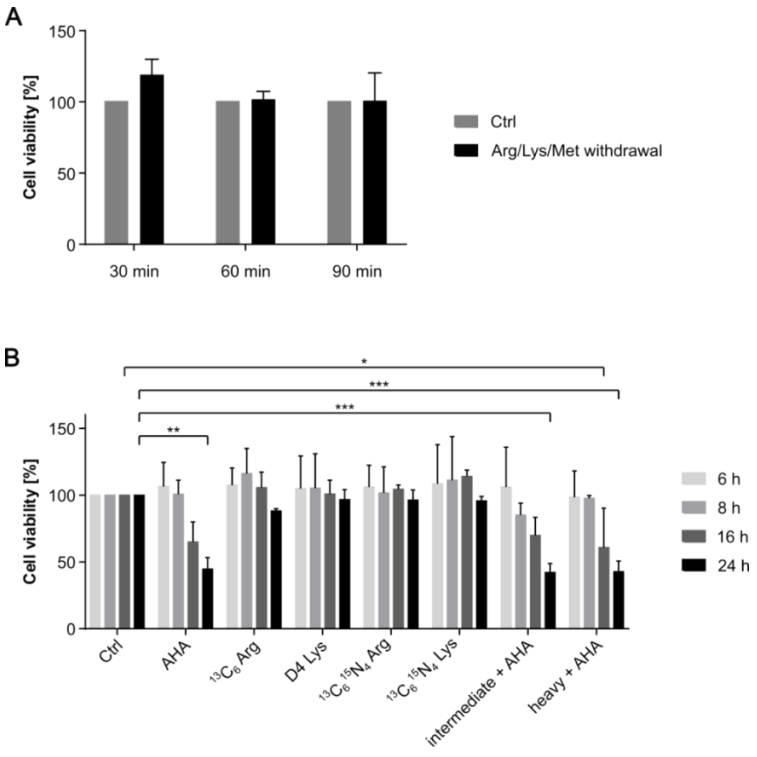

Figure 16: Arg, Lys, and Met depletion as well as the treatment with different amino acid isotopic analogues of Arg and Lys had no influence on murine CF viability, whereas L-azidohomoalanine (AHA) labeling decreased cell viability over time. A) Murine CF were depleted of Arg, Lys, and Met for 30 min, 60 min, and 90 min with medium lacking these amino acids. As a control, CF were cultivated with DMEM (Ctrl). **B)** CF were

depleted of Arg, Lys, and Met for 60 min and labeled with different amino acid isotopic analogues, $^{13}C_6$ Arg, [4,4,5,5-D4] Lys (D4 Lys), $^{13}C_6{}^{15}N_4$ Arg, and $^{13}C_6{}^{15}N_2$ Lys, or AHA instead of Met for 6 h, 8 h, 16 h, and 24 h. Additionally, cells were treated with a combination of intermediate $^{13}C_6$ Arg and D4 Lys and heavy $^{13}C_6{}^{15}N_4$ Arg and $^{13}C_6{}^{15}N_2$ Lys plus AHA. As a control (Ctrl), cells were treated with DMEM. Cell viability was measured in triplicates using CCK-8 and normalized to the control group with the assumption that the control group had a cell viability of 100%. Data points are presented as mean ± SEM (n=3). Two-way ANOVA followed by Tukey multiple comparisons test was used for statistical analysis (*P< 0.05; **P< 0.01; ***P< 0.001).

4.2.2 Click-chemistry

To validate the suitability of the click-chemistry mechanism for proteins secreted by murine CF and to confirm its ability to enrich newly synthesized proteins, CF were isolated and cultivated for 24 h followed by Arg, Lys, and Met depletion for 60 min. Thereafter, cells were labeled with Arg, Lys, and AHA for 24 h. As a control, CF were incubated with DMEM. After 8 h of incubation, cells were lysed and intracellular proteins were clicked to an alkyne biotin (see section 3.15.3), which can be detected via Western Blot (see section 3.12) using an AP-conjugated streptavidin and chemiluminescence measurement.

Only the intracellular proteins of AHA-treated CF showed a chemiluminescence signal (Figure 17) across various molecular weights, whereas no biotin-labeled proteins were detectable in the control (Figure 17 left). To ensure that the control sample was loaded in a comparable amount as the AHA-treated sample, the housekeeper protein β-actin, with a molecular weight of 42 kDa, was analyzed and found in both cell lysate samples (Figure 17 right). This indicates that click-chemistry mechanism is also sufficient for proteins of AHA-treated CF and that this method can be used for enrichment of novel secreted proteins.

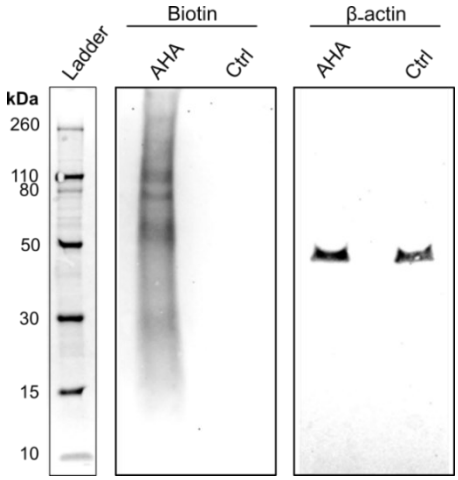

Figure 17: Click-chemistry reaction was suitable for AHA-labeled murine CF proteins. CF were isolated from C57Bl/6 mice and cultivated for 24 h in DMEM. After that, cells were either depleted of Met and labeled with AHA for 8 h or incubated with DMEM medium (Ctrl). Cells were lysed and intracellular proteins were coupled to an alkyne biotin via click-chemistry mechanism. Western Blot of AHA labeled intracellular proteins (AHA) and proteins of Ctrl CF showing biotin (left), which was detected via chemiluminescence using AP-coupled streptavidin. The housekeeper protein β-actin (MW 42 kDa) was detected via mouse anti-β-actin antibody and secondary antibody goat anti-mouse IgG AF 800 using a filter range of 810-850 nm (right). For Bis-Tris gel electrophoresis 20 ng of protein was applied per sample. Novex Sharp Pre-stained protein standard was used as a protein ladder (3 µl). Representative image of n=2 experiments.

4.3 Secretome analysis of cultured murine CF

After adjusting the washing steps compared to the described protocol of Eichelbaum and Krijgsveld and confirming of CF cell viability, the workflow shown in Figure 18 was employed for all further secretome analyses of cultured CF from the infarcted and Sham-operated heart by LC-MS/MS.

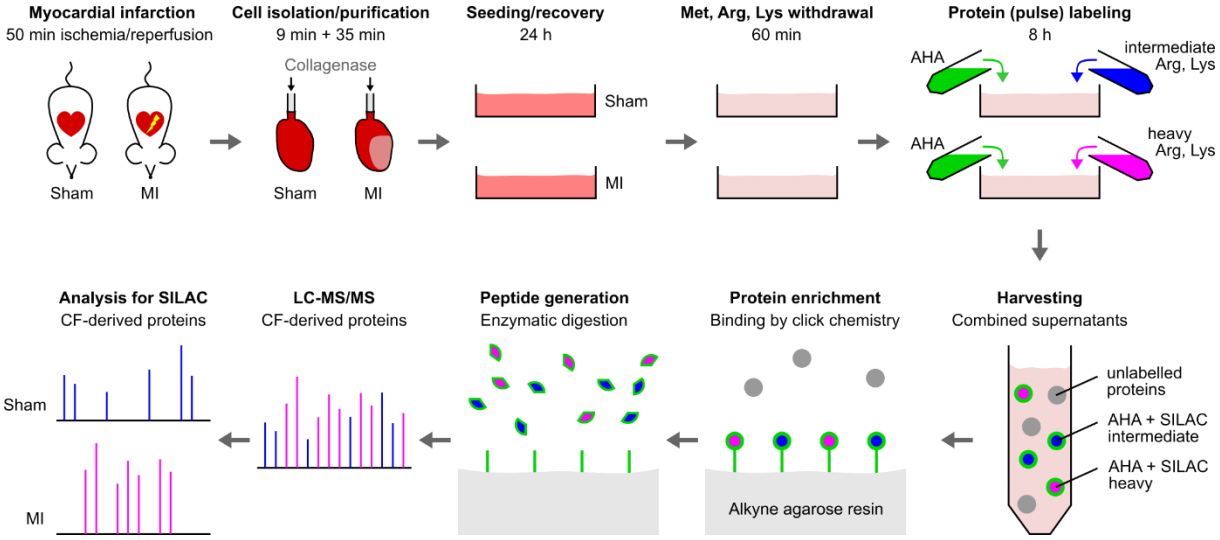

Figure 18: Workflow of comparative secretome analysis of cultured murine CF post MI/Sham. C57Bl/6 mice underwent MI (50 min ischemia/reperfusion) or Sham surgery. CF of three hearts were isolated using the Langendorff technique, pooled and cultivated for 24 h in a 10 cm dish in medium containing 10% FBS. After 60 min of Met, Arg, and Lys depletion, cells were labeled with either intermediate or heavy isotopes of Arg, Lys, and Met analogue L-azidohomoalanine (AHA) for 8 h. After pulse labeling, the supernatants were collected and pooled for protein enrichment. Newly synthesized AHA-bearing proteins were bound to an alkyne agarose resin via click-chemistry. After stringent washing, proteins were digested and eluted peptides were analyzed by LC-MS/MS in one approach.

4.3.1 Secretome analysis of cultured CF under basal conditions

Firstly, protein secretion of cultured CF from Sham-operated control hearts (5 d after Sham) was analyzed to obtain insights into the basal CF secretome (dataset see Appendix; Table 28). In this analysis, 126 proteins were identified. Out of these, 92% were predicted to be secreted by OutCyte[105] (Figure 19A) either conventionally (Conv) or unconventionally (UPS). Furthermore, 3% of the detected proteins were predicted to be transmembrane proteins (TM), and 2% intracellular proteins (IC). All in all, there were high proportions of proteins predicted to be secreted, and only a few proteins localized to be IC and TM proteins. This suggests that actively released proteins by CF can be measured, confirming the validity of the used methodology.

Detailed analysis showed that CF secreted several ECM-associated proteins (64% of total protein intensities) under basal conditions (Figure 19B). Collagen chains made up the highest intensity proportion of these proteins (24%). An additional 16% of intensity was contributed by matrix turnover proteins (Figure 19C), such as MMPs, disintegrin and metalloproteinases (ADAMs), and TIMPs, which are likely involved in a steady turnover and matrix maintenance. Another 13% of detected ECM-associated protein intensity was made up by matricellular proteins that are involved in metabolism and matrix synthesis, such as POSTN, osteonectin (SPARC), and connective tissue growth factor (CTGF). A Further 12% of intensity distribution

was contributed by matrix cross-linking proteins like LOX and lysyl hydroxylases (PLOD), followed by nidogens (NID), FN1, and nucleobindins (NUCB).

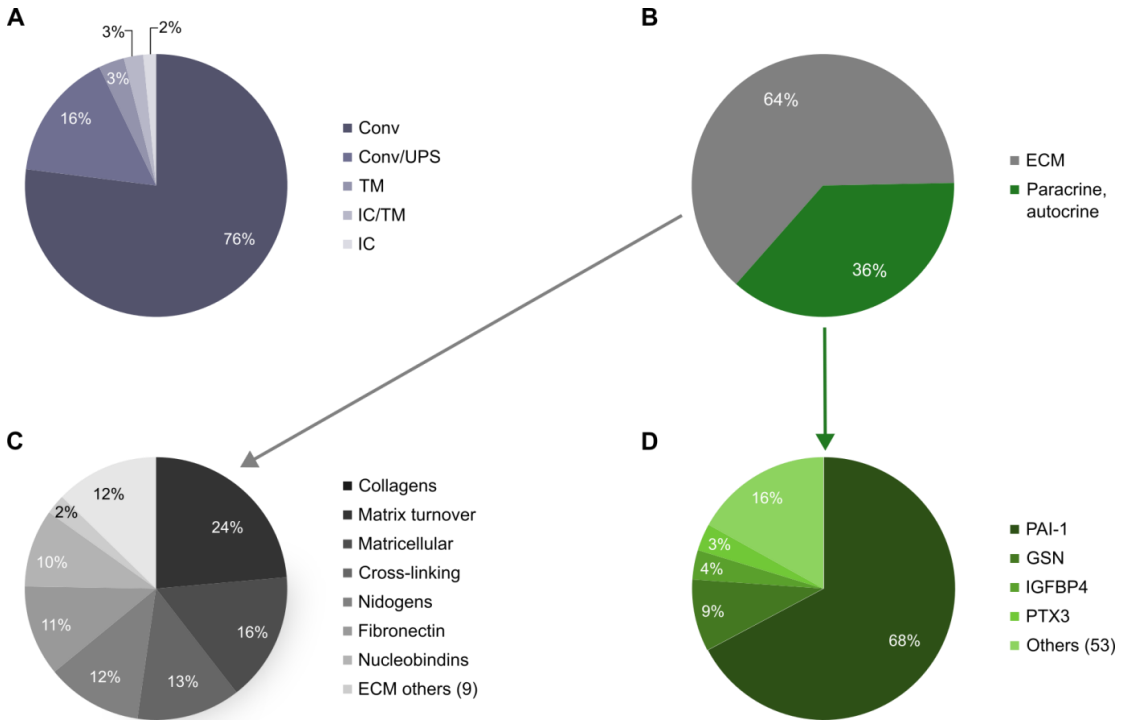

Figure 19: Basal protein secretion of cultivated CF identified 122 proteins. CF were isolated from C57Bl/6 mice 5 d post Sham surgery. Secretome was analyzed using LC-MS/MS and identified 122 proteins (n=4 CF preparations). **A)** Secretory pathways were predicted using prediction tool OutCyte[105]. Numbers of identified proteins that were conventionally secreted (Conv), unconventionally secreted (UPS), intracellular (IC) and transmembrane (TM) proteins are shown. **B)** Intensity distribution of extracellular matrix (ECM) related proteins and other paracrine and autocrine proteins categorized by KEGG annotation and PubMed search. **C)** Intensity distribution of different subcategories within ECM-related proteins. **D)** Intensity distribution of secreted paracrine and autocrine factors.

In addition to ECM-associated proteins, paracrine and autocrine factors were also detectable in the basal secretome, amounting to 36% of all measured protein intensities (Figure 19B). Among all these factors, plasminogen activator inhibitor 1 (PAI-1, *Serpine1*) showed by far the highest intensity distribution (68%), followed by gelsolin (GSN) with 9%, insulin like growth factor binding protein 4 (IGFBP4) showing an intensity distribution of 4%, and pentraxin-related protein 3 (PTX3) with 3% (Figure 19D).

To explore whether the identified proteins are predominantly expressed by CF or other cell types, previously published snRNA-seq data from hearts of healthy 12 weeks-old mice, as published by Vidal *et al.*[107], was analyzed for gene expression of identified proteins (Figure 20). This dataset included cardiomyocytes, immune cells, fibroblasts, pericytes and SMC, EC, endocardial cells, and Schwann cells. The ECM-associated secretome proteins, like different collagens, laminins, lysyl oxidases, decorin (DCN), and nidogen 1 (NID1), showed a notable gene expression in CF (Figure 20A). In addition, several autocrine/paracrine factors were preferentially expressed in CF like *Axl*, *Frzb*, *Fstl1*, *Gsn*, *Pcsk6*, *Serpinf1*, *Svep1,* and *Wisp2* (Figure 20B).

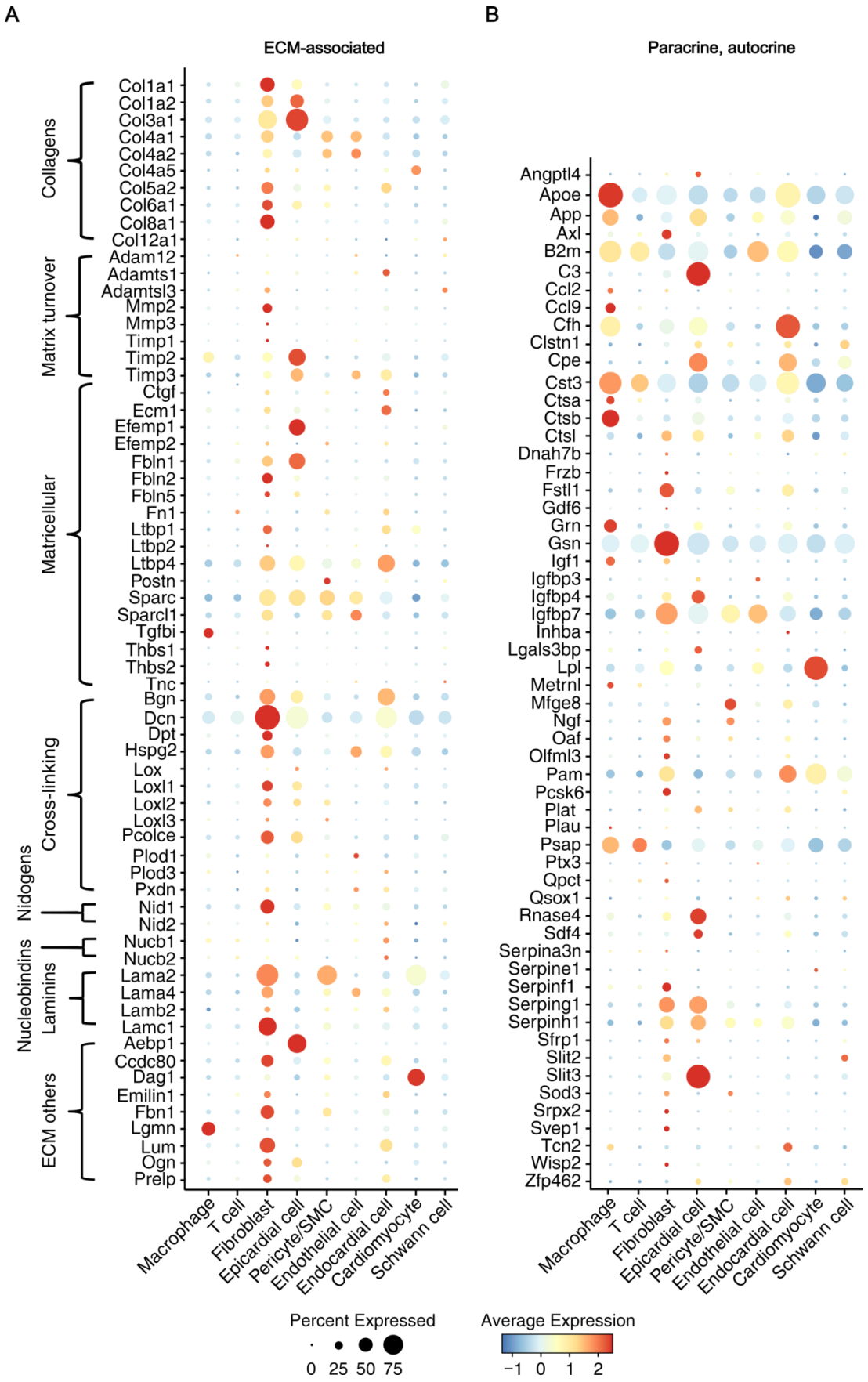

Figure 20: Genes of the identified basally secreted proteins were notably expressed by CF. Cardiac snRNA-seq data from a single healthy 12-week-old mouse, published by Vidal *et al.*[107] (sample Y1, 3790 cells), was analyzed for cellular gene expression distribution of **A)** ECM-related genes and **B)** paracrine/autocrine factors.

4.3.2 Secretome analysis of cultured CF after MI

To elucidate the impact of MI on the protein secretion of murine CF, a comparative quantitative secretome analysis was performed using the established method outlined in Figure 18. LC-MS/MS was employed to analyze the secretome of CF isolated 3 d or 5 d after MI (50 min ischemia/reperfusion) and Sham-operated controls.

The secretome analysis of CF isolated 3 d after MI identified a total of 129 proteins (dataset see Supplements Table 29), of which 49 were not detectable in the Sham-operated control secretome (Figure 21A). Among all secreted proteins, 79 showed significantly higher abundance after MI compared to control (Figure 21C). Analyzing the secretomes 5 d post MI and Sham (dataset see Appendix; Table 28) identified 31 proteins exclusively detectable post infarction, along with 122 proteins found in both secretomes (Figure 21B). Of these, 28 proteins displayed significantly higher abundance post MI compared to Sham (Figure 21D).

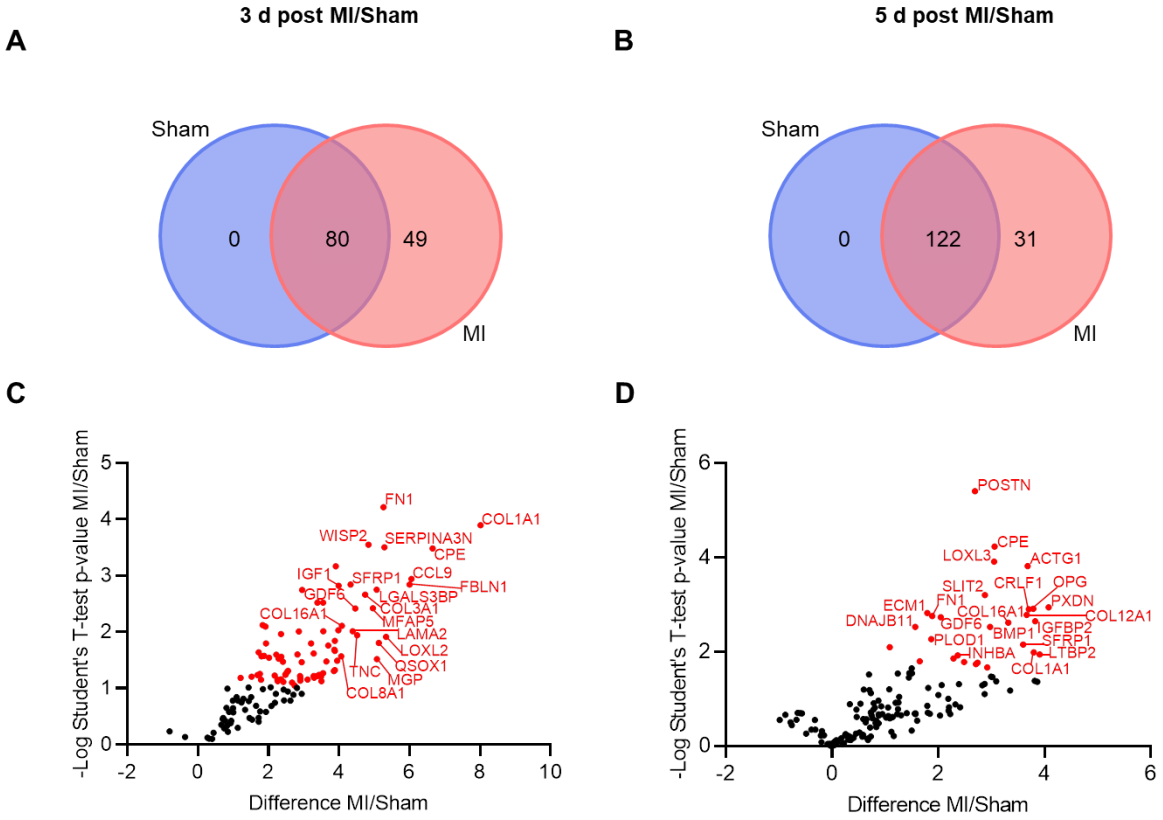

Figure 21: MI altered protein secretion of CF. CF were isolated from C57Bl/6 mice 3 d and 5 d after MI (50 min ischemia/reperfusion) and Sham and cultivated. Secreted proteins were analyzed using LC-MS/MS (n=4). **A-B)** Venn diagrams of identified proteins **A)** 3 d after surgery **B)** 5 d after surgery. **C-D)** Volcano plots of secreted proteins that were detected and quantified in the secretome of CF after MI compared to Sham **C)** 3 d and **D)** 5 d after surgery. To determine different abundant proteins, Student's t-test-based significance analysis of microarray approach (Tusher *et al.*, 2001)[103] was used. For statistical significance analysis of proteins exclusively detected post MI, an imputation approach of missing base values was performed, using values from a downshifted normal distribution. Proteins with significant differences in intensity (Student's t-test-based SAM analysis, 5% FDR, S_0=0.6) are highlighted in red. Top 20 significantly altered proteins with highest differences between MI and Sham are annotated. The shown differences refer to the difference of group mean values of Log_2 transformed intensities.

The identified proteins were once again categorized into ECM-related and paracrine/autocrine factors. ECM-related proteins were further subdivided into collagens, matrix turnover proteins, matricellular proteins, matrix cross-linkers, and laminins. Paracrine/autocrine proteins were classified based on their functions in growth regulation, Wnt-pathway regulation, inflammatory response, cell development, cell adhesion, angiogenesis, and signal transduction using KEGG annotation and PubMed search.

Out of the 71 ECM-related detected 3 d post MI/Sham, 43 were significantly higher abundant post MI (framed proteins in Figure 22A). The group of collagens, especially COL1A1 and COL16A1, showed the highest fold changes between MI and Sham (COL1A1: 159.3-fold, COL16A1: 112.1-fold), and COL12A1 was exclusively detectable post MI (shown in purple). Matrix turnover proteins, including matrix metalloproteinase 2 (MMP2: 3.4-fold) and nidogen 1 (NID1: 2.2-fold), were significantly increased, while A disintegrin and metalloproteinase 12 (ADAM12), A disintegrin and metalloproteinase with thrombospondin motifs 1 (ADAMTS1), and nidogen 2 (NID2) were exclusively detectable 3 d post MI. In the group of matricellular factors, almost all proteins were significantly higher abundant 3 d post MI compared to Sham, such as extracellular matrix protein 1 (ECM1: 6.5-fold), different fibulins (FBLN), latent TGF-β binding proteins (LTBP), FN1 (9.5-fold), SPARC (3.4-fold), POSTN (4.5-fold), and transforming growth factor inducible (TGFBI: 14.4-fold). LTBP3 and TNC were only detectable post infarction. Furthermore, matrix cross-linkers like LOX were significantly enhanced, with lysyl oxidase homolog 3 (LOXL3) showing the highest fold change (17.7-fold). Additionally, peroxidasin (PXDN) and procollagen C-endopeptidase enhancer 2 (PCOLCE2) were significantly altered and only detectable post MI. Out of four different detected laminins, three were significantly higher abundant 3 d post MI.

Within the paracrine and autocrine factors obtained 3 d post MI/Sham, 36 out of 58 proteins were significantly increased post MI (Figure 22A bottom). The growth regulators apolipoprotein E (APOE: 11.0-fold), growth differentiation factor 6 (GDF6: 8.2-fold), inhibin subunit beta A (INHBA: 3.5-fold), and quiescin sulfhydryl oxidase 1 (QSOX1: 9.1-fold) were significantly higher abundant 3 d post MI compared to Sham, while insulin-like growth factor 1 (IGF1) and insulin-like growth factor binding protein 7 (IGFBP7) were only detectable post MI. Detected proteins related with the Wnt-pathway were all elevated 3 d post MI compared to Sham, with frizzled related protein (FRZB: 4.0-fold) and sushi repeat-containing protein 2 (SRPX2: 2.9-fold) being significantly enhanced, and secreted frizzled-related protein-1 (SFRP1), WNT1-inducible-signaling pathway protein 2 (WISP2), and sushi repeat-containing protein (SRPX) being only detectable post MI. Proteins associated with inflammatory response, such as beta-2 microglobulin (B2M; 3.0-fold), C1-esterase-inhibitor (C1-INH; 6.7-fold), chemokine (C-C motif) ligand 9 (CCL9; 29.3-fold), and serine protease inhibitor A3N (SERPINA3N: only detectable post MI) were also significantly enhanced 3 d post MI compared to Sham. The following proteins associated with cell development were also significantly increased post MI: granulin (GRN: 3.3-fold), prosaposin (PSAP: 9.2-fold), and DNAJB11 (only detectable post MI). Among the proteins associated with cell adhesion, four were significantly increased, including milk fat globule EGF factor 8 (MFGE8: 3.7-fold) and galectin 3 binding protein (LGALS3BP: 22.3-fold). Furthermore, all proteins described with an angiogenic function (pigment epithelium-derived factor; PEDF: 5.1-fold, slit guidance ligand 2; SLIT2: 5.4-fold, slit guidance ligand 3; SLIT3: 12.0-fold, follistatin-related protein 1; FSTL: only detectable post MI) and signal transduction (carboxypeptidase E; CPE: 58.2-fold, osteoprotegerin; OPG: only detectable post MI) were significantly higher abundant 3 d post MI compared to Sham.

Most of the detected proteins 3 d post MI/Sham were also detectable 5 d post MI/Sham but showed a lower intensity distribution fold change between MI and Sham. Only 17 out of 79 ECM-related proteins were significantly higher abundant 5 d post MI compared to Sham (Figure 22B). Among them were three collagens: COL1A1 (9.9-fold), COL12A1 (11.1-fold), and COL16A1 (only detectable post MI). Additionally, metalloproteinase 3 inhibitor (TIMP3; 9.0-fold) was significantly increased post MI, while MMP3 was decreased (0.7-fold). Furthermore, four matricellular proteins (ECM1: 3.2-fold, FN1: 3.5-fold, LTBP2: 7.5-fold, and POSTN: 6.4-fold) and matrix cross-linkers (LOX: 2.0-fold, LOXL3: 8.4-fold, PLOD1:3.5-fold, and PXDN: 8.3-fold) were significantly elevated 5 d post MI compared to Sham. Only two laminins were still significantly elevated 5 d post MI: LAMA2 (3.4-fold) and LAMA4 (1.6-fold). Interestingly, fibromodulin (FMOD) was only detectable 5 d post MI, and further matrilin 2 (MATN2) was detectable only post MI (both 3 d and 5 d). Protein functions in the post MI heart will be discussed later (see section 5.3).

Among the paracrine/autocrine factors 11 (out of 74) were significantly altered 5 d post MI compared to Sham (Figure 22B bottom). The growth regulators GDF6 (4.0-fold) and INHBA (4.3-fold) were not only significantly altered 3 d post MI but also 5 d post MI compared to Sham. Additionally, IGFBP2 was only detectable 5 d post MI but in no other secretome. Within the Wnt/β-catenin pathway-related proteins only SFRP1 (4.6-fold) was still significantly elevated 5 d post MI compared to Sham. SEMA7A (only detected post MI) was the only protein among the inflammatory proteins which was significantly altered 5 d post MI compared to Sham. Whereas the cell developmental protein DNAJB11 again was significantly higher abundant and only detectable post MI. The angiogenic SLIT2, which had already been significantly increased 3 d post MI, was also elevated 5 d post MI compared to Sham (6.7-fold-fold). Furthermore, signal transduction proteins CPE (8.0-fold) and OPG (only detectable post MI) were again significantly higher abundant 5 d post MI, and cytokine receptor like factor 1 (CRLF1: only detectable post MI) was added at this timepoint.

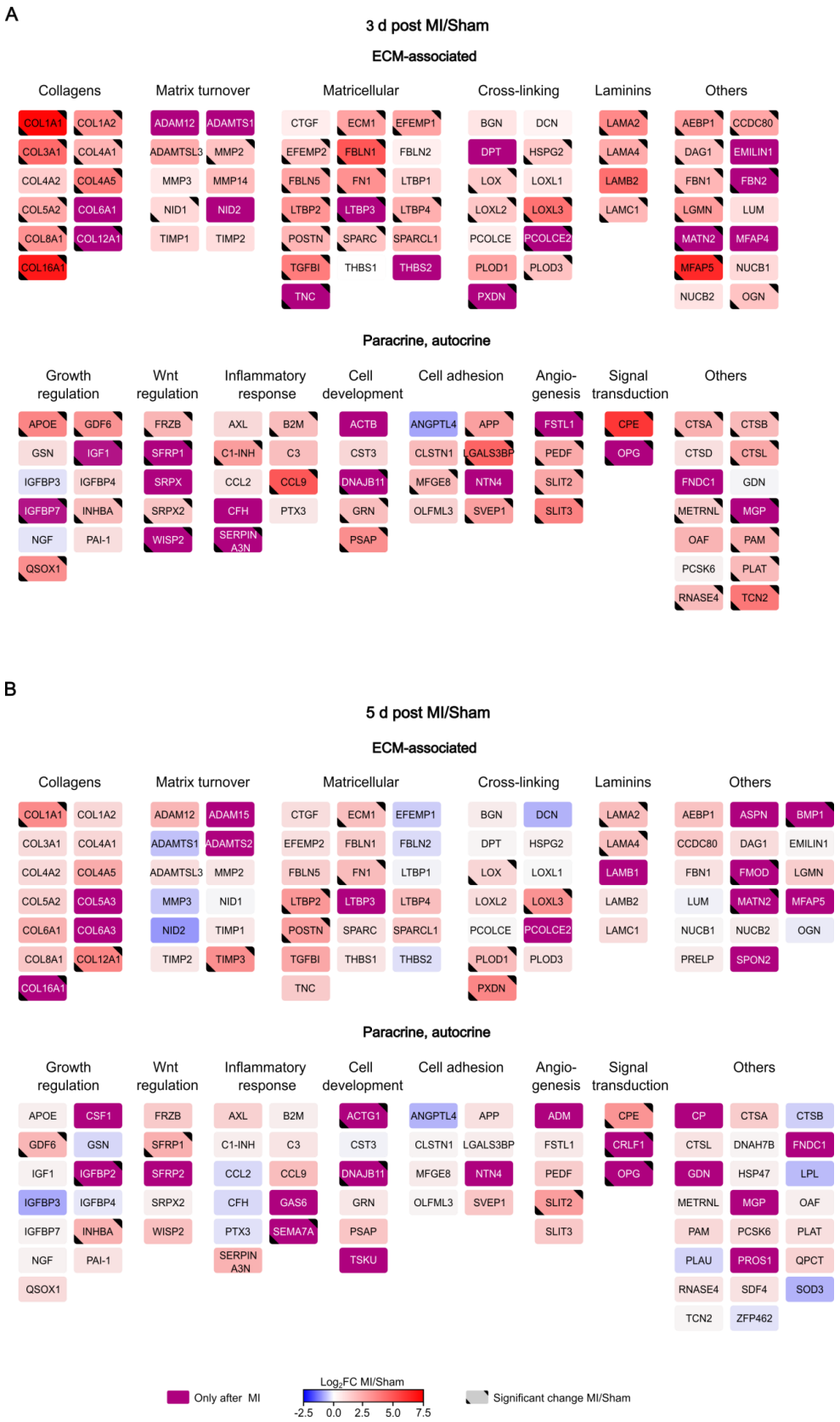

Figure 22: MI-induced changes in the secretome of cultivated CF 3 d/5 d post MI compared to Sham. CF from C57Bl/6 mice were isolated and cultivated 3 d and 5 d after MI (50 min ischemia/reperfusion) and Sham. Secreted proteins were analyzed using LC-MS/MS (n=4). Differences in proteins intensities between CF after MI and Sham surgery are shown as Log_2 fold changes (Log_2FC) of protein intensities **A)** 3 d post MI/Sham **B)** 5 d after intervention. Proteins were subcategorized into ECM-associated and paracrine/autocrine factors. Log_2FC is represented with fill color. Proteins only detectable post MI are shown in purple. Significant changes in proteins are shown with a black border (Student's t-test-based SAM analysis, 5% FDR, S_0=0.6).

4.3.3 Gene ontology analysis of CF-secreted proteins after MI

To identify the biological processes that are associated with CF-secreted proteins after MI, the 15 most significantly enriched GO biological process terms of secretome proteins significantly higher in abundance post MI compared to Sham were determined and listed based on their p-value (Figure 23). The analysis was conducted using the "David Functional Annotation Tool"[113,114] based on "GOTERM_BP_DIRECT".

Secreted proteins that exhibited a significantly higher abundance 3 d post MI were predominantly associated with extracellular matrix organization (27%) and cell adhesion (24%) (Figure 23A). Additionally, proteins were associated with angiogenesis (13%), collagen fibril organization (12%), and wound healing (10%).

Proteins significantly higher abundant 5 d post MI were primarily annotated with extracellular matrix organization (25%), and cell adhesion (25%) (Figure 23B). Furthermore, they were associated with response to drug (21%), collagen fibril organization (18%), angiogenesis (14%), positive regulation of cell migration (14%), axon guidance (14%), and wound healing (14%). This indicates that the identified secreted proteins likely play a role in regulating various CF responses to MI, especially in angiogenesis, cell adhesion, ECM organization, and collagen organization and assembly.

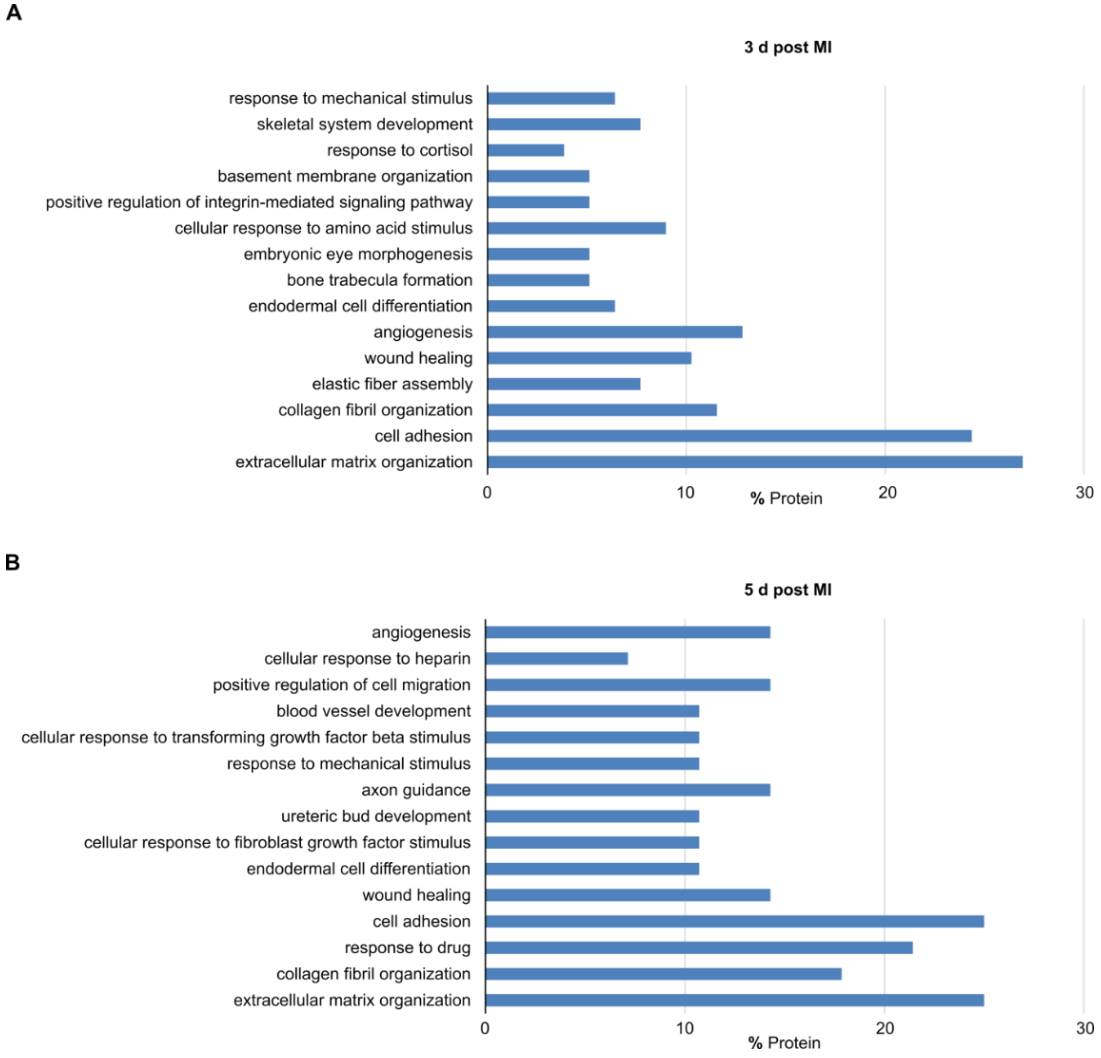

Figure 23: CF-secreted proteins post MI are associated with biological processes like ECM organization and cell adhesion. CF were isolated from C57Bl/6 mice 3 d and 5 d after MI (50 min ischemia/reperfusion) and

Sham and cultivated. The secreted proteins were analyzed using LC-MS/MS (n=4 CF preparations) and compared between MI and Sham samples. GO biological process terms annotated to the significantly higher abundant proteins post MI were identified and analyzed for enrichment using “David Functional Annotation Tool” based on “GOTERM_BP_DIRECT”. The 15 most significantly enriched GO biological process terms are listed according to their p-value **A)** for secreted proteins that were significantly higher abundant 3 d post MI and **B)** 5 d post MI compared to Sham.

4.3.4 Gene expression levels of CF-secreted proteins 5 d post MI compared to Sham

To explore whether the observations on protein level are mirrored at the gene level, published CF scRNA-seq data sets obtained under identical experimental conditions (CF isolated from C57Bl/6 Sham-operated control hearts and infarcted hearts 5 d post-surgery[109]) were analyzed for expression of the significantly altered secreted proteins 5 d post MI. As shown in Figure 24A, the expression of genes encoding ECM-associated proteins was mostly upregulated 5 d after MI compared to Sham (12 out of 17 transcript levels), and all paracrine/autocrine factors were higher expressed post MI. This indicates an interdependence between protein secretion and gene expression. To evaluate whether CF are the preferential source of the identified secretome proteins that were upregulated after MI, gene expression 5 d post MI was analyzed in published scRNA-seq data[108] of different heart cell types (including macrophages, dendritic cells (DC), granulocytes, T cells, B cells, nine subtypes of CF, EPDC, pericytes, and EC but excluding CM). Genes encoding the secreted proteins were mainly expressed by different subpopulations of CF (Figure 24B). Interestingly, some genes were also expressed by EPDC, pericytes, or endothelial cells, such as *Plod1* (procollagen-lysine, 2-oxoglutarate 5-dioxygenase 1), *Cpe*, or *Tnfrsf11b* (corresponding protein OPG). Most of the genes encoding the significantly altered secretome proteins (5 d post MI/Sham) were primarily expressed by CF, and approximately 70% of all genes were upregulated after MI compared to Sham.

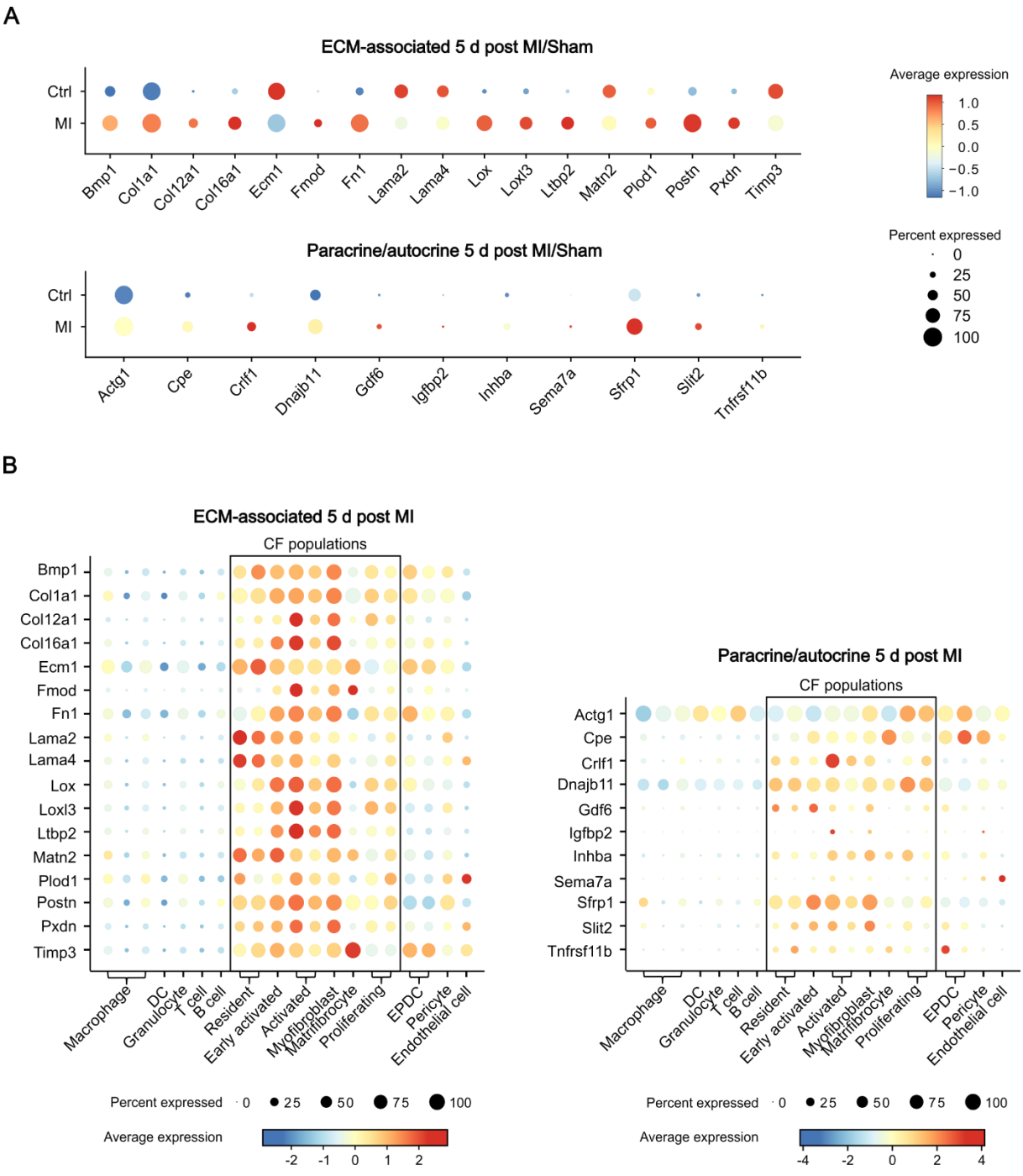

Figure 24: Corresponding genes of the upregulated proteins 5 d post MI were upregulated on gene level and mostly expressed by CF. A) CF gene expression levels of the significantly upregulated secretome proteins 5 d post MI (50 min ischemia/reperfusion) were analyzed in CF data of a published scRNA-seq analysis 5 d post MI/Sham (n=3 CF preparations)[109]. Expression levels in the total CF population are visualized as dot plots. **B)** Gene expression levels of the significantly upregulated secretome proteins 5 d post MI were analyzed in different cardiac cell types of a previously published scRNA-seq analysis 5 d post MI (n=3)[108] (macrophages, dendritic cells (DC), granulocytes, T cells, B cells, fibroblasts, epicardium-derived cells (EPDC), pericytes, and EC).

4.4 Specific *in vivo* secretome analysis of POSTN$^+$ CF

Given that the secretome of cultivated CF post MI, despite the short culture period, may not precisely reflect the *in vivo* situation, a CF-specific secretome analysis of CF *in vivo* was elaborated next, using proximity labeling according to Wei *et al.*, 2021[84], who developed this method for hepatocyte-specific secretome analysis in blood serum. As the majority of proteins found in the *in vitro* CF secretome analysis were conventionally secreted (see Figure 19), an ER-localized TurboID (ER-TurboID) seemed appropriate for biotin labeling of the secreted proteins. To target the dynamic changes of the CF post MI, which express *Postn* to a high extent, an AAV9 vector system with expression of ER-TurboID under the control of the *Postn* promoter (AAV9-POSTN-ER-TurboID) was generated (see Appendix; Figure 33). As CF represent only a small amount of heart cells (see Figure 1), proteins secreted by CF are most likely not easily detectable in blood serum. Therefore, previously labeled hearts were perfused with Krebs-Henseleit buffer, and coronary effluent was collected and analyzed for biotinylated proteins. Practically, AAV9-POSTN-ER-TurboID was injected into the tail vein of C57Bl/6 mice one day post MI/Sham, leading to the expression of ER-TurboID in POSTN$^+$ CF. For labeling proximate proteins with the help of TurboID, biotin was administered to mice via drinking water. After labeling, coronary effluent was collected from perfused hearts, biotinylated proteins enriched using streptavidin beads, and analyzed via LC-MS/MS (see Figure 9).

4.4.1 Establishment of POSTN$^+$ CF specific *in vivo* secretome analysis

In order to establish the POSTN$^+$ CF-specific secretome analysis under *in vivo* conditions, certain parameters, such as the level of TurboID expression and its cell-specificity, had to be validated before initiating the secretome analysis.

4.4.1.1 Validation of TurboID expression post MI

To ensure that ER-TurboID is exclusively expressed in POSTN$^+$ CF after transducing mice with AAV9-POSTN-ER-TurboID, an immunofluorescence staining of frozen heart sections (see section 3.14) from transduced mice 5 d after MI or Sham surgery was performed. ER-TurboID expression was detected using antibodies specific for its V5-tag (see Figure 9 and Appendix; Figure 32), and its distribution was compared to POSTN expression in the cardiac tissue. Immunofluorescence images of the Sham-operated control heart were negative for POSTN and V5 (Figure 25). In contrast, there were numerous POSTN-positive cells in the heart section after MI. Most importantly, there was a positive signal for V5-tagged TurboID, which overlapped with the POSTN signal.

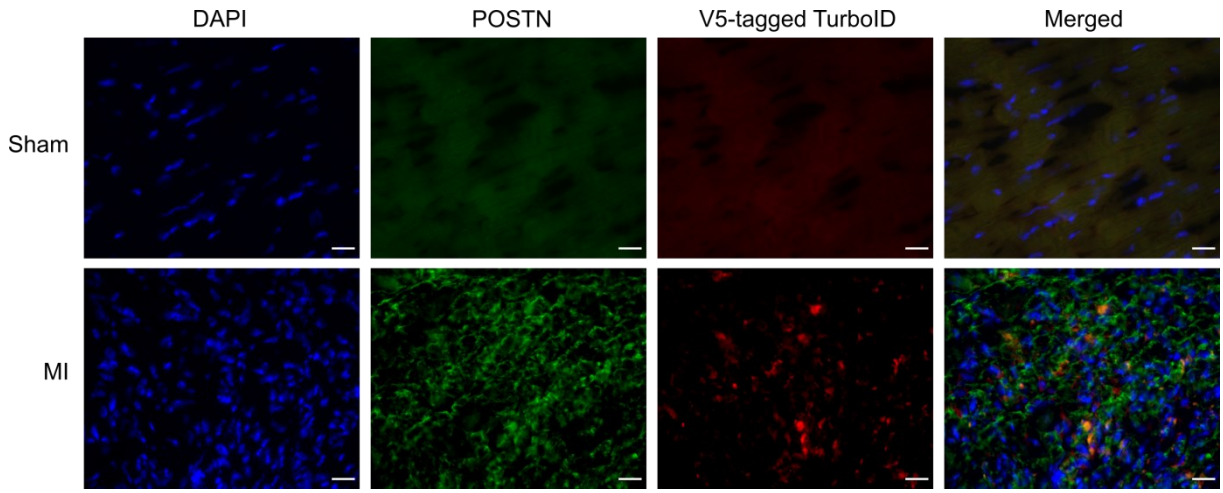

Figure 25: TurboID was expressed by POSTN⁺ CF after MI. Frozen heart sections from C57Bl/6 mice, 5 d after MI (50 min ischemia/reperfusion), or Sham surgery, which were transduced with AAV9-POSTN-ER-TurboID, were subjected to immunofluorescence staining for POSTN (green) and V5-tagged TurboID (red). Nuclei were counterstained with DAPI (blue). Scale bar: 20 µm. DAPI, AlexaFluor488, and AlexaFluor594 were used for staining. Representative image from n=3 experiments, including one heart each from Sham and MI conditions.

4.4.1.2 TurboID-mediated protein biotinylation in different tissues

The specificity of TurboID expression in POSTN-positive cells within the heart was confirmed by detecting TurboID exclusively in POSTN⁺ cells using its V5-tag. However, considering that AAV9 may target tissues beyond the heart, the expression of TurboID was assessed in other organs. Therefore, mice which underwent MI (50 min ischemia/reperfusion) or Sham surgery were transduced with AAV9-POSTN-ER-TurboID and received biotin via drinking water for three consecutive days. Untransduced MI-treated mice were used as controls. Five days after surgery, the organs were lysed (see section 3.16.3), and protein levels of POSTN, V5-tag, and Biotin were evaluated through Western Blot (see section 3.12).

V5-tagged TurboID (~51 kDa) was detectable in the liver tissue of AAV-transduced mice (Figure 26), confirming expression in extracardiac tissues. POSTN (~93 kDa) was observed in the liver, pancreas, and to a lesser extent, in kidney and spleen.

Notably, in the liver samples of AAV-transduced mice, a robust signal of biotinylated proteins (Figure 26) was observed, irrespective of whether the mice underwent MI or Sham. A similar pattern was also observed in lung and spleen, although the Biotin signal in these organs was generally lower. Given that the liver is a known producer of various plasma proteins and considering the assessment of POSTN and V5-tag in liver tissue, it is plausible that biotinylated liver proteins may also be present in blood plasma, which cannot be completely ruled out from the collected coronary effluent.

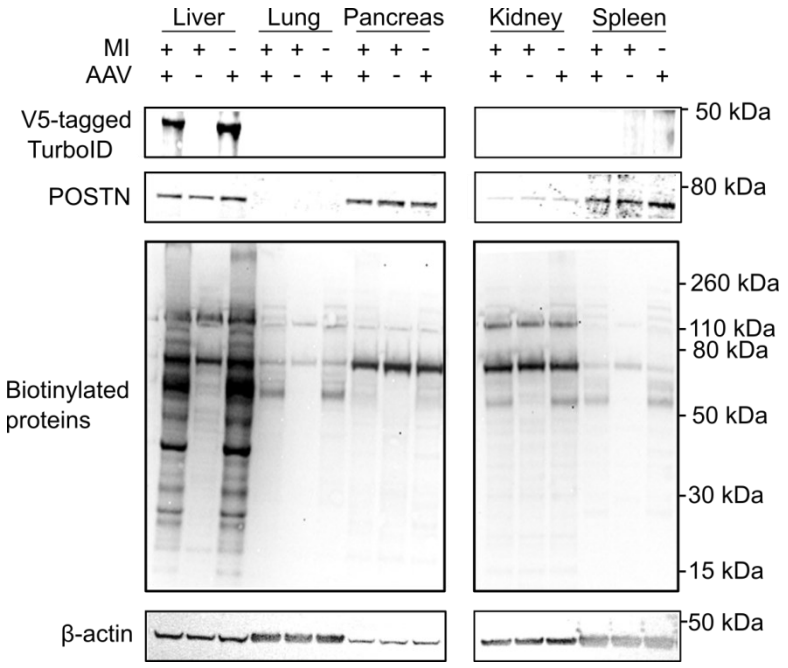

Figure 26: TurboID was expressed in the liver. Various organs from C57Bl/6 mice (excluding hearts, as they were utilized for the collection of coronary effluent) that were transduced with AAV9-POSTN-ER-TurboID after MI (50 min ischemia/reperfusion) or Sham surgery, along with organs from untransduced mice after MI, were lysed and analyzed by Western Blot for V5-tag, POSTN, and β-actin (loading control) protein levels via specific antibodies and biotinylated proteins. Detection of V5-tagged TurboID (~51 kDa) was performed by chemiluminescence using a mouse anti-V5 tag antibody and goat anti-mouse IgG secondary antibody coupled with HRP and SuperSignal West Femto Maximum Sensitivity Substrate. POSTN (~93 kDa) was detected via chemiluminescence using rabbit anti-V5 tag antibody and goat anti-rabbit coupled with HRP as secondary antibody and SuperSignal West Femto Maximum Sensitivity Substrate. Housekeeping protein β-actin (~42 kDa) was detected using a mouse anti-β-actin antibody and secondary antibody goat anti-mouse IgG AF-800 using a filter range of 810-850 nm. Biotinylated proteins were detected via chemiluminescence using AP-coupled streptavidin. For Bis-Tris gel electrophoresis, 20 ng of protein was applied per sample. Novex Sharp Pre-stained protein standard (3 µl) served as protein ladder. Representative image of n=3 experiments. All stainings were performed on the same blot, with the blot being stripped between different stainings using Restore Western Blot Stripping Buffer for 15-30 min.

4.4.1.3 Protein distribution in the coronary effluent

To assess the impact of liver-derived biotinylated plasma proteins on *in vivo* secretome analysis using biotinylated proteins from coronary effluent, the washout of these proteins from the isolated heart over time was investigated. Coronary effluent was collected (see section 3.5) at 10 min intervals for 60 min after the start of perfusion, and protein silver staining (see section 3.11.1) was performed. In the first fraction (0-10 min of perfusion), a prominent protein band between 60 kDa and 70 kDa was observed (Figure 27), corresponding to the molecular weight of the plasma protein albumin (66 kDa). Additionally, a robust protein band at 15 kDa, aligning with the molecular weight of hemoglobin, was also detected. Various proteins of different sizes were present in all fractions, with intensities decreasing over time. To minimize blood plasma contaminations for the subjected secretome analysist, the first 10 min of effluent were excluded.

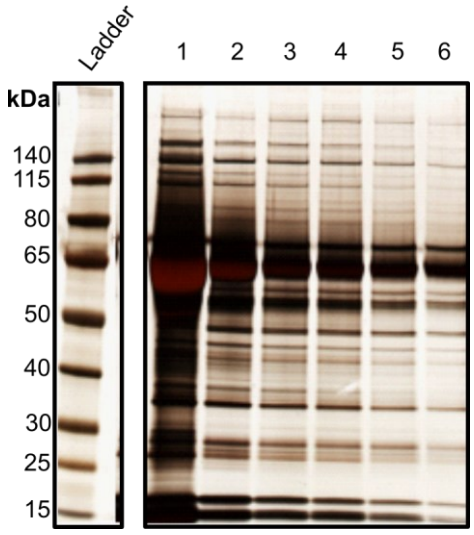

Figure 27: Protein concentrations in coronary effluent were highest in the first 10 min of effluent collection. A C57Bl/6 mouse heart was taken and cannulated via the aorta and perfused with Krebs-Henseleit buffer on a Langendorff apparatus under a constant pressure of 80 mmHg. Effluent was collected over 60 min in 10 min intervals (fractions 1-6). One-tenth of each effluent sample was loaded onto a polyacrylamide gel, and proteins were visualized using silver staining. To analyze protein sizes, PageRuler Prestained was used as a molecular weight ladder. Image of n=1 experiment.

4.4.1.4 Detection of TurboID-mediated biotinylated proteins in the coronary effluent

Since CF constitute only a minor fraction of all heart cells, it was investigated if biotinylated proteins are detectable in the coronary effluent using Western Blot. Therefore, coronary effluent was collected from AAV9-POSTN-ER-TurboID transduced mice post MI/Sham that received biotin via drinking water, and mice that did not receive exogenous biotin after with a 10 min washout period.

At the protein level, V5-tagged TurboID was detected in the MI effluents, while only a very faint signal was observed in Sham effluents (Figure 28, top). This observation aligns with the increase in the number of $POSTN^+$ CF and thus TurboID expressing CF after MI. POSTN was detectable in Sham and MI effluents (Figure 28, middle), indicating the presence of $POSTN^+$ CF in Sham hearts. In mice subjected with MI or Sham and given biotin over three days, biotin-labeled proteins were found in the coronary effluent, whereas no biotinylated proteins were found in the effluent of mice that did not receive biotin (Figure 28, bottom lane 1). This demonstrates the effectiveness of TurboID-mediated biotinylation in the experimental setting.

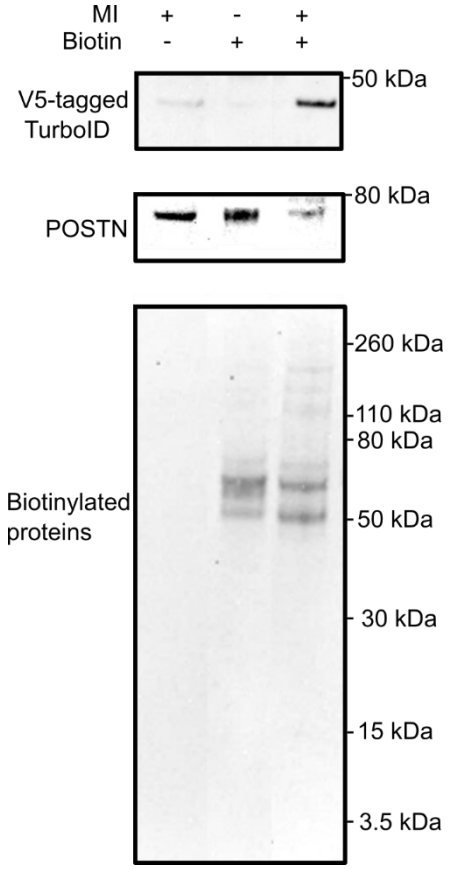

Figure 28: Biotinylated proteins in the coronary effluent were detected after TurboID-mediated biotinylation. Coronary effluents of C57Bl/6 mice, transduced with AAV9-POSTN-ER-TurboID after MI (50 min ischemia/reperfusion) or Sham surgery were analyzed by Western Blot for V5-tagged TurboID, POSTN, and biotinylated proteins. Mice received either biotin through drinking water or did not receive biotin. V5-tagged TurboID (~51 kDa) was visualized using chemiluminescence with mouse anti-V5 tag antibody, followed by a secondary antibody of goat anti-mouse IgG coupled with HRP and SuperSignal West Femto Maximum Sensitivity Substrate. POSTN (~93 kDa) was detected through chemiluminescence using rabbit anti-POSTN antibody and a secondary antibody of goat anti-rabbit IgG coupled with HRP and SuperSignal West Femto Maximum Sensitivity Substrate. Biotinylated proteins were detected through chemiluminescence utilizing AP-coupled streptavidin. For Bis-Tris gel electrophoresis, 20 ng of protein was applied per sample, and Novex Sharp Pre-stained protein standard served as protein ladder (3 µl). Representative image of n=2 experiments. All stainings were performed on the same blot, with intermediate stripping between different stainings using Restore Western Blot Stripping Buffer for 15-30 min.

4.4.2 *In vivo* secretome analysis of POSTN$^+$ CF

To characterize the protein secretion profile of *Postn*-expressing CF post MI *in vivo*, a secretome analysis was performed using TurboID-mediated protein biotinylation of POSTN$^+$ CF-secreted proteins (see 3.16 and Figure 9). To this end, coronary effluent was collected from AAV9-POSTN-ER-TurboID-transduced mice 5 d after MI or Sham surgery, and subsequently concentrated. Biotinylated proteins were enriched, and the secretome was identified using LC-MS/MS (see Figure 9).

The *in vivo* secretome of POSTN$^+$ CF identified 118 proteins (Figure 29A), with 116 proteins found after MI and 103 after Sham surgery. Seven proteins were significantly altered between MI and Sham (Figure 29B), including PEDF (3.5-fold). However, a notable heterogeneity was observed across different replicates (Figure 29C). Despite efforts to minimize plasma protein contamination by excluding the effluent from the first 10 min of perfusion, several identified

proteins likely originated from plasma contaminations, such as hemoglobin (HBB-B2, HBA2, HBBT1).

Interestingly, certain proteins that were upregulated in the secretome of cultivated CF 5 d post MI were also higher abundant in the *in vivo* secretome compared to Sham. These proteins include FN1 (6.7-fold), FBLN2 (1.4-fold), FBLN5 (only detectable post MI), BGN (only detectable post MI), NID1 (3.4-fold), and paracrine factors C1-INH (3.0-fold), SERPINA3N (2.4-fold), and C3 (2.0-fold). Overall, the measured intensity of all detected proteins in the coronary effluent was relatively low (see Figure 29C and Appendix; Table 29).

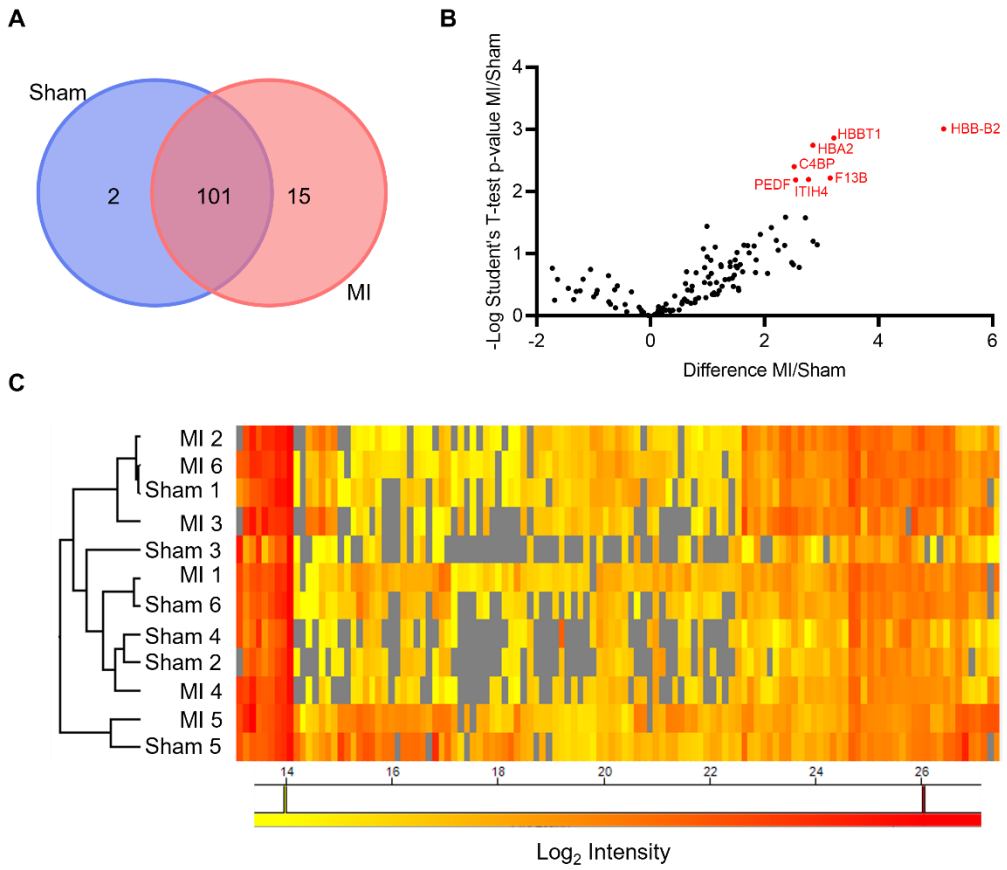

Figure 29: Secretome analysis of POSTN⁺ CF-secreted proteins *in vivo* was impeded by high plasma protein levels. MI and Sham-operated C57Bl/6 mice were transduced with AAV9-POSTN-ER-TurboID and received biotin via drinking water. Coronary effluents were collected 5 d after MI or Sham, and biotinylated proteins were enriched and analyzed by LC-MS/MS (n=6). **A)** Venn diagram of identified proteins. **B)** Volcano plot of identified proteins. To determine differentially abundant proteins, Student's t-test-based significance analysis of microarray approach (Tusher *et al.*, 2001)[103] was used. An imputation approach was applied to analyze secreted proteins detected only post MI, using values from a downshifted normal distribution. The displayed difference refers to the difference of group mean values of Log_2 transformed intensities. Proteins with significant differences in intensity (Student's t-test-based SAM analysis, 5% FDR, S_0=0.1) are highlighted in red. **C)** Peptides were analyzed via LC-MS/MS for their Log_2 intensity and distribution. Samples with similar profiles were linked.

4.4.3 Analysis of the POSTN⁺ CF-specific proteome

Due to challenges in achieving a successful secretome analysis of POSTN⁺ CF *in vivo*, primarily attributed to blood plasma contaminations and low of measured intensities, the examination of biotinylated proteins was redirected to the entire heart tissue. To this end,

perfused hearts were taken and lysed after effluent collection (see 3.16.3), followed by the enrichment of biotinylated proteins (see 3.16.5) and measurement using LC-MS/MS.

The proteome analysis identified 194 proteins (dataset see Appendix; Table 30), with 23 exclusively detectable 5 d post MI and 2 only detectable in the Sham-operated control (Figure 30A). There were 21 proteins which were significantly higher abundant post MI (Figure 30B) with HSP47 (16.8-fold), protein disulfide-isomerase (P4HB; 11.8-fold), and heat shock protein family A (Hsp70) member 5 (HSPA5; 6.5-fold) showing the highest fold changes. Furthermore, several proteins were only detectable post MI, including protein disulfide-isomerase A3 (PDIA3), melanoma inhibitory activity protein 3 (MIA3), reticulocalbin-3 (RCN3), coactosin-like protein (COTL1), and clusterin (CLU). Two of the significantly altered proteins were less abundant post MI: cytochrome c (CYC: 0.4-fold) and protein voltage-dependent anion-selective channel protein 1 (VDAC1: 0.5-fold). As expected, POSTN, coupled to TurboID and used as selective marker for aCF in this approach, was significantly higher abundant post MI compared to Sham.

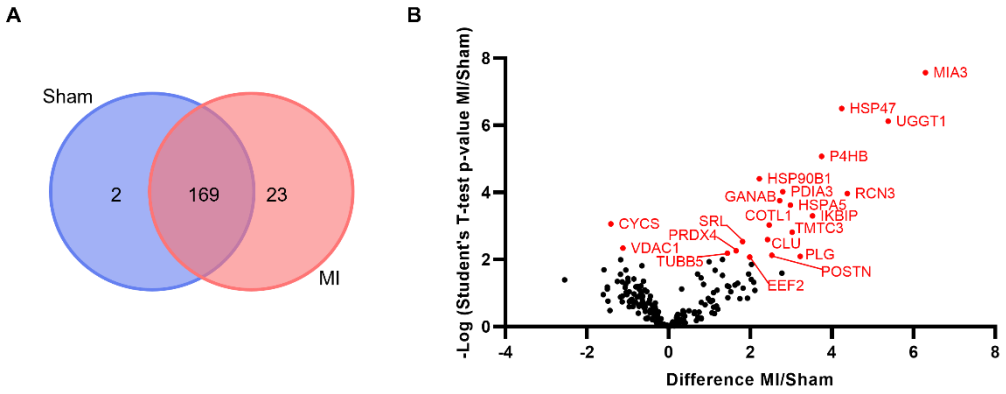

Figure 30: Actively produced intracellular proteins of POSTN$^+$ CF were detectable using *Postn*-controlled TurboID-mediated proximity biotinylation. Hearts from C57Bl/6 mice, transduced with AAV9-POSTN-ER-TurboID and receiving biotinylated drinking water, were taken 5 d after MI (50 min ischemia/reperfusion) or Sham. The hearts were digested after collection of coronary effluent. Biotinylated proteins were enriched from 300 µg cell lysate and analyzed using LC-MS/MS (n=6). **A)** Venn diagram of identified proteins. **B)** Volcano plot of identified proteins. To determine differentially abundant proteins, Student's t-test-based significance analysis of microarray approach (Tusher *et al.*, 2001)[103] was used. For the statistical significance analysis of secreted proteins exclusively detected post MI, an imputation approach of missing base values was applied, using values from a downshifted normal distribution. Proteins with significant differences in intensity (Student's t-test-based SAM analysis, 5% FDR, S_0=0.1) are highlighted in red and annotated. The shown difference represents the variance in group mean values of Log_2 transformed intensities.

Once more, scRNA-seq datasets obtained from CF isolated from C57Bl/6 Sham-operated control hearts and infarcted hearts 5 d post-surgery[109] were analyzed to identify intracellular proteins significantly altered *in vivo* 5 d post MI. The gene expression corresponding to significantly higher abundant proteins was upregulated in the majority of cases post MI (15 out of 19) (Figure 31A). Notably, gene expression of significantly lower abundant proteins such as VDAC1 was upregulated, while CYCS was downregulated, suggesting a correlation between protein production and gene expression. With the exception of *Cotl1* and *Eef2*, which were highly expressed by immune cells, genes were mainly expressed by CF or EPDC (Figure 31B). This observation indicates that these cell types serve as the primary cardiac source of proteins found to be significantly altered in the CF proteome.

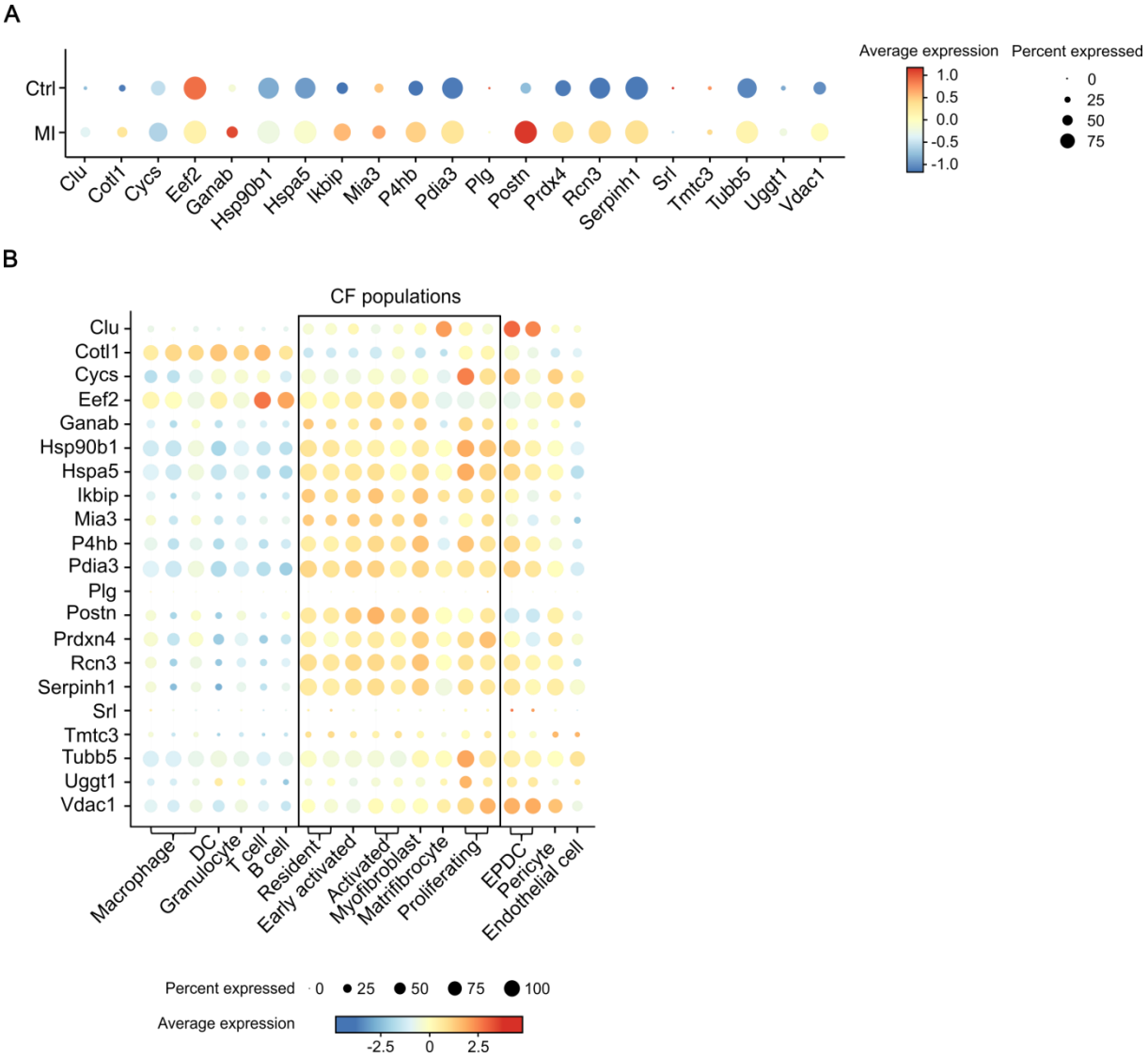

Figure 31: Production of significantly altered CF proteins 5 d post MI/Sham can be correlated to gene expression 5 d post MI/Sham. A) Analysis of CF gene expression levels for the significantly altered proteins of the *in vivo* proteome 5 d post MI/Sham. This analysis was conducted using previously published scRNA-seq CF data obtained 5 d post MI/Sham (n=3)[109]. Expression levels in the total CF population are visualized as dot plots. **B)** Gene expression levels of the significantly altered proteins in the *in vivo* proteome 5 d post MI were analyzed in the transcriptome of different cardiac cell types (macrophages, DC, granulocytes, T cells, B cells, CF, EPDC, pericytes, and endothelial cells) using previously published scRNA-seq analysis 5 d post MI (n=3)[108].

5. Discussion

In this study, secretome analysis of CF *in vitro* was successfully established using short term cultivation and pSILAC labeling combined with click-chemistry. Quantitative secretome analysis of CF post MI/Sham revealed that CF do not only secrete ECM-associated proteins but also various paracrine and autocrine molecules under both basal and post-ischemic conditions. These factors appear to play crucial roles in maintaining cardiac homeostasis and facilitating cardiac remodeling post MI.

Moreover, analysis of the *in vivo* CF proteome post MI was possible by implementing TurboID-mediated biotin labeling of the proteome of POSTN-positive CF in the heart. This innovative approach provided valuable insights into MI-mediated proteomic alterations of CF in the cardiac microenvironment.

5.1 Combining pSILAC labeling and click-chemistry for secretome analysis of fibroblasts

Secretome analysis of fibroblasts is challenging under serum-containing conditions due to the limitations in detection of low abundant proteins[76]. Previous studies, for this reason, resorted to serum starvation for exploring the CF secretome, although it is known that lower serum concentrations lead to changes in protein secretion[77]. This phenomenon was also observed in the present study (see Figure 15), using the fibroblast cell line NHDF for method validation and optimization. Serum starvation for 6 h already resulted in 123 significantly altered proteins compared to cultivation with medium containing 10% FBS. Additionally, the intensity distributions of proteins secreted under serum starvation were lower compared to the control.

To overcome these challenges and enrich bona fide secreted proteins from serum-containing supernatants, a combination of pSILAC labeling and click-chemistry[78] was adapted for fibroblasts and optimized to maintain optimal cultivation conditions. To this end, stable isotopes of Arg and Lys along with the Met analogue AHA, were used for labeling.

LC-MS/MS changes in cellular pathways of NHDF cells (see Figure 16) 6 h after AHA labeling, for example translational and ribosomal proteins were lower abundant in the proteome compared to control. These changes increased after 24 h of AHA labeling. Furthermore, proteins associated with the ER, glycosylation, and ECM were higher abundant after 24 h of AHA labeling. This suggests that classical protein secretion may be impaired when AHA labeling is used for longer time periods.

5.2 Defining the CF secretome under basal conditions

Upon closer examinations of secretion pathways from CF-secreted proteins, it was observed that 92% of the detected proteins were predicted to be secreted either conventionally or unconventionally (see Figure 19A). This clearly confirms the reliability of the established method for quantitative secretome analysis of proteins being secreted. Notably, transmembrane proteins were most likely released into the secretome through ectodomain shedding, a process mediated by metalloproteases such as ADAMs (which were also identified as being secreted by CF) known to cleave TM proteins in the trans-Golgi network[115].

Analysis of CF-secreted proteins under basal conditions (5 d post Sham) revealed the presence of both ECM-associated (64% of the total measured protein intensities) and paracrine/autocrine proteins (see Figure 19B). Among the ECM-associated proteins, collagens showed the highest intensity, followed by matrix turnover proteins, matricellular proteins, and matrix cross-linker (Figure 19C). This indicates that CF are highly likely to play a role in regulating the balance between ECM synthesis and degradation.

Table 23 summarizes the known functions of CF-secreted paracrine factors, identified in the secretome of basal CF. As depicted, PAI-1, representing 68% of the total intensity proportion (see Figure 19D), plays a crucial role in regulating the fibrinolytic system, MMP activities, TGF-β activation, and cell adhesion[116,117]. A global knockout of PAI-1 has been associated with cardiac fibrosis[118], emphasizing its importance in maintaining cardiac homeostasis and preserving cardiac function under stress conditions. Furthermore, cardiac fibrosis mediator[119] GSN showed a high intensity distribution of 9%. In contrast, the detected insulin like growth factor binding protein 4 (IGFBP4), known to be anti-fibrotic[120], may counterbalance the fibrotic effects. Additionally, proteins were detected that are involved in the complement cascade regulation[121], like pentraxin-related protein 3 (PTX3), complement C3 (C3) which activates the humoral immune system[122], and complement factor H (CFH) that inhibits C3[123]. Furthermore, detected CCL2 secretion promotes immune cell migration and infiltration[124], while CCL9 has an anti-inflammatory function[125]. Moreover, the measured superoxide dismutase 3 (SOD3) and tyrosine-protein kinase receptor UFO (AXL), although not known to be secreted by CF yet, play a role in immune homeostasis[126]. Several detected proteins are known to inhibit angiogenesis, such as PEDF[127] and angiopoietin-like 4 (ANGPTL4)[128], while beta-nerve growth factor (NGF) has pro-angiogenic effects[129], and follistatin-related protein 1 (FSTL1) maintains vascular wall homeostasis[130]. Proprotein convertase subtilis/kexin 6 (PCSK6), not previously described in any relation to CF, regulates growth factors and senescence within cardiomyocytes[131]. Furthermore, the secreted IGF1 contributes to hormone and growth regulation[132]. Additionally, the detected lipoprotein lipase (LPL) serves as a regulator of the fatty acid metabolism[133]. These findings indicate that CF-secreted proteins have diverse functions in maintaining cardiac homeostasis by controlling fibrotic and immune response, angiogenesis, and metabolism.

Table 23: Known functions of CF-secreted paracrine factors identified in the secretome of basal CF. Known functions of secreted proteins from CF isolated from the mouse heart 5 d after Sham surgery (n=4 preparations). The proteins were selected through a PubMed search and are listed in decreasing intensity.

Protein	Function	Ref.
Plasminogen activator inhibitor 1 (PAI-1); *Serpine1*	regulation of the fibrinolytic system	116
Gelsolin (GSN); *Gsn*	mediator of cardiac fibrosis	119
Insulin like growth factor binding protein 4 (IGFBP4); *Igfbp4*	anti-fibrotic and promotes cardiogenesis	120,134
Pentraxin-related protein 3 (PTX3); *Ptx3*	component of the innate immune system	121
Complement C3 (C3); *C3*	activation of humoral immune response	122
Chemokine (C-C motif) ligand 2 (CCL2); *Ccl2*	regulates migration and infiltration of immune cells	124
Pigment epithelium-derived factor (PEDF); *Serpinf1*	potent inhibitor of angiogenesis	127

Protein	Function	Ref.
Beta-nerve growth factor (NGF); *Ngf*	beneficial effects on cardiomyocytes and angiogenesis	[129]
Chemokine (C-C motif) ligand 9 (CCL9); *Ccl9*	inhibits inflammation and fibrosis	[125]
Insulin-like growth factor 1 (IGF1); *Igf1*	regulates contractility, metabolism, senescence, autophagy and apoptosis	[132]
Angiopoietin-like 4 (ANGPTL4); *Angptl4*	anti-angiogenic modulatory factor	[128]
Complement factor H (CFH); *Cfh*	inhibits complement activation	[123]
Proprotein convertase subtilis/kexin 6 (PCSK6); *Pcsk6*	regulates growth factors and hormones and proteases and modulates CM senescence	[131]
Follistatin-related protein 1 (FSTL1); *Fstl1*	regulates construction of vascular wall	[130]
Lipoprotein lipase (LPL); *Lpl*	regulates fatty acid metabolism	[133]
Superoxide dismutase (SOD3); *Sod3*	redox signaling and modulation of inflammatory response	[126]
Receptor protein tyrosine kinase receptor UFO (AXL); *Axl*	mediates inflammation	[135]

Comparison of basal secretome protein levels to gene expression levels in snRNA-seq data of a 12-week-old mouse under basal conditions[107] indicated that most ECM-associated proteins were predominantly CF-expressed (see Figure 20). Among the paracrine/autocrine factors, not all proteins were mainly expressed by CF. However, *Gsn*, *Serpinf1*, *Fstl1*, *Axl*, and *Pcsk6* were predominantly expressed by CF.

In summary, CF have the ability to secrete various paracrine factors under basal conditions. These factors play a crucial role in maintaining tissue integrity and homeostasis under unstressed conditions by signaling to different cell types within the heart, including cardiomyocytes, immune cells, endothelial cells, pericytes, smooth muscle cells, and Schwann cells. This likely underscores the essential role of CF in maintaining cardiac homeostasis, as the secreted proteins can have divers functions such as regulation of inflammation[125], angiogenesis [127,128], and metabolism[132]. Furthermore, these proteins can also signal in an autocrine manner, for example, to regulate fibrosis[119]. Some proteins, like PCSK6 or AXL, are not described in any relation to CF yet but are expressed and secreted by them. These proteins should be examined more closely in relation to their function in CF, as they could be important modulators of CF-mediated cardiac homeostasis.

5.3 Comparative secretome analysis of CF after MI and Sham

CF play a crucial role in cardiac homeostasis in the healthy heart[23]. As homeostasis is disturbed after MI, this study also compared CF secretome after MI and Sham 3 and 5 days after intervention. In doing so, CF secretome in the late inflammatory phase and in the beginning of the proliferation phase post MI was analyzed.

In the CF secretome 3 d post MI, 79 proteins were significantly higher abundant compared to control (see Figure 21C), while 5 d post MI fewer proteins (28) were significantly altered (see Figure 21D). ScRNA-seq data 5 d post MI/Sham[68,108] revealed that most of the secreted proteins which were identified 5 d post MI were selectively expressed by CF (see Figure 24B) and upregulated after MI on the gene level (see Figure 24A), supporting the experimental validity and strongly suggesting that these factors play an important role in cardiac remodeling post MI.

CF-secreted proteins were subdivided into ECM-related and paracrine/autocrine factors (see Figure 22). On day 3 post MI, a total of 43 ECM-related proteins was significantly enhanced compared to Sham, while 5 d post MI, 17 proteins were significantly higher abundant. Table 24 summarizes published functions of these proteins in cardiac ischemic stress response, such as cardiac fibrosis, inflammation, angiogenesis, and CM survival.

As observed, following matrix degradation in the early inflammatory phase, new collagens are produced for matrix regeneration and stability. In this stage, the fibrillar collagen types I and III are involved, with collagen type I known to enhance fiber stiffness[136]. Chains of both collagen types were significantly higher abundant 3 d post MI (see Figure 22A). Additionally, non-fibrillar collagens like COL VI and VIII were significantly upregulated 3 d post MI. These collagen types are involved in CF activation and fibrosis[136].

For improvement of matrix stability, collagen fibers have to be cross-linked, for example, by different lysyl oxidases (LOX, LOXL1-3) and lysyl hydroxylases (PLOD1;3), which all showed a higher abundance 3 d and 5 d post MI compared to control. LOXL3 was especially significantly upregulated on both days and might have a profound impact on matrix integrity. Laminins are important for basement membrane assembly. They link to collagens of type IV with the help of nidogens[137]. In the inflammatory stage (3 d post MI) LAMA2, LAMA4, LAMB2, and LAMC1 were significantly higher abundant, while only LAMA2 and LAMA4 were significantly higher abundant 5 d post MI. Further regulation of collagen fibers is done by different matricellular proteins. SPARC activates CF and is involved in collagen type I secretion through ADAMTS1[138]. Intensity distribution of ADAMTS1 was higher abundant 3 d post MI but not 5 d post MI. Additionally, SPARC, COL1A1 and COL1A2 showed a higher fold change in the early stage (3 d post MI). Profibrotic proteins like collagen type I might be downregulated over time, as they lead to myocardial stiffness.

The anti-inflammatory and matrix-stabilizing protein THBS1 is known to inhibit MMPs, especially MMP3[139] and was upregulated 5 d post MI, which went along with a downregulation of MMP3 (see Figure 22B). Furthermore, TNC, which activates CF, is also known to be upregulated in the acute phase post MI[140]. This was also observable in the secretome data, where TNC was significantly higher abundant 3 d post MI but not 5 d post MI. All in all, several pro-fibrotic proteins like FN1, POSTN, ECM1, PXDN, and LTBP2[141–144] were significantly upregulated on investigated timepoints after MI compared to Sham and could represent aCF biomarkers. The only anti-fibrotic ECM-associated proteins CCDC80[145] and FMOD[146] were

significantly higher abundant 3 d post MI and 5 d post MI, respectively. As FN1 deletion in CF is already known to minimize cardiac fibrosis[147], an inhibition of other fibrotic proteins or increase of anti-fibrotic factors like FMOD at the right time after MI should be further investigated for improving fibrosis. Matrilin-2 (MATN2), which was significantly higher abundant and only secreted post MI, is involved in forming fibrillar networks[148] but not described in remodeling after MI. This protein is therefore also interesting for further investigations, like identifying it as an aCF biomarker or as a potential target in ECM remodeling post MI.

Table 24: Significantly enhanced secreted ECM-related proteins of cultured CF 3 d/5 d post MI known to be involved in cardiac ischemic stress response.

Involved in cardiac fibrosis		
Protein/*gene*	**Function in cardiac ischemic stress response**	**Ref.**
Adipocyte enhancer-binding protein 1 (AEBP1); *Aebp1*	promotes cardiac fibrosis	149
Bone morphogenetic protein 1 (BMP1); *Bmp1*	promotes cardiac fibrosis	150
Coiled-coil domain containing 80 (CCDC80); *Ccdc80*	anti-fibrotic and protects against cardiac hypertrophy	145
Extracellular matrix protein 1 (ECM1); *Ecm1*	leads to CF activation and cardiac fibrosis	151,142
Fibromodulin (FMOD); *Fmod*	anti-fibrotic	146
Fibronectin (FN1); *Fn1*	promotes cardiac fibrosis	147
Lysyl oxidase (LOX); *Lox*	promotes cardiac fibrosis and marker of HF post MI	152,153
Lysyl oxidase homolog 2 (LOXL2); *Loxl2*	promotes cardiac fibrosis and marker of HF post MI	154
Lysyl oxidase homolog 3 (LOXL3); *Loxl3*	promotes cardiac fibrosis	155
Latent transforming growth factor beta binding protein 2 (LTBP2); *Ltbp2*	involved in cardiac fibrosis and oxidative stress injury and marker of HF	156,144
Nidogen 1 (NID1); *Nid1*	anti-fibrotic	157
Osteoglycin (OGN); *Ogn*	collagen maturation marker of HF	158
Periostin (POSTN); *Postn*	involved in fibrosis	141

Peroxidasin (PXDN); *Pxdn*	promotes cardiac fibrosis	143
Tenascin-C (TNC); *Tnc*	pro-fibrotic	159
Secreted protein acidic and cysteine rich (SPARC); *Sparc*	regulates CF migration	160
Effect on CM		
Fibronectin (FN1); *Fn1*	CM apoptosis	161
Legumain (LGMN); *Lgmn*	clearance of apoptotic CM	162
Nidogen 1 (NID1); *Nid1*	CM survival	157
Involved in inflammation		
Fibronectin (FN1); *Fn1*	pro-inflammatory	161
Tenascin-C (TNC); *Tnc*	pro-inflammatory	159
Tissue inhibitor of metalloproteinase 3 (TIMP3); *Timp3*	anti-inflammatory	163
Involved in angiogenesis		
Heparin sulfate proteoglycan 2 (HSPG2); *Hspg2*	pro-angiogenic	164
Nidogen 1 (NID1); *Nid1*	pro-angiogenic	157
Tissue inhibitor of metalloproteinase 3 (TIMP3); *Timp3*	pro-angiogenic	165

In addition to ECM-associated proteins, paracrine and autocrine factors were altered post MI. On day 3 post MI, 37 paracrine/autocrine factors were significantly upregulated. On day 5 post MI, 11 proteins were significantly higher abundant. A total of 7 proteins (GDF6, INHBA, SFRP1, DNAJB11, SLIT2, CPE, and OPG) were significantly higher abundant on both days (see Figure 22). Several of these proteins also have known functions in ischemic stress response, such as maintaining cardiac function, angiogenesis, and inflammatory response, and some are described as HF biomarkers (Table 25).

This study underlines that CF do not only contribute to matrix remodeling post MI but can also interact with a wide range of different cardiac cell types. Paracrine CF can signal to cardiomyocytes, and protective effects have already been described in a co-culture

experiment[166]. This study contributes to understanding which factors might be involved in cardioprotection. CPE and Wnt-inhibitor SFRP1 were significantly higher abundant on both days post MI and are known to inhibit CM apoptosis[167]. Additionally CPE is described to enhance proliferation of primary CM[168]. Similar functions are described for FSTL1[169], which was significantly upregulated 3 d post MI. The significantly enhanced SLIT2 is known to maintain contractility by regulating myofilament activation and calcium sensitivity[170]. In contrast, the INHBA dimer ACTIVIN-A impairs human cardiomyocyte function, e.g., by downregulating genes that maintain calcium levels[171] and was significantly upregulated on day 3 and 5 post MI. It is furthermore elevated in the serum of heart failure patients[172]. Therefore, the inhibition of this protein, for example with monoclonal antibodies, or upregulation of SLIT2 to counteract CM impairment, could be therapeutic targets to improve the outcome post MI.

CF-secreted mediators can also signal to endothelial cells and enhance angiogenesis, as described for GDF6[173], which can also have positive effects on vascular SMC growth[174], METRNL[175], and FSTL1[176]. The latter of them can additionally prevent the heart from cardiac rupture, as it can signal to CF in an autocrine manner and promote early activation and proliferation[177]. Furthermore, CRLF1 which was only detectable 5 d post MI, promotes CF proliferation, viability and collagen production[178]. Among the paracrine/autocrine mediators, there were also factors with pro-fibrotic functions like B2M and SLIT3, which were significantly increased 3 d post MI but not on day 5. In contrast to that, WISP2, which decreases the switch of fibroblast into myofibroblasts[179], was significantly more abundant 3 d post MI. Furthermore, the fibrosis reducing SFRP1[167] was significantly higher abundant on day 3 and 5 post MI.

CF-secreted proteins can additionally affect the inflammatory response and signal to immune cells. On day 3 post MI, proteins of the inflammatory response were highly upregulated in the secretome (see Figure 22). Regulators of the innate immune system, like complement system activator C1-INH[180] and C3, which is associate with myocardial necrosis post MI[181], were higher abundant. Additionally, the C3 inhibitor[123] CFH was elevated. CCL2, which stimulates migration of immune cells[124], was also upregulated on day 3 post MI, as well as the anti-inflammatory CCL9[125]. These proteins showed fewer fold changes 5 d post MI compared to Sham or were even less abundant 5 d post MI, such as CCL2 and CFH. This might reflect the different remodeling phases (late inflammatory phase 3 d post MI and early proliferative phase 5 d post MI), as at the end of the inflammatory phase, anti-inflammatory proteins are secreted, and CF activation is strongly induced[14]. Additionally, IGF1 and C1-INH, which are known to have anti-inflammatory effects[180,182], were significantly elevated 3 d post MI compared to Sham.

Some of the identified proteins have been recognized as HF biomarkers. The glycoprotein OPG, which was significantly enhanced on day 3 and 5 post MI, is already a known predictor of poor prognosis post MI[183] and upregulated in serum of patients in the acute phase after MI[184]. Additionally, IGFBP7,QSOX1, and CTSB, which were significantly upregulated 3d post MI, are known biomarkers in heart failure and showed a decrease in fold change 5 d post MI/Sham, with HF biomarker IGFBP2 being significantly higher abundant 5 d post MI. The decrease in HF biomarker secretion over time could be a hint for a well-progressing scar formation and reduced risk of fibrosis

Table 25: Significantly enhanced secreted paracrine/autocrine proteins of cultured CF 3 d/5 d post MI known to be involved in cardiac ischemic stress response.

Involved in cardiac fibrosis		
Protein/*gene*	**Function in cardiac ischemic stress response**	**Ref.**
Beta-2 microglobulin (B2M); *B2m*	involved in CF activation and cardiac fibrosis	185
Cytokine receptor like factor 1 (CRLF1); *Crlf1*	increases collagen production, CF proliferation, viability and myofibroblast differentiation	178
Follistatin like 1 (FSTL1); *Fstl1*	anti-fibrotic	186
Secreted frizzled-related protein 1 (SFRP1); *Sfrp1*	anti-fibrotic	167
Slit homolog 3 protein (SLIT3); *Slit3*	activation of CF and promotion of collagen production	187
WNT1-inducible-signaling pathway protein 2 (WISP2); *Wisp2*	anti-fibrotic	179
Effect on CM		
Carboxypeptidase E (CPE); *Cpe*	inhibits CM apoptosis and promotes CM proliferation	168
Activin-A (INHBA dimer); *Inhba*	impairs cardiomyocyte contractile function	171
Milk fat globule-EGF factor 8 (MFGE8); *Mfge8*	clearance of apoptotic CM	188
Pigment epithelium-derived factor (PEDF); *Serpinf1*	reduces CM apoptosis and infarct size	189
Secreted frizzled-related protein 1 (SFRP1); *Sfrp1*	inhibits CM apoptosis and improves cardiac function	167
Slit homolog 2 protein (SLIT2); *Slit2*	maintains myofilament contractility	170

Effect on cardiac function		
Cathepsin-A (CTSA); *Ctsa*	inhibition post MI is cardioprotective	190
Cathepsin-L (CTSL); *Ctsl*	improves remodeling and cardiac function	191
Tissue plasminogen activator (PLAT); *Plat*	preserves LV function and reduces infarct size	192
Involved in inflammation		
C1-Esterase-inhibitor (C1-INH); *Serping1*	regulation of complement activity post MI	180
Insulin like growth factor 1 (IGF1); *Igf1*	anti-inflammatory	182
Semaphorin 7A (SEMA7A); *Sema7a*	resolution of severe systemic inflammation	193
Slit homolog 2 protein (SLIT2); *Slit2*	anti-inflammatory	170
Involved in angiogenesis		
Follistatin like 1 (FSTL1); *Fstl1*	pro angiogenic	176
Growth differentiation factor 6 (GDF6); *Gdf6*	enhances endothelial angiogenesis	173
Meteorin-like protein (METRNL); *Metrnl*	pro-angiogenic and involved in tissue repair	175
Biomarkers		
Cathepsin-B (CTSB); *Ctsb*	marker of HF	194
Insulin-like growth factor binding protein-2 (IGFBP2); *Igfbp2*	marker of HF	195
Insulin-like growth factor binding protein-7 (IGFBP7); *Igfbp7*	marker of HF	196
Osteoprotegerin (OPG); *Tnfrsf11b*	marker of HF	197
Quiescin sulfhydryl oxidase 1 (QSOX1); *Qsox1*	marker of LV dysfunction	198

Interestingly, there were factors significantly higher abundant post MI in the CF secretome that have not considered in CF signaling yet, such as SEMA7A, CPE, and SLIT2. Additionally, LGALS3BP, Sushi von Willebrand factor type A (SVEP1), and PSAP have no reported function in cardiac remodeling. These proteins should be further investigated for their potential in CF signaling and ischemic response. Furthermore, DNAJB11 was only detectable post MI but is not known for any participation in cardiac remodeling or CF signaling. Gene expression data 5 d post MI/Sham[68,108] showed that it was higher expressed post MI and specific for CF (see Figure 24), so it is very likely that this factor has an impact on the post-ischemic heart and could serve as novel drug target or could serve as a marker for MI-induced aCF.

Taken together, this study identified a panel of proteins through which CF exert important known functions after MI, such as ECM remodeling and scar formation. Additionally, this study supports the notions that CF can communicate with other cell types like EC, immune cells and CM to regulate angiogenesis, inflammatory response, or CM survival, and therefore affect cardiac remodeling in many partially unknown ways. Specific drug targeting of these identified proteins might be a fruitful future research avenue for improving cardiac remodeling and decreasing the risk of heart failure.

5.4 Method for POSTN$^+$ CF-specific *in vivo* secretome analysis post MI

Even though the protocol for CF secretome analysis with short-term cultured CF and labeling times of 8 h was carefully developed to minimize culture-dependent changes, there could still be differences compared to the *in vivo* situation. Additionally, proteins with a turnover rate higher than 8 h are not measurable using this protocol. To explore the possibility of measuring protein secretion under *in vivo* condition in the beating heart, POSTN$^+$ CF-specific secretome analysis was established for the first time by adapting the protocol of Wei *et al*.[84] who described cell type-specific *in vivo* secretomics of hepatocytes using biotin labeling for three consecutive days. There is no specific marker for targeting all CF, as these cells are very heterogenous and marker genes are also expressed by other cell types[16,29]. but there is a high amount of aCF in the infarct zone[199]. For this reason, *Postn* a marker gene for aCF was used for cell type-specific protein tracking. To this end, an AAV carrying plasmid with an ER-located biotin ligase (TurboID) sequence behind a *Postn* promoter (see Figure 9) was used. Immunofluorescence imaging ensured that TurboID was expressed by POSTN$^+$ CF in the infarcted area (see Figure 25) but further investigations showed, that TurboID was also expressed in other organs especially in the liver (see Figure 26). This may lead to a high amount of liver-secreted, biotinylated proteins in the blood plasma.

As a high amount of plasma proteins like albumin and hemoglobin was still found in the coronary effluent, especially in the first 10 min of collection (see Figure 27), this portion of the sample was discarded, considering that the total protein concentration decreased over time as well. Although plasma proteins in the coronary effluent were minimized, there were still interfering signals of biotinylated plasma proteins in the LC-MS/MS analysis of POSTN$^+$ CF 5 d post MI/Sham as p(see Figure 29) Only 7 proteins were significantly altered between MI and Sham and the most prevalent fold changes were detected for plasma proteins (see Figure 29B), such as HBB-B2, HBBT1, and F13B, which is known to play a part in blood coagulation. Additionally, heterogeneity within the different replicates and low intensity distribution of ECM-associated and paracrine/autocrine proteins in the coronary effluent impaired the analysis (see Figure 29C). However, interesting consistencies between *in vitro* and *in vivo* secretome

analysis were observed. Some proteins that were significantly altered in the secretome of cultivated CF post MI were also found to be increased in the post MI *in vivo* secretome of POSTN$^+$ CF. For example, the FN1, FBLN2, FBLN5, COL1A1, BGN, NID1, and paracrine factors C1-INH, SERPINA3N, and C3 were secreted post MI and upregulated compared to Sham-operated control (see Appendix Table 29).

Taken together, the results shown are promising and demonstrate the general feasibility of *in vivo* secretome analysis in the beating heart, Future studies must explore whether different fibroblast promoters may be advantageous, particularly when one would like to compare the *in vivo* CF control secretome with that under infarct conditions.

5.5 POSTN$^+$ CF-specific *in vivo* proteome analysis post MI

Specific secretome analysis of POSTN$^+$ CF after MI was limited by biotinylated plasma proteins and a low intensity distribution of proteins. To further study the feasibility of the *in vivo* biotinylation using TurboID heart tissue of the virus transduced mice was lysed after collecting the coronary effluent and enriched for biotinylated proteins. In total 194 proteins were detectable (see Figure 30A), from which 19 were significantly higher and 2 lower in abundance post MI compared to Sham.

As summarized in table 26, these proteins have different functions in cardiac remodeling post MI. For example, HSPA5, PDIA3, and PRDX4 play a role in ischemic stress response as they protect against oxidative stress[200–202]. Furthermore, many proteins are involved in collagen secretion, like HSP47[203] and MIA3[204], while RCN3 reduces collagen expression[205]. Additionally, COTL1 and the significantly lower abundant protein VDAC1 are known to have anti-fibrotic properties[206,207]. Some proteins are not associated with CF but are described to protect against apoptosis of other cell types like CM and EC (P4HB[208,209] and CLU[210]). On this account, these proteins may protect CF from apoptosis as well.

All in all, this data underlines the importance of POSTN$^+$ CF in MI remodeling and maintaining cardiac structure. Interesting proteins that are described for oxidative stress response and regulating fibrosis were significantly altered in the *in vivo* proteome of POSTN$^+$ CF after MI compared to Sham.

Table 26: Significantly altered proteins in the POSTN$^+$ CF proteome 5 d post MI known to be involved in cardiac ischemic stress response.

Higher abundant post MI		
Protein/*gene*	**Function in cardiac ischemic stress response**	**Ref.**
Clusterin (CLU); *Clu*	protects against oxidative stress and inhibits apoptosis of CM	210
Coactosin-like protein (COTL1); *Cotl1*	regulates TGF-β signaling and reduces fibrosis	206
Heat shock protein 47 (HSP47); *Serpinh1*	collagen secretion, processing, fibril assembly and ECM deposition	203
Heat Shock Protein Family A (Hsp70) Member 5 (HSPA5); *Hspa5*	protects against oxidative stress	200
Melanoma inhibitory activity protein 3	exports collagen from ER	204

(MIA3); *Mia3*		
Protein disulfide–isomerase (P4HB/PDI); *P4hb*	inhibits apoptosis of CM and EC	208,209
Protein disulfide-isomerase A3 (PDIA3); *Pdia3*	protects against oxidative stress	201
Plasminogen (PLG); *Plg*	stem cell-mediated cardiac repair after MI	211
Peroxiredoxin-4 (PRDX4), *Prdx4*	protects against oxidative stress	202
Reticulocalbin-3 (RCN3); *Rcn3*	decreases collagen expression	205
Transmembrane and TPR repeat-containing protein 3 (TMTC3); *Tmtc3*	cellular adherence and migration	212
UDP-glucose: glycoprotein glycosyltransferase 1 (UGGT1), *Uggt1*	improves glycoprotein quality control	213

Lower abundant post MI		
Protein/*gene*	**Function in cardiac ischemic stress response**	**Ref.**
Cytochrome C (CYCS); *Cycs*	biomarker of poor prognosis post MI and has pro-apoptotic functions	214,215
Voltage-dependent anion-selective channel protein 1 (VDAC1); *Vdac1*	alleviates CF activation and has anti-fibrotic functions	207

Gene expression analysis of the significantly higher abundant secretome proteins revealed that most of the proteins were CF- and EPDC-specific (see Figure 31B). Furthermore, most of the higher abundant proteins post MI were also higher expressed on the gene level post MI in comparison to Sham (see Figure 30B), indicating that the increased protein secretion might directly result from an induction of gene expression. Additionally, most of the detected proteins, like HSP47, UGGT1, HSPA5, MIA3, P4HB, RCN3, and TMTC3, are described to be ER associated[200,204,205,209,212,213,216]. This nicely correlates with the ER-specific location of the used TurboID enzyme and indicates that the biotinylation mechanism of the method is functional.

5.6 Outlook

In this thesis, secretome analysis using pSILAC labeling and click-chemistry was optimized for cultivated CF and for comparative secretome analysis of CF-secreted proteins post MI/Sham. It was shown that there are significant differences in the secretome of cultivated CF post MI and Sham, and that CF secrete several well-known proteins post MI. These results are in support of the validity of the used method.

As the individual components of the CF secretome under basal conditions and post MI could be identified in this study, they now provide a resource for analyzing their contribution to intracellular signaling and for evaluation as therapeutic targets or CF activation markers and HF biomarkers. Identifying central nodes and mediators is important for understanding the complex cellular crosstalk and signaling networks post MI.

Significantly increased proteins 5 d post MI were also upregulated at the gene level of CF 5 d post MI compared to Sham and were highly expressed by CF compared to other cell types. These proteins such as FMOD, DNAJB11, or CLRF1 could, therefore, serve as selective markers for infarct-induced aCF. In a next step, human data should be analyzed for a CF-dependent upregulation of these proteins and genes post MI. Detected CF-secreted proteins post MI could also serve as therapeutical targets to attenuate fibrosis. Therefore, identified pro-fibrotic proteins, that were significantly enhanced post MI, such as B2M, LTBP2, LOX, and LOXL3 could be targeted via neutralizing antibodies to decrease the fibrotic response post MI. Additionally, anti-fibrotic proteins that were elevated post MI like SFRP1, WISP2, and FMOD could be used as drugs to minimize the risk of fibrosis development. Therefore, these proteins should be further analyzed regarding their concentration and timing in post-MI treatment.

Secretome analysis of CF using pSILAC and click-chemistry is not without limitations. Analyzed CF were obtained from healthy 10-12-weeks-old C57Bl/6 mice, representing an age group optimal for cardiac remodeling and recovery post MI. In future studies, CF secretome of aged mice and mice with underlying health conditions like type 2 diabetes can now be analyzed and compared to CF secretome of healthy mice after MI to identify factors that worsen cardiac remodeling and disturb the essential balance of inflammation, scar building, and angiogenesis. Additionally, the present CF secretome study concentrated on day 3 and 5 post MI and, therefore, did not investigate the early phase of inflammation, the late proliferative phase and the maturation phase. For deeper insights into these phases of cardiac remodeling, timepoints like 1 d, 14 d, and 21 d post MI might be interesting to analyze in the future.

The possibility that cell isolation, cultivation, and AHA labeling could impact the secretome even under optimal conditions cannot be completely ruled out. Due to AHA toxicity, secreted proteins could only be assessed with an 8 h labeling period. Consequently, only proteins synthesized and secreted during this specific time frame were captured in the analysis. Proteins synthesized before labeling and secreted during this time period, or proteins synthesized during this time frame but not secreted, were not detected by this analysis.

To validate the obtained *in vitro* results, a method for *in vivo* aCF-specific secretome analysis using ER-TurboID-mediated biotinylation was developed and applied in this study. *In vivo* secretomics of $POSTN^+$ CF exhibited many similarities in detected proteins from both *in vivo* and *in vitro* secretome analysis approaches. Unfortunately, the *in vivo* secretome analysis was hampered by low intensity distributions of biotinylated proteins and the presence of biotinylated

plasma proteins, primarily originating from the liver, as *Postn* expression is specific to aCF in the heart but not systemically, due to its expression in the liver .

To optimize this protocol, the number of replicates should be increased and, in order to decrease biotinylated blood plasma contaminants, a liver-specific microRNA (miR122) could be used to suppress AAV liver transfer[217,218]. It was shown that AAV9 vectors containing at least three miR122 target site repeats in the 3'-untranslated region avoid undesired liver targeting without impacting vector expression in the heart[218]. Using this target site for AAV9-mediated TurboID expression could resolve the impairment of CF *in vivo* secretome analysis through blood plasma proteins, as liver-secreted proteins that are still washed out into the coronary effluent are no longer biotinylated and enriched, and therefore should no longer influence the LC-MS/MS measurements.

In vivo secretome study was focused on POSTN^{+} CF-secreted proteins because *Postn* is a biomarker for aCF which make up a high proportion in the post-MI heart, especially in the infarcted area. Genes such as *Vim*, *Cd90*, *Ddr2*, or *Col1a1* are highly expressed by different CF subpopulations and could serve as potential markers. However, these genes are not CF-specific, as other cell types like EC, SMC, or immune cells also express them[219]. Additionally, the CF marker gene *Pdgfrα* is also detectable in pericytes[220]. Another marker, *α-SMA*, similar to *Postn*, does not encompass the entire heterogenous CF population[221], but only activated CF. In summary, identifying a CF-specific marker that encompasses all heterogenous CF populations is challenging.

Another approach to minimize protein contamination from sources other than CF could involve the use of CF reporter mice. One such example is the *Postn^{LacZ}* reporter mouse[222], which could be employed for aCF tracking. Additionally, a reporter mouse featuring green fluorescent protein (GFP) coupled with fibroblast-specific protein 1 (FSP1-GFP) has been utilized for CF tracking. However, a challenge arises with *Fsp1* as it is also expressed by immune cells and EC[223]. Moreover, mouse lines such as *Postn*-Cre and *Fsp1*-Cre are available[224]. It is important to note that genetic manipulation of mice may alter proteins secretion, as the insertion of loxP sites and vector sequences into a gene has been reported to attenuate gene expression or even result in gene disruption[225]. Furthermore, the difficulty persists in generating a reporter mouse specifically tailored for all CF.

Liu and colleagues developed a reporter mouse that localizes a modified BirA enzyme called BioID in the ER (ER-BioID)[226]. BioID, derived from *E.coli* is a known biotin ligase and the precursor to the third generation TurboID[227]. This reporter mouse can be bred with Cre-recombinase mice for cell-specific expression of ER-BioID, as demonstrated in vascular EC and skeletal muscle cells[226]. Therefore, it is feasible to cross this reporter mouse with the CF-specific Cre mice mentioned above, facilitating *in vivo* biotinylation of CF-secreted proteins. To enable biotinylation, exogenous biotin was introduced by Liu *et al*., 2021[226] through intraperitoneal and subcutaneous injections, along with biotin-containing chow. Subsequently, biotinylated proteins can be enriched with streptavidin beads and analyzed via MS. In comparison to TurboID, BioID has the drawback of requiring more than 18 h on average to produce detectable biotinylation[227]. Given that TurboID achieves faster biotinylation with lower biotin consumption (as demonstrated in this thesis, where administration of biotin via drinking water was sufficient for protein biotinylation), a TurboID reporter mouse may be worthwhile to create for further studies. This mouse could be crossed with CF-specific Cre mice lines, such as *Fsp1*-Cre.

In vivo proteome data of lysed heart tissue revealed that -mediated biotinylation was ER-specific, active in POSTN$^+$ CF, and was suitable to target POSTN$^+$ CF-produced proteins. Thus, it should be possible to detect POSTN$^+$ CF-secreted proteins in the effluent to assess the secretome of POSTN$^+$ CF *in vivo* after adjusting the protocol with the above discussed modifications in the future. Several of the detected POSTN$^+$ CF-specific intracellular proteins were described to protect against oxidative stress or fibrosis, and some are known to be secreted by CF, like POSTN, PRDX4[202], and HSP47. Furthermore, the significantly decreased protein VDAC1 was described to alleviate CF activation and has already been suggested as potential drug candidate for inhibiting cardiac fibrosis[207].

In summary, this study discovered basic insights into CF-mediated cell-cell communication in the mouse heart and can be used as resource for further investigations. In the future it might be worthwhile to analyze if these discovered results are transferable to humans and if the detected CF protein secretion is reflected in human CF post MI. As the identified CF-secreted proteins are likely to be critically involved in cardiac remodeling after MI, they could be targeted in therapeutic approaches of fibrosis in heart failure or used as biomarkers for heart failure or markers for MI-induced aCF.

6. References

1. Mutschler, E., Schaible, H.-G. & Vaupel, P. *Anatomie, Physiologie, Pathophysiologie des Menschen*. (2007).
2. Schrader, J., Gödecke, A. & Kelm, M. Das Herz. in *Physiologie* (eds. Klinke, R., Pape, H.-C., Kurtz, A. & Silbernagel, S.) 134–171 (Georg Thieme Verlag, 2009).
3. Gomes, J. A. Demystifying the Heart. *Rhythms of Broken Hearts* 21–29 (2021) doi:10.1007/978-3-030-77382-3_3.
4. Jean-Francis Berry. Heart Anatomy. Preprint at (2020).
5. Lafuse, W. P., Wozniak, D. J. & Rajaram, M. V. S. Role of Cardiac Macrophages on Cardiac Inflammation, Fibrosis and Tissue Repair. *Cells 2021, Vol. 10, Page 51* **10**, 51 (2020).
6. Pinto, A. R. *et al.* Revisiting Cardiac Cellular Composition. *Circ Res* **118**, 400–409 (2016).
7. Woodcock, E. A. & Matkovich, S. J. Cardiomyocytes structure, function and associated pathologies. *Int J Biochem Cell Biol* **37**, 1746–1751 (2005).
8. Hara, A. & Tallquist, M. D. Fibroblast and Immune Cell Cross-Talk in Cardiac Fibrosis. *Curr Cardiol Rep* **25**, 485–493 (2023).
9. Zhuge, Y. *et al.* Role of smooth muscle cells in Cardiovascular Disease. *Int J Biol Sci* **16**, 2741 (2020).
10. Lee, L. L. & Chintalgattu, V. Pericytes in the heart. *Adv Exp Med Biol* **1122**, 187–210 (2019).
11. Aird, W. C. Phenotypic Heterogeneity of the Endothelium. *Circ Res* **100**, 158–173 (2007).
12. Epelman, S., Liu, P. P. & Mann, D. L. Role of innate and adaptive immune mechanisms in cardiac injury and repair. *Nature Reviews Immunology 2015 15:2* **15**, 117–129 (2015).
13. Tzahor, E. & Dimmeler, S. A coalition to heal-the impact of the cardiac microenvironment. *Science* **377**, (2022).
14. Humeres, C. & Frangogiannis, N. G. Fibroblasts in the Infarcted, Remodeling, and Failing Heart. *JACC Basic Transl Sci* **4**, 449–467 (2019).
15. Furtado, M. B., Costa, M. W. & Rosenthal, N. A. The cardiac fibroblast: Origin, identity and role in homeostasis and disease. *Differentiation* **92**, 93–101 (2016).
16. Doppler, S. A. *et al.* Cardiac fibroblasts: more than mechanical support. *J Thorac Dis* **9**, S36–S51 (2017).

17. Perez-Pomares, J. M. *et al.* Origin of coronary endothelial cells from epicardial mesothelium in avian embryos. *International Journal of Developmental Biology* **46**, 1005–1013 (2002).

18. Acharya, A. *et al.* The bHLH transcription factor Tcf21 is required for lineage-specific EMT of cardiac fibroblast progenitors. *Development* **139**, 2139–2149 (2012).

19. Tallquist, M. D. & Molkentin, J. D. Redefining the identity of cardiac fibroblasts. *Nat Rev Cardiol* **14**, 484 (2017).

20. Ali, S. R. *et al.* Developmental heterogeneity of cardiac fibroblasts does not predict pathological proliferation and activation. *Circ Res* **115**, 625–635 (2014).

21. Ivey, M. J. & Tallquist, M. D. Defining the Cardiac Fibroblast: A New Hope. *Circ J* **80**, 2269 (2016).

22. Souders, C. A., Bowers, S. L. K. & Baudino, T. A. Cardiac Fibroblast: The Renaissance Cell. *Circ Res* **105**, 1164 (2009).

23. Camelliti, P., Borg, T. K. & Kohl, P. Structural and functional characterisation of cardiac fibroblasts. *Cardiovasc Res* **65**, 40–51 (2005).

24. Muhl, L. *et al.* Single-cell analysis uncovers fibroblast heterogeneity and criteria for fibroblast and mural cell identification and discrimination. *Nature Communications 2020 11:1* **11**, 1–18 (2020).

25. Goldsmith, E. C. *et al.* Organization of fibroblasts in the heart. *Developmental Dynamics* **230**, 787–794 (2004).

26. Rossert, J., Terraz, C. & Dupont, S. Regulation of type I collagen genes expression. *Nephrology Dialysis Transplantation* **15**, 66–68 (2000).

27. Smith, C. L., Baek, S. T., Sung, C. Y. & Tallquist, M. D. Epicardial-Derived Cell Epithelial-to-Mesenchymal Transition and Fate Specification Require PDGF Receptor Signaling. *Circ Res* **108**, (2011).

28. Lajiness, J. D. & Conway, S. J. Origin, development, and differentiation of cardiac fibroblasts. *J Mol Cell Cardiol* **0**, 2 (2014).

29. Tarbit, E., Singh, I., Peart, J. N. & Rose'Meyer, R. B. Biomarkers for the identification of cardiac fibroblast and myofibroblast cells. *Heart Fail Rev* **24**, 1–15 (2019).

30. Mutschler, E., Schaible, H.-G. & Vaupel, P. *Anatomie, Physiologie, Pathophysiologie des Menschen*. (2007).

31. WHO | Top 10 causes of death. *WHO* (2019).

32. De Lemos, J. A., Newby, L. K. & Mills, N. L. A Proposal for Modest Revision of the Definition of Type 1 and Type 2 Myocardial Infarction. *Circulation* **140**, 1773–1775 (2019).

33. Thygesen, K. *et al.* Fourth Universal Definition of Myocardial Infarction (2018). *Circulation* **138**, e618–e651 (2018).

34. Gard, A. *et al.* Diagnosing type 2 myocardial infarction in clinical routine. A validation study. *Scandinavian Cardiovascular Journal* **53**, 259–265 (2019).

35. Singh, A. *et al.* Cardiovascular Mortality After Type 1 and Type 2 Myocardial Infarction in Young Adults. *J Am Coll Cardiol* **75**, 1003–1013 (2020).

36. Myocardial Infarction (Heart Attack). Preprint at (2022).

37. Sandoval, Y. & Jaffe, A. S. Type 2 Myocardial Infarction: JACC Review Topic of the Week. *J Am Coll Cardiol* **73**, 1846–1860 (2019).

38. Thygesen, K. *et al.* How to use high-sensitivity cardiac troponins in acute cardiac care. *Eur Heart J* **33**, 2252–2257 (2012).

39. Katrukha, I. A. Human cardiac troponin complex. structure and functions. *Biochemistry (Moscow)* **78**, 1447–1465 (2013).

40. Twerenbold, R. *et al.* Clinical Use of High-Sensitivity Cardiac Troponin in Patients With Suspected Myocardial Infarction. *J Am Coll Cardiol* **70**, 996–1012 (2017).

41. Welch, T. D., Yang, E. H., Reeder, G. S. & Gersh, B. J. Modern Management of Acute Myocardial Infarction. *Curr Probl Cardiol* **37**, 237–310 (2012).

42. Gerber, Y. *et al.* Mortality Associated with Heart Failure after Myocardial Infarction: A Contemporary Community Perspective. *Circ Heart Fail* **9**, (2016).

43. Sweeney, M., Corden, B. & Cook, S. A. Targeting cardiac fibrosis in heart failure with preserved ejection fraction: mirage or miracle? *EMBO Mol Med* **12**, e10865 (2020).

44. Frangogiannis, N. G. Regulation of the inflammatory response in cardiac repair. *Circ Res* **110**, 159 (2012).

45. Talman, V. & Ruskoaho, H. Cardiac fibrosis in myocardial infarction—from repair and remodeling to regeneration. *Cell Tissue Res* **365**, 563 (2016).

46. Ma, Y., Iyer, R. P., Jung, M., Czubryt, M. P. & Lindsey, M. L. Cardiac Fibroblast Activation Post-Myocardial Infarction: Current Knowledge Gaps. *Trends Pharmacol Sci* **38**, 448–458 (2017).

47. Prabhu, S. D. & Frangogiannis, N. G. The Biological Basis for Cardiac Repair After Myocardial Infarction: From Inflammation to Fibrosis. *Circ Res* **119**, 91 (2016).

48. Chen, W. & Frangogiannis, N. G. Fibroblasts in post-infarction inflammation and cardiac repair. *Biochimica et Biophysica Acta (BBA) - Molecular Cell Research* **1833**, 945–953 (2013).

49. Timmers, L. *et al.* The innate immune response in reperfused myocardium. *Cardiovasc Res* **94**, 276–283 (2012).

50. Vinten-Johansen, J. Involvement of neutrophils in the pathogenesis of lethal myocardial reperfusion injury. *Cardiovasc Res* **61**, 481–497 (2004).

51. Frangogiannis, N. G. The immune system and cardiac repair. *Pharmacol Res* **58**, 88–111 (2008).

52. Yan, X. *et al.* Temporal dynamics of cardiac immune cell accumulation following acute myocardial infarction. *J Mol Cell Cardiol* **62**, 24–35 (2013).

53. Dobaczewski, M., Gonzalez-Quesada, C. & Frangogiannis, N. G. The extracellular matrix as a modulator of the inflammatory and reparative response following myocardial infarction. *J Mol Cell Cardiol* **48**, 504–511 (2010).

54. Weil, B. R. & Neelamegham, S. Selectins and immune cells in aucte mycardial infarction and post-infarction ventricular remodelings: Pathophysiology and novel treatments. *Front Immunol* **10**, 300 (2019).

55. Kologrivova, I., Shtatolkina, M., Suslova, T. & Ryabov, V. Cells of the Immune System in Cardiac Remodeling: Main Players in Resolution of Inflammation and Repair After Myocardial Infarction. *Front Immunol* **12**, 664457 (2021).

56. Hofmann, U. *et al.* Activation of CD4 + T lymphocytes improves wound healing and survival after experimental myocardial infarction in mice. *Circulation* **125**, 1652–1663 (2012).

57. Daseke, M. J., Tenkorang, M. A. A., Chalise, U., Konfrst, S. R. & Lindsey, M. L. Cardiac fibroblast activation during myocardial infarction wound healing: Fibroblast polarization after MI. *Matrix Biology* **91–92**, 109–116 (2020).

58. Sun, Y. & Weber, K. T. Infarct scar: A dynamic tissue. *Cardiovasc Res* **46**, 250–256 (2000).

59. Shinde, A. v. & Frangogiannis, N. G. Fibroblasts in myocardial infarction: A role in inflammation and repair. *Journal of Molecular and Cellular Cardiology* vol. 70 74–82 Preprint at https://doi.org/10.1016/j.yjmcc.2013.11.015 (2014).

60. Frangogiannis, N. G. Matricellular proteins in cardiac adaptation and disease. *Physiol Rev* **92**, 635–688 (2012).

61. Forte, E., Furtado, M. B. & Rosenthal, N. The interstitium in cardiac repair: role of the immune–stromal cell interplay. *Nature Reviews Cardiology* vol. 15 601–616 Preprint at https://doi.org/10.1038/s41569-018-0077-x (2018).

62. Frangogiannis, N. G., Michael, L. H. & Entman, M. L. Myofibroblasts in reperfused myocardial infarcts express the embryonic form of smooth muscle myosin heavy chain (SMemb). *Cardiovasc Res* **48**, 89–100 (2000).

63. Fu, X. *et al.* Specialized fibroblast differentiated states underlie scar formation in the infarcted mouse heart. *J Clin Invest* **128**, 2127 (2018).

64. van den Borne, S. W. M. *et al.* Myocardial remodeling after infarction: the role of myofibroblasts. *Nature Reviews Cardiology 2010 7:1* **7**, 30–37 (2009).

65. Venugopal, H., Hanna, A., Humeres, C. & Frangogiannis, N. G. Properties and Functions of Fibroblasts and Myofibroblasts in Myocardial Infarction. *Cells 2022, Vol. 11, Page 1386* **11**, 1386 (2022).

66. Holmes, J. W., Borg, T. K. & Covell, J. W. Structure and Mechanics of Healing Myocardial Infarcts. *Annu Rev Biomed Eng* **7**, 223–253 (2005).

67. Farbehi, N. *et al.* Single-cell expression profiling reveals dynamic flux of cardiac stromal, vascular and immune cells in health and injury. *Elife* **8**, (2019).

68. Hesse, J. *et al.* Single-cell transcriptomics defines heterogeneity of epicardial cells and fibroblasts within the infarcted murine heart. *Elife* **10**, (2021).

69. Forte, E. *et al.* Dynamic Interstitial Cell Response during Myocardial Infarction Predicts Resilience to Rupture in Genetically Diverse Mice. *Cell Rep* **30**, 3149-3163.e6 (2020).

70. Poschmann, G. *et al.* Secretomics-A Key to a Comprehensive Picture of Unconventional Protein Secretion. *Front Cell Dev Biol* **10**, (2022).

71. Lee, M. C. S., Miller, E. A., Goldberg, J., Orci, L. & Schekman, R. BI-DIRECTIONAL PROTEIN TRANSPORT BETWEEN THE ER AND GOLGI. *https://doi.org/10.1146/annurev.cellbio.20.010403.105307* **20**, 87–123 (2004).

72. Nickel, W. & Seedorf, M. Unconventional Mechanisms of Protein Transport to the Cell Surface of Eukaryotic Cells. (2008) doi:10.1146/annurev.cellbio.24.110707.175320.

73. Hathout, Y. Approaches to the study of the cell secretome. *https://doi.org/10.1586/14789450.4.2.239* **4**, 239–248 (2014).

74. Stastna, M. & van Eyk, J. E. Secreted proteins as a fundamental source for biomarker discovery. *Proteomics* **12**, 722–735 (2012).

75. Doroudgar, S. & Glembotski, C. C. The Cardiomyokine Story Unfolds: Investigating Stress-induced Protein Secretion in the Heart. *Trends Mol Med* **17**, 207 (2011).

76. Dowling, P. & Clynes, M. Conditioned media from cell lines: A complementary model to clinical specimens for the discovery of disease-specific biomarkers. *Proteomics* vol. 11 794–804 Preprint at https://doi.org/10.1002/pmic.201000530 (2011).

77. Raimondo, F., Morosi, L., Chinello, C., Magni, F. & Pitto, M. Advances in membranous vesicle and exosome proteomics improving biological understanding and biomarker discovery. *Proteomics* vol. 11 709–720 Preprint at https://doi.org/10.1002/pmic.201000422 (2011).

78. Eichelbaum, K. & Krijgsveld, J. Combining pulsed SILAC labeling and click-chemistry for quantitative secretome analysis. *Methods in Molecular Biology* **1174**, 101–114 (2014).

79. Ong, S. E. *et al.* Stable Isotope Labeling by Amino Acids in Cell Culture, SILAC, as a Simple and Accurate Approach to Expression Proteomics. *Molecular & Cellular Proteomics* **1**, 376–386 (2002).

80. Eichelbaum, K., Winter, M., Diaz, M. B., Herzig, S. & Krijgsveld, J. Selective enrichment of newly synthesized proteins for quantitative secretome analysis. *Nat Biotechnol* **30**, 984–990 (2012).

81. invitrogen. Click-iT Metabolic Labeling Reagents for Proteins. https://www.thermofisher.com/document-connect/document-connect.html?url=https%3A%2F%2Fassets.thermofisher.com%2FTFS-

Assets%2FLSG%2Fmanuals%2Fmp10186.pdf&title=Q2xpY2staVQgTWV0YWJvbGlJ
ExhYmVsaW5nIFJlYWdlbnRzIGZvciBQcm90ZWlucw==.

82. Imami, K. & Yasuda, T. Measuring Protein Synthesis during Cell Cycle by Azidohomoalanine (AHA) Labeling and Flow Cytometric Analysis. *Bio Protoc* **9**, (2019).

83. Innovative Peptide Solutions. Click Chemistry. https://www.jpt.com/products/click-chemistry?breadcrumbPath=462.

84. Wei, W. *et al.* Cell type-selective secretome profiling in vivo. *Nat Chem Biol* **17**, 326–334 (2021).

85. Branon, T. C. *et al.* Efficient proximity labeling in living cells and organisms with TurboID. *Nat Biotechnol* **36**, 880–898 (2018).

86. Roux, K. J., Kim, D. I., Raida, M. & Burke, B. A promiscuous biotin ligase fusion protein identifies proximal and interacting proteins in mammalian cells. *Journal of Cell Biology* **196**, 801–810 (2012).

87. Cho, K. F. *et al.* Proximity labeling in mammalian cells with TurboID and split-TurboID. *Nat Protoc* **15**, 3971–3999 (2020).

88. Lino, J. B., Robert, A. W., Stimamiglio, M. A. & de Aguiar, A. M. Comparative analysis of the potential of the secretomes of cardiac resident stromal cells and fibroblasts. *IUBMB Life* (2021) doi:10.1002/IUB.2557.

89. Bräuninger, H. *et al.* Cytokine-Mediated Alterations of Human Cardiac Fibroblast's Secretome. *Int J Mol Sci* **22**, (2021).

90. Ceccato, T. L. *et al.* Defining the Cardiac Fibroblast Secretome in a Fibrotic Microenvironment. *J Am Heart Assoc* **9**, (2020).

91. Cosme, J., Guo, H., Hadipour-Lakmehsari, S., Emili, A. & Gramolini, A. O. Hypoxia-Induced Changes in the Fibroblast Secretome, Exosome, and Whole-Cell Proteome Using Cultured, Cardiac-Derived Cells Isolated from Neonatal Mice. *J Proteome Res* **16**, 2836–2847 (2017).

92. Landry, N. M., Rattan, S. G. & Dixon, I. M. C. An Improved Method of Maintaining Primary Murine Cardiac Fibroblasts in Two-Dimensional Cell Culture. *Scientific Reports 2019 9:1* **9**, 1–13 (2019).

93. Shin, J. *et al.* Comparative analysis of differentially secreted proteins in serum-free and serum-containing media by using BONCAT and pulsed SILAC. *Scientific Reports 2019 9:1* **9**, 1–12 (2019).

94. Fang, H. *et al.* Comparison of Adeno-Associated Virus Serotypes and Delivery Methods for Cardiac Gene Transfer. *Hum Gene Ther Methods* **23**, 234 (2012).

95. Piras, B. A. *et al.* Systemic injection of AAV9 carrying a periostin promoter targets gene expression to a myofibroblast-like lineage in mouse hearts after reperfused myocardial infarction. *Gene Ther* **23**, 469–478 (2016).

96. Lindsley, A. *et al.* Identification and characterization of a novel Schwann and outflow tract endocardial cushion lineage-restricted periostin enhancer. *Dev Biol* **307**, 340–355 (2007).

97. Cheah, J. S. & Yamada, S. A simple elution strategy for biotinylated proteins bound to streptavidin conjugated beads using excess biotin and heat. *Biochem Biophys Res Commun* **493**, 1522–1527 (2017).

98. Røberg-Larsen, H., Lundanes, E., Nyman, T. A., Berven, F. S. & Wilson, S. R. Liquid chromatography, a key tool for the advancement of single-cell omics analysis. *Anal Chim Acta* **1178**, 338551 (2021).

99. Gross, J. H. *Massenspektrometrie*. (Springer Berlin Heidelberg, 2012). doi:10.1007/978-3-8274-2981-0.

100. Ho, C. S. *et al.* Electrospray Ionisation Mass Spectrometry: Principles and Clinical Applications. *Clin Biochem Rev* **24**, 3 (2003).

101. Mittal, R. D. Tandem Mass Spectroscopy in Diagnosis and Clinical Research. *Indian Journal of Clinical Biochemistry* **30**, 121 (2015).

102. Brenig, K. *et al.* The Proteomic Landscape of Cysteine Oxidation That Underpins Retinoic Acid-Induced Neuronal Differentiation. *J Proteome Res* **19**, 1923–1940 (2020).

103. Tusher, V. G., Tibshirani, R. & Chu, G. Significance analysis of microarrays applied to the ionizing radiation response. *Proceedings of the National Academy of Sciences* **98**, 5116–5121 (2001).

104. Cox, J. & Mann, M. 1D and 2D annotation enrichment: a statistical method integrating quantitative proteomics with complementary high-throughput data. *BMC Bioinformatics* **13 Suppl 16**, 1–11 (2012).

105. Zhao, L. *et al.* OutCyte: a novel tool for predicting unconventional protein secretion. *Sci Rep* **9**, (2019).

106. Butler, A., Hoffman, P., Smibert, P., Papalexi, E. & Satija, R. Integrating single-cell transcriptomic data across different conditions, technologies, and species. *Nature Biotechnology 2018 36:5* **36**, 411–420 (2018).

107. Vidal, R. *et al.* Transcriptional heterogeneity of fibroblasts is a hallmark of the aging heart. *JCI Insight* **4**, (2019).

108. Alter, C. *et al.* IL-6 in the infarcted heart is preferentially formed by fibroblasts and is modulated by purinergic signaling. *Journal of Clinical Investigation* (2023) doi:10.1172/JCI163799.

109. Hesse, J. *et al.* Single-cell transcriptomics defines heterogeneity of epicardial cells and fibroblasts within the infarcted murine heart. *Elife* **10**, (2021).

110. Shi, S. Y. *et al.* Recent Advances in Single-Cell Profiling and Multispecific Therapeutics: Paving the Way for a New Era of Precision Medicine Targeting Cardiac Fibroblasts. *Curr Cardiol Rep* **23**, (2021).

111. Kiick, K. L., Saxon, E., Tirrell, D. A. & Bertozzi, C. R. Incorporation of azides into recombinant proteins for chemoselective modification by the Staudinger ligation. *Proc Natl Acad Sci U S A* **99**, 19–24 (2002).

112. Kiick, K. L., Saxon, E., Tirrell, D. A. & Bertozzi, C. R. Incorporation of azides into recombinant proteins for chemoselective modification by the Staudinger ligation. *Proc Natl Acad Sci U S A* **99**, 19–24 (2002).

113. Huang, D. W., Sherman, B. T. & Lempicki, R. A. Systematic and integrative analysis of large gene lists using DAVID bioinformatics resources. *Nat Protoc* **4**, 44–57 (2009).

114. Sherman, B. T. *et al.* DAVID: a web server for functional enrichment analysis and functional annotation of gene lists (2021 update). *Nucleic Acids Res* **50**, W216–W221 (2022).

115. Lichtenthaler, S. F., Lemberg, M. K. & Fluhrer, R. Proteolytic ectodomain shedding of membrane proteins in mammals—hardware, concepts, and recent developments. *EMBO J* **37**, 99456 (2018).

116. Morrow, G. B., Whyte, C. S. & Mutch, N. J. A Serpin With a Finger in Many PAIs: PAI-1's Central Function in Thromboinflammation and Cardiovascular Disease. *Front Cardiovasc Med* **8**, 180 (2021).

117. Ghosh, A. K. & Vaughan, D. E. PAI-1 in tissue fibrosis. *J Cell Physiol* **227**, 493–507 (2012).

118. Ghosh, A. K. *et al.* Cardiomyocyte PAI-1 influences the cardiac transcriptome and limits the extent of cardiac fibrosis in response to left ventricular pressure overload. *Cell Signal* **104**, (2023).

119. Jana, S. *et al.* Gelsolin is an important mediator of Angiotensin II-induced activation of cardiac fibroblasts and fibrosis. *The FASEB Journal* **35**, e21932 (2021).

120. Su, Y. Y. *et al.* Insulin-like growth factor binding protein-4 exerts antifibrotic activity by reducing levels of connective tissue growth factor and the C-X-C chemokine receptor 4. *FASEB Bioadv* **1**, 167–179 (2019).

121. Chiari, D. *et al.* The crossroad between autoimmune disorder, tissue remodeling and cancer of the thyroid: The long pentraxin 3 (PTX3). *Front Endocrinol (Lausanne)* **14**, (2023).

122. Erdei, A. *et al.* The versatile functions of complement C3-derived ligands. *Immunol Rev* **274**, 127–140 (2016).

123. Cserhalmi, M., Papp, A., Brandus, B., Uzonyi, B. & Józsi, M. Regulation of regulators: Role of the complement factor H-related proteins. *Semin Immunol* **45**, (2019).

124. Zhang, H. *et al.* Role of the CCL2-CCR2 axis in cardiovascular disease: Pathogenesis and clinical implications. *Front Immunol* **13**, 4894 (2022).

125. Hemmers, C. *et al.* Chemokine CCL9 Is Upregulated Early in Chronic Kidney Disease and Counteracts Kidney Inflammation and Fibrosis. *Biomedicines* **10**, (2022).

126. Hu, L., Zachariae, E. D., Larsen, U. G., Vilhardt, F. & Petersen, S. V. The dynamic uptake and release of SOD3 from intracellular stores in macrophages modulates the inflammatory response. *Redox Biol* **26**, (2019).

127. Zhang, H. *et al.* PEDF and 34-mer inhibit angiogenesis in the heart by inducing tip cells apoptosis via up-regulating PPAR-γ to increase surface FasL. *Apoptosis* **21**, 60–68 (2016).

128. Ito, Y. *et al.* Inhibition of angiogenesis and vascular leakiness by angiopoietin-related protein 4. *Cancer Res* **63**, 6651–6657 (2003).

129. Pius-Sadowska, E. & Machaliński, B. Pleiotropic activity of nerve growth factor in regulating cardiac functions and counteracting pathogenesis. *ESC Heart Fail* **8**, 974–987 (2021).

130. Jiang, H. *et al.* Angiocrine FSTL1 (Follistatin-Like Protein 1) Insufficiency Leads to Atrial and Venous Wall Fibrosis via SMAD3 Activation. *Arterioscler Thromb Vasc Biol* **40**, 958–972 (2020).

131. Zhan, W. *et al.* Pcsk6 Deficiency Promotes Cardiomyocyte Senescence by Modulating Ddit3-Mediated ER Stress. *Genes (Basel)* **13**, (2022).

132. Ren, J. & Anversa, P. The insulin-like growth factor I system: Physiological and pathophysiological implication in cardiovascular diseases associated with metabolic syndrome. *Biochem Pharmacol* **93**, 409–417 (2015).

133. Wang, Y. & Rodrigues, B. Intrinsic and extrinsic regulation of cardiac lipoprotein lipase following diabetes. *Biochim Biophys Acta* **1851**, 163–171 (2015).

134. Zhu, W. *et al.* IGFBP-4 is an inhibitor of canonical Wnt signalling required for cardiogenesis. *Nature 2008 454:7202* **454**, 345–349 (2008).

135. Pop, O.-T. *et al.* AXL expression on homeostatic resident liver macrophages is reduced in cirrhosis following GAS6 production by hepatic stellate cells. *Cell Mol Gastroenterol Hepatol* (2023) doi:10.1016/J.JCMGH.2023.03.007.

136. Frangogiannis, N. G. Cardiac fibrosis. *Cardiovasc Res* **117**, 1450–1488 (2021).

137. McKee, K. K., Harrison, D., Capizzi, S. & Yurchenco, P. D. Role of laminin terminal globular domains in basement membrane assembly. *Journal of Biological Chemistry* **282**, 21437–21447 (2007).

138. Toba, H. *et al.* Increased ADAMTS1 mediates SPARC-dependent collagen deposition in the aging myocardium. *Am J Physiol Endocrinol Metab* **310**, E1027–E1035 (2016).

139. Xia, Y. *et al.* Endogenous thrombospondin 1 protects the pressure-overloaded myocardium by modulating fibroblast phenotype and matrix metabolism. *Hypertension* **58**, 902–911 (2011).

140. Tamaoki, M. *et al.* Tenascin-C regulates recruitment of myofibroblasts during tissue repair after myocardial injury. *American Journal of Pathology* **167**, 71–80 (2005).

141. Ladage, D. *et al.* Stimulating Myocardial Regeneration with Periostin Peptide in Large Mammals Improves Function Post-Myocardial Infarction but Increases Myocardial Fibrosis. *PLoS One* **8**, e59656 (2013).

142. Hardy, S. A. *et al.* Novel role of extracellular matrix protein 1 (ECM1) in cardiac aging and myocardial infarction. *PLoS One* **14**, (2019).

143. Liu, Z. *et al.* Vascular peroxidase 1 is a novel regulator of cardiac fibrosis after myocardial infarction. *Redox Biol* **22**, 101151 (2019).

144. Pang, X. F., Lin, X., Du, J. J. & Zeng, D. Y. LTBP2 knockdown by siRNA reverses myocardial oxidative stress injury, fibrosis and remodelling during dilated cardiomyopathy. *Acta Physiologica* **228**, e13377 (2020).

145. Yin, A. *et al.* Exercise-derived peptide protects against pathological cardiac remodeling. *EBioMedicine* **82**, 104164 (2022).

146. Andenæs, K. *et al.* The extracellular matrix proteoglycan fibromodulin is upregulated in clinical and experimental heart failure and affects cardiac remodeling. *PLoS One* **13**, e0201422 (2018).

147. Valiente-Alandi, I. *et al.* Inhibiting Fibronectin Attenuates Fibrosis and Improves Cardiac Function in a Model of Heart Failure. *Circulation* **138**, 1236–1252 (2018).

148. Piecha, D. *et al.* Matrilin-2, a large, oligomeric matrix protein, is expressed by a great variety of cells and forms fibrillar networks. *J Biol Chem* **274**, 13353–13361 (1999).

149. Rao, M. *et al.* Resolving the intertwining of inflammation and fibrosis in human heart failure at single-cell level. *Basic Res Cardiol* **116**, (2021).

150. Vukicevic, S. *et al.* Bone morphogenetic protein 1.3 inhibition decreases scar formation and supports cardiomyocyte survival after myocardial infarction. doi:10.1038/s41467-021-27622-9.

151. McLellan, M. A. *et al.* High-Resolution Transcriptomic Profiling of the Heart During Chronic Stress Reveals Cellular Drivers of Cardiac Fibrosis and Hypertrophy. *Circulation* 1448–1463 (2020) doi:10.1161/CIRCULATIONAHA.119.045115.

152. López, B. *et al.* Impact of Treatment on Myocardial Lysyl Oxidase Expression and Collagen Cross-Linking in Patients With Heart Failure. *Hypertension* **53**, 236–242 (2009).

153. Allen, B. G. & Nattel, S. Role of the lysyl oxidase enzyme family in cardiac function and disease. doi:10.1093/cvr/cvz176.

154. Yang, J. *et al.* Targeting LOXL2 for cardiac interstitial fibrosis and heart failure treatment. *Nature Communications 2016 7:1* **7**, 1–15 (2016).

155. Schilter, H. *et al.* The lysyl oxidase like 2/3 enzymatic inhibitor, PXS-5153A, reduces crosslinks and ameliorates fibrosis. *J Cell Mol Med* **23**, 1759–1770 (2019).

156. Bai, Y. *et al.* LTBP-2 acts as a novel marker in human heart failure - a preliminary study. *Biomarkers* **17**, 407–415 (2012).

157. Zbinden, A. *et al.* Nidogen-1 Mitigates Ischemia and Promotes Tissue Survival and Regeneration. *Advanced Science* **8**, (2021).

158. Van Aelst, L. N. L. *et al.* Osteoglycin prevents cardiac dilatation and dysfunction after myocardial infarction through infarct collagen strengthening. *Circ Res* **116**, 425–436 (2015).

159. Imanaka-Yoshida, K., Tawara, I. & Yoshida, T. Tenascin-C in cardiac disease: a sophisticated controller of inflammation, repair, and fibrosis. *Am J Physiol Cell Physiol* **319**, C781–C796 (2020).

160. Wu, R. X. *et al.* Fibroblast migration after myocardial infarction is regulated by transient SPARC expression. *J Mol Med* **84**, 241–252 (2006).

161. Zhang, Y. L., Li, P. B., Han, X., Zhang, B. & Li, H. H. Blockage of Fibronectin 1 Ameliorates Myocardial Ischemia/Reperfusion Injury in Association with Activation of AMP-LKB1-AMPK Signaling Pathway. *Oxid Med Cell Longev* **2022**, (2022).

162. Jia, D. *et al.* Cardiac Resident Macrophage-Derived Legumain Improves Cardiac Repair by Promoting Clearance and Degradation of Apoptotic Cardiomyocytes After Myocardial Infarction. *Circulation* **145**, 1542–1556 (2022).

163. Fan, D. & Kassiri, Z. Biology of Tissue Inhibitor of Metalloproteinase 3 (TIMP3), and Its Therapeutic Implications in Cardiovascular Pathology. *Front Physiol* **11**, 661 (2020).

164. Li, X. *et al.* Neonatal Plasma Exosomes Contribute to Endothelial Cell-Mediated Angiogenesis and Cardiac Repair after Acute Myocardial Infarction. *Int J Mol Sci* **24**, (2023).

165. Takawale, A. *et al.* Myocardial overexpression of TIMP3 after myocardial infarction exerts beneficial effects by promoting angiogenesis and suppressing early proteolysis. *Am J Physiol Heart Circ Physiol* **313**, H224–H236 (2017).

166. Constantinou, C. *et al.* Human pluripotent stem cell-derived cardiomyocytes as a target platform for paracrine protection by cardiac mesenchymal stromal cells. *Sci Rep* **10**, (2020).

167. Tao, J. *et al.* Sfrp1 protects against acute myocardial ischemia (AMI) injury in aged mice by inhibiting the Wnt/β-catenin signaling pathway. *J Cardiothorac Surg* **16**, 1–10 (2021).

168. Li, J. *et al.* CPE Regulates Proliferation and Apoptosis of Primary Myocardial Cells Mediated by Ischemia and Hypoxia Injury. *J Healthc Eng* **2022**, (2022).

169. Peters, M. C. *et al.* Follistatin-like 1 promotes proliferation of matured human hypoxic iPSC-cardiomyocytes and is secreted by cardiac fibroblasts. *Mol Ther Methods Clin Dev* **25**, 3–16 (2022).

170. Li, X. *et al.* Slit2 Protects Hearts Against Ischemia-Reperfusion Injury by Inhibiting Inflammatory Responses and Maintaining Myofilament Contractile Properties. *Front Physiol* **0**, 228 (2020).

171. MacDonnell, S. *et al.* Activin A directly impairs human cardiomyocyte contractile function indicating a potential role in heart failure development. *Front Cardiovasc Med* **9**, 3114 (2022).

172. Yndestad, A. *et al.* Elevated Levels of Activin A in Heart Failure. *Circulation* **109**, 1379–1385 (2004).

173. Wu, R. *et al.* A Novel Human Long Noncoding RNA SCDAL Promotes Angiogenesis through SNF5-Mediated GDF6 Expression. *Advanced Science* **8**, 2004629 (2021).

174. Harrison, C. B. *et al.* Fibroblast Nox2 (NADPH Oxidase-2) Regulates ANG II (Angiotensin II)-Induced Vascular Remodeling and Hypertension via Paracrine Signaling to Vascular Smooth Muscle Cells. *Arterioscler Thromb Vasc Biol* **41**, 698–710 (2021).

175. Reboll, M. R. *et al.* Meteorin-like promotes heart repair through endothelial KIT receptor tyrosine kinase. *Science* **376**, 1343–1347 (2022).

176. Xi, Y. *et al.* Dynamic resistance exercise increases skeletal muscle-derived FSTL1 inducing cardiac angiogenesis via DIP2A-Smad2/3 in rats following myocardial infarction. *J Sport Health Sci* **10**, 594–603 (2021).

177. Maruyama, S. *et al.* Follistatin-like 1 promotes cardiac fibroblast activation and protects the heart from rupture. *EMBO Mol Med* **8**, 949–966 (2016).

178. Luo, S. *et al.* Cytokine receptor-like factor 1 (CRLF1) promotes cardiac fibrosis via ERK1/2 signaling pathway. *J Zhejiang Univ Sci B* **24**, 682–697 (2023).

179. Xu, H. *et al.* CCN5 attenuates profibrotic phenotypes of fibroblasts through the Smad6-CCN2 pathway: Potential role in epidural fibrosis. *Int J Mol Med* **36**, 123 (2015).

180. Emmens, R. W. *et al.* Endogenous C1-inhibitor production and expression in the heart after acute myocardial infarction. *Cardiovasc Pathol* **25**, 33–39 (2016).

181. Fang, Z. *et al.* The role of complement C3 in the outcome of regional myocardial infarction. *Biochem Biophys Rep* **33**, 101434 (2023).

182. Heinen, A. *et al.* IGF1 Treatment Improves Cardiac Remodeling after Infarction by Targeting Myeloid Cells. *Mol Ther* **27**, 46–58 (2019).

183. Dutka, M. *et al.* Osteoprotegerin and RANKL-RANK-OPG-TRAIL signalling axis in heart failure and other cardiovascular diseases. *Heart Failure Reviews 2021 27:4* **27**, 1395–1411 (2021).

184. Secchiero, P. *et al.* An imbalanced OPG/TRAIL ratio is associated to severe acute myocardial infarction. *Atherosclerosis* **210**, 274–277 (2010).

185. Molenaar, B. *et al.* Single-cell transcriptomics following ischemic injury identifies a role for B2M in cardiac repair. *Commun Biol* **4**, (2021).

186. Lu, L. *et al.* FSTL1-USP10-Notch1 Signaling Axis Protects Against Cardiac Dysfunction Through Inhibition of Myocardial Fibrosis in Diabetic Mice. *Front Cell Dev Biol* **9**, (2021).

187. Gong, L. *et al.* SLIT3 deficiency attenuates pressure overload-induced cardiac fibrosis and remodeling. *JCI Insight* **5**, (2020).

188. Howangyin, K. Y. *et al.* Myeloid-Epithelial-Reproductive Receptor Tyrosine Kinase and Milk Fat Globule Epidermal Growth Factor 8 Coordinately Improve Remodeling After Myocardial Infarction via Local Delivery of Vascular Endothelial Growth Factor. *Circulation* **133**, 826–839 (2016).

189. Zhang, H. *et al.* PEDF improves cardiac function in rats with acute myocardial infarction via inhibiting vascular permeability and cardiomyocyte apoptosis. *Int J Mol Sci* **16**, 5618–5634 (2015).

190. Petrera, A. *et al.* Cathepsin A inhibition attenuates myocardial infarction-induced heart failure on the functional and proteomic levels. *J Transl Med* **14**, 1–11 (2016).

191. Sun, M. *et al.* Cathepsin-L contributes to cardiac repair and remodelling post-infarction. *Cardiovasc Res* **89**, 374–383 (2011).

192. Van de Werf, F. & Arnold, A. E. R. Intravenous tissue plasminogen activator and size of infarct, left ventricular function, and survival in acute myocardial infarction. *BMJ* **297**, 1374–1379 (1988).

193. Körner, A. *et al.* Sema7A is crucial for resolution of severe inflammation. *Proc Natl Acad Sci U S A* **118**, (2021).

194. Ge, J. *et al.* Enhanced myocardial cathepsin B expression in patients with dilated cardiomyopathy. *Eur J Heart Fail* **8**, 284–289 (2006).

195. Girerd, N., Bresso, E., Devignes, M. D. & Rossignol, P. Insulin-like growth factor binding protein 2: A prognostic biomarker for heart failure hardly redundant with natriuretic peptides. *Int J Cardiol* **300**, 252–254 (2020).

196. Bracun, V. *et al.* Insulin-like growth factor binding protein 7 (IGFBP7), a link between heart failure and senescence. *ESC Heart Fail* **9**, (2022).

197. Ma, T. *et al.* Plasma osteoprotegerin predicts adverse cardiovascular events in stable coronary artery disease: the PEACE trial. *Front Cardiovasc Med* **10**, 1178153 (2023).

198. Vanhaverbeke, M. *et al.* Peripheral Blood RNA Levels of QSOX1 and PLBD1 Are New Independent Predictors of Left Ventricular Dysfunction After Acute Myocardial Infarction. *Circ Genom Precis Med* **12**, 561–572 (2019).

199. Fu, X. *et al.* Specialized fibroblast differentiated states underlie scar formation in the infarcted mouse heart. *J Clin Invest* **128**, 2127–2143 (2018).

200. Qin, C., Wu, X. L., Gu, J., Du, D. & Guo, Y. Mitochondrial Dysfunction Secondary to Endoplasmic Reticulum Stress in Acute Myocardial Ischemic Injury in Rats. *Med Sci Monit* **26**, (2020).

201. Yoo, D. Y. *et al.* Protein disulfide-isomerase A3 significantly reduces ischemia-induced damage by reducing oxidative and endoplasmic reticulum stress. *Neurochem Int* **122**, 19–30 (2019).

202. Ibarrola, J. *et al.* Galectin-3 down-regulates antioxidant peroxiredoxin-4 in human cardiac fibroblasts: a new pathway to induce cardiac damage. *Clin Sci (Lond)* **132**, 1471–1485 (2018).

203. Rusu-Nastase, E. G. *et al.* MiR-29a Increase in Aging May Function as a Compensatory Mechanism Against Cardiac Fibrosis Through SERPINH1 Downregulation. *Front Cardiovasc Med* **8**, 810241 (2022).

204. García-Bermúdez, M. *et al.* Association study of MIA3 rs17465637 polymorphism with cardiovascular disease in rheumatoid arthritis patients. *DNA Cell Biol* **31**, 1412–1417 (2012).

205. Martínez-Martínez, E. *et al.* Differential Proteomics Identifies Reticulocalbin-3 as a Novel Negative Mediator of Collagen Production in Human Cardiac Fibroblasts. *Sci Rep* **7**, (2017).

206. Zhang, F. *et al.* Long noncoding RNA Cfast regulates cardiac fibrosis. *Mol Ther Nucleic Acids* **23**, 377–392 (2021).

207. Tian, G. *et al.* Voltage-dependent anion channel 1 (VDAC1) overexpression alleviates cardiac fibroblast activation in cardiac fibrosis via regulating fatty acid metabolism. *Redox Biol* **67**, (2023).

208. Tian, F. *et al.* Protein disulfide isomerase increases in myocardial endothelial cells in mice exposed to chronic hypoxia: a stimulatory role in angiogenesis. *Am J Physiol Heart Circ Physiol* **297**, (2009).

209. Toldo, S., Severino, A., Abbate, A. & Baldi, A. The Role of PDI as a Survival Factor in Cardiomyocyte Ischemia. *Methods Enzymol* **489**, 47–65 (2011).

210. Pereira, R. M. *et al.* Protective molecular mechanisms of clusterin against apoptosis in cardiomyocytes. *Heart Fail Rev* **23**, 123–129 (2018).

211. Gong, Y., Zhao, Y., Li, Y., Fan, Y. & Hoover-Plow, J. Plasminogen regulates cardiac repair after myocardial infarction through its noncanonical function in stem cell homing to the infarcted heart. *J Am Coll Cardiol* **63**, 2862–2872 (2014).

212. Graham, J. B. *et al.* Endoplasmic reticulum transmembrane protein TMTC3 contributes to O-mannosylation of E-cadherin, cellular adherence, and embryonic gastrulation. *Mol Biol Cell* **31**, 167–183 (2020).

213. Ferris, S. P., Jaber, N. S., Molinari, M., Arvan, P. & Kaufman, R. J. UDP-glucose:glycoprotein glucosyltransferase (UGGT1) promotes substrate solubility in the endoplasmic reticulum. *Mol Biol Cell* **24**, 2597–2608 (2013).

214. Liu, Z. B., Fu, X. H., Wei, G. & Gao, J. L. Cytochrome c release in acute myocardial infarction predicts poor prognosis and myocardial reperfusion on contrast-enhanced magnetic resonance imaging. *Coron Artery Dis* **25**, 66–72 (2014).

215. Anzell, A. R., Maizy, R., Przyklenk, K. & Sanderson, T. H. Mitochondrial Quality Control and Disease: Insights into Ischemia-Reperfusion Injury. *Molecular Neurobiology 2017 55:3* **55**, 2547–2564 (2017).

216. Köhler, A. *et al.* New specific HSP47 functions in collagen subfamily chaperoning. *FASEB J* **34**, 12040–12052 (2020).

217. Geisler, A. *et al.* microRNA122-regulated transgene expression increases specificity of cardiac gene transfer upon intravenous delivery of AAV9 vectors. *Gene Ther* **18**, 199–209 (2011).

218. Qiao, C. *et al.* Liver-specific microRNA-122 target sequences incorporated in AAV vectors efficiently inhibits transgene expression in the liver. *Gene Ther* **18**, 403–410 (2011).

219. Ivey, M. J. & Tallquist, M. D. Defining the Cardiac Fibroblast. *Circulation Journal* **80**, 2269–2276 (2016).

220. Alex, L. *et al.* Cardiac Pericytes Acquire a Fibrogenic Phenotype and Contribute to Vascular Maturation After Myocardial Infarction. *Circulation* **148**, 882–898 (2023).

221. Travers, J. G., Kamal, F. A., Robbins, J., Yutzey, K. E. & Blaxall, B. C. Cardiac Fibrosis: The Fibroblast Awakens. *Circ Res* **118**, 1021–1040 (2016).

222. Snider, P. *et al.* Origin of cardiac fibroblasts and the role of periostin. *Circ Res* **105**, 934–947 (2009).

223. Zeisberg, E. M. *et al.* Endothelial-to-mesenchymal transition contributes to cardiac fibrosis. *Nat Med* **13**, 952–961 (2007).

224. Swonger, J. M., Liu, J. S., Ivey, M. J. & Tallquist, M. D. Genetic tools for identifying and manipulating fibroblasts in the mouse. *Differentiation* **92**, 66–83 (2016).

225. Kissel, H. *et al.* Point mutation in kit receptor tyrosine kinase reveals essential roles for kit signaling in spermatogenesis and oogenesis without affecting other kit responses. *EMBO J* **19**, 1312–1326 (2000).

226. Liu, J., Jang, J. Y., Pirooznia, M., Liu, S. & Finkel, T. The secretome mouse provides a genetic platform to delineate tissue-specific in vivo secretion. *Proc Natl Acad Sci U S A* **118**, (2021).

227. Branon, T. C. *et al.* Efficient proximity labeling in living cells and organisms with TurboID. *Nature Biotechnology 2018 36:9* **36**, 880–887 (2018).

7. Appendix

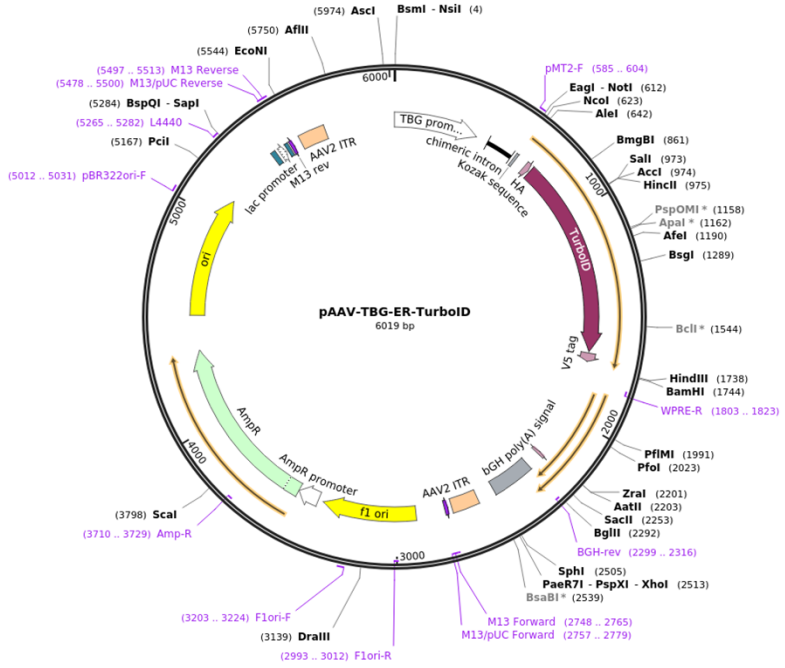

Figure 32: Scheme of plasmid *pAAV-TBG-ER-TurboID.* The plasmid was purchased from Addgene (#149415)[84]

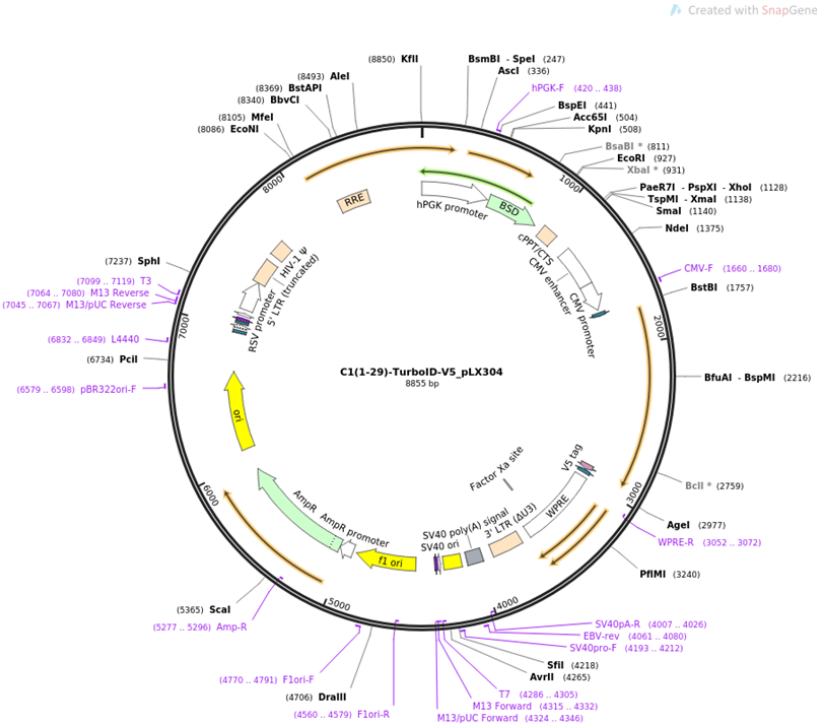

Figure 33: Scheme of the pAAV-POSTN-ER-TurboID plasmid with an ER-located TurboID sequence. The plasmid was constructed by the research group of Prof. Dr. Patrick Most, University Medical Center Freiburg using *pAAV-TBG-ER-TurboID* purchased from Addgene (#149415) and exchanging the *TBG* promoter for the *Periostin* promoter from Lindsley *et al.*[96].

Table 27: CF-secreted proteins 5 d post MI and 5 d post Sham. Proteins are presented with their secretion pathway, subcategories, and subclasses. LC-MS/MS intensities are depicted as means with SD, along with their corresponding -Log p-values, differences between MI and Sham and fold changes between MI and Sham. Significantly altered proteins between MI and Sham are annotated in red.

Protein	OutCyte	Subcategory	Subclass	Mean Sham	SD Sham	Mean MI	SD MI	-Log p-value	Difference	Fold change
POSTN	Conv	ECM	Matricellular	1,68E+08	3,21E+07	1,07E+09	1,08E+08	5,41	2,69	6,38
CPE	Conv	P/A	Signal transduction	3,47E+07	1,28E+07	2,77E+08	4,33E+07	4,23	3,06	7,98
ACTG1	UPS	P/A	Cell development	NaN	NaN	9,00E+06	5,52E+06	3,82	3,68	NaN
LOXL3	Conv	ECM	Cross-linking	2,65E+06	7,42E+05	2,23E+07	7,58E+06	3,91	3,05	8,41
SLIT2	Conv/UPS	P/A	Angiogenesis	9,85E+06	4,46E+06	6,61E+07	1,24E+07	3,20	2,88	6,71
PXDN	Conv	ECM	Cross-linking	1,67E+06	1,46E+06	1,81E+07	8,55E+06	2,94	4,08	10,83
OPG/ TNFRSF11B	Conv	P/A	Signal transduction	NaN	NaN	7,52E+06	4,52E+06	2,91	3,79	NaN
CRLF1	Conv/UPS	P/A	Signal transduction	NaN	NaN	1,29E+07	8,81E+06	2,90	3,70	NaN
COL12A1	Conv	ECM	Collagens	1,87E+06	1,28E+06	2,07E+07	1,34E+07	2,78	3,67	11,05
IGFBP2	Conv	P/A	Growth regulation	NaN	NaN	8,50E+06	8,05E+06	2,65	3,83	NaN
COL16A1	Conv	ECM	Collagens	NaN	NaN	5,36E+06	2,14E+06	2,62	3,32	NaN
ECM1	Conv	ECM	Matricellular	2,90E+07	1,22E+07	9,40E+07	8,66E+06	2,82	1,80	3,24
GDF6	Conv	P/A	Growth regulation	7,24E+06	2,75E+06	2,87E+07	7,39E+06	2,73	2,05	3,96
FN1	Conv/UPS	ECM	Matricellular	1,72E+09	6,57E+08	5,96E+09	7,76E+08	2,76	1,89	3,46
BMP1	Conv	ECM	Others	NaN	NaN	6,69E+06	2,60E+06	2,53	2,97	NaN
DNAJB11	Conv	P/A	Cell development	NaN	NaN	3,62E+06	1,07E+06	2,53	1,56	NaN
SFRP1	Conv	P/A	Wnt regulation	2,74E+06	2,44E+06	1,26E+07	6,07E+06	2,15	3,60	4,59
PLOD1	Conv/UPS	ECM	Cross-linking	2,60E+06	6,53E+05	9,04E+06	5,29E+06	2,27	1,87	3,47
LTBP2	Conv/UPS	ECM	Matricellular	5,60E+06	2,37E+06	4,22E+07	2,85E+07	1,99	3,80	7,53
COL1A1	Conv	ECM	Collagens	8,36E+07	6,15E+07	8,29E+08	3,34E+08	1,94	3,91	9,92
INHBA	Conv	P/A	Growth regulation	6,88E+07	3,73E+07	2,99E+08	8,69E+07	1,92	2,37	4,34
LAMA2	Conv	ECM	Laminins	6,81E+06	4,18E+06	2,31E+07	1,15E+07	1,86	2,29	3,39
SEMA7A	Conv	P/A	Inflammatory response	NaN	NaN	4,36E+06	2,36E+06	1,77	2,74	NaN
TIMP3	Conv/UPS	ECM	Matrix turnover	1,31E+06	1,36E+05	1,17E+07	1,20E+07	1,78	2,49	8,97
MATN2	Conv	ECM	Others	NaN	NaN	7,66E+06	8,55E+06	1,74	2,71	NaN

Protein	OutCyte	Subcategory	Subclass	Mean Sham	SD Sham	Mean MI	SD MI	-Log p-value	Difference	Fold change
LOX	Conv	ECM	Cross-linking	4,97E+08	1,69E+08	1,01E+09	1,16E+08	2,10	1,09	2,03
LAMA4	Conv	ECM	Laminins	3,60E+06	8,21E+04	1,12E+07	6,02E+06	1,67	2,92	3,10
FMOD	Conv	ECM	Others	NaN	NaN	1,42E+06	2,74E+05	1,80	1,65	NaN
CCDC80	Conv	ECM	Others	2,64E+07	1,28E+07	7,28E+07	2,69E+07	1,65	1,50	2,76
PSAP	Conv	P/A	Cell development	1,54E+07	2,12E+07	4,45E+07	1,98E+07	1,47	2,99	2,88
COL4A5	Conv	ECM	Collagens	6,82E+06	4,45E+06	3,39E+07	2,45E+07	1,46	3,02	4,97
MGP	Conv	P/A	Others	NaN	NaN	3,31E+07	1,56E+07	1,38	3,81	NaN
PEDF	Conv	P/A	Angiogenesis	2,96E+07	1,46E+07	7,25E+07	9,29E+06	1,54	1,50	2,45
FBLN5	Conv	ECM	Matricellular	2,91E+07	1,95E+07	7,06E+07	1,91E+07	1,55	1,46	2,42
SFRP2	Conv	P/A	Wnt regulation	NaN	NaN	2,23E+07	1,11E+07	1,36	3,86	NaN
WISP2	Conv	P/A	Wnt regulation	9,23E+06	8,31E+06	2,93E+07	1,27E+07	1,37	3,09	3,17
AXL	Conv	P/A	Inflammatory response	2,64E+06	1,44E+06	5,82E+06	1,81E+06	1,54	1,24	2,21
AEBP1	Conv	ECM	Others	1,08E+07	3,90E+06	3,32E+07	2,48E+07	1,45	1,45	3,08
LTBP4	Conv	ECM	Matricellular	6,98E+06	3,51E+06	2,34E+07	7,99E+06	1,32	2,87	3,34
CTSA	Conv	P/A	Others	2,95E+06	2,33E+06	7,31E+06	2,18E+06	1,31	2,39	2,48
COL6A1	Conv	ECM	Collagens	3,02E+06	2,54E+06	1,31E+07	1,06E+07	1,29	2,83	4,33
ADAM12	Conv/UPS	ECM	Matrix turnover	1,33E+06	2,08E+05	5,20E+06	3,96E+06	1,29	2,07	3,90
TNC	Conv	ECM	Matricellular	1,52E+07	1,99E+07	3,93E+07	2,36E+07	1,18	3,35	2,59
SVEP1	Conv	P/A	Cell adhesion	9,52E+06	8,31E+06	2,69E+07	1,30E+07	1,23	1,81	2,83
EFEMP2	Conv/UPS	ECM	Matricellular	4,37E+08	5,61E+07	7,29E+08	2,18E+08	1,52	0,70	1,67
CCL9	Conv	P/A	Inflammatory response	1,82E+07	1,21E+07	6,23E+07	4,13E+07	1,10	2,87	3,42
ADAMTS2	Conv	ECM	Matrix turnover	NaN	NaN	3,46E+06	2,68E+06	1,08	2,00	NaN
COL1A2	Conv	ECM	Collagens	1,60E+09	7,67E+08	3,13E+09	8,05E+08	1,20	1,08	1,95
SERPINA3N	Conv/UPS	P/A	Inflammatory response	3,08E+06	3,84E+05	1,31E+07	1,06E+07	1,00	2,19	4,25
COL5A2	Conv	ECM	Collagens	5,93E+08	2,76E+08	1,37E+09	6,83E+08	1,04	1,27	2,32
PAI-1	Conv	P/A	Growth regulation	7,06E+09	2,37E+09	1,11E+10	2,07E+09	1,19	0,71	1,57
FBN1	Conv	ECM	Others	2,03E+09	7,07E+08	3,20E+09	5,67E+08	1,12	0,73	1,58
TIMP2	Conv/UPS	ECM	Matrix turnover	1,87E+08	6,72E+07	2,70E+08	1,29E+07	1,20	0,60	1,44

Protein	OutCyte	Subcategory	Subclass	Mean Sham	SD Sham	Mean MI	SD MI	-Log p-value	Difference	Fold change
MFAP5	Conv	ECM	Others	NaN	NaN	1,42E+07	1,14E+07	0,88	2,32	NaN
LTBP3	Conv	ECM	Matricellular	NaN	NaN	2,64E+06	1,59E+06	0,92	1,25	NaN
COL8A1	Conv	ECM	Collagens	1,86E+08	5,59E+07	5,19E+08	3,41E+08	0,92	1,20	2,79
APP	Conv	P/A	Cell adhesion	1,32E+07	6,83E+06	2,16E+07	5,67E+06	0,85	1,79	1,63
SPARC	Conv	ECM	Matricellular	2,69E+08	1,33E+08	4,52E+08	1,18E+08	0,96	0,87	1,68
FNDC1	Conv	P/A	Others	3,18E+06	NaN	1,20E+07	1,09E+07	0,82	2,41	3,76
FSTL1	Conv	P/A	Angiogenesis	9,91E+06	3,45E+06	1,36E+07	1,02E+07	0,82	2,20	1,37
DAG1	Conv	ECM	Others	2,75E+07	1,11E+07	4,88E+07	2,07E+07	0,91	0,78	1,77
LOXL2	Conv	ECM	Cross-linking	2,51E+07	1,68E+07	4,45E+07	1,95E+07	0,84	0,93	1,78
LAMB2	TM	ECM	Laminins	1,04E+07	7,36E+06	1,57E+07	4,11E+06	0,75	2,19	1,51
EMILIN1	Conv	ECM	Others	2,84E+06	2,13E+06	3,12E+06	1,03E+06	0,82	1,06	1,10
FBLN1	Conv	ECM	Matricellular	1,43E+07	8,91E+06	3,64E+07	2,80E+07	0,78	1,24	2,55
PCSK6	Conv	P/A	Others	1,30E+07	5,56E+06	2,30E+07	9,71E+06	0,81	0,81	1,76
LAMC1	Conv/UPS	ECM	Laminins	2,00E+07	1,86E+07	3,62E+07	1,11E+07	0,71	1,80	1,81
HSP47	Conv	P/A	Others	1,84E+06	6,22E+05	2,21E+06	6,09E+05	0,90	0,54	1,20
IGFBP7	Conv	P/A	Growth regulation	2,20E+07	2,92E+07	2,46E+07	1,35E+07	0,68	2,23	1,12
SPON2	Conv	ECM	Others	5,44E+06	NaN	3,83E+06	3,01E+06	0,68	1,84	0,70
SLIT3	Conv	P/A	Angiogenesis	4,24E+06	2,10E+06	1,15E+07	1,33E+07	0,69	1,57	2,72
PCOLCE2	Conv	ECM	Cross-linking	2,40E+06	NaN	2,32E+06	9,89E+05	0,77	0,78	0,96
QSOX1	Conv	P/A	Growth regulation	3,46E+07	4,19E+07	6,25E+07	3,89E+07	0,69	1,56	1,81
ADAM15	Conv	ECM	Matrix turnover	NaN	NaN	3,47E+06	4,72E+06	0,70	1,41	NaN
ASPN	Conv	ECM	Others	NaN	NaN	5,10E+06	1,79E+06	0,68	1,57	NaN
CSF1	Conv/UPS	P/A	Growth regulation	NaN	NaN	9,01E+06	3,48E+06	0,65	2,04	NaN
METRNL	Conv	P/A	Others	6,57E+06	3,95E+06	8,33E+06	2,48E+06	0,68	1,23	1,27
SPARCL1	Conv	ECM	Matricellular	1,73E+06	5,78E+05	4,72E+06	3,23E+06	0,65	1,30	2,73
COL4A1	Conv	ECM	Collagens	4,64E+08	2,46E+08	9,40E+08	5,83E+08	0,68	0,95	2,02
THBS1	Conv	ECM	Matricellular	2,18E+08	1,21E+08	3,26E+08	9,18E+07	0,71	0,73	1,49
CTSL	Conv/UPS	P/A	Others	4,72E+07	3,39E+07	7,17E+07	2,19E+07	0,67	0,88	1,52
COL3A1	TM	ECM	Collagens	5,67E+08	3,36E+08	1,03E+09	5,10E+08	0,64	1,06	1,81

Protein	OutCyte	Subcategory	Subclass	Mean Sham	SD Sham	Mean MI	SD MI	-Log p-value	Difference	Fold change
COL4A2	TM	ECM	Collagens	7,35E+08	4,07E+08	1,38E+09	7,62E+08	0,65	0,88	1,87
LGMN	Conv	ECM	Others	1,90E+06	7,87E+05	4,56E+06	3,53E+06	0,62	1,15	2,40
MMP2	Conv/UPS	ECM	Matrix turnover	4,78E+07	9,75E+06	6,77E+07	2,16E+07	0,77	0,46	1,42
BGN	Conv	ECM	Cross-linking	4,97E+08	5,93E+07	6,38E+08	1,58E+08	0,89	0,34	1,28
PAM	Conv/UPS	P/A	Others	6,70E+06	1,77E+06	1,28E+07	7,58E+06	0,65	0,75	1,91
COL5A3	TM	ECM	Collagens	NaN	NaN	1,83E+06	1,40E+06	0,60	1,12	NaN
RNASE4	Conv	P/A	Others	4,74E+07	3,73E+07	6,89E+07	1,57E+07	0,60	1,02	1,45
NTN4	Conv	P/A	Cell adhesion	NaN	NaN	2,26E+06	1,74E+06	0,59	1,09	NaN
CLSTN1	Conv	P/A	Cell adhesion	1,84E+07	1,43E+07	1,98E+07	1,15E+07	0,54	1,60	1,08
PLAT	Conv	P/A	Others	1,42E+07	6,61E+06	2,36E+07	1,12E+07	0,59	0,76	1,66
CTGF	Conv	ECM	Matricellular	3,21E+08	1,35E+08	5,54E+08	3,34E+08	0,57	0,65	1,72
GDN	Conv/UPS	P/A	Others	NaN	NaN	3,77E+06	2,88E+06	0,54	0,83	NaN
GRN	Conv/UPS	P/A	Cell development	1,28E+08	4,11E+07	1,81E+08	7,54E+07	0,62	0,46	1,41
PLOD3	Conv	ECM	Cross-linking	2,18E+07	7,64E+06	3,51E+07	1,88E+07	0,57	0,59	1,61
QPCT	Conv	P/A	Others	1,43E+06	4,86E+05	3,13E+06	1,06E+06	0,48	0,88	2,19
MFGE8	Conv	P/A	Cell adhesion	8,32E+07	6,36E+07	1,09E+08	3,00E+07	0,49	0,82	1,32
TIMP1	Conv	ECM	Matrix turnover	5,99E+08	3,33E+08	8,43E+08	3,09E+08	0,50	0,63	1,41
LGALS3BP	Conv	P/A	Cell adhesion	5,95E+07	4,07E+07	7,46E+07	1,94E+07	0,40	0,83	1,25
OAF	Conv	P/A	Others	4,90E+06	3,86E+06	5,88E+06	3,68E+06	0,39	0,72	1,20
CCL2	Conv	P/A	Inflammatory response	8,71E+07	3,45E+07	7,07E+07	3,03E+07	0,33	1,50	0,81
ADAMTSL3	IC/TM	ECM	Matrix turnover	4,89E+06	3,18E+06	8,37E+06	5,00E+06	0,30	1,12	1,71
SDF4	Conv	P/A	Others	4,40E+06	2,01E+06	6,91E+06	3,24E+06	0,29	0,52	1,57
HSPG2	Conv	ECM	Cross-linking	3,78E+08	3,13E+08	4,45E+08	2,52E+08	0,26	0,45	1,18
NID2	Conv	ECM	Matrix turnover	5,68E+06	3,42E+06	2,90E+06	1,33E+06	0,24	0,59	0,51
ADM	Conv	P/A	Angiogenesis	NaN	NaN	2,71E+07	2,21E+07	0,21	1,16	NaN
NUCB2	Conv	ECM	Others	1,16E+07	3,69E+06	1,43E+07	6,31E+06	0,25	0,26	1,23
THBS2	Conv	ECM	Matricellular	8,34E+06	8,88E+06	7,05E+06	2,60E+06	0,20	0,73	0,85
DPT	Conv	ECM	Cross-linking	3,04E+06	1,76E+05	3,22E+06	1,83E+06	0,22	0,29	1,06

Protein	OutCyte	Subcategory	Subclass	Mean Sham	SD Sham	Mean MI	SD MI	-Log p-value	Difference	Fold change
TCN2	Conv	P/A	Others	9,88E+06	5,93E+06	1,06E+07	2,34E+06	0,23	0,25	1,07
FRZB	Conv	P/A	Wnt regulation	2,98E+07	2,31E+07	7,65E+07	1,17E+08	0,20	0,57	2,56
COL6A3	Conv	ECM	Collagens	NaN	NaN	1,22E+06	7,32E+05	0,21	0,32	NaN
CTSB	Conv	P/A	Others	1,83E+07	2,42E+07	1,38E+07	2,09E+06	0,18	0,37	0,76
OLFML3	Conv	P/A	Cell adhesion	1,73E+07	1,23E+07	1,87E+07	9,52E+06	0,17	0,41	1,08
TGFBI	Conv	ECM	Matricellular	5,80E+06	4,30E+06	3,11E+07	2,47E+07	0,16	0,67	5,37
LOXL1	Conv	ECM	Cross-linking	2,77E+08	1,54E+08	2,77E+08	1,72E+07	0,16	0,17	1,00
ADAMTS1	IC/TM	ECM	Matrix turnover	5,35E+06	4,61E+06	3,66E+06	1,71E+06	0,14	0,34	0,69
C3	Conv/UPS	P/A	Inflammatory response	1,34E+08	6,82E+07	2,01E+08	1,75E+08	0,14	0,31	1,50
B2M	Conv	P/A	Inflammatory response	1,13E+08	7,44E+07	1,39E+08	1,05E+08	0,13	0,68	1,23
LAMB1	TM	ECM	Laminins	NaN	NaN	2,15E+06	1,94E+06	0,13	0,35	NaN
NUCB1	Conv	ECM	Others	4,27E+08	9,96E+07	4,50E+08	9,78E+07	0,12	0,08	1,05
NGF	IC/TM	P/A	Growth regulation	2,11E+07	5,77E+06	2,38E+07	9,90E+06	0,10	0,11	1,13
PRELP	Conv	ECM	Others	3,26E+06	2,25E+06	4,16E+06	2,05E+06	0,06	0,23	1,28
PCOLCE	Conv/UPS	ECM	Cross-linking	2,36E+08	5,16E+07	2,40E+08	2,62E+07	0,09	0,04	1,02
C1-INH	Conv	P/A	Inflammatory response	2,77E+07	4,31E+06	3,42E+07	2,14E+07	0,06	0,08	1,23
CFH	Conv/UPS	P/A	Inflammatory response	1,35E+07	1,84E+07	1,10E+07	6,76E+06	0,04	0,20	0,81
CST3	Conv	P/A	Cell development	1,53E+08	6,55E+07	1,46E+08	2,05E+07	0,04	0,05	0,96
NID1	Conv	ECM	Matrix turnover	2,00E+09	5,70E+08	1,97E+09	1,56E+08	0,04	0,02	0,98
GAS6	Conv	P/A	Inflammatory response	NaN	NaN	5,40E+05	1,86E+05	0,02	0,04	NaN
SRPX2	Conv	P/A	Wnt regulation	4,83E+07	1,77E+07	5,89E+07	4,12E+07	0,02	0,03	1,22
IGF1	TM	P/A	Growth regulation	1,57E+07	4,92E+06	1,76E+07	2,30E+06	0,01	-0,03	1,12
LUM	Conv	ECM	Others	9,98E+07	4,21E+07	9,48E+07	3,66E+07	0,02	-0,03	0,95
OGN	Conv	ECM	Others	6,72E+06	4,02E+06	6,15E+06	3,93E+06	0,04	-0,08	0,91
LTBP1	Conv	ECM	Matricellular	4,35E+07	1,33E+07	4,19E+07	1,03E+07	0,05	-0,04	0,96
APOE	Conv	P/A	Growth regulation	5,91E+07	1,50E+07	7,10E+07	5,79E+07	0,04	-0,08	1,20
PROS1	Conv	P/A	Others	NaN	NaN	2,12E+06	1,26E+06	0,08	-0,20	NaN

Protein	OutCyte	Subcategory	Subclass	Mean Sham	SD Sham	Mean MI	SD MI	-Log p-value	Difference	Fold change
ZFP462	IC	P/A	Others	9,17E+06	2,94E+06	7,93E+06	6,17E+05	0,23	-0,15	0,87
FBLN2	Conv	ECM	Matricellular	7,18E+08	3,07E+08	5,91E+08	1,55E+08	0,22	-0,21	0,82
PTX3	Conv	P/A	Inflammatory response	3,51E+08	1,04E+08	3,00E+08	4,56E+07	0,32	-0,19	0,85
EFEMP1	Conv/UPS	ECM	Matricellular	9,52E+07	6,37E+07	7,10E+07	5,78E+07	0,26	-0,49	0,75
PLAU	Conv	P/A	Others	1,71E+06	6,65E+05	1,34E+06	4,35E+05	0,35	-0,31	0,78
IGFBP4	Conv/UPS	P/A	Growth regulation	3,81E+08	5,13E+07	3,38E+08	2,05E+08	0,35	-0,39	0,89
GSN	Conv/UPS	P/A	Growth regulation	9,31E+08	2,49E+08	7,45E+08	1,96E+08	0,55	-0,32	0,80
SOD3	Conv	P/A	Others	3,17E+06	2,05E+06	1,95E+06	3,45E+05	0,44	-0,76	0,62
LPL	Conv	P/A	Others	3,37E+06	5,61E+05	2,21E+06	1,63E+05	0,50	-0,78	0,66
TSKU	Conv	P/A	Cell development	1,13E+06	NaN	7,39E+05	4,21E+05	0,56	-0,67	0,66
CP	Conv/UPS	P/A	Others	NaN	NaN	7,91E+05	7,69E+05	0,55	-0,98	NaN
ANGPTL4	Conv	P/A	Cell adhesion	1,50E+07	7,18E+06	9,29E+06	1,71E+06	0,69	-0,57	0,62
DCN	Conv	ECM	Cross-linking	2,03E+08	9,63E+07	1,25E+08	3,13E+07	0,70	-0,60	0,61
MMP3	Conv	ECM	Matrix turnover	2,00E+09	4,08E+08	1,43E+09	8,44E+08	0,70	-0,65	0,71
IGFBP3	Conv	P/A	Growth regulation	4,40E+07	1,96E+07	2,54E+07	1,69E+07	0,66	-0,88	0,58
DNAH7B	IC	P/A	Others	1,10E+08	4,89E+07	1,19E+08	4,67E+07	NaN	NaN	1,08

Table 28: CF-secreted proteins 3 d post MI and 3 d post Sham. Proteins are presented with their subcategories and subclasses. LC-MS/MS intensities are depicted as means with SD, along with their corresponding -Log p-values, differences between MI and Sham and fold changes between MI and Sham. Significantly altered proteins between MI and Sham are annotated in red.

Protein	Subcategory	Subclass	Mean Sham	SD Sham	Mean MI	SD MI	-Log p-value	Difference	Fold change
COL1A1	ECM	Collagens	5,91E+06	5,97E+06	9,41E+08	6,27E+08	3,89	8,02	159,18
CPE	P/A	Signal transduction	3,94E+06	3,11E+06	2,29E+08	1,05E+08	3,48	6,66	58,18
WISP2	P/A	Wnt regulation	NaN	NaN	1,67E+07	8,18E+06	3,55	4,84	NaN
SERPINA3N	P/A	Inflammatory response	NaN	NaN	1,93E+07	1,62E+07	3,50	5,29	NaN
COL4A5	ECM	Collagens	1,51E+06	2,03E+05	2,04E+07	1,65E+07	3,17	3,91	13,55
CCL9	P/A	Inflammatory response	2,97E+06	8,94E+05	8,69E+07	5,79E+07	2,94	6,06	29,25
FBLN1	ECM	Matricellular	1,29E+06	NaN	4,07E+07	3,38E+07	2,84	6,00	31,54

Protein	Subcategory	Subclass	Mean Sham	SD Sham	Mean MI	SD MI	-Log p-value	Difference	Fold change
SFRP1	P/A	Wnt regulation	NaN	NaN	1,27E+07	1,04E+07	2,84	4,33	NaN
IGF1	P/A	Growth regulation	NaN	NaN	9,33E+06	7,62E+06	2,82	3,99	NaN
LGALS3BP	P/A	Cell adhesion	4,77E+06	3,08E+06	1,06E+08	7,44E+07	2,75	5,07	22,25
FN1	ECM	Matricellular	5,91E+08	3,79E+08	5,59E+09	1,96E+09	2,83	3,44	9,46
COL3A1	ECM	Collagens	4,44E+07	3,54E+07	9,17E+08	5,10E+08	2,66	4,74	20,66
DNAJB11	P/A	Cell development	NaN	NaN	3,20E+06	2,12E+06	2,74	2,96	NaN
CTSA	P/A	Others	1,53E+06	NaN	6,77E+06	4,07E+06	2,52	3,55	4,44
COL1A2	ECM	Collagens	3,67E+08	2,46E+08	3,46E+09	1,79E+09	2,52	3,39	9,44
MFAP5	ECM	Others	2,97E+05	NaN	2,37E+07	1,58E+07	2,42	4,97	79,66
GDF6	P/A	Growth regulation	3,02E+06	NaN	2,46E+07	1,63E+07	2,41	4,46	8,16
COL16A1	ECM	Collagens	7,89E+04	NaN	8,84E+06	5,48E+06	2,11	4,08	112,09
COL12A1	ECM	Collagens	NaN	NaN	2,14E+07	2,75E+07	2,03	3,99	NaN
LAMA2	ECM	Laminins	1,71E+06	NaN	1,90E+07	1,22E+07	2,01	4,39	11,14
TCN2	P/A	Others	1,18E+06	5,95E+05	1,74E+07	1,86E+07	2,01	3,56	14,68
TNC	ECM	Matricellular	NaN	NaN	2,51E+07	2,08E+07	1,94	4,52	NaN
LOXL2	ECM	Cross-linking	1,80E+07	NaN	5,59E+07	3,85E+07	1,91	5,34	3,11
COL5A2	ECM	Collagens	1,98E+08	1,86E+08	1,19E+09	6,32E+08	2,01	2,87	6,00
EFEMP2	ECM	Matricellular	1,95E+08	8,35E+07	6,80E+08	2,45E+08	2,12	1,84	3,48
DAG1	ECM	Others	1,09E+07	5,43E+06	4,01E+07	1,61E+07	2,09	1,92	3,69
CTSL	P/A	Others	1,14E+07	6,25E+06	6,08E+07	3,36E+07	1,96	2,36	5,32
QSOX1	P/A	Growth regulation	8,31E+06	7,27E+06	7,60E+07	5,89E+07	1,80	5,13	9,14
PXDN	ECM	Cross-linking	NaN	NaN	1,25E+07	9,69E+06	1,84	3,88	NaN
TGFBI	ECM	Matricellular	1,46E+06	1,86E+05	2,11E+07	2,74E+07	1,79	3,21	14,42
FBLN5	ECM	Matricellular	9,02E+06	3,63E+06	5,85E+07	2,49E+07	1,76	3,70	6,48
SLIT2	P/A	Angiogenesis	7,42E+06	2,70E+05	4,03E+07	3,77E+07	1,68	3,87	5,43
SVEP1	P/A	Cell adhesion	3,34E+06	NaN	2,14E+07	1,91E+07	1,66	3,89	6,40
METRNL	P/A	Others	2,53E+06	1,95E+06	6,21E+06	3,08E+06	1,79	1,93	2,45
ECM1	ECM	Matricellular	1,51E+07	2,04E+07	9,82E+07	7,75E+07	1,61	3,28	6,49

Protein	Subcategory	Subclass	Mean Sham	SD Sham	Mean MI	SD MI	-Log p-value	Difference	Fold change
COL8A1	ECM	Collagens	5,79E+07	4,81E+07	5,31E+08	2,59E+08	1,57	4,06	9,16
LTBP4	ECM	Matricellular	2,10E+06	NaN	1,07E+07	8,60E+06	1,60	2,83	5,12
MGP	P/A	Others	NaN	NaN	5,06E+07	5,88E+07	1,51	5,08	NaN
COL4A1	ECM	Collagens	1,30E+08	9,11E+07	6,07E+08	4,79E+08	1,60	2,23	4,67
AEBP1	ECM	Others	5,29E+06	3,71E+06	3,73E+07	2,83E+07	1,48	3,95	7,05
HSPG2	ECM	Cross-linking	7,64E+07	4,49E+07	2,35E+08	1,00E+08	1,64	1,72	3,07
POSTN	ECM	Matricellular	1,68E+08	1,29E+08	7,55E+08	4,29E+08	1,56	2,37	4,50
EFEMP1	ECM	Matricellular	1,44E+07	1,12E+07	9,50E+07	6,92E+07	1,47	3,64	6,58
PCOLCE2	ECM	Cross-linking	NaN	NaN	1,85E+06	1,66E+06	1,57	1,88	NaN
FBN1	ECM	Others	7,72E+08	5,24E+08	3,40E+09	1,62E+09	1,52	2,29	4,40
MFGE8	P/A	Cell adhesion	2,85E+07	1,76E+07	1,04E+08	5,34E+07	1,54	2,02	3,65
B2M	P/A	Inflammatory response	4,79E+07	2,82E+07	1,63E+08	8,86E+07	1,56	1,81	3,40
CCDC80	ECM	Others	9,90E+06	8,92E+06	6,03E+07	4,46E+07	1,46	2,95	6,09
RNASE4	P/A	Others	1,58E+07	1,69E+07	5,61E+07	2,18E+07	1,47	2,41	3,55
APOE	P/A	Growth regulation	1,16E+07	8,85E+06	1,28E+08	1,79E+08	1,32	3,88	11,05
IGFBP7	P/A	Growth regulation	NaN	NaN	2,79E+07	9,44E+06	1,30	3,86	NaN
PLAT	P/A	Others	5,80E+06	6,52E+06	2,11E+07	1,44E+07	1,31	2,56	3,63
LOXL3	ECM	Cross-linking	1,98E+06	1,43E+06	3,51E+07	4,04E+07	1,26	3,55	17,72
LTBP3	ECM	Matricellular	NaN	NaN	5,34E+06	2,87E+06	1,28	2,52	NaN
PSAP	P/A	Cell development	2,99E+06	2,34E+06	2,74E+07	2,66E+07	1,24	3,44	9,17
LTBP2	ECM	Matricellular	3,79E+06	NaN	3,39E+07	1,86E+07	1,21	3,38	8,94
FSTL1	P/A	Angiogenesis	NaN	NaN	1,58E+07	4,13E+06	1,21	3,28	NaN
FBN2	ECM	Matricellular	NaN	NaN	1,53E+07	1,25E+07	1,20	3,49	NaN
LGMN	ECM	Others	1,10E+06	3,24E+05	8,35E+06	5,97E+06	1,24	2,48	7,59
FRZB	P/A	Wnt regulation	1,92E+07	2,69E+07	7,69E+07	7,15E+07	1,24	2,49	4,00
C1-INH	P/A	Inflammatory response	8,72E+06	7,09E+06	5,85E+07	6,46E+07	1,22	2,89	6,71
OGN	ECM	Others	4,04E+06	NaN	1,36E+07	1,37E+07	1,20	3,30	3,36
MATN2	ECM	Others	NaN	NaN	1,79E+07	1,18E+07	1,19	3,30	NaN

Protein	Subcategory	Subclass	Mean Sham	SD Sham	Mean MI	SD MI	-Log p-value	Difference	Fold change
MMP2	ECM	Matrix turnover	1,55E+07	1,93E+07	5,30E+07	3,40E+07	1,22	2,18	3,41
SRPX2	P/A	Wnt regulation	1,70E+07	1,42E+07	4,89E+07	2,29E+07	1,25	1,76	2,88
PEDF	P/A	Angiogenesis	1,49E+07	1,64E+07	7,59E+07	6,05E+07	1,17	2,91	5,09
PLOD3	ECM	Cross-linking	9,05E+06	8,62E+06	3,13E+07	2,16E+07	1,15	3,11	3,46
LOX	ECM	Cross-linking	2,46E+08	1,45E+08	7,01E+08	2,75E+08	1,23	1,69	2,85
LAMC1	ECM	Laminins	6,08E+06	1,96E+06	2,62E+07	2,24E+07	1,12	3,50	4,32
CTSB	P/A	Others	5,07E+06	1,87E+06	1,83E+07	1,62E+07	1,13	2,90	3,61
PAM	P/A	Others	1,51E+06	7,04E+05	7,00E+06	7,64E+06	1,16	2,35	4,64
OPG/ TNFRSF11B	P/A	Signal transduction	NaN	NaN	4,49E+06	5,18E+05	1,15	2,26	NaN
GRN	P/A	Cell development	5,64E+07	2,28E+07	1,87E+08	1,19E+08	1,20	1,52	3,31
LAMA4	ECM	Laminins	1,42E+06	NaN	7,80E+06	7,43E+06	1,12	2,26	5,49
INHBA	P/A	Growth regulation	5,91E+07	5,26E+07	2,04E+08	1,28E+08	1,11	2,42	3,45
SLIT3	P/A	Angiogenesis	8,29E+05	NaN	9,97E+06	1,02E+07	1,10	2,67	12,02
SPARC	ECM	Matricellular	1,01E+08	7,00E+07	3,45E+08	2,05E+08	1,15	1,79	3,40
NID1	ECM	Matrix turnover	7,19E+08	3,70E+08	1,59E+09	6,46E+08	1,18	1,21	2,21
APP	P/A	Cell adhesion	3,72E+06	NaN	2,31E+07	1,25E+07	1,04	2,74	6,23
THBS2	ECM	Matricellular	NaN	NaN	9,59E+06	1,08E+07	1,00	2,81	NaN
ADAM12	ECM	Matrix turnover	NaN	NaN	5,23E+06	4,48E+06	1,01	2,07	NaN
NUCB2	ECM	Others	5,28E+06	2,40E+06	9,30E+06	8,39E+06	0,97	2,43	1,76
COL4A2	ECM	Collagens	3,09E+08	3,08E+08	8,63E+08	6,41E+08	0,98	1,84	2,80
NTN4	P/A	Cell adhesion	NaN	NaN	2,16E+06	7,46E+05	1,01	1,44	NaN
LAMB2	ECM	Laminins	9,52E+05	NaN	1,78E+07	4,09E+06	0,94	2,55	18,68
C3	P/A	Inflammatory response	8,37E+07	9,44E+07	2,80E+08	3,42E+08	0,90	2,94	3,35
OLFML3	P/A	Cell adhesion	7,82E+06	8,87E+06	1,75E+07	1,76E+07	0,88	2,71	2,23
CFH	P/A	Inflammatory response	NaN	NaN	9,11E+06	8,91E+06	0,90	2,21	NaN
LOXL1	ECM	Cross-linking	1,06E+08	4,84E+07	1,83E+08	6,27E+07	0,99	0,84	1,72
TIMP1	ECM	Matrix turnover	2,60E+08	2,20E+08	5,93E+08	4,00E+08	0,84	1,51	2,28
PLOD1	ECM	Cross-linking	1,65E+06	NaN	1,03E+07	7,25E+06	0,78	2,45	6,23

Protein	Subcategory	Subclass	Mean Sham	SD Sham	Mean MI	SD MI	-Log p-value	Difference	Fold change
SRPX	P/A	Wnt regulation	NaN	NaN	6,92E+06	6,13E+06	0,78	2,62	NaN
CST3	P/A	Cell development	5,71E+07	3,63E+07	1,14E+08	6,06E+07	0,84	1,10	2,00
NUCB1	ECM	Others	1,30E+08	9,88E+07	2,81E+08	1,55E+08	0,81	1,29	2,16
COL6A1	ECM	Collagens	NaN	NaN	1,25E+07	8,34E+06	0,74	2,19	NaN
LTBP1	ECM	Matricellular	1,23E+07	7,73E+06	2,80E+07	1,52E+07	0,77	1,44	2,28
EMILIN1	ECM	Others	NaN	NaN	2,40E+06	1,55E+06	0,78	1,14	NaN
PAI-1	P/A	Growth regulation	5,26E+09	3,72E+09	8,87E+09	2,85E+09	0,78	0,99	1,69
IGFBP4	P/A	Growth regulation	1,12E+08	8,23E+07	2,29E+08	1,60E+08	0,75	1,24	2,05
FNDC1	P/A	Others	NaN	NaN	1,46E+07	2,36E+07	0,68	2,08	NaN
DPT	ECM	Cross-linking	NaN	NaN	5,83E+06	7,59E+06	0,69	1,65	NaN
BGN	ECM	Cross-linking	3,36E+08	2,76E+08	5,71E+08	3,37E+08	0,64	1,00	1,70
ADAMTS1	ECM	Matrix turnover	NaN	NaN	3,20E+06	1,83E+06	0,61	1,34	NaN
ADAMTSL3	ECM	Matrix turnover	1,68E+06	1,07E+06	8,97E+06	1,95E+06	0,58	1,77	5,35
MMP3	ECM	Matrix turnover	6,37E+08	4,16E+08	9,89E+08	3,98E+08	0,65	0,81	1,55
CCL2	P/A	Inflammatory response	1,49E+07	7,97E+06	2,27E+07	1,58E+07	0,58	1,93	1,53
GSN	P/A	Growth regulation	3,10E+08	2,38E+08	5,36E+08	3,94E+08	0,58	0,89	1,73
OAF	P/A	Others	2,97E+06	5,81E+05	1,21E+07	7,92E+06	0,47	1,73	4,09
MMP14	ECM	Matrix turnover	3,43E+06	1,36E+06	1,38E+07	8,64E+06	0,47	1,46	4,04
LUM	ECM	Others	4,04E+07	4,36E+07	7,85E+07	7,91E+07	0,44	1,54	1,94
FBLN2	ECM	Matricellular	3,17E+08	2,28E+08	4,39E+08	1,86E+08	0,47	0,72	1,38
AXL	P/A	Inflammatory response	1,73E+06	NaN	3,22E+06	2,86E+06	0,45	0,70	1,86
CLSTN1	P/A	Cell adhesion	3,21E+06	1,10E+06	1,14E+07	7,02E+06	0,40	1,73	3,53
ACTB	P/A	Cell development	NaN	NaN	2,72E+06	3,58E+06	0,42	0,94	NaN
TIMP2	ECM	Matrix turnover	9,49E+07	5,31E+07	1,89E+08	1,30E+08	0,42	0,78	1,99
SPARCL1	ECM	Matricellular	7,60E+05	NaN	3,57E+06	2,81E+06	0,38	0,93	4,70
CTSD	P/A	Others	1,82E+06	NaN	3,02E+06	3,10E+06	0,34	0,84	1,66
PCOLCE	ECM	Cross-linking	1,22E+08	9,62E+07	1,79E+08	1,08E+08	0,35	0,66	1,47
PCSK6	P/A	Others	9,71E+06	1,09E+07	1,11E+07	5,46E+06	0,32	0,80	1,15

Protein	Subcategory	Subclass	Mean Sham	SD Sham	Mean MI	SD MI	-Log p-value	Difference	Fold change
NGF	P/A	Growth regulation	1,34E+07	1,42E+07	1,18E+07	3,65E+06	0,29	1,13	0,88
PTX3	P/A	Inflammatory response	1,18E+08	9,87E+07	1,68E+08	1,59E+08	0,29	0,74	1,42
DCN	ECM	Cross-linking	7,58E+07	7,95E+07	9,69E+07	8,82E+07	0,22	0,85	1,28
CTGF	ECM	Matricellular	2,38E+08	1,69E+08	3,42E+08	2,89E+08	0,21	0,45	1,44
NID2	ECM	Matrix turnover	NaN	NaN	1,43E+06	1,03E+06	0,12	0,27	NaN
THBS1	ECM	Matricellular	1,62E+08	1,57E+08	1,67E+08	1,63E+08	0,10	0,32	1,03
GDN	P/A	Others	5,34E+06	NaN	5,25E+06	4,43E+06	0,10	0,40	0,98
IGFBP3	P/A	Growth regulation	3,85E+07	2,69E+07	3,29E+07	2,76E+07	0,13	-0,36	0,86
ANGPTL4	P/A	Cell adhesion	7,56E+06	5,28E+06	4,23E+06	2,08E+06	0,23	-0,81	0,56
MFAP4	ECM	Others	NaN	NaN	6,25E+06	3,56E+06	NaN	NaN	NaN

Table 29: POSTN^{+}CF-secreted proteins *in vivo* 5 d post MI and 5 d post Sham. LC-MS/MS intensities are depicted as means with SD, along with their corresponding -Log p-values, differences between MI and Sham and fold changes between MI and Sham. Significantly altered proteins between MI and Sham are annotated in red.

Proteins	Mean Sham	SD Sham	Mean MI	SD MI	-Log p-value	Difference	Fold change
FN1	2,03E+05	3,02E+05	1,37E+06	1,63E+06	-1,48	1,20	6,74
GAPDH	4,02E+06	8,00E+06	9,69E+05	1,45E+06	-1,23	0,31	0,24
GM8797	1,70E+05	7,66E+04	1,32E+05	9,01E+04	-1,17	0,48	0,78
VIM	4,93E+04	2,35E+04	2,30E+05	2,23E+05	-1,05	0,23	4,66
HIST1H2AA	2,58E+05	1,45E+05	1,52E+05	5,75E+04	-3,02	0,09	0,59
C9	1,08E+05	1,25E+05	4,36E+05	4,55E+05	3,60	0,35	4,04
KNG1	8,74E+05	7,91E+05	1,05E+06	5,98E+05	4,01	0,41	1,20
HRG	3,29E+05	2,80E+05	8,28E+05	4,77E+05	5,07	1,14	2,51
	4,99E+06	4,13E+06	7,97E+06	4,35E+06	3,92	0,78	1,60
SERPINA1A	2,01E+05	1,41E+05	1,10E+05	4,41E+04	3,42	0,27	0,55
BTD	7,44E+04	1,67E+04	8,15E+04	1,86E+04	3,46	1,31	1,09
BLVRB	NaN	NaN	9,62E+04	4,55E+04	2,40	1,59	NaN
GPX3	1,20E+05	8,98E+04	1,08E+05	1,11E+05	-0,42	0,66	0,89
FBLN5	NaN	NaN	1,37E+05	1,17E+05	0,25	0,90	NaN

Proteins	Mean Sham	SD Sham	Mean MI	SD MI	-Log p-value	Difference	Fold change
AI182371	1,14E+05	3,96E+04	2,78E+05	1,96E+05	5,18	1,12	2,45
AGT	2,08E+05	6,04E+04	1,30E+05	1,91E+04	3,50	0,30	0,62
LDHB	5,67E+05	9,12E+05	NaN	NaN	-2,37	0,13	NaN
C8A	9,17E+04	9,78E+04	5,23E+05	5,58E+05	4,33	0,83	5,70
ITIH4	9,22E+04	6,01E+04	6,82E+05	5,97E+05	4,48	2,19	7,40
ALDOA	7,58E+05	1,46E+06	3,27E+05	4,74E+05	-0,73	0,44	0,43
HBBT1	3,16E+06	1,40E+06	4,06E+07	4,15E+07	-0,75	2,86	12,84
ANXA2	1,26E+05	5,85E+04	8,04E+04	5,74E+04	-1,48	0,75	0,64
PRDX1	4,67E+05	7,62E+05	1,82E+05	2,43E+05	-0,75	0,01	0,39
GM20547	2,27E+05	3,79E+05	2,75E+05	2,53E+05	3,19	0,71	1,21
GPD1	4,90E+05	8,99E+05	3,65E+04	2,54E+04	-1,28	0,40	0,07
FGA	7,01E+05	8,04E+05	1,56E+06	1,36E+06	0,21	0,29	2,22
TFDP2	6,78E+05	1,19E+06	6,20E+04	1,50E+04	-2,18	0,41	0,09
HSPG2	6,18E+04	9,69E+04	1,11E+05	1,75E+05	-1,31	0,21	1,79
CP	2,78E+05	2,40E+05	5,65E+05	5,40E+05	5,38	0,54	2,04
GM4788	2,08E+05	7,28E+04	6,71E+05	4,38E+05	5,18	1,42	3,22
CFH	2,10E+05	2,39E+05	1,33E+06	1,65E+06	4,82	1,14	6,35
CUX1	1,37E+06	5,41E+05	1,12E+06	4,51E+05	5,18	0,59	0,82
C4BP	NaN	NaN	1,03E+05	2,72E+04	4,04	2,40	NaN
ITIH1	1,13E+05	8,35E+04	1,64E+05	5,14E+04	2,54	0,37	1,45
SERPINA3N	4,22E+05	2,94E+05	1,03E+06	9,72E+05	6,19	0,80	2,44
F2	2,69E+05	3,15E+05	1,36E+05	8,75E+04	1,85	0,48	0,51
PGAM2	7,85E+04	2,08E+04	NaN	3,60E+05	NaN	0,36	NaN
GPLD1	4,46E+04	3,14E+03	7,49E+04	2,38E+04	3,18	1,02	1,68
WDR1	NaN	NaN	3,57E+04	1,50E+04	0,69	0,05	NaN
AFM	1,25E+05	1,10E+05	1,78E+05	1,37E+05	3,21	0,52	1,42
CA2	2,60E+05	1,52E+05	4,13E+05	2,76E+05	2,00	0,52	1,59
C3	1,01E+06	7,09E+05	2,04E+06	1,63E+06	3,50	0,90	2,01
C4B	5,43E+05	5,09E+05	1,45E+06	1,12E+06	6,80	1,02	2,67

Proteins	Mean Sham	SD Sham	Mean MI	SD MI	-Log p-value	Difference	Fold change
HBB-B2	3,74E+04	1,78E+04	1,77E+06	1,60E+06	0,30	3,01	47,33
FABP4	2,28E+05	1,25E+05	6,32E+05	7,51E+05	1,56	0,09	2,77
MB	3,37E+05	5,25E+05	1,46E+05	1,61E+05	-0,76	0,77	0,43
TUBA1B	2,08E+05	2,73E+05	1,64E+05	1,37E+05	-0,88	0,05	0,79
LDHA	NaN	NaN	2,19E+05	2,44E+05	-1,61	0,41	NaN
C5	8,72E+04	9,76E+04	3,40E+05	5,39E+05	3,80	0,68	3,90
APOA4	1,82E+05	6,21E+04	2,01E+05	6,42E+04	3,83	0,54	1,11
TTR	9,14E+05	7,93E+05	7,87E+05	5,09E+05	4,49	0,35	0,86
CKM	3,45E+06	6,52E+06	3,80E+05	5,31E+05	-2,30	0,26	0,11
ALB	1,62E+07	1,15E+07	1,70E+07	6,16E+06	1,93	0,32	1,05
EEF1A1	1,47E+05	3,51E+04	1,13E+05	5,74E+04	0,73	0,23	0,77
NID1	1,32E+05	9,05E+04	4,48E+05	4,41E+05	-0,55	0,45	3,38
EIF4A2	NaN	NaN	5,17E+04	1,97E+04	-0,62	0,09	NaN
FABP3	1,08E+05	6,12E+04	2,72E+05	3,81E+05	-0,14	0,02	2,52
HSP90AB1	NaN	NaN	1,27E+05	1,95E+05	2,46	0,90	NaN
GSN	5,72E+05	7,90E+05	4,73E+05	5,68E+05	0,22	0,08	0,83
PLG	2,18E+06	1,26E+06	3,93E+06	1,57E+06	7,05	1,11	1,80
GC	4,16E+06	2,85E+06	3,33E+06	1,63E+06	6,81	0,14	0,80
SERPINA1B	1,04E+06	9,20E+05	1,20E+06	5,24E+05	4,39	0,48	1,15
CES1C	1,13E+06	1,11E+06	1,08E+06	5,34E+05	6,13	0,41	0,96
KLKB1	2,76E+05	2,49E+05	5,92E+05	4,97E+05	6,16	0,78	2,14
BGN	NaN	NaN	3,71E+05	3,95E+05	0,08	0,86	NaN
MUG1	8,34E+05	9,57E+05	2,40E+06	2,71E+06	5,27	0,78	2,88
ATIII	1,19E+06	1,41E+06	1,53E+06	1,05E+06	4,87	0,59	1,29
FBLN2	2,52E+05	1,58E+05	3,52E+05	4,47E+05	-1,99	0,34	1,39
MBL1	3,45E+05	1,84E+05	6,77E+05	3,76E+05	5,22	1,08	1,96
MBL2	1,01E+05	2,94E+04	8,22E+04	2,11E+04	4,02	0,82	0,82
LIFR	1,29E+06	7,88E+05	1,35E+06	7,00E+05	7,36	0,13	1,05
HEP2	1,17E+05	1,07E+05	1,14E+05	7,78E+04	1,57	0,05	0,98

Proteins	Mean Sham	SD Sham	Mean MI	SD MI	-Log p-value	Difference	Fold change
LUM	6,48E+05	7,51E+05	2,64E+05	3,00E+05	-0,13	0,21	0,41
ACTB	1,51E+06	1,20E+06	1,10E+06	9,22E+05	-1,13	0,42	0,73
YWHAE	1,14E+05	4,19E+04	1,27E+05	5,04E+04	-1,62	0,59	1,11
EEF1A2	9,50E+05	1,70E+06	4,09E+05	5,48E+05	-1,85	0,23	0,43
ACTC1	9,84E+05	9,99E+05	5,31E+05	8,35E+05	-0,21	0,10	0,54
HIST1H4A	2,81E+05	7,21E+04	2,19E+05	1,41E+05	-1,62	0,65	0,78
HSPA8	1,41E+05	2,05E+05	3,65E+05	4,87E+05	-0,02	0,02	2,59
TUBB4B	4,69E+05	6,95E+05	3,05E+05	2,52E+05	-1,26	0,39	0,65
C1-INH	6,86E+05	6,05E+05	2,07E+06	1,47E+06	6,45	1,13	3,02
PEDF	1,88E+05	1,88E+05	6,60E+05	1,66E+05	4,94	2,19	3,51
APOA1	1,30E+06	6,99E+05	1,19E+06	3,85E+05	3,42	0,47	0,91
SERPINA1C	1,28E+06	1,36E+06	1,85E+06	1,23E+06	2,99	0,69	1,44
SERPINA1D	1,35E+07	1,22E+07	1,78E+07	7,35E+06	3,11	0,70	1,32
SERPINA1E	6,76E+05	4,26E+05	8,04E+05	5,84E+05	1,88	0,06	1,19
EGFR	8,52E+05	2,72E+05	1,85E+06	8,65E+05	7,87	1,44	2,17
APOH	1,28E+06	4,51E+05	1,98E+06	8,54E+05	8,04	0,71	1,55
SERPINA3M	NaN	NaN	1,21E+05	1,26E+05	2,59	1,13	NaN
SERPINA6	1,13E+05	7,55E+04	1,49E+05	1,08E+05	4,04	0,12	1,32
CLU	NaN	NaN	1,01E+05	3,49E+04	1,80	0,80	NaN
AMBP	8,78E+04	5,58E+04	1,06E+05	5,01E+04	2,57	0,87	1,20
F13B	NaN	NaN	1,15E+05	4,19E+04	4,38	2,22	NaN
FGG	2,78E+05	3,01E+05	6,55E+05	6,06E+05	-0,21	0,58	2,35
KRT76	1,02E+07	1,16E+07	6,68E+06	2,58E+06	-4,47	0,25	0,65
CFI	2,07E+05	1,18E+05	4,02E+05	2,06E+05	5,60	0,95	1,94
PRDX2	4,26E+05	6,71E+05	2,41E+05	2,90E+05	-0,78	0,19	0,56
A2AP	1,60E+05	7,94E+04	2,41E+05	1,33E+05	4,10	0,63	1,51
A2M	2,45E+06	2,56E+06	1,19E+07	1,12E+07	5,77	1,58	4,87
OGN	NaN	NaN	2,77E+05	3,66E+05	0,98	1,06	NaN
POSTN	NaN	NaN	2,04E+05	2,89E+05	-0,91	1,22	NaN

Proteins	Mean Sham	SD Sham	Mean MI	SD MI	-Log p-value	Difference	Fold change
KNG2	8,42E+04	2,07E+04	1,01E+05	4,50E+04	1,47	0,61	1,20
C8B	NaN	NaN	9,23E+04	3,25E+04	2,46	0,83	NaN
FGB	4,33E+05	5,17E+05	9,55E+05	8,99E+05	0,10	0,70	2,21
C8G	2,83E+05	2,11E+05	4,87E+05	4,16E+05	3,20	0,86	1,72
HBA2	1,04E+06	5,44E+05	8,65E+06	6,66E+06	-0,76	2,74	8,30
C6	2,30E+05	1,80E+05	9,18E+05	8,71E+05	6,86	0,79	3,99
HPX	8,02E+06	6,38E+06	6,29E+06	4,46E+06	6,20	0,10	0,78
LRG1	1,15E+06	7,44E+05	1,14E+06	6,02E+05	7,07	0,09	0,99
UGP2	2,83E+05	4,39E+05	7,27E+04	4,38E+04	-0,63	0,19	0,26
TF	7,31E+07	2,88E+07	6,11E+07	2,92E+07	6,30	0,39	0,84
CPN2	NaN	NaN	2,22E+04	3,51E+03	1,46	0,27	NaN
ICA	5,41E+05	4,11E+05	7,95E+05	4,96E+05	6,17	0,42	1,47
CPB2	7,78E+05	3,51E+05	8,64E+05	3,58E+05	6,32	0,15	1,11
ACTN2	5,73E+05	1,11E+06	2,28E+05	2,85E+05	-0,26	0,04	0,40
FETUB	2,39E+05	1,33E+05	2,78E+05	1,40E+05	5,25	0,19	1,16
HGFAC	1,98E+05	5,11E+04	1,62E+05	8,90E+04	4,16	0,20	0,82
PYGM	2,28E+06	3,88E+06	3,97E+05	4,02E+05	-1,17	0,07	0,17

Table 30: *In vivo* POSTN$^+$ CF proteome from heart tissue 5 d post MI and 5 d post Sham. LC-MS/MS intensities are depicted as means with SD, along with their corresponding -Log p-values, differences between MI and Sham and fold changes between MI and Sham. Significantly altered proteins between MI and Sham are annotated in red.

Protein	Mean Sham	SD Sham	Mean MI	SD MI	-Log p-value	Difference	Fold change
ACACB	1,07E+09	3,29E+08	8,30E+08	2,55E+08	0,58	-0,37	0,78
PCCA	1,08E+10	3,19E+09	7,82E+09	1,82E+09	0,91	-0,45	0,73
PCX	2,93E+09	1,01E+09	2,25E+09	5,00E+08	0,59	-0,33	0,77
ACACA	1,47E+08	7,78E+07	1,75E+08	5,21E+07	0,44	0,37	1,19
MCCC1	4,81E+09	1,49E+09	3,50E+09	9,82E+08	0,81	-0,46	0,73
PCCB	9,30E+07	2,92E+07	7,13E+07	1,15E+07	0,71	-0,33	0,77

Protein	Mean Sham	SD Sham	Mean MI	SD MI	-Log p-value	Difference	Fold change
ATP2A2	3,53E+07	1,45E+07	2,24E+07	8,29E+06	0,84	-0,65	0,64
ACAA2	3,81E+07	1,28E+07	3,93E+07	1,80E+07	0,02	-0,02	1,03
ATP5F1A	4,43E+07	1,10E+07	3,04E+07	1,42E+07	1,01	-0,67	0,69
ACO2	2,90E+07	9,11E+06	1,79E+07	6,83E+06	1,20	-0,75	0,62
MB	2,61E+07	9,85E+06	1,68E+07	7,64E+06	0,76	-0,64	0,64
C4B	2,14E+06	1,99E+06	8,30E+06	9,17E+06	1,32	2,09	3,88
COL6A3	6,49E+05	8,57E+05	8,26E+06	1,15E+07	0,03	0,14	12,71
GAPDH	4,46E+07	1,20E+07	3,63E+07	1,07E+07	0,52	-0,32	0,81
TUBB4B	1,84E+07	4,78E+06	1,91E+07	6,18E+06	0,01	0,01	1,04
HADHA	2,00E+07	5,44E+06	1,40E+07	6,27E+06	0,91	-0,63	0,70
TUBB5	8,49E+05	5,03E+05	1,97E+06	3,93E+05	2,19	1,44	2,33
ACTB	1,25E+07	4,92E+06	2,06E+07	4,99E+06	1,46	0,80	1,64
PZP	8,33E+06	4,11E+06	1,05E+07	5,09E+06	0,37	0,34	1,26
HBB-BS	5,72E+06	4,28E+06	3,13E+07	4,20E+07	1,41	2,03	5,47
ETFA	1,77E+07	6,38E+06	8,85E+06	6,34E+06	1,35	-1,26	0,50
TUBB2A	NaN	NaN	1,95E+05	5,11E+04	1,20	1,47	NaN
HSPA8	8,19E+06	2,82E+06	9,33E+06	2,67E+06	0,29	0,21	1,14
ACTA2	5,64E+06	2,50E+06	5,32E+06	1,10E+06	0,05	0,05	0,94
TUBA1A	2,20E+06	1,03E+06	4,93E+06	1,31E+06	2,00	1,32	2,24
HSP90B1	3,17E+06	1,20E+06	1,48E+07	4,86E+06	4,41	2,22	4,66
TUBA4A	6,81E+06	1,87E+06	1,10E+07	2,75E+06	1,57	0,71	1,61
IDH2	1,23E+07	2,42E+06	8,35E+06	2,97E+06	1,36	-0,62	0,68
ALB	5,83E+06	2,43E+06	6,27E+06	1,41E+06	0,27	0,19	1,08
SLC25A4	5,15E+07	1,14E+07	3,41E+07	1,32E+07	1,22	-0,68	0,66
PLG	3,10E+05	1,67E+05	1,72E+06	2,06E+06	2,10	3,22	5,57
ALDOA	5,25E+06	1,65E+06	4,74E+06	1,69E+06	0,24	-0,18	0,90
MYBPC3	3,71E+06	1,35E+06	2,98E+06	1,25E+06	0,38	-0,36	0,80
SERPINA3K	7,38E+06	3,74E+06	6,88E+06	1,63E+06	0,03	0,03	0,93
ETFB	8,50E+06	2,62E+06	4,78E+06	2,85E+06	1,44	-1,00	0,56

Protein	Mean Sham	SD Sham	Mean MI	SD MI	-Log p-value	Difference	Fold change
TUBB3	NaN	NaN	1,24E+05	3,68E+04	0,77	1,01	NaN
HSPA9	7,88E+06	2,18E+06	6,04E+06	2,64E+06	0,71	-0,47	0,77
TUFM	8,70E+06	2,34E+06	6,81E+06	2,06E+06	0,62	-0,37	0,78
MCCC2	6,74E+06	2,62E+06	4,87E+06	1,16E+06	0,63	-0,40	0,72
MIA3	NaN	NaN	3,58E+06	8,63E+05	7,57	6,29	NaN
HBA-A1	4,62E+06	3,00E+06	1,47E+07	1,61E+07	1,22	1,44	3,18
P4HB	6,91E+05	4,17E+05	8,15E+06	2,35E+06	5,07	3,75	11,79
SLC25A5	1,05E+06	3,32E+05	8,74E+05	3,34E+05	0,42	-0,29	0,83
CSRP3	7,06E+06	1,42E+06	8,71E+06	1,13E+06	1,13	0,32	1,23
MUG1	2,10E+06	9,93E+05	3,23E+06	2,21E+06	0,32	0,39	1,53
MDH2	3,46E+06	1,65E+06	5,66E+06	3,70E+06	0,45	0,64	1,64
ACADVL	4,03E+06	1,91E+06	3,00E+06	1,75E+06	0,42	-0,45	0,74
CKMT2	3,61E+06	1,50E+06	3,46E+06	1,86E+06	0,07	-0,11	0,96
COL6A1	3,65E+05	2,80E+05	3,35E+06	5,64E+06	0,07	-0,28	9,18
ATP5F1B	6,45E+06	2,76E+06	8,62E+06	6,88E+06	0,05	0,09	1,34
HADHB	7,05E+06	1,63E+06	4,74E+06	2,21E+06	1,11	-0,71	0,67
SRL	2,18E+06	1,27E+06	6,76E+06	2,44E+06	2,54	1,81	3,10
HSPD1	2,75E+06	9,42E+05	2,43E+06	8,11E+05	0,24	-0,18	0,88
SUCLA2	6,21E+06	1,49E+06	4,75E+06	1,99E+06	0,72	-0,50	0,76
EEF1A1	6,80E+05	3,86E+05	1,45E+06	4,03E+05	1,53	1,32	2,13
HSPA5	5,22E+05	3,22E+05	3,39E+06	1,06E+06	3,62	2,98	6,49
HBB-B2	NaN	NaN	5,72E+05	6,76E+05	1,09	2,11	NaN
C3	8,66E+05	8,61E+05	1,25E+06	1,07E+06	0,19	0,68	1,45
ATP5PO	9,09E+06	3,91E+06	6,06E+06	2,89E+06	0,67	-0,60	0,67
ACAT1	3,46E+06	1,72E+06	2,08E+06	1,35E+06	0,81	-0,90	0,60
UQCRC2	2,44E+06	8,30E+05	1,89E+06	8,67E+05	0,50	-0,45	0,77
VDAC2	7,09E+06	1,83E+06	3,71E+06	1,56E+06	1,69	-1,05	0,52
ATP1A1	3,22E+06	1,02E+06	1,95E+06	1,07E+06	1,19	-0,80	0,60
CPT1B	3,70E+06	1,29E+06	2,81E+06	1,51E+06	0,59	-0,57	0,76

Protein	Mean Sham	SD Sham	Mean MI	SD MI	-Log p-value	Difference	Fold change
PDHB	3,95E+06	2,35E+06	2,54E+06	2,29E+06	0,74	-1,13	0,64
UQCRFS1	5,59E+06	3,45E+06	2,42E+06	1,40E+06	1,34	-1,14	0,43
TGM2	4,88E+05	1,56E+05	1,67E+06	2,92E+06	0,26	0,80	3,42
EEF1A2	7,22E+06	2,68E+06	8,03E+06	1,56E+06	0,37	0,23	1,11
PDHA1	6,38E+06	3,24E+06	3,51E+06	1,71E+06	0,98	-0,85	0,55
CS	1,19E+07	5,23E+06	7,95E+06	4,42E+06	0,61	-0,73	0,67
CYCS	2,59E+07	1,11E+07	9,10E+06	1,88E+06	3,06	-1,42	0,35
NDUFS1	3,37E+06	1,73E+06	1,76E+06	9,28E+05	0,96	-1,02	0,52
IDH3A	4,00E+06	1,43E+06	2,87E+06	1,41E+06	0,63	-0,63	0,72
VDAC3	7,63E+06	3,24E+06	3,61E+06	1,97E+06	1,56	-1,18	0,47
FGG	7,23E+05	6,62E+05	1,99E+06	9,02E+05	1,57	1,96	2,75
HSP90AB1	2,21E+06	1,00E+06	3,15E+06	1,44E+06	0,48	0,50	1,42
SUCLG1	7,46E+06	1,41E+06	4,26E+06	1,68E+06	1,35	-0,99	0,57
ATP5C1	4,94E+06	1,30E+06	3,04E+06	1,90E+06	1,03	-1,04	0,61
TF	4,07E+06	1,60E+06	3,95E+06	1,42E+06	0,02	-0,02	0,97
UGGT1	NaN	NaN	2,94E+06	8,71E+05	6,13	5,38	NaN
DLAT	2,61E+06	1,37E+06	1,55E+06	7,38E+05	0,89	-0,77	0,60
PRDX5	4,47E+06	2,06E+06	2,83E+06	1,50E+06	0,69	-0,66	0,63
CFH	6,80E+05	8,94E+05	3,68E+05	4,53E+05	0,13	0,36	0,54
GATD3	4,17E+06	1,13E+06	2,86E+06	9,57E+05	1,10	-0,58	0,69
KRT76	1,02E+07	2,74E+06	1,02E+07	3,65E+06	0,05	-0,04	1,00
UQCRC1	3,12E+06	1,44E+06	1,82E+06	1,10E+06	0,76	-0,89	0,58
PYGM	5,56E+05	4,03E+05	1,84E+05	1,31E+05	1,19	-1,50	0,33
PRDX4	1,80E+06	9,76E+05	5,10E+06	2,03E+06	2,26	1,65	2,83
VDAC1	5,32E+06	2,10E+06	2,38E+06	6,29E+05	2,34	-1,12	0,45
ERO1A	1,29E+06	9,50E+05	2,52E+06	9,10E+05	1,60	2,77	1,96
GOT2	1,47E+06	7,07E+05	2,13E+06	1,43E+06	0,39	1,12	1,45
HSP47	1,45E+05	2,56E+04	2,44E+06	9,47E+05	6,51	4,24	16,83
LDHB	3,24E+06	8,42E+05	2,75E+06	8,87E+05	0,37	-0,27	0,85

Protein	Mean Sham	SD Sham	Mean MI	SD MI	-Log p-value	Difference	Fold change
FGB	7,87E+05	5,77E+05	1,37E+06	7,66E+05	0,75	1,04	1,75
PKM	1,60E+06	1,15E+06	1,70E+06	8,16E+05	0,22	0,29	1,06
RACK1	1,74E+06	1,04E+06	2,85E+06	8,31E+05	1,26	0,86	1,64
ATP5PD	1,88E+06	5,80E+05	1,16E+06	4,95E+05	0,95	-1,60	0,62
ANXA2	7,08E+05	6,46E+05	8,38E+05	3,52E+05	0,61	1,17	1,18
ECHS1	7,40E+05	4,77E+05	8,08E+05	4,83E+05	0,13	0,25	1,09
HSPB1	6,33E+05	5,18E+05	9,52E+05	5,19E+05	0,65	0,89	1,50
RCN3	NaN	NaN	1,36E+06	5,14E+05	3,97	4,38	NaN
FGA	1,69E+06	1,25E+06	2,36E+06	8,31E+05	0,72	0,80	1,40
PYGB	1,36E+06	6,21E+05	9,81E+05	2,35E+05	0,33	-0,31	0,72
GPX4	1,78E+06	6,25E+05	1,97E+06	4,21E+05	0,33	0,20	1,11
CKM	6,65E+05	4,84E+05	8,77E+05	6,94E+05	0,19	0,37	1,32
PRDX2	8,56E+05	5,53E+05	8,45E+05	4,23E+05	0,07	0,12	0,99
SDHA	7,65E+05	3,05E+05	5,12E+05	3,51E+05	0,04	-0,09	0,67
VIM	5,77E+05	4,96E+05	5,87E+05	3,38E+05	0,84	1,75	1,02
LDB3	1,06E+06	4,93E+05	1,08E+06	6,64E+05	0,01	-0,02	1,02
CKAP4	NaN	NaN	7,09E+05	6,39E+05	0,85	1,93	NaN
SERPINA3N	1,07E+06	4,93E+05	8,34E+05	3,10E+05	0,24	-0,26	0,78
SQOR	6,93E+05	2,66E+05	7,68E+05	4,24E+05	0,05	-0,08	1,11
CLU	NaN	NaN	4,44E+05	2,86E+05	2,60	2,43	NaN
VDAC1	8,10E+05	3,81E+05	4,70E+05	2,00E+05	0,78	-0,92	0,58
ACADM	1,31E+06	6,63E+05	8,14E+05	4,47E+05	0,73	-0,82	0,62
MYH6	NaN	NaN	8,14E+05	5,56E+05	0,52	1,20	NaN
TMTC3	2,94E+05	1,64E+05	1,23E+06	3,86E+05	2,82	3,03	4,17
OGDH	1,23E+06	5,22E+05	1,22E+06	3,69E+05	0,07	0,07	1,00
COL6A2	1,53E+05	8,65E+04	NaN	NaN	0,12	0,40	NaN
SLC25A3	3,15E+06	5,18E+05	2,31E+06	8,12E+05	1,05	-0,53	0,73
PGK1	5,88E+05	2,74E+05	5,48E+05	1,72E+05	0,03	-0,04	0,93
SLC25A12	5,76E+06	3,15E+06	3,15E+06	1,92E+06	0,75	-0,96	0,55

Protein	Mean Sham	SD Sham	Mean MI	SD MI	-Log p-value	Difference	Fold change
IDH3B	1,04E+06	6,74E+05	1,04E+06	9,51E+05	0,14	-0,30	1,00
DECR1	9,17E+05	5,47E+05	5,86E+05	3,38E+05	0,57	-0,60	0,64
PRDX1	9,07E+05	4,32E+05	1,06E+06	2,12E+05	0,47	0,35	1,17
ACOT13	4,22E+06	7,79E+05	2,74E+06	7,44E+05	1,82	-0,65	0,65
PFN1	1,26E+06	6,29E+05	2,13E+06	7,79E+05	0,84	0,97	1,69
SDHB	3,26E+06	1,24E+06	2,07E+06	1,03E+06	0,91	-0,73	0,64
ALDH2	3,29E+05	1,64E+05	2,47E+05	1,49E+05	0,46	-0,57	0,75
FABP3	8,67E+05	5,99E+05	1,45E+06	1,15E+06	0,40	0,62	1,67
VWA8	2,32E+06	1,40E+06	1,09E+06	7,83E+05	0,60	-0,97	0,47
AK1	1,04E+06	5,04E+05	8,46E+05	3,35E+05	0,28	-0,26	0,82
NDRG2	1,60E+06	8,01E+05	8,68E+05	6,67E+05	0,92	-1,13	0,54
HADH	1,42E+06	8,75E+05	8,23E+05	3,25E+05	0,61	-0,64	0,58
HLCS	7,29E+05	4,82E+05	5,10E+05	3,26E+05	0,08	-0,17	0,70
RAB10	2,25E+05	1,33E+05	2,87E+05	2,10E+05	0,01	0,03	1,28
IKBIP	NaN	NaN	1,11E+06	5,39E+05	3,30	3,52	NaN
COTL1	NaN	NaN	3,42E+05	1,53E+05	3,03	2,46	NaN
ACSL1	1,68E+06	6,52E+05	9,19E+05	5,04E+05	1,05	-0,97	0,55
RAB1A	2,03E+06	4,83E+05	1,74E+06	9,01E+05	0,45	-0,40	0,86
ACOT2	9,70E+05	5,52E+05	9,05E+05	2,78E+05	0,07	0,09	0,93
C5	1,77E+05	3,86E+04	4,87E+05	3,60E+05	0,86	1,45	2,75
APOA1	2,91E+05	2,29E+05	6,38E+05	3,44E+05	1,30	1,69	2,20
CDC42	1,37E+05	6,52E+04	2,28E+05	4,84E+04	1,94	0,99	1,67
SERPING1	NaN	NaN	5,73E+05	4,71E+05	1,15	1,82	NaN
H1-4	9,87E+05	2,83E+05	7,08E+05	5,31E+05	0,77	-0,94	0,72
MDH1	1,16E+06	6,90E+05	1,37E+06	7,14E+05	0,24	0,80	1,19
HSD17B10	1,20E+06	6,39E+05	6,10E+05	3,56E+05	0,23	-0,53	0,51
ANXA7	5,00E+05	3,55E+05	4,33E+05	3,93E+05	0,06	0,16	0,87
EGFR	2,51E+05	8,36E+04	5,46E+05	5,01E+05	0,29	0,72	2,17
COQ8A	1,36E+06	6,37E+05	9,09E+05	5,29E+05	0,60	-0,87	0,67

Protein	Mean Sham	SD Sham	Mean MI	SD MI	-Log p-value	Difference	Fold change
NDUFS8	5,23E+05	2,75E+05	4,32E+05	1,43E+05	0,48	-1,44	0,83
NDUFS7	8,22E+05	4,77E+05	2,75E+05	1,52E+05	1,69	-1,59	0,33
FH	2,58E+05	2,39E+05	1,59E+05	1,60E+05	0,12	-0,26	0,62
H6PD	NaN	NaN	4,00E+05	3,55E+05	1,86	2,03	NaN
AHNAK	NaN	NaN	2,46E+05	1,63E+05	0,78	1,07	NaN
RDX	3,92E+05	2,42E+05	6,20E+05	2,21E+05	1,68	1,14	1,58
H1-2	6,91E+05	7,09E+05	4,12E+05	1,91E+05	0,26	-0,38	0,60
GANAB	NaN	NaN	6,14E+05	3,49E+05	3,75	2,72	NaN
DLD	7,17E+05	1,62E+05	4,49E+05	2,37E+05	0,40	-0,74	0,63
UBC	8,01E+05	2,70E+05	8,97E+05	3,82E+05	0,14	0,16	1,12
MMUT	3,96E+05	2,80E+05	NaN	NaN	1,12	-1,50	NaN
MBL1	1,31E+05	7,42E+04	4,17E+05	2,11E+05	1,04	1,52	3,19
H1-3	4,67E+05	3,19E+05	2,00E+05	8,30E+04	0,01	0,02	0,43
SDHC	1,41E+06	5,90E+05	8,21E+05	2,44E+05	0,03	-0,06	0,58
PFKM	2,91E+05	1,26E+05	2,15E+05	1,79E+05	0,02	-0,05	0,74
ARPC1B	NaN	NaN	2,49E+05	1,92E+05	0,12	0,26	NaN
FERMT2	1,50E+05	5,30E+04	1,49E+05	7,13E+04	0,24	-0,56	0,99
COL1A1	NaN	NaN	1,48E+05	2,18E+05	0,76	-1,49	NaN
H2BC3	2,17E+06	1,81E+06	1,61E+06	6,21E+05	0,02	0,04	0,74
SLC25A20	1,26E+06	3,07E+05	7,47E+05	2,59E+05	1,43	-0,85	0,59
ACADL	3,27E+05	6,94E+04	4,12E+05	2,69E+05	0,44	0,75	1,26
COX7A1	1,15E+06	5,97E+05	6,26E+05	3,31E+05	0,66	-0,74	0,54
PDIA3	NaN	NaN	4,08E+05	2,13E+05	4,03	2,80	NaN
MTCO2	2,09E+06	1,46E+06	7,78E+05	2,69E+05	1,39	-2,55	0,37
ATP1B1	5,30E+05	1,31E+05	5,82E+05	1,89E+05	0,14	0,10	1,10
	7,34E+04	1,63E+04	6,29E+04	6,08E+03	0,14	0,19	0,86
C8A	2,76E+05	2,02E+05	2,94E+05	1,17E+05	0,10	-0,19	1,06
H4C1	1,33E+06	8,10E+05	1,20E+06	3,33E+05	0,00	0,00	0,90
NDUFA12	2,07E+05	1,66E+05	1,46E+05	1,59E+05	0,89	-1,18	0,71

Protein	Mean Sham	SD Sham	Mean MI	SD MI	-Log p-value	Difference	Fold change
JUP	NaN	NaN	3,36E+05	1,08E+05	1,24	1,62	NaN
POSTN	NaN	NaN	5,36E+05	3,28E+05	2,13	2,53	NaN
MTND4	2,60E+05	1,02E+05	1,51E+05	6,52E+04	1,26	-1,05	0,58
ECI1	6,64E+05	4,53E+05	5,80E+05	4,66E+05	0,21	-0,40	0,87
ATP5F1D	NaN	NaN	1,82E+05	1,07E+05	0,58	1,10	NaN
PUF60	3,09E+05	2,50E+05	2,01E+05	7,37E+04	0,16	-0,25	0,65
PHB1	5,49E+05	2,67E+05	5,97E+05	3,88E+05	0,27	-0,51	1,09
ATP5MG	1,72E+07	6,13E+06	1,41E+07	3,31E+06	0,44	-0,25	0,82
CFHR4	NaN	NaN	1,51E+05	8,22E+04	1,02	1,10	NaN
COX5B	6,51E+05	2,53E+05	2,90E+05	9,97E+04	2,00	-1,17	0,45
PPIB	9,77E+05	3,59E+05	9,56E+05	3,75E+05	0,42	1,06	0,98
LRPAP1	3,84E+05	2,71E+05	5,40E+05	2,35E+05	1,09	1,19	1,40
EEF2	NaN	NaN	3,66E+05	2,04E+05	2,07	1,99	NaN
ATP5F1E	1,13E+06	1,90E+05	6,62E+05	3,28E+05	1,17	-1,07	0,59

8. Acknowledgement

At the conclusion of this thesis, I extend my gratitude to everyone who supported me during my doctoral journey.

Special thanks to Prof. Dr. Jürgen Schrader for supervising me and providing me with the opportunity to write my dissertation at the Department of Molecular Cardiology in this fascinating field of research. I express my appreciation to all members of this research group, especially Dr. Julia Hesse, who was always available for scientific discussion and advice, and Dr. Ding who conducted all the MI and Sham surgeries.

Furthermore, my sincere thanks go to Prof. Dr. Axel Gödecke for his unwavering support during my work and for serving as my second assessor.

I would like to specifically acknowledge Dr. Gereon Poschmann, Prof. Dr. Kai Stühler and the staff of the Biological-Medical Research Centre (BMFZ). The collaboration with you was amazing on both scientific and personal levels. Your advice has been invaluable, contributing to the success of this this great project.

I also express my gratitude to the group of Prof. Dr. Patrick Most in Heidelberg. Special thanks goes to Dr. Andreas Jungmann and Dr. Martin Busch for their assistance in producing the AAV9 plasmid and protocol advices, enabling the *in vivo* secretome analysis of aCF.

Beyond this, I appreciate the support of the graduate school IRTG for letting me participate in numerous interesting lectures, symposiums ,and for the opportunity to spend three months abroad at the Cardiovascular Research Center at the University of Virginia. Special thanks to Sandra Berger for always being attentive and assisting us with various issues.

Thanks to Prof. Dr. Kenneth Walsh, Dr. Nick Chavkin, and all members of the research team of the UVA for providing insights into your work and supervising me during my time abroad. This experience was very special for me and expanded my horizon.

In particular, I want to thank my colleagues Julia Steinhausen, Vera Flocke and Ria Zalfen (die Bertis). Work colleagues who turned into best friends. I will really miss our morning kitchen chats and seeing you every day! You played a crucial role in making this work successful.

Thank you, Arlen Martinez, for the adventurous travels to Mannheim. We had a very enjoyable time.

I want to thank Anne Hemmers and Justus Julebert Jonas for the great moments in Charlottesville. You were the best roommates I could have imagined. There is only one Charlottes Ville! In this context, I would also like to thank the Prax family, who welcomed us like family and introduced us to many different activities in Charlottesville.

Of course, my heartfelt thanks go to my family, who has always supported me in my life and my academic career. Thank you, Mum, Dad and Isabelle. Thanks to my grandparents Heidi, Karl, Jutta, Marianne and Hans-Joachim. Special thanks to my husband Kevin, who helped me to believe in myself and uplifted me during challenging times. I also want to thank Kevin's family for supporting me.

Last but not least, I want to thank all my friends who always believed in me and supported me through struggles. Special thanks to Saskia Rainer, Ronja Stephan, Maren Berendonck, Ali

Burdur, Stephanie Obst, Mara Duven, my second family (Ralf & Barbara Drückes, Judith Sting-Rabeneck), and to my Water polo girls.

9. Affidavit

I solemnly affirm, under penalty of perjury, that the dissertation titled “Quantitative secretome analysis of cardiac fibroblasts in the control heart and after myocardial infarction” was written by me independently and without improper outside assistance, adhering to the “principles for the assurance of good scientific practice at the Heinrich-Heine-University Düsseldorf”. The dissertation has not been submitted to any other institution or in comparable form. Furthermore, I have not made any unsuccessful attempts at obtaining a doctorate to date.

Düsseldorf, 23.12.2023 _____

Jasmin Bahr